STUDY OF THERMAL PROTECTION

REQUIREMENTS FOR A LIFTING BODY

ENTRY VEHICLE SUITABLE FOR

NEAR-EARTH MISSIONS

Final Report

by

M. J. Brunner
C. Dolan
R. Grasier
S. Kottock
G. Merlo

GENERAL 🌀 ELECTRIC

FOREWORD

STUDY OF THERMAL PROTECTION REQUIREMENTS FOR A LIFTING BODY ENTRY VEHICLE SUITABLE FOR NEAR-EARTH MISSIONS

Final Report

by

M. J. Brunner
C. Dolan
R. Grasier
S. Kottock
G. Merlo

NASA Contract No. NAS-2-2974

prepared for

National Aeronautics and Space Administration
Mission Analysis Division
Office of Advanced Research and Technology
Moffett Field, California

TABLE OF CONTENTS

LIST OF ILLUSTRATIONS

LIST OF ILLUSTRATIONS (Cont'd)

LIST OF ILLUSTRATIONS (Cont'd)

LIST OF TABLES

1. ABSTRACT

A study was made of the thermal protection requirements for the M2-F2 vehicle for a wide variety of vehicle sizes, weights, and re-entry conditions. The effects of ascent and abort were included for the Titan II, Titan III-C, and Saturn I-B boosters. Heat protection requirements were established for systems which include ablation, re-radiation, and ablation over re-radiation, separately or in combination, as required. Requirements were established for refurbishible systems having various materials and backface temperatures.

2. NOMENCLATURE

A	Pre-exponential factor in the Arrhenius equation; reference area
BF	Backface
C_D	Coefficient of drag
C_L	Coefficient of lift
C_g	Specific heat of pyrolysis gases
C_p	Specific heat of solid; pressure coefficient
E	Activation energy in the Arrhenius equation
H	Latent heat
h	Enthalpy; altitude
K	Thermal conductivity
L	Reference length
$\dot{m}$	Ablated mass loss rate at surface of solid
$\dot{m}_g$	Pyrolysis gas generation rate
M	Mach number
$\bar{M}$	Molecular Weight
n	Order of Reaction
Pr	Prandtl number
p	Pressure
q	Dynamic pressure
$\dot{q}$	Heat flux
Q	Total Heating
Q^*_{HW}	Hot wall heat of ablation
R	Universal gas constant
r	Radius
S	Surface erosion
s	Surface length
t	Time; thickness
T	Temperature

2

2. NOMENCLATURE (Cont'd)

TH	Thickness
u	Velocity (local)
V	Velocity
x	Co-ordinate distance from original surface of solid material
α	Angle of attack
β	Area ratio = (char solid/char solid + char porous)
γ	Ratio of specific heats; flight path angle
ϵ	Emissivity
Δ	distance from body to flow separation boundary, standoff distance
η	(see equation 16)
Λ	Sweep angle
λ	Mean free path
θ	Body Angle
μ	Viscosity
Φ	Bank angle
ρ	Density
σ	Stefan Boltzmann Constant
τ	Shear stress
∞	Free stream

Subscripts

b	Base
BF	Backface
BL	Boundary layer
Block	Blocked
C	Convective
c	Char
cal	Calorimeter

2. NOMENCLATURE (Cont'd)

cg	Gas combustion
CR	Char removal
D	Degradation
e	Edge boundary layer; erosion
f	Final
g	Gas
gf	Gas formation
HGR	Hot gas radiation
HW	Hot wall
i	i^{th} leg of the modified Arrhenius plot; ionization
ins	Insulation
k	Cracking or recombination
LD	Laminar detached
LE	Leading edge
m	Mass
mtl	Material
n	Nose
o	Stagnation point
R	Radius
R	Recovery
Re	Reynolds number
RR	Re-radiation
S	Stagnation
s	Entropy
subl.	Sublimation
turb.	Turbulent

2. <u>NOMENCLATURE</u> (Cont'd)

TD   Turbulent detached

traj.   Trajectory

V   Virgin

W   Wall

<u>Superscripts</u>

*   Reference conditions (Eckert)

3. INTRODUCTION

There is considerable interest in lifting-body entry vehicles for future manned space missions. These missions are usually constrained to altitudes lower than for synchronous orbits, and in general dictate a need for moderate lifting capability such as exhibited by the M2-F2 vehicle.

The shape of most applicable lifting bodies is such that there is a considerable variation of heating rates over the vehicle surface. In addition, a wide variation in thermal environments exists along the flight path. These variations, and the likely existence of turbulent flow over portions of the vehicle surface, complicate the design of efficient thermal protection systems for lifting entry vehicles.

The study discussed in this final report was initiated to assess the thermal protection requirements, to obtain accurate evaluations of shield weight requirements, and to delineate problem areas which may require increased research effort. Both ablative and combinations of ablative, re-radiative, and ablative over re-radiative thermal protection systems with refurbishable capability were considered for a wide range of M2-F2 vehicle sizes and weights capable of entry from a range of near-earth orbits.

The scope of the study may be summarized as follows:

Vehicle	NASA/Ames M2-F2 configuration as shown in Figure 1
Booster	Titan II, Titan III-C, Saturn I-B
Vehicle Weight	3172, 4536, 6804 kg nominal weight and ± 10% (7000, 10,000, 15,000 lb)
Vehicle Length	6.71, 7.92, 9.14 m nominal length and ±10% (22, 26, 30 ft)

Trajectories

Ascent	Titan II, Titan III-C, Saturn I-B
Abort	From the above boosters
Entry	7,468 m/sec (24,500 ft/sec)
	9,144 m/sec (30,000 ft/sec)
	10,363 m/sec (34,000 ft/sec)

Heat Protection Systems

Ablation

Re-radiation

Ablation over re-radiation

Materials

Ablation	Microballoon Phenolic Nylon (MPN)
	Elastomeric Shield Material (ESM)
Re-radiation	René 41, TZM
Insulation	Ablation system - ablation material (ESM, MPN)
	Re-radiation system - microquartz (MQ)
	foamed pyrolytic graphite (FPG)

Structure Temperature (Max. allowable)

$422^{\circ}K$ $(300^{\circ}F)$

$589^{\circ}K$ $(600^{\circ}F)$

Heat Protection System Weights

(include refurbishment and attachment weights)

The scope of the study is illustrated by examining the vehicle weight and $W/C_L A$ variation with vehicle length on Figure 2. These vehicles will be studied for the variety of flight trajectories and heat protection systems stated above.

4. DISCUSSION OF RESULTS

4.1 TRAJECTORY ANALYSIS

4.1.1 ENTRY

4.1.1.1 Flight Path Definition

4.1.1.1.1 Sub-Circular Entry

The flight paths for the sub-circular entry velocity flights were generated as follows:

(1) Starting with the initial velocity and flight path angle at 122 km (400,000 ft), the vehicle is trimmed to the attitude for $L/D = 1$, and a zero bank angle is maintained. The vehicle is flown at $L/D = 1$ until a horizontal flight path is achieved.

(2) At pullout the pitch attitude is modulated to provide the lift necessary to maintain horizontal flight. A zero bank angle is held throughout the horizontal flight. The pitch attitude is modulated throughout the horizontal flight until a predetermined attitude is achieved, and then a terminal equilibrium glide phase is initiated. The latter portion of the trajectory was flown in three different ways, namely:

   (a) The equilibrium glide begins when $L/D = L/D$ max is achieved, and zero bank angle is maintained during the equilibrium glide.

   (b) The equilibrium glide begins when $C_L = C_{L \, max}$. $C_{L \, max}$ and a 60-degree roll angle are maintained during the equilibrium glide.

   (c) Another equilibrium glide was flown at $C_{L \, max}$ as in item (b), but with a zero bank angle.

4.1.1.1.2 Super-Circular Entry

The flight paths for the super-circular velocities considered were generated as follows:

(1) Starting with the initial velocity and flight path angle at 122 km (400,000 ft), the vehicle is trimmed to the attitude for $L/D = 1$, and a zero bank angle is maintained. The vehicle is flown at $L/D = 1$ until a horizontal flight path is achieved.

(2) At pullout the vehicle is rolled while $L/D = 1$ is maintained until the lift vector just balances the vertical forces on the vehicle, and a constant altitude is maintained. The horizontal lift vector effects a cross-range maneuver during the horizontal flight phase. The roll angle is modulated to maintain horizontal flight until the vehicle is eventually rolled back to zero bank angle.

(3) When a zero bank angle is achieved, the vehicle commences a terminal equilibrium glide at the attitude for $L/D = 1$ and a constant zero bank angle.

8

4.1.1.2 Overshoot Boundary for Super-circular Entry

The overshoot boundary for the super-circular entry flight conditions was determined in the following manner:

(1) For a range of entry path angles, the vehicle is flown in the attitude for $L/D = 1$ until pullout ($\gamma = 0$) is achieved.

(2) At each pullout flight condition, the required downward lift force necessary to maintain constant attitude flight is computed.

(3) The available negative lift ($-C_L$), using the C_L for $L/D = 1$, is computed. The maximum available negative lift (where $C_L = C_{L\,max}$) is also computed.

A typical variation of the required negative lift and the available lift as a function of entry path angle is shown in Figure 3. The intersection of the required and the available lift curves defines the overshoot boundary for the given entry velocity and $W/C_L A$. The entry path angle, determined by selecting the available lift for $L/D = 1$, is seen to be only slightly steeper than the allowable path angle for $C_L = C_{L\,max}$; thus, the selected overshoot boundary is slightly conservative. Figure 4 shows the overshoot boundary (i.e., minimum entry path angle) as a function of $W/C_L A$ for entry velocities of 9144 m/sec (30,000 ft/sec) and 10,363 m/sec (34,000 ft/sec). The overshoot boundary does not vary greatly with $W/C_L A$ for the range of $W/C_L A$ considered; a 50 percent increase in $W/C_L A$ changes the overshoot boundary approximately 0.15 degrees.

Subsequent to the definition of the super-circular entry overshoot boundary, the complete re-entry flight profiles were computed. Figure 5 shows typical altitude time histories for the 10,363 m/sec (34,000 ft/sec) entry velocity condition. Note the small difference between the flight profiles for the minimum and maximum values of $W/C_L A$. The typical velocity time histories shown in Figure 6 exhibit only slight differences for the extreme $W/C_L A$ values. The overshoot boundary trajectories represent flights which have the greatest flight time and consequently have the most severe thermal soak exposure.

4.1.1.3 Undershoot Boundary for Super-circular Entry

The undershoot boundary is determined by consideration of the g forces on the pilot during the pullout phase of the re-entry flight. During pullout, the pilot experiences acceleration in an essentially normal direction. A reasonable tolerance level for acceleration in this direction is 5 g (Reference 1). The backward acceleration component is relatively small, and since the tolerance level in this direction is large (about 12 g's), normal acceleration is the critical factor. A 5-g normal acceleration at pullout was taken as the undershoot boundary.

The undershoot boundary was determined by flying a series of pullouts with the attitude for $L/D = 1$ and increasingly steep entry path angles. Figure 7 shows the variation of pullout peak g's with entry path angle for the two super-circular velocities considered

9

in this study. The undershoot boundary (i.e., maximum entry path angle) is seen to be approximately seven degrees down from the horizontal. Once the undershoot boundary was determined, complete trajectories were run for the two super-circular velocities and the nominal weight and $W/C_L A$. The heat flux histories for the undershoot boundary trajectories are shown in Figure 8 along with the heat flux histories for two overshoot boundary trajectories and a sub-circular re-entry case.

The undershoot boundary provides the severest trajectory from the standpoint of maximum heat flux for a given value of $W/C_L A$ while the overshoot boundary provides the severest trajectory for total heating. Since an ablative thermal protection system is most sensitive to the total heat load and since it can be seen from Figure 8 that the values of the maximum heat flux for the undershoot boundaries are so large as to prohibit the use of a re-radiative system, the overshoot boundary is adopted, for the purposes of this study, as the design trajectory for the super-circular cases. It should be noted that the thermal protection system designs utilizing re-radiation is thus limited to the upper part of the flight corridor for the super-circular cases.

The velocity-altitude histories for the undershoot, overshoot, and sub-circular cases are shown in Figure 9.

4.1.2 ASCENT AND ABORT

4.1.2.1 Critical Ascent Abort

The critical conditions for abort on the ascent trajectory are those which produce maximum heat flux, maximum total heating, and maximum total acceleration. Three types of trajectories were flown for a family of points on the ascent trajectory prior to orbit injection. The three trajectory types are:

(1) **L/D = 1 constant**

The L/D is held constant at L/D = 1, and the bank angle is maintained at zero. This type of trajectory goes through a series of altitude oscillations until an equilibrium glide condition is achieved.

(2) **L/D = 1, 3-Phase**

A pullout at L/D = 1 is made. When a horizontal flight path is attained, the vehicle is roll modulated to maintain a constant altitude with L/D = 1 held constant. When the roll angle is modulated back to zero, the vehicle begins an equilibrium glide at L/D = 1.

(3) **L/D max, 3-Phase**

Similar to item (2) but the entire trajectory is flown with L/D = L/D max rather than L/D = 1.

10

The maximum heat rate and total acceleration both occur just prior to the initial pullout. Up to this point, the L/D = 1 constant and L/D = 1, 3-phase trajectories are identical, so the maximum heat flux and total accelerations are plotted for only one of the two flight modes. Figures 10 through 12 show the maximum total acceleration and maximum heat flux as a function of abort velocity on the ascent trajectory for the three boosters, the maximum and minimum $W/C_L A$, and the L/D = 1, 3-phase and L/D max, 3-phase flight modes. In every case it is seen that L/D max results in more severe loads and heating rates. In all cases, the maximum total heating was less than for the critical re-entry flights. The effect of L/D on the maximum heat flux is large; an increase in L/D from 1 to L/D max increases the maximum heat rate by as much as 70 percent. The effect of L/D on maximum total acceleration is relatively small: one g or less. The maximum total acceleration is seen to occur for an abort at relatively low velocity on the ascent trajectory: from about 3000 to 4000 m/sec. The maximum heat rate occurs for abort at somewhat higher velocity: from about 5500 to 6500 m/sec. Several typical 3-phase flight profiles (altitude vs. range) for aborts from the ascent trajectory are shown on Figure 13.

4.1.2.2   Maximum Dynamic Pressure Abort

The maximum dynamic pressure abort condition for the ascent trajectory can produce high values of total acceleration. The maximum total acceleration occurs at relatively low altitude: approximately 8.5 km. Figure 14 shows the variation of maximum total acceleration with $W/C_L A$ for the Titan II, Titan III-C, and Saturn I-B. Figure 15 shows time histories of total acceleration for aborts from each of the three boost trajectories for the nominal weight and $W/C_L A$ associated with each booster. It is noted that the acceleration for the maximum dynamic pressure abort condition is in an axial direction instead of normal as in the other critical ascent abort cases discussed previously. Although the g's are numerically higher (in the axial direction) they are actually less critical from a human-tolerance standpoint. The maximum acceleration in both normal and axial directions must be considered in any actual vehicle design.

4.2 FLOW FIELD AND HEATING ANALYSES

4.2.1 FLOW FIELDS

Estimated trimmed lift and drag for the M2-F2 vehicle are presented in Reference 2, as derived from NASA-supplied and -reported test data. The methods of estimation and a discussion of data limitations are contained in the reference.

Both axisymmetric flow field and arbitrary body methodology was applied to the problem of estimating windward pressures at various angles of attack, then comparing these theoretical results with surface pressure data and pertinent reports. The leeward pressures followed the same procedure, except that more reliance was placed on various data sources. The details of the analysis and presentation of data may be found in Reference 2.

The pressure distributions for 0, 10, and 30-degree pitch angles, resulting from the flow field and arbitrary body computations, wind tunnel data, and data interpolations, data extrapolation, combinations, and comparisons, are presented in Reference 2 as functions of X/L, the axial distance from the nose, and meridian angle, measured perpendicular to the vertical plane of symmetry from the bottom centerline.

The pressure distribution data available for the fins and boat-tail areas is quite limited. A definition of the local flow field in the fin/boat-tail region by use of Schlieren/shadowgraph information was attempted.

The flow pictures obtained at Rhodes and Bloxsom did not have enough detail to enable flow field definition, but did indicate the possibility of both a strong interaction shock region at the base of the fin leading edge and a large area of separated flow on the upper surface boat-tail area extending forward almost to the canopy for the M2-F2 model tested. The data from the fin pressure pickups just above, aft, and parallel to the side meridian from the reported test data were not sufficient to define the fin/boat-tail flow field, particularily since the F1, rather than the current F2, model was tested.

4.2.2 HEATING ANALYSIS

4.2.2.1 Model Test Results

A model test was performed to experimentally determine the heat transfer distribution over the M2-F2 vehicle at a 30-degree angle of attack for a Mach number of 22. The technique used at Rhodes and Bloxsom employs a special temperature-sensitive paint. The local heat flux is obtained by evaluating the local thermal coating color changes with respect to a calibration sphere. The detail results of the model tests are given in Reference 2.

4.2.2.2 Method of Analysis

4.2.2.2.1 Convective Heating

a. Attached

The stagnation heat flux for the M2-F2 vehicle was calculated using Lee's classical laminar solution for hypersonic heating combined with Eckert's reference enthalpy relationship. The equation for this is given (Reference 3) as:

$$\dot{q}_s = \frac{0.778}{P_r^{2/3}} \left[\rho^* \, \mu^* \left(\frac{d u_e}{d s} \right)_{s=0} \right]^{1/2} (h - h_w) \tag{1}$$

For body locations off the stagnation point, both laminar and turbulent heat fluxes were calculated. The off-stagnation-point laminar heat fluxes were computed using a compressible reference enthalpy relation based on Lee's solution. The equation for the laminar heat fluxes is given (Reference 3) as:

$$\dot{q}_L = \frac{0.389}{P_r^{2/3}} \frac{\rho^* \, \mu^* \, u_e \, r \, (h_r - h_w)}{\left[\int_0^s \rho^* \, \mu^* \, u_e \, r^2 \, d s \right]^{1/2}} \tag{2}$$

The off-stagnation point turbulent heat fluxes were computed using the GE turbulent integral equation employing Eckert's reference enthalpy relationship. The equation for the turbulent heat fluxes is given (Reference 3) as:

13

$$\dot{q}_t = \frac{0.0296}{P_r^{2/3}} \frac{\rho_e u_e \mu_e^{.25} (\mu^*/\mu_e)^{0.2} (\rho^*/\rho_e)^{0.8} r^{0.25}}{\left[\int_0^s \rho_e u_e \mu_e^{0.25} r^{1.25}\, ds\right]^{0.2}} (h_r - h_w) \quad (3)$$

This equation satisfies both the momentum and energy integral equations and includes the effect of a finite pressure gradient. The solution was obtained by use of the Blasius incompressible flat plate skin friction coefficients modified for compressible flow employing Eckert's reference enthalpy relationship.

All heat fluxes are based on real gas relationships and properties of air in chemical equilibrium (Reference 4). In addition, the effect of entropy gradients has been factored into the analysis even though these effects may be small for this vehicle.

b. Separated

The convective heat fluxes to the afterbody for the region of separated flow were determined by semi-empirical methods developed from flight test data from the Mark 2 Re-entry Vehicle. Results show the convective heating for laminar and turbulent separated flow, which are given (References 5 and 6) by the following equations:

$$\dot{q}_{LD} = 0.0192\, R_{e_\Delta}^{0.5}\, \frac{\mu_e}{\Delta} (h_o - h_w) \quad (4)$$

$$\dot{q}_{tD} = 0.0069\, R_{e_\Delta}^{0.8}\, \frac{\mu_e}{\Delta} (h_o - h_w) \quad (5)$$

where

$$R_{e_\Delta} = \frac{\rho_e u_e \Delta}{\mu_e}$$

4.2.2.2.2 Radiative Heating

The radiative heat flux to the vehicle from the gas cap was evaluated by the following equation:

$$\dot{q}_r = \Delta \epsilon \sigma T^4, \quad \epsilon = f(\rho, T) \quad (6)$$

14

The emissivity was obtained for the various radiating species for a given value of local density and temperature (References 7, 8).

There are a number of sophisticated programs available (Reference 9) to evaluate the incident and absorbed radiative heat flux over a re-entry vehicle for a non-optically thin radiating gas layer. These programs are very costly and complex but produce accurate evaluations of the radiative heating. This sophistication is only warranted when radiative heating is an important contribution to the thermal environment. In most cases the more rigorous computations produce heat fluxes which are lower than given above. The magnitude of the radiative heating for this application is small compared to the convective; therefore only the incident, optically thin radiation was evaluated.

4.2.2.2.3 Angle of Attack

The local heat flux distribution around a vehicle such as the M2-F2 at zero angle of attack can be quite adequately evaluated by methods previously discussed except in local areas where special interactions exist. Heating evaluations at large angle of attack, however, are quite another matter. Rigorous methods of heating predictions except for simple shapes are not generally adequate. Engineering methods, however, are available for predicting local heat flux distributions at relatively large angle of attack for both laminar and turbulent flow (References 10 and 11). Correlation parameters have been developed to predict heating at angle of attack as follows:

Laminar flow - Windward Ray

$$\frac{\dot{q}_L}{\dot{q}_{L_{\alpha=0}}} = \left[\frac{(\rho^* \mu^* u_e)}{(\rho^* \mu^* u_e)_{\alpha=0}} \left(\frac{2 K + 1}{3} \right) \right]^{1/2} \frac{(h_r - h_w)}{(h_r - h_w)_{\alpha=0}} \tag{7}$$

Laminar flow - Leeward Ray

$$\frac{\dot{q}_L}{\dot{q}_{L_{\alpha=0}}} = \left[\frac{(\rho^* \mu^* u_e)}{(\rho^* \mu^* u_e)_{\alpha=0}} \cos \alpha \right]^{1/2} \frac{(h_r - h_w)}{(h_r - h_w)_{\alpha=0}} \tag{8}$$

15

Turbulent flow - Windward Ray

$$\frac{\dot{q}_T}{\dot{q}_{T_{\alpha=0}}} = \left[\frac{(\rho^* u_e)}{(\rho^* u_e)_{\alpha=0}}\right]^{0.8} \left[\frac{\mu^*}{\mu^*_{\alpha=0}}\right]^{0.2} \left[\frac{1.25\,K+1}{2.25}\right]^{0.2} \frac{(h_r - h_w)}{(h_r - h_w)_{\alpha=0}} \quad (9)$$

Turbulent flow - Leeward Ray

$$\frac{\dot{q}_T}{\dot{q}_{T_{\alpha=0}}} = \left[\frac{(\rho^* u_e)}{(\rho^* u_e)_{\alpha=0}}\right]^{0.8} \left(\frac{\mu^*}{\mu^*_{\alpha=0}}\right)^{0.2} \frac{h_r - h_w)}{(h_r - h_w)_{\alpha=0}} \quad (10)$$

where

$$K = 1 + \frac{\sin \alpha \cot \theta}{\cos \alpha + \theta}$$

For the above angle of attack correlations, the local properties employed are based on an isentropic expansion from the stagnation conditions on the downstream side of the normal shock to the local pressure on the body. The methods on the windward ray generally show that correlation with data is within $\pm$ 15 percent for both laminar and turbulent flow. The methods on the leeward ray show that correlations with data are somewhat worse due to considerable scatter in the data. The leeward correlations used, however, are believed to be conservative.

4.2.2.2.4 General Heating Approximations

Evaluations of the thermal environment for the wide variety of flights and vehicle sizes and weights may be obtained without the detailed knowledge of the flow field by utilizing simplifications to the local gas properties at the edge of the boundary layer for hypersonic flow. It should be noted that all portions of the study requiring detailed knowledge of the flow properties and heating such as for the REKAP analysis, transition studies, etc., the more rigorous methods described previously were utilized. The approximate methods developed for convective heat input are summarized as follows (Reference 12):

Stagnation - Heat Flux

$$\dot{q}_s = f(C_s)\, R_n^{-1/2}\, \rho_\infty^{1/2}\, V_\infty^{3} \quad (11)$$

$$f(C_s) = C_s\, C_{T_s}\, C_{i_s}$$

$$C_s = 3.47 \times 10^{-9}$$

16

Laminar Heat Flux

$$\dot{q}_L = f(C_L) \, S^{-1/2} \, \rho_\infty^{1/2} \, V_\infty^3 \tag{12}$$

$$f(C_L) = C_L \, C_{T_L} \, C_{i_L} \, C_{s_L}$$

$$C_L = 2.74 \times 10^{-9} \left(\frac{P_e}{P_s}\right)^{0.5 + 0.39\,(\gamma-1)/\gamma} \left[1 - \left(\frac{P_e}{P_s}\right)^{\gamma-1/\gamma}\right]^{1/4}$$

$$\left[1 + \left(\frac{P_e}{P_s}\right)^{\gamma-1/\gamma}\right]^{-0.14}$$

Turbulent Heat Flux

$$\dot{q}_T = f(C_T) \, S^{-0.2} \, \rho_\infty^{0.8} \, V_\infty^3 \tag{13}$$

$$f(C_T) = C_T \, C_{T_T} \, C_{i_T} \, C_{s_T}$$

$$C_T = 2.49 \times 10^{-7} \left(\frac{P_e}{P_s}\right)^{0.8 + 0.56\,(\gamma-1)/\gamma} \left[1 - \left(\frac{P_e}{P_s}\right)^{\gamma-1/\gamma}\right]^{0.4}$$

$$\left[1 + 1.272 \left(\frac{P_e}{P_s}\right)^{\gamma-1/\gamma}\right]^{-0.46}$$

The temperature correction $(C_{T_{s,\,\ell,\,T}})$ may be evaluated as:

$$C_T = \left[1 - h_w/h_s\right] \left[\frac{1 + 1.272\, h_e/h_s}{1 + 1.272\, h_e/h_s + 2.72\, h_w/h_s}\right]^n \tag{14}$$

$$n = 0.14 \text{ for } C_{T_S} \text{ and } C_{T_L}$$

$$n = 0.46 \text{ for } C_{T_T}$$

$$h_s \simeq \frac{V_\infty^2}{2 g J}$$

$$\frac{h_e}{h_s} \simeq \left(\frac{P_e}{P_s}\right)^{\gamma - 1/\gamma} = 1.0 \text{ for } C_{T_S}$$

where:

quantity	units
$\dot{q}$	$Btu/ft^2 sec$
Q	Btu/ft^2
ρ	lb/ft^3
s, R	ft
V	ft/sec

4.2.2.2.5 Heating in Special Areas

The heating on the leading edge of the fin was established for the current application by the following relation:

$$\dot{q}_{LE}/\dot{q}_s = \sqrt{\frac{1}{2} \frac{R_N}{R_{LE}}} \cos^n \Lambda_e \tag{15}$$

where

$$\cos^2 \Lambda_e = 1 - \sin^2 \Lambda \cos^2 \alpha$$

$$n = 1.0$$

The value n can vary depending on the local flow conditions and sweep angle. It can in some cases be as high as 1.5. Using n = 1 should produce conservative heating estimates. It should be noted that the above relationship approaches zero as $\Lambda_e \simeq 90$ degrees. The local heating on the fin should not, however, be less than that obtained along the surface of a cylinder based on the local flow properties at the edge of the boundary layer as described previously.

The heating on the flaps and canopy were obtained by methods described previously with the exception that the local boundary layer was initiated at the forward position as required for the specific item, instead of from the stagnation point. Previous model tests and other pertinent information were utilized in making these predictions (References 13, 14).

There are local regions on this vehicle, as in most other lifting vehicles, which are subjected to increased heating due to interactions with various local flows around joining abrupt sections. Such areas are adjacent to the flaps, fins, canopy, rudder, and all local gaps or protuberances on the vehicle. These areas are generally quite small in width but may extend over a considerable length. The local heating in these interaction areas can be appreciably higher than the undisturbed region depending on the local geometry, Mach number, Reynolds number, and flow condition (laminar or turbulent) (Reference 15). These local areas, although small in area compared to the total vehicle area, must be individually analyzed and then protected by an adequate heat protection system.

4.2.2.2.6 Viscous Effects

A problem existing for some lifting vehicle flights is that of predicting aerodynamic and thermodynamic characteristics at high speeds and high altitudes. The flow field in this regime may be sufficiently rarefied so that the mean free path becomes too large for application of classical boundary layer theory, but not large enough for free molecule flow concepts to apply. Classical boundary layer theory applies at high Reynolds numbers in the continuum regime. Continuum flow exists when the local mean free path is small compared to the characteristic length of interest. The rarefied gas flow regimes may be classified (Reference 16) according to the degree of rarefaction as determined by comparing the mean free path to a characteristic dimension as $\lambda_s/\Delta \sim \lambda_\infty/R_b$. A convenient classification (Reference 17) of the various intermediate regimes between continuum and free molecule flow is given in the order of decreasing Reynolds number as:

(1) Vorticity Interaction Regime

$$\lambda_\infty/R_b << \epsilon \qquad \text{where } \epsilon \sim \Delta/R_b = \rho_\infty/\rho_s$$

(2) Viscous Layer Regime

$$\lambda_\infty/R_b << \epsilon^{1/2}$$

(3) Incipient Merged Layer Regime

$$\lambda_\infty/R_b << 1$$

(4) Fully Merged Layer Regime

$$\lambda_\infty/R_b < 1$$

(5) Transitional Layer Regime

$$\lambda_\infty / R_b > 1$$

(6) First Order Collision Regime

$$\lambda_\infty / R_b >> 1$$

The M2 - F2 trajectories of interest, in terms of the general flight conditions representing these intermediate gas flow regimes, are shown as follows:

	Approximate altitude $R_b = 0.457m$ (1.5 ft)	
Regime	km	ft x 10^{-3}
Vorticity Interaction	76.2	250
Viscous Layer	85.3	280
Incipient Merged Layer	93.0	305
Fully Merged Layer	100.5	330
Transitional Layer	109.6	360

For this application, the vorticity interaction regime exists from about 76.2 km (250,000 ft) to 85.3 km (280,000 ft) and the viscous layer exists up to about 93 km (305,000 ft) altitude. The other regimes occur at higher altitudes. All re-entry flights pass through these regions but the comparable time and heating experienced in these regimes are relatively low compared to the remaining portion of flight. The pullout phase and constant-altitude phase of flight occur at lower altitudes. The only regime of particular concern is the vorticity interaction regime which occurs higher in altitude than the major and critical portion of flight but is close enough to warrant further investigation.

4.2.2.2.7 Low Reynolds Number Effects

In high-altitude regions where the Reynolds Number is below that for thin boundary layer flow, several effects appear which require special consideration. Ferri and Libby (Reference 18) in 1954 began studies of the interaction between the vorticity generated by shockwave curvature at the nose of a blunt body and the surface shear generated vorticity of the boundary layer. This was one of several effects of the same order of magnitude but quantitatively the most important for blunt vehicles in

hypersonic flow. In addition to vorticity, other effects (Reference 19) occur due to longitudinal and transverse curvature, velocity slip at the surface, temperature jump at the surface, entropy gradients in the outer flow, stagnation enthalpy gradients in the outer flow, and displacement of the outer flow by the inner flow (the outer flow being inviscid and the inner flow being viscous). These second order effects are frequently referred to as vorticity effects.

An evaluation of these effects have been made by Van Dyke (Reference 19), Lenard (Reference 20) and Maslen (Reference 21), whereas Davis (Reference 22), Ferri (Reference 18), and Hickman (Reference 23) have evaluated only the vorticity effect. Of the methods available, Davis (Reference 22) and Van Dyke (Reference 19) appear to be the most complete and useful. Van Dykes' (Reference 24) calculation of the second order effects as high Mach number for a highly cooled wall show the heating to be:

$$\dot{q}/\dot{q}_{ref} = 1 + 0.483 \, \eta$$

where

$$\eta = \frac{\left[(\gamma - 1) \, M_\infty^2 \right]^{\omega/2}}{R_e} \qquad \omega = 1/2$$

$\dot{q}_{ref}$ = heat transfer rate without second order effects.

The second order effects can be estimated for a typical M2-F2 flight.

As an illustration, the re-entry flight at velocity of 9144 m/sec (30,000 ft/sec) for the nominal $W/C_L A$ vehicle was examined as follows:

time	altitude			$\dot{q}/\dot{q}_{v=0}$			
(sec)	KM	(ft x 10^{-3})	$\dot{q}/\dot{q}_{max}$	Item (1)	Item (2)	Item (3)	Item (4)
50	96.2	(316)	0.16	1.129	1.05	1.49	1.10
100	79.8	(262)	0.75	1.024	1.02	1.16	1.04
140	75.5	(248)	1.00	1.018	1.01	1.14	1.03
1000	75.3	(247)	0.45	1.019	1.01	1.14	1.03

(1) Van Dyke (Reference 24)
(2) Hickman (Reference 23)
(3) Ferri (Reference 25)
(4) Davis (Reference 22)

It is noted that the calculations of Items 1, 2, and 4 are in close agreement, while Item 3 is high. It is believed that Items 4 and 1 are the most accurate estimates. Therefore, at the maximum heat flux condition, it is believed that the secondary or vorticity effects represent a correction of about one to three percent on the stagnation heating. Considerably less than this will occur at locations away from the stagnation point (Reference 25). As the vehicle flies at higher Reynolds Number (lower altitude), these effects will become negligible. The heating in the stagnation area then should be increased about three percent to account for secondary effects.

4.2.2.3 Transition Criteria

The magnitude of the local heating during flight depends not only on the local pressure and geometry of the vehicle, but also on whether the flow is laminar or turbulent. The transition criteria should be the most reliable one available, based on the latest available flight and ground test data. A great deal of study has been devoted recently to the subject of transition (Reference 26). The transition from laminar to turbulent flow is a function of such variables as roughness, angle of attack, mass addition rate, wall cooling ratio, vehicle geometry (bluntness ratio, cone angle, nose radius), and local boundary layer properties (Mach number, Reynolds number). Evaluation of the influence of each of these specific variables on transition is currently beyond the state of the art. There is, however, a wealth of both flight and ground test data which have resulted in a reasonable transition criteria which can be readily evaluated for a given vehicle application.

The transition criteria used in this study is shown in Figure 16. The transition Reynolds number is based on the local properties at the edge of the boundary layer based on wetted length, and is a function of local Mach number. This criteria is based on thermal, observable, pressure, and radar tracking data, and it is believed to be representative of realistic flights of both ablating and non-ablating bodies.

The effect of transition on the local heat flux and total heating can then be evaluated from the flight path and local pressure distribution over the vehicle. The effect of transition on total heating will be a function of W/C_LA, vehicle length, and the position on the vehicle expressed by the local heat flux ratio $(\dot{q}/\dot{q}_s)_m$ for each re-entry trajectory. The influence of transition on the total heating is shown on Figure 17 as a function of the local heat flux ratio for re-entry at 7468 m/sec (24,500 ft/sec) for various values of W/C_LA and vehicle length (L). The influence of the various re-entry conditions on the effect of transition is shown on Figure 18 for a nominal typical value of W/C_LA and L. The effect on total heating is greatest for the lowest re-entry velocity flight, 7468 m/sec (24,500 ft/sec), and the smallest effect for the highest super-orbital velocity flights. The effect of transition on the maximum heat flux is shown on Figure 19. Only at very low heat flux ratios does the maximum turbulent heat flux exceed the maximum local laminar heat flux. The maximum effect is obtained for the lowest re-entry velocity condition.

4.2.2.4 Reference Heat Flux Evaluation

The thermal environment for the M2-F2 will depend primarily on the flight path and angle of attack time history. The maximum heating will occur at the stagnation point for laminar flow and at a location off the stagnation point on the spherical section for turbulent flow. The distribution around the vehicle will vary considerably from the maximum values. The lowest heating will occur on the top surfaces and the after-body, while the highest values will occur on the leading edges, pitch flaps, and wind-ward side; the relative magnitude of each varies with the angle of attack. The heating during ascent, abort, and re-entry must be evaluated as it will affect the heat pro-tection system requirements.

The ascent phase stagnation heating is shown on Figure 20 as a function of time for the three applicable boosters (Titan II, Titan III-C, and Saturn I-B). The maximum refer-ence stagnation heat flux reaches about 13.6 W/cm^2 (12 Btu/ft^2-sec) (nose radius = 0.305m (1 ft)) for the Titan II booster. The maximum total stagnation heating reaches about 1.18KJ/cm^2 (1040 Btu/ft^2) (nose radius = 0.305m (1 ft)) for this Titan II ascent flight. Both the maximum heat flux and total heating associated with the ascent phase is appreciably lower than either abort or re-entry, as will be shown later.

The typical re-entry convective stagnation heating is shown on Figure 21 for the three basic trajectories of this study [(i.e., re-entry at 7468 m/sec (24,500 ft/sec) and re-entry along the overshoot boundary at 9144 m/sec and 10,363 m/sec (30,000 ft/sec and 34,000 ft/sec)]. The maximum re-entry heat flux and total heating occur for flights which have the highest re-entry velocity 10,363 m/sec (34,000ft/sec). The stagnation heat flux for re-entry at 7468 m/sec (24,500 ft/sec) is higher than that for re-entry at 9144 m/sec (30,000 ft/sec) due to the manner of defining the design trajectories (see section 4.1.1). The correspond-ing maximum turbulent heating is shown on Figure 22 for these same trajectories. A com-parison of these two maximum heating conditions shows that the highest values of heat flux occur at the stagnation point during the early phase of re-entry (the pullout phase). It is also evident that the maximum turbulent heating becomes greater than the stagnation values only at the latter phases of re-entry. The maximum turbulent heating normally occurs on the spherical nose away from the stagnation point near the sonic point. It is clear then that the occurrence of turbulent flow will affect the total heating on the vehicle, depending not only on transition but the variations of the local to maximum heating values or vehicle position.

The maximum value of hot gas radiation will occur at the stagnation point for the re-entry flights where the local temperature and density of the radiating gas are maximum. Representative values of the hot gas radiation for these referenced re-entry trajectories are shown on Figure 23 as a function of time. The maximum value of the referenced radiation heat flux is only about 1.135 w/cm^2 (1 Btu/ft^2 sec) for the highest re-entry condition. This represents less than one percent of the maximum convective heat flux, and it occurs over a very short time period during the early phases of flight. The total radiation heating is therefore negligible compared to the total for re-entry. The radiation for the ascent and abort flights are considerably less than for re-entry.

23

The abort heating will depend on the booster and condition of abort for each ascent trajectory. The typical abort stagnation heat flux is shown as a function time for operation at L/D max on Figure 24 and at L/D = 1 on Figure 25. Calculations have shown that the critical abort conditions for each booster will in most cases result in the maximum heat flux environment. Of importance is the maximum heat flux as well as the maximum total heating condition. It should be noted that the critical abort mission for maximum heat flux occurs at a different condition than that for maximum total heating.

It is evident that, compared to the convective heating during re-entry and abort, the heating during ascent is negligible. The radiative component of the heating is also negligible even at re-entry. The local heat flux during abort and re-entry must be examined closely for the proper heat protection system design. Heat flux during abort may well preclude the use of re-radiative panels in certain areas of the vehicle. The maximum heat flux during the critical ascent abort may be higher than for re-entry depending on the booster and the re-entry condition considered. The total heating during re-entry, however, is by far the maximum.

The critical thermal environment during operation in orbit will be the range in shield temperatures experienced during flight. This depends not only on the orbit inclination but on the number of orbits and the vehicle surface conditions. The most critical orbit condition of cold soak is obtained when the vehicle is in polar orbit with one side continuously exposed to the sun. The maximum soak conditions expected for a typical vehicle application having up to 17 orbits will be 394°K ($+250^{\circ}$F) to 144°K (-200°F). A change in orbit inclinations of 45 degrees may relieve these maximum temperatures by approximately 27.7°K (50°F).

4.2.2.5   Reference Heat Flux Distribution

The heat flux distribution over the M2-F2 vehicle will vary with the position, angle of attack, and flow condition (laminar or turbulent). The local heating can be conveniently compared to the maximum heating as a function of angle of attack. The reference value will be the stagnation heating for laminar flow and the maximum turbulent heating for turbulent flow. The local heating compared to the reference value will depend primarily on the local pressure distribution and local flow conditions as developed for bodies at angle of attack by methods of analyses discussed previously in Section 4.2.2.2.

The local reference heat flux is shown as a function of position and angle of attack for laminar flow on Figure 26 for the windward ray. The local heating for angles of attack of 10, 30 and 40 degrees includes the effect of local increased heating due to the influence of the flow properties (referenced density, viscosity, and velocity),

24

and influence of streamline divergence (Reference 11). The range of angle of attack of interest is between 0 to 30 degrees; however, 40 degrees was also included for this windward ray because of interest in operation at C_L max condition. The prediction of local heat flux on the windward ray would be somewhat lower than shown if an accounting only were made for the local flow property changes, which are influenced primarily by the local pressure as shown for the 10, 30, and 40-degree angle of attack conditions.

The referenced heat flux for the leeward ray is shown on Figure 27 for the various values of angle of attack and as a function of local body station. The utilization of Equations 4 and 5 for the heat flux evaluation on the leeward surface depends on the magnitude of the standoff distance between the body surface and the boundary flow. A good definition of this boundary surface across the leeward surface was not available for this configuration. The heat flux evaluation shown on Figure 27 was then obtained by using corrections (Reference 27) for separated flow for both laminar (0.56) and turbulent (0.60) heating. The local heating values were established by methods described previously which primarily depend on the local pressure distribution.

Similar heat flux ratios are shown in Figure 28 for the side meridian. It is noted that the heat flux varies only a relatively small amount with angle of attack at the side meridian. The corresponding variation on the windward ray is quite large due primarily to the large pressure variation.

A typical variation of the local laminar heat flux distribution over the vehicle at a 30-degree angle of attack is shown on Figure 29. It is of interest to note the contours of constant heat flux along the vehicle side. A heat protection system based primarily on the magnitude of the heat flux will ideally be designed along such lines. Of course, for practical reasons, such application is not desirable due to large changes in position with angle of attack and yaw. Local values of heat flux ratios for the fin leading edge, flap, rudder, and canopy are shown on Figure 30 as a function of angle of attack. The heating on the rudder is shown for deflections of both zero and 25 degrees.

The local turbulent reference heat flux ratio for the windward, leeward, and side meridians are shown as a function of position and angle of attack on Figures 31, 32, and 33, respectively. The turbulent heat flux ratio for the canopy, flap, and rudder are shown on Figure 34.

4.2.2.6 Maximum Heat Flux and Total Heating

The maximum heat flux and total heating on the vehicle is of interest for the design of the vehicle heat protection system. The maximum heat flux is of particular interest

for the re-radiation type of system where the upper temperature limit is the limiting criterion and the total heating the primary requirement for the ablation type of system. The major concern for maximum heating may be limited to the re-entry and abort conditions. A comparison of the maximum heat flux and total heating for both re-entry and abort is shown on Figure 35. It is clear that the maximum heat flux is obtained during abort at L/D max condition. This is reduced somewhat when operating at L/D = 1, but it still will produce the highest heat flux for all cases, with the exception of normal re-entry at 10,363 m/sec (34,000 ft/sec). The total heating is highest for re-entry. For the abort flights, both the maximum heat flux and total heating is lower for the L/D = 1 condition. It is evident that the heating during ascent and, of course, over the top phase is small compared to both re-entry and abort.

The maximum heat flux for the re-entry phase is shown on Figure 36 as a function of $W/C_L A$. The highest re-entry velocity, of course, produces the highest maximum heat flux. The maximum heat flux for the other re-entry velocities are quite similar, but the lower re-entry velocity produces the slightly higher maximum values for a given value of $W/C_L A$ (see section 4.2.2.4). The maximum heat flux during the re-entry occurs during pullout for all re-entry conditions.

The total heating during re-entry is shown on Figure 37 as a function of $W/C_L A$. The total heating increases with re-entry velocity and $W/C_L A$. It should be noted that both of the super-circular re-entry flights were performed in a similar manner (see section 4.1.1.3) operating at essentially a constant angle of attack. The sub-circular re-entry flight path was flown in a variety of ways (see section 4.1.1.3.2), but after pullout the flight had varying angle of attack. This total heating is shown for three types of flights; namely, at L/D max, C_L max at $\varphi = 0$, and C_L max at $\varphi = 60$. The largest value of total heating is for the L/D max flight. Flying at C_L max condition will reduce the total heating by about 25 percent. The comparison between the banked and unbanked flights shows that reduction in heating of about an additional 5 percent occurs for the banked flight. The maximum heating for this re-entry velocity was used for the heat protection requirements. The maximum heat flux for all the sub-circular re-entry flights noted previously are identical, since the initial pullout phase produced the maximum heating and was identical for each case.

26

4.3 THERMAL PROTECTION EVALUATION

The heat protection system application for the wide variety of vehicle sizes (weights and lengths) and flight paths will depend on the system used, the materials, and the thermal and structural performance.

4.3.1 MATERIALS

4.3.1.1 Ablation Materials

The ablation materials considered in this study included both an elastomeric shield material (ESM) and microballoon phenolic nylon (MPN).

4.3.1.1.1 Formulation and Fabrication of ESM

a. Composition

The ESM 1000 Series (References 28 and 29) are char-forming materials consisting of chemically blown, phenyl-methyl-silicone elastomeric foams. The ESM 1004 materials used in this analysis contain from 6 to 20 percent of fibrous aluminum silicate, and are available in densities from 0.32 to 0.96 g/cm^3 (20 to 60 lb/ft^3) depending on the concentration of blowing agent and curing conditions used in the particular composition. A typical formulation, ESM 1004A P, uses the base elastomer RTV-560, contains 12 percent aluminum silicate fibers, and has a density of 0.56 g/cm^3 (35 lb/ft^3).

A materials specification document (Reference 30) established the process and material requirements, formulations, and the quality assurance provisions for free-foam elastomeric ablators used for thermal protection as sheet stock or molded parts. Specific formulation and processing information is GE-RSD "Company Proprietary." Sufficient general information is provided to describe the process. All raw materials are covered by the following GE-RSD materials acceptance specifications:

156A9874	RTV-560
128A5481	Silicone Fluids
146A9268	Catalyst for Silicone Rubber Compounds
147A1256	Curing Agent, Stannous Octoate
156A4410	Fibrous Aluminum Silicate
128A5500	Cabosil M-5.

The identification of the component elastomer materials as commercial products follows:

RTV-560

A liquid synthetic rubber made by adding suitable compounding ingredients to a silicone polymer that cures at room temperature after the addition of a catalyst.

Nuocure 28

Stannous octoate with a stannous tin concentration of 28 percent.

SF-96

Dimethyl polysiloxane silicone fluids are clear, water white, oily liquids. They are non-toxic, inert, tasteless, and essentially odorless.

RTV-921

A proprietary blowing agent for foaming room-temperature vulcanizing silicone rubber compounds.

b. Fabrication

1) General

The polymerization and cure of the siloxane polymers are condensation processes producing water and/or alcohol as the volatile species. The silicone blowing agents are materials containing silicon-hydrogen bonds which break to liberate hydrogen under the influence of the same catalysts used to promote polymerization. The by-product from this reaction forms a reactive species capable of reacting with itself to form a resin, or enters into the overall polymeric network by reacting with the polymer.

There are three basic methods of fabricating ESM: sheet, molded, and spray. Sheet material is formed by foaming large "buns" of ESM in an open pan mold which are slit to desired sheet thickness. Molded parts are cast to the final desired shape without pressure in low-cost molds. This technique is often used in the fabrication of relatively thick sections and/or for application over surfaces of small radii such as leading edges and stagnation areas. The spray technique is used as an alternate to sheet fabrication and is particularly applicable where small thicknesses of ablation material are required; e.g., 2.54 mm (100 mils).

2) Base Formulation

For each fabrication procedure, the base formulation is made in the same manner; it consists of the base elastomer, SF-96 silicone fluid, and the aluminum silicate fibers. The aluminum silicate fibers are passed once through a rotary cutter equipped with a perforated screen. The component materials are weighed and mixed for one hour. This material is then passed through a three-roll paint mill three times with controlled gap settings to incorporate and disperse the fibers into the base elastomer.

3) Sheet and Molded Fabrication

The next step in the process is identical for both sheet and molded ESM. A simple "cake pan" mold is constructed for the sheet material and for molded sections on an inexpensive, two-part, open mold of the final configuration. The mold surfaces are cleaned by solvent wiping but are not treated with mold release. The proper proportions of base formulation, blowing agent, and catalyst are weighed. The blowing agent and catalyst are added to the base formulation and mixed for five minutes in an open container with a high-speed propeller-type mixer. The material then foams and cures for several hours either at room temperature or $344^{\circ}k$ ($160^{\circ}F$) in an oven, depending upon the formulation, followed by an oven cure at $366^{\circ}k$ ($200^{\circ}F$) for several hours.

The material is removed from the mold, and the skin is sanded or machined from the top surface of the bun and the inner or bonding surface of the molded part. The material is then post-cured an additional ten hours in an oven at $422^{\circ}k$ ($300^{\circ}F$) to complete the cure and remove any unreacted, residual volatiles from the material. This final post-cure dimensionally stabilizes the material.

After final trimming, the molded part is ready for application to the vehicle. For sheet stock, one surface of the bun is machined flat. The bun may then be slit into sheets of desired thickness with a commercial foam rubber slicer. The sheet thickness tolerance can be maintained at $\pm$.076 mm ($\pm$3 mils).

4) Spray Application

The same basic ESM formulation is used in the spray application as is used in the fabrication of sheet stock. Freon is used as a diluent to adjust viscosity. During the spray application, the low-boiling-point Freon flashes away, preventing solvent entrapment in the applied material. The blowing agent is mixed with the base formulation. The catalyst, also diluted with Freon, is introduced in the fan of the spray at the nozzle, thus providing a continuous process.

The spray equipment consists of a spray gun with a special catalyst nozzle. The flow of all components is controlled at the trigger. Component pressures are controlled by five controlled outlets. The system is pressurized with either filtered compressed air or cylinder nitrogen.

The spray would nominally be applied to a cleaned primed surface, either to the section of the vehicle structure or to the surface of the selected refurbishment technique. In this application, the material foams and cures in place, thus eliminating a separate bonding operation. "Sagging" is prevented by the use of controlled concentrations of thixotropic agents in the base elastomer. The final material thickness depends on the amount of applied material. This technique is currently capable of providing thicknesses from 0.25 to 5.0 mm (10 to 200 mils).

5) Manufacturing Experience

ESM sheet stock and molded parts are fabricated as standard production items, but are proprietary to GE-RSD. Their manufacture and bonding are controlled by material, processing, and quality control specifications including complete in-process inspection. In addition to fabrication and application to the leading edge, ventral fin, and speed brakes for flight test on the X-15, an ESM thermal shield has been fabricated in sheet and molded sections for a re-entry satellite vehicle for a full-scale flight test.

The spray application of ESM was demonstrated in the field by coating the ventral fin and lower speed brakes on the X-15-1 on September 3, 1965. Solid propellant rocket cases have also been coated with spray ESM both in-house and in the field.

A brief summary of this material follows:

(1) ESM is a foamed phenyl-methyl-silicone elastomer containing controlled concentrations of fibrous aluminum silicate.

(2) The fabrication of sheet and molded ESM is a standard production process proprietary to GE-RSD.

(3) The application of spray ESM has been demonstrated but is not yet a standard production item.

(4) The fabrication of ESM is reliable and relatively inexpensive, since it does not require expensive tooling and equipment.

4.3.1.1.2   Formulation and Fabrication of MPN

a.   Composition

MPN is a generic composition of phenolic resin, phenolic microballoons, and ground nylon. Many modifications have been formulated of this basic composition (References

30

31 to 37), all of which have been termed MPN. The basic formulation of MPN is as follows:

Phenolic Resin (BRP 5549)	25.0%
Nylon (Zytel)	50.0%
Phenolic Microballoons	25.0%
Density	0.576 g/cm^3 (36 lb/ft^3)

The BRP-5549 phenolic is a two-stage dry resin. It is commercially available and does not have a limited shelf life at room temperature. GE specification No. 128A5511 defines the quality control tests required on this material for receiving acceptance.

The phenolic microballoons are also commercially available. This material absorbs atmospheric moisture and must be stored in sealed, dry containers. The material has a low auto-ignition temperature and cannot be dried in air at even slightly elevated temperatures. In addition, the size of the microballoon spheres varies considerably from lot to lot and between lots.* Mesh screening may be used to assure uniformity.

Zytel nylon resin molding powders are commercially available as solid granular material, cube-cut or chopped. Fine mesh sizes are available from specialty grinding suppliers. Zytel is characterized as rigid, highest melting nylon with high fluidity at molding temperatures, good machinability, and high impact strength with maximum stiffness. Zytel resins have relatively sharp melting points, 519 – 530°K (475-495°F), below which they remain rigid and above which they have a fluidity like that of lubricating oil. Zytel resins are insoluble in common solvents, alkalies, dilute mineral acids, and most organic acids. All Zytel compositions may be dissolved in phenols and in formic acid. Since all nylons are hygroscopic and will absorb moisture from the atmosphere, the resins should be stored in dry, sealed containers. The nylon does not melt at molding temperatures for MPN. The nylon partially dissolves in the liquid phenolic resin during cure of the system. The rate of solution is dependent on the particle size of effective surface area of the nylon, and on the time and temperature during which it is in contact with the phenolic resin in the liquid state.

b.   Fabrication

Phenolic resins cure by a condensation reaction with water as the by-product. Phenolics must be cured either under very high pressures, 4.79 – 14.37 N/cm^2 (1000 – 3000 psi), to maintain the water in the molded part or at lower pressures under vacuum to remove the water of condensation as it is formed. The low pressure-vacuum technique

* Phenolic microballoons have a specific gravity of 0.25 to 0.30.

must be used for MPN, since high pressures would crush the microballoons and produce a high–density part.

Relatively small test samples of MPN have been produced to date and these have been hot-press molded. NASA-LRC has fabricated small nose cap sections in a press using matched metal molds with a vacuum tap. The materials were carefully dried and blended to reduce the volatile content during cure. Even with careful selection and screening of the raw materials, the molded parts have varied in density within the part and from part to part. The use of matched metal molds is almost mandatory, since the blended material is in the form of a dry powder. Thus, matched metal molds would have to be fabricated for each surface contour for the M2-F2 vehicle. Molding pressures of less than 7180 N/M^2 (150 psi) must be used to prevent crushing of the phenolic microballoons. Tooling costs would be extremely high in the production of large shield sections in a press, since the matched metal molds would also have to be cored to maintain temperature control for steam under pressure.

A vacuum–bag autoclave molding technique provides adequate pressure and could be used with matched metal molds in the production of full–scale parts. Shield sections have not been manufactured with this technique, however, and a scale–up development program would be required to define the process parameters.

The raw materials should be blended by the fabricator in the molding of MPN to maintain quality acceptance control over the components. After the process has been defined, the sections would be fabricated in matched metal molds in a vacuum–bag autoclave. The part should be post-cured in one or both of the mold sections to prevent distortion.

A summary of this material follows:

(1) MPN is composed of: 25 percent dry phenolic resin with minimum B-stage development, 25 percent phenolic microballoons, and 50 percent ground, powered nylon resin.

(2) The raw materials must be stored and blended under very carefully controlled conditions.

(3) The process for the production of large–scale, quality parts has been neither defined nor demonstrated.

(4) The process would be very expensive requiring matched metal molds for each configurational part and vacuum, pressure, and temperature control during cure.

4.3.1.2   Re-Radiation

In considering materials for a re-radiative thermal protection system, two candidates were selected as representatives of different classes of materials, namely: (1) the

high-temperature super-alloys which have found widespread applications in the jet engine field, and (2) the more exotic refractory metal alloys. Rene'41 was selected as the super-alloy, while TZM molybdenum alloy with a silicide coating was the refactory metal alloy selected.

Rene'41 has a life expectancy of at least 100 hours in air at 1255^OK (1800^OF) and a tensile yield strength of 30,000 psi. A comparison of significant properties of Rene'41 at 1255^OK (1800^OF) and TZM at 1810^OK (2800^OF) is shown in Table 1. Emittance values given are for both: (1) a pre-oxidized matte finish, and (2) a typical application for Rene'41 and TZM with protective coating. The TZM material would be more suscep-tible to mechanical damage due to sand abrasion and pebble impact.

4.3.1.3 Insulating Materials

A re-radiative thermal protection system would require use of high-efficiency, high-temperature thermal insulators to minimize heat inputs to the structure. Properties of two of the most efficient insulators are listed below. Microquartz is a high purity silica fiber available in a 0.048 to 0.096 $g/_{cm}3$ (3 to 6 lb/ft^3) density range and a temperature capability of 1366^OK (2000^OF). Dyna quartz (temperature stabilized micro-quartz) has been utilized to extend the operating range to over 1810^UK (2800^OF). The foamed pyrolytic graphite is a very-high-purity graphite produced by pyrolytic decom-position of methane or other hydrocarbon gases and further processed to obtain a high-efficiency insulator with temperature capability in excess of 3030^OK (5000^OF) and densities ranging from 0.032 to 2.09 $g/_{cm}^3$ (2 to 130 lb/ft^3).

Either microquartz or foamed pyrolytic graphite (PG) could be used with Rene'41, while the foamed PG is very effective as an insulator at higher temperatures. The limitations on pyrolytic graphite lies in its tendency to oxidize in air at temperatures above 1090^OK (1500^OF). However, oxidation rates are not significant below 1925^OK (3000^OF), and the surface protection provided by the TZM panels at high altitudes would result in a useful life comparable to that of the TZM panel.

4.3.1.4 Refurbishment Attachment Systems

Several factors must be considered in the evaluation of the selected refurbishment, thermal protection, attachment systems. These include reliability, applicability, ease of fabrication, application, and refurbishment cost and weight.

4.3.1.4.1 Refurbishment Attachment System Weights

A summary of the estimated weights of each attachment system for MPN (microballoon phenolic nylon) and for both sheet and spray ESM (elastomeric shield material) is

presented in Table 2. These weights include the weight of the refurbishment technique and the weight of adhesive required to attach the refurbishment technique to the shield and structure. A discussion of the basis for the calculations for each refurbishment technique follows:

a. Elastomeric Bond

The weight of the elastomeric bond was based on the density of RTV-560 (1.44 g/cm^3) (90 lb/ft^3) and a nominal thickness of 0.254 mm (10 mils). The thickness of this bond is 0.254 mm $\pm$ .127 mm (10 mils $\pm$ 5 mils). The weight of the required primer was considered insignificant and was not included in this estimate.

Although there is an effective bondline thickness in each refurbishment system in the application of spray ESM of 0.127 to 0.254 mm (5 to 10 mils), its weight is calculated as part of the shield density. Spray ESM should only be considered in areas where the shield thickness requirement falls between 0.127 and 6.35 mm (5 and 250 mils). Sheet ESM can be fabricated only in thicknesses down to 1.52 mm (60 mils).

b. Perforated Scrim

A 5.08 by 7.62 cm (2 by 3 inch) sample of the teflon-glass scrim weighed 0.4850 grams. This weight is equivalent to 1.22 g/cm^2 (0.025 lb/ft^2). This scrim cloth has a thickness of 0.102 mm (4 mils). No allowance was made for the slight reduction in weight accompanying the loss of scrim material in the perforations. The weight of 0.254 mm (10 mils) of the elastomeric bond on the shield is added to the scrim weight for the total weight of this attachment system.

c. Nut and Bolt

Based on the weight of a 3.18 mm (1/8 inch)-diameter, 1.27 cm (1/2 inch)-long steel bolt, nut, and washer, the weight of a similar phenolic-glass bolt assembly was calculated to be 1 gram. Assuming that five bolts of this size would be required for each square foot, the estimated weight for this system is 0.536 g/cm^2 (0.011 lb/ft^2). This estimate can vary considerably depending upon the size and spacing of these bolt systems. The reduction or addition of structural weight due to the holes in the structure was not included in the estimate. Additional weight, which was not included in this estimate, may also be required in the shield for the 589°K (600°F) backface condition to provide a thickness of virgin shield material as the load bearing surface for the washer.

d. Elastomeric Pillars

The weight of this system can also vary considerably depending upon the diameter, height and spacing of these pillars. For this calculation it was assumed that the pillars were 3.18 mm (1/8 inch) in diameter, 3.18 mm (1/8 inch) high, and were spaced in rows 6.36 mm (1/4 inch) apart. Using the RTV-560 density of 1.44 g/cm^3 (90 lb/ft^3), the solid pillars would weigh 3.98 g/cm^2 (0.0815 lb/ft^2). For use with MPN, the pillars would have to be fabricated with a 0.254 mm (10 mil) RTV-560 backing which would then have to be bonded to the MPN with an additional 0.254 mm (10 mils) of RTV-560. For attachment to the ESM, the pillars can be fabricated and attached to the ESM surface in one step, thus eliminating one of the two 0.254 (10 mil) layers of RTV-560. If foamed pillars have sufficient strength to carry the shield load, an additional weight reduction is possible.

The possible reduction in shield weight, especially in the case of the 300°F backface requirement, due to the insulating function of this system, was not included in this calculation. Additional consideration must also be made for this system used with MPN in its potential as a compressible bond to provide shield integrity over the orbital cycle, temperature extremes.

e. High-Temperature Loop and Pile

This all-metal, high-temperature material has a weight of 21 g/cm^2 (0.43 lb/ft^2) for both the loop and for the pile as reported by the manufacturer (Velcro Corporation). This weight is doubled to include both the loop and pile and is added to two thicknesses of 0.254 mm (10 mils) of RTV-560 used to bond the system to the shield and to the structure. In an alternate approach, one-half of the system may be spot-welded to the stainless steel structure, rather than adhesively bonded. Although the comparative weight of this system is high, it still has significant potential in ease of refurbishment.

f. Mid-Temperature Loop and Pile

The same considerations apply in the use of this technique as in the previous section, except for the spot-welding feature. The weight for this system is one-half the weight of the all-metal closure for both the loop and for the pile.

g. Mystic Tape No. 7000

Mystic tape has a reported density of 3.07 g/cm^2 (0.063 lb/ft^2) and is added to the weight of 0.254 mm (10 mils) of RTV-560 required to bond the back of the tape to sheet ESM. The attachment to the structure is made with the pressure-sensitive adhesive on the tape surface.

4.3.2   HEAT PROTECTION SYSTEM ANALYSIS

4.3.2.1   Performance

4.3.2.1.1   Ablation System

a.   Analysis

There is a wide variety of ablation materials available for re-entry vehicle applications such as the M2-F2. The materials may be used as a single material or as a composite as required for the application. The performance of ablation materials generally depends on the type of material and on the manner in which it performs. Some of the typical materials may be classified into 1) materials that melt and vaporize, such as quartz, 2) plastics that depolymerize to a gas, such as teflon, 3) materials that pyrolyze and form a carbonaceous char layer, such as ESM or MPN, and 4) materials that ablate by oxidation and sublimation, such as graphite. Of course, the plastic materials that form a char can also act in a manner similar to the graphite of the char surface but are complicated by the other processes occurring in depth.

The ablation of the char-forming material generally is considered to be the most difficult to evaluate because of the complexity of the processes going on in depth through the material. When the material is exposed to a typical re-entry thermal environment of a ballistic-type vehicle, the performance, and thus the material selection, will naturally depend on the actual application. A material ideal for a very high, short-time heat pulse generally will not be ideal for a glide-type re-entry having a low-heat-flux, long-time environment. However, the mathematical model used to describe the performance of the materials usually can be described in a similar manner. The external environment when imposed on the material will cause the process of ablation, char formation, and char removal.

The external thermal environment, in general, consists of a heat flux input caused by convection, hot gas radiation, and combustion. This environment will cause the surface temperature of the material to increase because of the heat conduction process through the material. This increase in surface temperature will increase the radiation away from the material, and it will decrease the convective heating, both tending to reduce the net heat input to the material. When this surface material reaches a given temperature, it undergoes chemical reactions that produce thermal degradation. The charring ablators undergo these pyrolysis reactions and produces gaseous products and a residual carbonaceous matrix, or char. The reinforcement of the material, when used, is generally trapped in the char and undergoes melting and vaporization or depolymerization. The char not only includes these but additional materials that result from chemical reactions between the char and the reinforcement material. The gases produced in the process are forced through the

36

porous char into the boundary layer. This will introduce thermal energy by friction and by chemical changes in the gas, because of cracking or recombination, and by heat transfer between the gas and char. This gas flow through the material into the boundary layer will block a portion of the convective heat flux. As additional heat enters the body, the reacting layer of material progresses deeper into the body. The outer surface erodes because of oxidation and/or vaporization, depending on the local temperature and pressure and also, in some cases, because of mechanical failure of the char.

The preceding description of the process can be formulated approximately by examining the external and internal heat fluxes. An attempt to describe this process is done with a reaction kinetics ablation program. It is easily possible to make the formulation much more sophisticated than is necessary and thus make the prediction of performance too unwieldy. Therefore, it is necessary to employ a procedure of reasonable complexity that will accurately predict the actual performance for a wide variety of environments. The prediction will be based on establishing the net heat flux and then evaluating the material performance.

1) Method of Analysis of Charring Ablators

The semi-empirical analytical model described below was used for the prediction of the response of the charring ablators investigated in this study. The digital computer model described (defined as REKAP-Reaction Kinetics Ablation Program) includes the three significant regions of interest in the interaction and coupling between the material degradation and the hypersonic environment: 1) the gas-phase boundary layer, 2) the condensed phase, and 3) the interactions between phases.

The system of conservation equations used for this mathematical model are described briefly. The equations describing the condensed-phase region are considered first; the gas phase and interaction phase may then be considered as boundary conditions for the solution of the complete charring ablation problem.

For any point in the condensed-phase region:

$$\nabla \cdot h \nabla T = \rho C_P \frac{\partial T}{\partial t} + \Delta H (\rho - \rho_c) A e^{-\Delta E/RT}$$

$$+ C_{P_g} \left[(1 - \beta)^{3/2} \rho_g \frac{\partial T}{\partial t} + \dot{m} (\nabla T) \right] + \dot{m} \left\{ \frac{\partial H_K}{\partial T} \nabla T + \frac{\partial H_K}{\partial P} \nabla P \right\}$$

$$+ \rho_g (1 - \beta)^{3/2} \left\{ \frac{\partial H_K}{\partial T} \frac{\partial T}{\partial t} + \frac{\partial H_K}{\partial P} \frac{\partial P}{\partial t} \right\} \tag{17}$$

Where the term $\nabla \cdot k \nabla T$ represents the heat conducted into any element in the condensed phase.

$$\rho C_P \frac{\partial T}{\partial t}$$ represents the heat stored in the condensed phase.

$$\Delta H (\rho - \rho_c) Ae^{-\Delta E/RT}$$ represents the heat absorbed in reaction.

$$C_{Pg} \left[(1 - \beta)^{3/2} \rho_g \frac{\partial T}{\partial t} + \dot{m} (\nabla T) \right]$$ represents thermal energy stored in the evolved gases.

The last two major terms in Equation (17) represent the energy absorbed in evolved gas "cracking".

The evolved gas passing through any location x within the condensed phase in a given time period is assumed to be generated by all elements interior to this location during the same time period, i.e.

$$\dot{m}_x = \int_x^{x_{BACKFACE}} (\rho - \rho_c) Ae^{-\Delta E/RT} \, dx \qquad (18)$$

Within the condensed phase, the thermal conductivity and specific heat properties are included as a function of temperature. Evolved gas-product enthalpy, specific heat, and gas-product molecular weight are included as a function of both temperature and pressure. At the backface,

$$\left[\frac{\partial T}{\partial x} \right]_{BACKFACE} = 0 \qquad (19)$$

At the interface between the boundary layer gas phase and the condensed-phase region:

$$\nabla \cdot k \nabla T = \dot{q}_c + \dot{q}_{GAS\ RADIATION} + \dot{q}_{COMBUSTION} - \dot{q}_{SURFACE\ RADIATION}$$

$$- \dot{q}_{MASS\ TRANSFER} \qquad (20)$$

where the convective, gas radiation, and combustion heat sources are obtained from independent analyses, although coupling exists between the mass and species of the evolved gas products and the gas-phase boundary layer.

38

$$\dot{q}_{\text{SURFACE RADIATION}} = \sigma \epsilon T^4 \tag{21}$$

For the mass transfer effects

$$\left(\dot{q}/\dot{q}_{\dot{m}=0}\right)_{\text{LAMINAR}} = \left[0.69 \left(\frac{\overline{M}_{BL}}{\overline{M}_g}\right)^{1/3} \frac{\Phi_o}{P_r^{1/3}}\right] \tag{22}$$

$$\left(\dot{q}/\dot{q}_{\dot{m}=0}\right)_{\text{TURBULENT}} = \left[1 - e^{0.38 \, (\overline{C}_{P_g}/\overline{C}_{PBL}) \, \Phi_o}\right] \tag{23}$$

$$\Phi_o = \dot{m}_w \frac{\Delta h}{\dot{q}_c} \tag{24}$$

The semi-empirical relations presented above are the result of extensive correlations of mass transfer effects on the reduction of laminar and turbulent heat transfer as a function of injected species, injectant rate, and local edge of boundary layer Mach number.

Combustion of the evolved-gas species heterogeneously with the char layer and the boundary layer is treated empirically by expressing the combustion energy source term as a function of species and pressure.

The aerodynamic heating rates are determined by well-established methods for the particular velocity regime of interest. The local heat flux for laminar flow (stagnation point and other locations) and turbulent flow are obtained by Equations (1), (2), and (3) given in Section 4.2.2.2.

The gas-condensed-phase boundary movement is controlled either by chemical erosion resulting from evolved gas-char reactions or char-boundary layer reactions, i.e., oxidation reaction or sublimation of the carbon residue, or by mechanical forces resulting from aerodynamic shear, from evolved-gas-product internal pressure force, by thermal structural forces, or by combinations of all three mechanical forces. For silica-reinforced charring ablators, the surface boundary is normally controlled by liquid layer flow and vaporization under the viscous shear forces at the gas-liquid layer boundary.

For refractory-reinforced phenolics which form a dense char, the gas-condensed-phase boundary movement is assumed to be controlled by boundary layer diffusion oxidation and sublimation. The oxidation and sublimation of carbon in air has been

analyzed in detail and confirmed experimentally over the complete temperature and pressure range for laminar flow. The results were correlated, and the resulting equations are:

For laminar and turbulent flow

$$\dot{m} = \dot{m}_D \left[1 + 2.64 \times 10^9 \ P_e^{-0.67} \ e^{-11.05 \times 10^{-4}/Tw} \right] \tag{25}$$

Where $\dot{m}_D$ is the mass loss within the diffusion-controlled regime

$$\dot{m}_D = \frac{\dot{q}_c}{Q^*} = \frac{\dot{q}_c}{K_1 + K_2 \ (h_r - C_{P_{BL}} \ Tw)} \tag{26}$$

The quantities K_1 and K_2 are input constants. For turbulent flow, their values are 4240 and 5.77, respectively; for laminar flow 5370 and 5.37, respectively. The rate of front face recession is given by:

$$\dot{S} = \frac{\dot{m}_T}{\rho_{SURFACE}} \tag{27}$$

The heat balance at the front face is given by:

$$-K \nabla T = \dot{q}_c' + \dot{q}_{GAS} - \dot{q}_{SURFACE} - \dot{q}_{MASS} \tag{28}$$
$$\phantom{-K \nabla T = \dot{q}_c' +} \text{RADIATION} \quad \text{RADIATION} \quad \text{TRANSFER}$$

where:

$$\dot{q}_c' = \dot{q}_c \left[1 - S^* \ (396 \times 10^8) \ P_e^{-0.67} \ e^{-11.05 \times 10^4/Tw} \right] \tag{29}$$

The local boundary layer edge pressure, P_e, is an input quantity which is a function of time; S^* is a function of the recovery enthalpy.

For phenolic nylon, the surface boundary movement is controlled by a combination of chemical erosion and mechanical shear according to the equations and limits, as follows:

For surface shear stress values less than 718 N/m^2 (15 lb/ft^2) the char is assumed to be removed according to the oxidation and sublimation relations assumed for refractory-reinforced phenolic. Above surface shear levels of 718 N/m^2 (15 lb/ft^2),

aerodynamic shear appears to dominate, and the char layer thickness to the 589°K (600°F) isotherm is given as

$$t_{CHAR} = \frac{0.15}{4 + \tau}$$ (30)

The addition of microballoons (to phenolic nylon) makes the char somewhat more frangible and therefore more susceptible to mechanical shear removal. But the shear levels encountered for the M2-F2 environment — much less than 238 N/m^2 (5 lb/ft^2) — are so small that this type of erosion should not effect shield performance (see Section 4.5).

For the silicone elastomer, ESM, the front face surface recession has been correlated as

$$\dot{S} = f\ (P_e,\ \dot{q}_{AERO},\ \rho)$$ (31)

The heat balance at the front face is then

$$\nabla \cdot KT = \dot{q}_c + \dot{q}_{RADIATION} + \dot{q}_{COMB.} - \dot{q}_{SURFACE}$$
$$_{RADIATION}$$

$$- \dot{q}_{MASS} - (\rho_c L)\ \dot{s}$$ (32)
$$_{TRANSFER}$$

In general, the analytical model used for this study provides reasonable agreement with ground test data. Since all results are normalized to a reference thermo-physical value, greater sophistication in the analytical model used over that described was not required.

The REKAP program, with its developed and proven capabilities, has been used by GE-RSD in the design of re-entry vehicles for a number of successful ballistic and satellite flight test programs. Using REKAP, RSD has obtained excellent correlations of experimental and theoretical data on temperature responses and internal degradation on ESM subjected to typical thermal environments encountered on the upper surface and stagnation region or lower surface of the X-15 lifting vehicle.

b. Ablation System Performance

The performance of the two reference ablation materials (ESM and MPN)* was studied by REKAP analysis for a number of typical thermal environments for each of the three applicable re-entry velocities.

The REKAP analysis provides the temperature and material density as a function of depth through the material based on the heat flux input specified at the surface as a function of time, as described previously in Section 4.3.2.1.1.1. The performance will then depend not only on the material but on the heat flux that varies over the body and with re-entry condition. Typical performance calculations are shown on Figures 41 to 44 for a re-entry velocity of 9,144 m/sec (30,000 ft/sec). Figure 41 shows the location in depth through 0.576 g/cm^3 (36 lb/ft^3) MPN material for temperatures of 422°K (300°F) and 589°K (600°F) as a function of time for several typical heat flux locations from the stagnation point to points with less than ten percent of stagnation values. The degradation and ablation are shown on Figure 42 as a function of time for these same heat flux conditions. The degradation shown represents the distance from the front face to a point where the density is 95 percent of the virgin material density. The amount of ablation shown represents the amount of erosion calculated for these same conditions. It is noted that there is no erosion calculated for the low heating condition.

Similar performance calculations for 0.465 g/cm^3 (29 lb/ft^3) ESM are shown in Figure 43 for the location in depth of the specified temperatures and in Figure 44 for the amount of degradation and erosion as a function of time. For this material there is no erosion for the lower two heating conditions shown. The performance of ESM is such that for heat fluxes of about 34.1 w/cm^2 (30 Btu/ft^2 sec) and lower, there is essentially no erosion.

It is of interest to establish the influence on material performance of extended soak-out times additional to the flight path requirements.** Therefore the effect of prolonged soak-out time was studied for the two backface temperature conditions 422°K (300°F) and 589°K (600°F) and for the two ablation materials (MPN, ESM) which were of prime interest in the M2-F2 Program. Emphasis was placed on low heating conditions because of their applicability to the major portion of the vehicle. The M2-F2

---

*The performance of the ESM and MPN was based on the material properties presented on Figures 38 to 40 (also see Reference 38) and Section 7.1.

**A brief study was made to determine the possible effect on the nominal trajectory by including a typical landing maneuver during the latter phase of flight. It was determined that, in general, the execution of landing would result in a flight time about the same as the total time established for the nominal trajectories with negligible change in the total heating.

shield requirements are based on the maximum allowable backface temperatures cited previously for trajectories of about 2400 seconds. A study was made, for reference purposes, on the effect of an additional 1000-second soak on these requirements. This study indicates that it is a function of both the location on the vehicle and the allowable backface temperature. In the high heat flux regions, the backface temperatures will rise somewhat beyond the allowable temperatures, at the end of flight, for both ablation and backface materials.

In the low heat regions, the backface temperature peaks at approximately 3200 seconds for the aluminum system. The backface temperature for ESM, shown on Figure 45 as a function of time for total heating of about 5.56 KJ/cm^2 (4900 Btu/ft^2) is typical for the low backface temperature condition (aluminum structure). The temperatures at the extended time are between 22.2 to 77.8°K (40 to 140°F) higher for material sized without consideration of soak. Approximately 5.68 to 11.35 J/cm^2 (5 - 10 Btu/ft^2) would have to be removed to maintain the low backface temperature condition. With a steel structure, the backface temperature peaks at about 2200 seconds for the ESM material, as shown on Figure 46. The maximum temperature occurs before the extended soak-out begins and therefore the extended soak-out has no influence on the backface temperature for this condition. Therefore, in the low heat regions, the present steel system is sufficient for extended soak times, but the aluminum system will show somewhat higher backface temperatures unless there is a small amount of cooling.

c. Heat Shield Requirements

The ablation material performance calculations have been performed, for the various re-entry velocities for a variety of local heating conditions. The application of this individual material performance to local conditions, which differ from the calculated points, may be accomplished successfully by using the total heating as the correlation parameter (Reference 39). The total material degradation, erosion, maximum surface temperature, and insulation requirements can be correlated with total heating based on a given re-entry velocity for a wide variation of local heating values that represent various locations over the entire re-entry vehicle. The material functional relations may be written as:

Total thickness	$t_t = t_D \times (SF) + t_{ins}$	(33)
Total degradation	$t_D = t_D (Q_c, \text{Mtl, traj})$	(34)
Total insulation	$t_{ins} = t_{ins} (T_{BF}, \text{mtl, traj})$	(35)
Surface erosion	$t_e = t_e (Q_c, \text{mtl, traj})$	(36)
Surface temperature	$T_W = T_W (Q_c, \text{mtl, traj})$	(37)

The maximum surface temperature for both MPN and ESM is shown on Figure 47 as a function of total convective heating. The maximum temperature shown was insensitive to the re-entry trajectories studied but, rather, was a function primarily of the total heating. The ESM produces surface temperatures of about 111 to 277°K (200 to 500°F) higher than MPN, depending on the magnitude of the total heating.

The degradation calculated for ESM material is shown on Figure 48 as a function of total heating. It is noted that the degradation is essentially identical for the lower two re-entry trajectories for a given value of total heating. It should be noted, however, that any individual local position on the vehicle will have a different degraded thickness for each trajectory, since the total heating differs (for that point) for each trajectory, as discussed previously. There is considerably higher degradation produced for the highest re-entry velocity trajectory. The high heat flux exhibited by this flight produces relatively greater degradation for ESM than that exhibited for the lower re-entry velocities. The degradation shown is based on the material thickness at which the local density is 95 percent of the virgin material. The corresponding degradation for MPN is shown on Figure 49. The degradation for MPN is very similar for the three re-entry trajectories for a given value of total heating; a different trend than that exhibited for ESM. It should be noted, however, that the degradation required for ESM at the two lower entry velocities is considerably less than for MPN.

The insulation requirements for ESM is shown on Figure 50 as a function of total heating for backface temperatures of 422 and 589°K (300 and 600°F) for each re-entry velocity. The corresponding insulation thickness for MPN is shown on Figure 51 as a function of total heating. It is clear that the insulation requirement for each material is considerably reduced for the larger backface temperature. It is also noted that the insulation requirement even vanishes for both materials at the lower values of total heating which occur over the major portion of the vehicle surface area, such as on the leeward surface and on the aft regions of the windward surface.

The surface erosion for both ESM and MPN is shown on Figure 52 as a function of total heating. The erosion of MPN for all the re-entry velocities may be represented by a single line, while the ESM erosion shows two distinct values similar to that exhibited by the degradation. The surface erosion for ESM is substantially lower than that for MPN except at the very highest total heating values for the high re-entry condition. The low surface erosion characteristic is of importance in order to maintain the desirable performance characteristic during flight. Both ESM and MPN have the characteristic that a higher density material may be added as an outer layer in order to reduce this erosion, if desired.

The ESM material used for these performance calculations has a density of 0.465 g/cm^3 (29 lb/ft^3). An outer layer having a density of about 1.04 g/cm^3 (65 lb/ft^3) can be used to reduce the erosion loss. This outer layer can be made of the same basic

material which permits essentially one material having graded properties without a bond reliability problem. Such a composite may reduce the erosion by an amount that is almost proportional to the density; however, the weight loss will be about the same. The MPN can also be made in a similar manner, with PN as the outer layer. PN has a density of 1.2 g/cm^3 (75 lb/ft^3) compared to the basic density of MPN of 0.576 g/cm^3 (36 lb/ft^3). Combining the PN with MPN, however, is a more difficult process than making an ESM Composite.

4.3.2.1.2 Re-radiation System

One of the heat protection systems studied was re-radiation. The system requirements for this approach are very closely associated with the materials used and the specific application. The prime area of application is in low heat flux areas, since the applicable system is temperature-limited by the materials employed for the system.

a. Analysis

The re-radiation systems evaluated were based on the following:

- Re-radiation materials - René 41, TZM with coating

- Insulation materials - micro quartz (MQ)
                                   foamed pyrolytic graphite (FPG)

- Cooling - passive
                     active

The re-radiation system was designed to provide the same degree of protection as the ablation system; that is, a maximum of 422°K (300°F) backface temperature with an aluminum structure and 589°K (600°F) for a steel structure — both exposed to the M2 – F2 thermal environment. The re-radiation system was limited in allowable maximum re-radiation temperature of 1255°K (1800°F) for René 41 and 1755°K (2700°F) for TZM with coating.

A critical problem area in the design of metallic re-radiative shields is support of the outer surface without introducing excessive thermal stresses in the primary structure. The usual approach is to support a thin, high-temperature-resistant metal surface some distance outboard from the primary structure with a minimum of flexible supports. Insulation is installed between the thin metal surface and the primary structure to achieve the required backface temperature. The idealized support 1) carries air pressure loads from the outer skin into the primary structure,

2) is flexible enough to allow differential expansion between the skin and the primary structure, 3) is not a heat sink, 4) minimizes conduction of heat to the primary structure, and 5) allows quick and easy panel refurbishment.

The attachment system in Figure 53A uses diamond-shaped overlapping panels, forming an external re-radiative erosion shield that is supported by flexible attachment clips welded to an inner attachment frame, also diamond-shaped. Each diamond-shaped panel is securely fastened at the aft apex by a single bolt through the vehicle shell to a self-locking nut inside the stiffening ring. The forward edges of each diamond interlock with, and are restrained by, the adjacent panels in such a fashion that they may freely expand under thermal differentials but remain firmly anchored to the vehicle. All external overlaps are in the downstream direction, avoiding local flow and heating problems associated with forward-facing steps. Attachment bolts are covered and protected by installation of the following panel.

The second re-radiative panel concept is the clip attachment system, shown in Figure 53B. This basic concept is presently being tested by NASA Langley (Reference 40). It consists of a rectangular panel, corrugated to add longitudinal stiffness and transverse flexibility to accommodate thermal expansion. The shield supports are designed to essentially "fix" the panel at its center and to permit expansion away from this point in all directions. Easy refurbishability is provided by the "rod" attachment scheme which also increases the conduction path length to the primary structure. This design avoids threaded fasteners and access holes in the outer shield. Insulation pads are retained between the panel and the vehicle skin.

The two re-radiation system concepts shown in Figure 53 represent refurbishable re-radiative heat protection systems capable of being fabricated from either René 41 nickel alloy or TZM molybdenum alloy. Since the corrugated panel has been further developed (Reference 40) it was selected as the typical re-radiative heat protection system for this study. (A closer detail of the panel and clips are shown on Figure 54.) Using this system as a base, three radiation cooling concepts were selected for the detailed study. These systems included a completely passive system (heat shield, insulation, air gap, and structure) and two active systems (heat shield, insulation, with and without air gap, structure, and active cooling).

The thermal response of the re-radiation system to the M2 – F2 environment was determined by transient-conduction-solution computer programs. The material properties used for the analysis are shown on Figure 55 for the specific heat and on Figure 56 for the thermal conductivity as a function of temperature for the various combinations of materials. Over the major portion of the temperature range of interest for this application, the TZM material has a lower specific heat while the René 41 has lower thermal conductivity.

The temperature histories for three typical radiation concepts are depicted on Figure 57 as a function of time. As shown, for a given surface profile, the intermediate temperatures vary, depending on the system used. It is clear that for this application, the maximum temperature occurs for a relatively short time. Since the outer material is temperature-limited, this short time of operation will establish the extent of application of the system. The active systems provide a more uniform constant temperature with time at the structure, while the passive system backface temperature increases with time. The air gap provides lower temperatures at the backface for a given system and amount of coolant. The air gap will require less total weight, but there is a greater total shield thickness requirement. The typical temperature profiles for each of these systems are shown on Figure 58 as a function of thickness for various flight times. The characteristic decrease in temperature in the air gap is evident for both cases with and without cooling. The thicknesses of insulation selected for these studies were 12.7 cm (5 inches) for the passive system and 6.35 cm (2.5 inches) for the active systems.

b. Temperature Control

The re-radiation systems were designed for backface temperatures of 422°K (300°F) and 589°K (600°F) for an aluminum and steel structure, respectively. Both passive and active cooling of the interior structure were considered. The passive system is the simplest and most reliable system; however, it has the disadvantage of requiring a greater thickness that may limit its application to areas other than those severely limited volumewise (the fins and rudders), and it will generally require greater total weight for a given shield application, which can be a great disadvantage for any critical application.

The active system concepts must consider reliability, complexity, refurbishability, and overall system aspects, with the overall system weight being of prime importance for this study. This involves a weight trade-off between passive insulation requirements and the combined weight of reduced insulation plus cooling system in order to obtain the optimum thermal protection concept. Even if the active system did not show a weight saving, it may be necessary in areas of the vehicle where the shield-structure thickness is limited. Two basic approaches were investigated; namely, 1) a transport system where the coolant is transferred through tubing to and along the surface to be cooled, and 2) a passive concept where the coolant is stored at the surface in a gelatin or wicking matrix. Both open- and closed-loop systems were considered. The closed-loop system contains a single-phase fluid (ethylene-glycol water solution) which is pumped through tubes where the thermal energy is removed by convection. The fluid is returned to a water boiler where the temperature is lowered by the removal of thermal energy in the open-loop system the water temperature is increased (and vaporized) within the tubes while passing along the surface being cooled. The vapor is then discharged overboard.

The active system selected for this study was the closed-loop system which has the advantage over the open-loop system in that it requires less weight, is more reliable, and is easily refurbished. The passive-gelatin or wicking-matrix type was not used primarily because of its disadvantage in refurbishability, effectiveness, and adaptability to varying thermal loads that occur during flight.

The internal cooling system (Reference 41) considered is of the water circulation system type. Heat exchanger tubes, through which the water is pumped, are attached to the back surface of the metal structural skin. The metal skin acts as a fin to conduct the received thermal energy to the water. The heated water, in turn, is pumped through a boiler heat exchanger where the water is cooled down to 380°K (225°F) by boiling, with the steam vented overboard. The cooled water is recycled through the coolant passages attached to the vehicle skin.

The cooling requirements shown on Figure 59 are presented as weight-per-unit-area of an internal cooling system as a function of the peak-received-heat-flux. The weights given are the minimum ones for systems having either an aluminum or a stainless steel skin material. The weight for the lower backface temperature (aluminum skin) is somewhat lower than that for steel. The weight-per-unit-area of the internal cooling system is composed of the weight of the skin or panel material, the weight of the coolant tubes, and the weight of the coolant contained within the tubes. In addition to these weights, it is necessary to add the weight of the circulation pump, the boiler heat exchanger, and the expendable coolant and its storage system to obtain the total weight of the internal cooling system. The weight of the electrical power supply for the pump was neglected, since it is assumed that the required power can be obtained from the vehicle power source.

c. Heat Shield Requirements

The heat shield weight was obtained from both the insulation and coolant requirements for various amounts of cooling. Typical shield weight optimization for the various active cooling systems was obtained as a function of insulation thickness, as shown in Figure 60. The minimum shield weight for the system using microquartz, air gap, and active cooling to a maximum backface temperature of 422°K (300°F) is about 15.9 kg/m^2 (3.28 lb/ft^2). The minimum total weight (see Figure 60) is not very sensitive to insulation thickness. A 20 percent decrease in insulation thickness for the example shown produces a total shield weight increase of only two percent. A decrease in total shield thickness may be desirable for special locations at the expense of a small increase in shield weight.

The passive system could maintain the same backface temperature as the active system simply by supplying the proper thickness of insulation. The typical amount of insulation required for the passive system is shown on Figure 61 for both microquartz

and foamed pyrolytic graphite. The large thickness required for the application makes the passive system unattractive. About 13.2 cm (5 in.) of microquartz is required for the passive system at the high backface temperature requirement. The requirements for foamed pyrolytic graphite are even greater.

A typical weight comparison for the various systems considered is shown on Figure 62. The system requiring the minimum weight consists of microquartz insulation, an air gap, and active cooling. The use of pyrolytic graphite increases the weight some five percent for the minimum-weight system. The active cooling system without an air gap increases the weight some five percent, but the passive system shows an increase of about 40 percent for the conditions shown. The trade-off of the desirability of decreased shield thickness by elimination of the air gap for a weight penalty of five percent can be made in many cases, depending on the area of application. The air gap is on the order of 1.27 cm (0.5 in.).

The weight of the coolant, plumbing, and insulation can be shown on Figure 63 as a function of maximum heat flux for the re-radiation heat protection system. The increase in unit weight with increasing heat flux and the increased weights for the TZM system when compared to René 41 at similar conditions are quite obvious.

The total weight requirement for the re-radiation heat protection system can then be presented in terms of the total heating for each trajectory for both re-radiating materials and backface temperatures. The minimum shield weight is shown on Figure 64 for both René 41 and TZM for the three re-entry trajectories. The weight shown is based on the system that produces the minimum weight; namely, microquartz insulation, air gap, and active cooling. The limits shown for René 41 and TZM are temperature-dependent. A maximum temperature of $1255^{\circ}K$ ($1800^{\circ}F$) for René 41 and $1755^{\circ}K$ ($2700^{\circ}F$) for TZM was used, which corresponds to a maximum heat flux of about $11.35 \, w/cm^2$ ($10 \, Btu/ft^2 \, sec$) and $42 \, w/cm^2$ ($37 \, Btu/ft^2 \, sec$), respectively. It is noted that where applicable, the René 41 system will provide the lightest re-radiation system. The extent of the TZM application, therefore, is shown only for conditions in excess of $1255^{\circ}K$ ($1800^{\circ}F$). The effect of increased backface temperature, as noted on Figure 63, is quite small for this system (three to eight percent weight saving). This is considerably smaller than the effect shown for the ablating systems discussed in Section 4.3.2.1.1.

4.3.2.1.3 Ablation Over Re-radiation System

The heat protection system that has the ablation material over the re-radiation material can extend the applicability of the re-radiation system to higher heat flux regimes. The capability of this system still depends primarily on the re-radiator. The higher the allowable re-radiation temperature, the more efficient is this combined system. The outer ablation material, as a minimum, must be capable of preventing the basic re-radiation surface temperature from exceeding its limiting capability.

a. Analysis

The requirement for this system is dependent on the capability of each part of the system (ablation and re-radiation). The application providing greatest efficiency is obtained when the re-radiation material operates at its maximum capability and at heat flux locations on the vehicle considerably in excess of the re-radiation material capability alone. The use of the ablation system will extend from the beginning of flight until a time in flight where the heat flux is equal to or less than the maximum allowable limit for the re-radiation system.

The performance of the total system can be obtained for a given combination of ablation and re-radiation materials by establishing the requirements in terms of total heating by considering the re-radiation system applicable over a certain portion of the total flight. The ablation system performance can be established from the REKAP analysis as a function of the percentage of the total flight time for the system. The degradation calculated for typical re-entry conditions for ESM and MPN is shown on Figures 65 and 66, respectively. The performance for each material is presented in terms of the total heating during flight and clearly shows the effect of flight time on the degradation. The degradation is not necessarily proportional to the total heating. The requirement for the re-radiation system is presented in Figure 64 as a function of total heating for both René 41 and TZM, as described in Section 4.3.2.1.2. The re-radiation system for this application is based on reaching the maximum allowable surface material temperature during the given portion of flight.

Combining the ablation system with the radiation system produces the total weight requirement as shown in Figures 67 and 68 for ESM-René 41, ESM-TZM, and MPN-René 41, MPN-TZM, respectively. The requirement shown is based on a safety factor of 1.2 on the ablation material. The minimum ablation material from a practical standpoint needed for the lower total heating locations was included as follows:

Material	Minimum Thickness
ESM	mm (inches)
bond	0.254 (.010)
material	2.54 (.10)
MPN	
bond	1.02 (.040)
material	2.54 (.10)

50

Since the combined ablation over re-radiation system will be used in areas where the local heat flux reaches values higher than the re-radiation system alone can withstand, it is desirable to examine the minimum ablation required for the system. As the critical environment exists for abort and re-entry, both must be considered. The typical comparison of the stagnation heat flux variation for both abort and re-entry is shown in Figure 69 as a function of time for the maximum W/C_LA. Since the maximum total heating occurs for re-entry, an ablation system will be sized primarily for this application. However, since the critical abort flights may have higher heat flux, the amount of initial outer ablation material must be capable of withstanding the heating up to the point where the re-radiation material application is satisfactory. This critical amount occurs close to the limit application of re-radiation on the windward ray. The material performance is based on REKAP analyses for the region near maximum heat flux. The material thickness for ESM and MPN is shown in Figure 70 as a function of total heating. The typical minimum ablation thickness requirement is shown in Table 3 for the most critical abort flight (Saturn I-B, L/D max.) for various re-entry conditions for the TZM material application. The requirements for the René 41 material and for all conditions for other less-critical abort flights show thicknesses which are considerably less than stated in Table 3. The minimum thickness provided is adequate for the intended application.

4.3.2.1.4 Performance Comparison

The individual performance of the ablation, re-radiation, and ablation over re-radiation heat protection systems were established in the previous sections. It is of interest to compare the various systems to determine their applicability. The performance of each system can be stated in terms of weight-per-unit-area as a function of total heating, as shown on Figure 71 for ESM for both $422^{\circ}K$ ($300^{\circ}F$) and $589^{\circ}K$ $600^{\circ}F$ backface temperature. The value of total heating for a typical trajectory essentially determines the applicable location on the vehicle, subject to heat flux constraints. As shown, the high heating region is applicable roughly to the nose, followed by lower heating on the windward and leeward sides. The weight advantage of both the re-radiation system and the ablation over re-radiation system is clearly evident when applicable to the low temperature condition for specific portions of the vehicle. The definite advantage for the ablation system for the high temperature condition is also shown. The ablation systems shown include a safety factor of 1.0. The corresponding comparisons for the MPN material are shown on Figure 72 and similar trends are shown, as discussed previously.

4.3.2.2 Heat Protection System Application

4.3.2.2.1 Application

The various heat protection systems considered in this study include ablation, re-radiation, and ablation over re-radiation. The application of each system depends

primarily on the adequacy of the limiting parameter of the system and the most critical environment to which it will be subjected on the vehicle. Although the low-density ablation systems used for this study (ESM and MPN) may be somewhat limited in efficiency when operating at very high heat flux and shear conditions, the present application of these materials appears adequate for the comtemplated conditions over all parts of the vehicle. The design requirement for the application, then is, essentially total-heating-dependent for a given total flight time. In general, for a given flight path, a greater material thickness is required as the total heating is increased for similar backface temperature, safety margins, material, refurbishment techniques, and thermal stress considerations.

The re-radiation system is temperature-limited, indicating that the application is severely limited, depending on the local environmental requirements. Therefore, the use in this study of Rene 41 and TZM will determine the limit of application on a vehicle exposed to a given environment. The maximum temperature for this re-radiation system will determine the extent of application of this system.

The ablation over re-radiation system is essentially a combination of both the ablation and the re-radiation systems. The usefulness of the composite is based primarily on the re-radiation material capability-the higher the allowable temperature becomes, the more efficient is the system. The ablation material is used to extend the temperature range of the re-radiation system to heat fluxes much greater than are allowable for re-radiation alone.

The application of the various heat protection systems to the M2-F2 vehicle may be determined by considering the thermal environment imposed during flight with the limitation of the particular heat protection system. The ablation system, of course, can be applied to any portion of the vehicle as desired. The only major difference in requirement is the detailed ablation material thickness requirement, which will vary over the vehicle.

The application of the various re-radiation systems to the different re-entry and abort cases is shown in Table 4. Since the material is temperature-limited, not only re-entry but abort must be carefully evaluated. Table 4 shows the application to the top, bottom, canopy, fin, flap, and leading edge.

The composite type (ablation over re-radiation) heat protection system is partially limited in application because of the individual component material capability. The outer ablation material will be used during the initial phase of flight and will withstand the maximum peak heat flux imposed by both re-entry and abort trajectories. The application of this system, then, will extend the use of the re-radiation material over portions of the body subjected to higher heat fluxes than the re-radiation material alone could withstand. This system would be used on the windward sides of the M2-F2 vehicle only. The nose, fin leading edge, flaps, and canopy would use the ablating

system due to considerations of volume and reliability. It is noted that for this system, the re-entry portion of flight will impose the most critical environment; therefore, it is the limiting condition for the application. A typical heat protection system application is shown on Figure 73.

4.3.2.2.2 Typical Joint Considerations

The heat protection system that appears most applicable and versatile for the M2-F2 application is the all-ablation system. With this system, the adaptability to many other missions with quite different variations in local heating (e.g., yaw, other trajectory modes, etc.) can be readily accommodated by the basic system. Since the re-radiation system alone is not suitable for the entire vehicle, a combination of various heat protection systems must be used with it. A mixture of ablation, re-radiation, and ablation over re-radiation systems, each of different material combinations, may be used on one vehicle as discussed previously. The joint between any two dissimilar heat protection systems will present a problem. Some typical locations of joints and joint concepts are shown in Figure 74. There is a joint similar to the others between the upper surface and the side of the vehicle in a longitudinal plane, but this joint is subjected to a different flow direction. It should be noted that the material slopes, tapers, and thickness shown are schematic. The joint between the ablation and re-radiation surface will be designed so that as surface erosion of the ablation material takes place, there remains a continuous surface between the two systems and in no case is a forward facing step formed. It should be noted that the erosion at the location of such a joint is usually very low. Since ESM does not erode at heat fluxes of about 34 to 45.4 W/CM^2 (30-40 Btu/ft^2 sec) or below, there will be no initial material build-up required between the adjacent surfaces of the ablating and a re-radiation material of René 41 or TZM. The rearward sloping outer ablation material shown in Figure 75A is just enough to prevent the possibility of a forward step being formed during flight. The slope of the joint mating pieces below the surface will be determined by the material properties and the thermal environment. The angle may be as high as 80 to 90 degrees in some cases. There are other joint configurations (Reference 42) which, although more complex, can even adjust to the required aligned position during flight.

4.3.2.2.3 Application of MPN and ESM to Special Areas

The thermal protection system for several areas of a lifting re-entry vehicle requires special consideration. The following areas are considered with respect to requirements and possible design approaches using both MPN and ESM shield materials.

a. Joints, Gaps

With ESM there are no gaps — all shield sections are butt-jointed. With the MPN thermal shield, gaps must be provided, the sizes of which depend on the panel size, the differential coefficient of expansion of shield and structure, and the environmental temperature range. Gap-sealant materials are currently available such as RTV-102 or RTV-108 that may be applied in the gap to thermally protect the underlying structure. The sealants must have sufficient stress-strain and adhesive characteristics so as not to fail when the gap size increases (when the temperature is lowered), and must have a low compression modulus to allow the gap size to decrease when the temperature increases.

b. Access Panels Interaction Zones

There will be special design considerations to minimize edge gaps between the thermal shield attached to access panels and the thermal shield material surrounding the access doors. With ESM, there need be no gap since the edges can be butt-jointed. There must be gaps, however, when MPN is used as the thermal shield.

Edge gaps can be controlled between thermal shield-covered access panels and the surrounding thermal shield in several ways. One is shown in Figure 75. Here templated matching edges are provided to eliminate the gap. The levels are oriented to eliminate up-stream edge lifting.

An alternative solution is to apply a sealing fillet of ESM along the edges for the ESM external shield, or a sealant such as RTV-102 or RTV-108 for MPN. This technique has been successfully used by GE, and its desirable properties of adequate strength, compatability, and rapid cure cycle have been established.

Access panels must be attached to the vehicle, usually by counter-sunk bolts as illustrated in Figure 75A. Thermal shielding must be provided, in the form of plugs, for the head of the bolt.

In the case of ESM, the plug can be removed by a device such as a cork-borer and can be retained until the access panel is closed for the last time. The edges of the plug are coated with a fast-curing silicone adhesive, and the plug is inserted into the hole.

With MPN, there is more difficulty. The plug must be drilled out, and it cannot be re-used to fill in the hole. A new plug must be machined from a different piece of shield material. At the final closing of the access panel, the plug must be bonded into the gap with a fast-curing adhesive such as an amine-cured epoxy.

54

c. Control Surface Gaps

This problem area includes the vertical and horizontal control surfaces where minimization of heat shield gaps is required. There is also the requirement that full travel of these components must be unimpeded, that high-temperature, high-velocity flow be eliminated or minimized into interior regions behind these components, and that their actuating mechanisms be thermally protected.

For control of edge gaps around the boundaries of movable fins and rudders, a fiber-reinforced ESM "hinge" for the leading edge, as shown in Figure 75B, is offered as a possible solution. Fitted beveled edges are proposed for other edge gap regions. The characteristics of the hinge are such that rotation and displacement can be accommodated, at the same time preserving a sealing action along the leading edge. The hinge would be fabricated and tailored independently of the rest of the movable surface thermal shield and would be fitted and attached separately. For the gap regions other than at the leading edge, carefully fitted, matched beveled edges could be considered, possibly with a reinforcing matrix for the increased edge stiffness to minimize the joint gaps.

The ESM hinge could be used with either type of thermal shield. For the movable surfaces, the required all-movable pitch, roll, and yaw control motions of the control surfaces require relative rotation of the surfaces with respect to the fuselage. At the same time, thermal covering and sealing must be provided. The available gap between fuselage and inboard edges of the control surfaces may permit surfacing of these regions with thermal shield. It appears to be desirable to consider high-density material for this area in view of the limited clearance available between fuselage and stabilizers and the need for preserving clearance for thermal expansion.

d. Expansion Joints

To provide a heat shield in the regions of fuselage expansion joints, the following concepts appear feasible:

(1) The heat shield joint can be installed with an initial pre-stretched deflection (applicable to ESM) which is partially relieved when the structural expansion gaps close.

(2) The heat shield joint can be fabricated with low-density material filling the joint such that at joint closing under elevated temperature, the filler will be partially compressed.

4.3.3 STRUCTURAL CONSIDERATIONS

4.3.3.1 Attachment Requirements

4.3.3.1.1 Ablation

The attachment requirements and refurbishment techniques (Section 4.3.1.4) will require a specific weight for each system as shown on Table 2. Two candidate refurbishment systems for the MPN are elastomeric pillars and the nut and bolt system. The elastomeric pillars were chosen over the nut and bolt system for the following reasons:

(a) Pillars allow the shield to relieve itself of thermal strain.

(b) They provide a more uniform support for the prevention of flutter.

(c) They enable more uniform shear distribution.

(d) The bolt system will require the drilling of holes that will induce stress concentrations.

Assuming a normal pressure of 1.43 N/cm^2 (300 lb/ft^2), the stress level in the elastomeric pillars is equal to a compressive stress of 10 psi, which is negligible.

The three candidate refurbishment system for the ESM are mystic tape, loop and pile, and perforated scrim. Based on the very high weight of the loop and pile system, it was eliminated in favor of the perforated scrim and mystic tape which have similar weights, 4.88 and 6.73 g/cm^2 (0.100 and 0.138 lb/ft^2), respectively. The choice of either one depends on the operating structural backface temperature and the desired reliability of each of the systems.

The weight of the perforated scrim consists of teflon-glass plus an elastomeric bond on the shield. The weight of the loop and pile includes the pile material plus two thicknesses of RTV-560 used to bond the system to the shield and the structure.

The mystic tape consists of the material itself plus the RTV-560 required to bond the back of the tape to the sheet ESM.

The resultant weight comparisons for various types of ablation materials and backface temperatures are shown on Figure 76 and, for all practical purposes, are independent of the type of refurbishment system used (those discussed above). The weight of the refurbishment system is essentially constant for a given material and vehicle size, since it can be reduced to a given weight-per-unit-area. The differences shown for a given material for varying backface temperature simply reflect the difference in total heat protection system weight, not the refurbishment weight.

4.3.3.1.2 Re-radiation

Table 5 depicts the criteria that was used to calculate the weight of the re-radiative system.

Weights for the outer surface material, supports and attachments, refurbishment channels, and rods were determined from Reference 43.

The structural supports must be capable of carrying the external pressure loads and shear to the vehicle substructure. These supports must also be capable of relieving the panel of any thermal stresses resulting from the differential expansion between the re-radiation panel and the vehicle substructure.

4.3.3.1.3 Ablation over Re-radiation

For this type of heat protection system, the same refurbishment system will apply as in the case of the re-radiation panels. The ablation material will be bonded directly on to the re-radiation panel, and after one flight, the entire panel can be replaced with a new one.

4.3.3.2 Thermal Stress Consideration

Figure 77 shows experimental and analytical evaluation of the ESM ablative system bonded to three different substructures; aluminum, steel, and phenolic glass. The critical condition of cold-soak associated with orbital environment is considered. Both applied thermal stresses and ultimate strength data are shown as a function of the cold-soak temperature. The two test points available are:

(1) No failure of ESM/aluminum at temperatures less than $89^{\circ}K$ $(-300^{\circ}F)$.

(2) No failure of ESM/steel at temperatures less than $89^{\circ}K$ $(-300^{\circ}F)$.

The test points indicate close agreement with analytical predictions, and the results of these curves indicate that the ESM/aluminum and ESM/steel are more than adequate to survive the thermal stresses associated with the orbital environment.

Figure 78 shows the analytical evaluation of the MPN ablative system bonded to two different substructures. Again, the critical condition of cold-soak associated with orbital environment is considered. Both applied thermal stresses and ultimate strength data are shown as a function of the cold-soak temperature. Material properties

for the MPN material were obtained from Reference 44 which gives data from two separate research institutions; Melpar Incorporated and Southwest Research Institute. As shown in Figure 78, a discrepancy exists in the ultimate strength data of the material at cold temperature. However, using the lower strength (Melpar) data, the material appears to be capable of a cold-soak orbit environment of $150^{\circ}K$ ($-190^{\circ}F$). This temperature is somewhat higher than the minimum cold-soak temperature for a polar orbit, as discussed in Section 4.2.2.4. Although the thermal stress analysis was conducted for a shield/substructure thickness of 10, Figure 79 shows that this ratio has negligible effect on the cold-soak capability of the material. It is noted that test data are not available to verify the analysis, so the applicability of MPN is dependent upon the accuracy of the material properties used. It should be noted that experience on various full-sized vehicles with materials such as phenolic nylon, which is even stronger than MPN, exhibited limitations in their cold-soak application.

4.3.4 HEAT PROTECTION SYSTEM WEIGHTS

4.3.4.1 Method of Analysis

Thermal protection system weights were established with the aid of a digital computer program, WALRVS (Weight of Ames Lifting Re-entry Vehicle Shield). The approach used in developing this program was 1) to use Fortran, a standard engineering computer language, and 2) to use the GE time-sharing computer system. This computer system (DSCS: Desk Side Computer System) is well-adapted to the type of program considered here, and allows rapid program development in terms of elapsed time. The results of the program are provided in terms of a weight listing for each of the material systems for a given vehicle weight, length, and safety factor. Two types of program output are available to the user: 1) a detailed weight list of 39 items, and 2) a subtotal weight list of seven items, along with the total vehicle shield weight. The seven items included in the subtotal weight list are:

(1)	Nose cap	(5)	Fins
(2)	Upper surface	(6)	Control surfaces
(3)	Lower surface	(7)	Canopy
(4)	Sides		

Input for the program is composed of five items: length, weight, safety factor, trajectory selection, and the type of heat protection system that is desired in a given vehicle location. The program has the capability of handling the ablation, re-radiation, and ablation over re-radiation heat protection systems. The referenced area, nose radius, and lift parameter are then computed. Table of heating distribution and entry heating, including transition effects, are used next to determine the local heat load

at each location. Given the heat load, the shield thickness requirements for the ablation, re-radiation, or ablation over re-radiation heat protection systems are determined from a stored table, depending upon the type of system specified. The necessary refurbishment weight is added to the heat protection weight, resulting in the net weight of the system for that particular local area. The weights are then given as output in a manner previously described.

4.3.4.2 Weight Requirements for Refurbishment

The weight requirements for the refurbishment systems have been stated in Section 4.3.3.1 and are as follows:

(1) Ablation

    (a) ESM — 4.88 to 6.73 g/cm^2 (0.100 to 0.138 lb/ft^2)

    (b) MPN — 11.3 g/cm^2 (0.232 lb/ft^2)

(2) Re-radiation — 10.2 g/cm^2 (0.209 lb/ft^2)

(3) Ablation over re-radiation - same as that for the re-radiation panel.

4.3.4.3 Heat Protection System Weights

4.3.4.3.1 General

Heat protection system weights are presented for an all-ablative vehicle and various combinations of ablation, re-radiation, and ablation over re-radiation. The design philosophy of a combined heat protection system can follow two approaches. In the first approach ablative materials are used on those portions of the vehicle that experience heat fluxes too high for re-radiative materials, while refractory metal alloys and super-alloys are used on the lower heat flux areas. In the second approach, an ablative material is used to handle peak heating during early re-entry. During the latter period, the ablator is removed and the re-radiative surface of the vehicle handles the heat load. Both concepts present attractive features along with problems that limit their range of application.

The limiting factor for the ablation over re-radiation system is the high temperature capability of the bond attaching the ablator to the structure. At present, bond systems are generally temperature-limited to a soak condition of about $644^{o}K$ ($700^{o}F$). The thickness of the ablator on the vehicle varies and would be minimum where the ablative system ended and the re-radiative system began. Since a Rene' 41 shield can operate at about $1255^{o}K$ ($1800^{o}F$) and a TZM shield at $1755^{o}K$ ($2700^{o}F$), the ablative system

would require sufficient insulation thickness to prevent flow of excessive heat to the ablator bond at the juncture area, since this would cause premature failure of the bond.

The other approach consists of the re-radiator which is completely coated with an ablator. The ablator functions during peak heating in early re-entry and is later jettisoned to permit the re-radiative structure to take over during later stages of re-entry. A method of achieving a clean re-radiative surface has been examined. By incorporating a sheet of magnesium foil in the bond layer, positive control in jettisoning the ablator may be possible. Laboratory tests (Reference 45) have shown that magnesium foil can be used for this purpose.

Magnesium foil less than 0.382 mm (0.015 in.) thick will ignite without melting. Since burning magnesium will react with most compounds containing oxygen, a strip of foil coated with a silicone elastomer over about 75 percent of its length was ignited. The magnesium burned under the silicone coating and left a white ash. This indicated that the reaction between burning magnesium and the elastomeric bond may be used to destroy the bond and effect the removal of the ablator.

Another test was made on a sample heat protection system panel. A layer of RTV-560, 0.254 mm (0.010 in.) thick, was placed on a 5.08 x 7.62 cm (2 x 3 in.) sheet of 0.788 mm (0.031 in.) aluminum. Strips of 0.152 mm (0.006 in.) magnesium foil were placed on the RTV, and ESM-1004 was then bonded on the prepared substrate. The first layer of RTV protected the aluminum from the heat of the burning magnesium. One edge of the ESM layer was peeled away to expose the magnesium. A small weight was attached to this edge to simulate the peeling action of the air stream. The magnesium foil was ignited and it burned, destroying the RTV bond without damaging the aluminum substrate.

Since this concept may permit positive control of the removal of the ablator at command time, transition from an ablative to a re-radiative system may be programmed. However, the 644°K (700°F) bond temperature limit still would require sufficient material of the ablator to insulate the bond until removal of the ablator is desired.

4.3.4.3.2 Total Shield Weight for Each Trajectory

a. Ablation

Figures 80, 81, and 82 show the ablator shield weights for the nominal vehicle (See Figure 2) and various trajectories. The shield represents from about 9 to 24 percent of the total vehicle weight, depending on the material, backface temperature, vehicle size, and re-entry conditions. The shield weight ratio (W_S/W_T) decreases with increasing vehicle length. As indicated, the lightest heat protection system is the MPN for a backface temperature of 422°K (300°F) and the ESM for a backface temperature of

589°K (600°F). The MPN appears superior at low backface temperatures because of its better insulating qualities. However, the ESM at the higher backface temperature operates closer to the degradation temperature requiring a minimum of insulation. Figure 83 shows the distribution of ablation shield weights in terms of the nose cap, upper surface, lower surface, sides, fins, control surface, and canopy. As shown, the lower surface provides the greatest portion of the shield weights.

The detailed weight comparison for one typical vehicle and trajectory application as shown on the above-mentioned figures is presented on Table 6. The weights are given for both ablation materials and both backface temperatures. The weight was calculated for each individual section (39 total, see Figure 84), with subtotals shown for the seven individual larger sections. For each material, it is clear that a large weight advantage exists for the higher backface temperature. It is of interest to note that for the nose cap, both ESM and MPN show similar weights at the 422°K (300°F), but ESM is lighter at 589°K (600°F). Both the ablating materials show similar weights for the upper surface at 589°K (600°F), but MPN is the lightest at the lower backface temperature. The other sections show that at 422°K (300°F), MPN is lighter but at 589°K (600°F), ESM is lighter. The weight variations with materials and vehicle heating was given in Section 4.3.2.1.1 .

b. Ablation Plus Re-radiation

This system consists of ablation in areas of high heat fluxes and re-radiation in the areas where ablation is not required. Two types were considered: ablation plus René 41 re-radiation and ablation plus TZM re-radiation. Two types of ablation material (ESM and MPN) were used with the two types of re-radiation material (René 41 and TZM). The heat protection system employing TZM also used René 41 where applicable. This combination for TZM was used for greater reliability and minimum weight since René 41 is a simpler system that does not require a coating and, in addition, requires less weight for a given heating load. For ablation plus René 41 re-radiation, the ablation was used in all areas except where René 41 was used (Section 4.3.2.2). Figures 85, 86, and 87 depict the shield weights for the ablation plus René 41 re-radiation. For the backface temperature equal to 422°K (300°F), the MPN shows the lightest weight system, and at 600°F the ESM is the lightest. The shield weights are somewhat lower than those for an ablating system for the low backface temperature case, but the reverse trend occurs for the high temperature case. This follows the same trend as the all-ablation system and becomes obvious from Figures 88 and 89 which show that for the ablation plus re-radiation systems, the ablator represents as much as 80 percent of the total shield weight.

Figures 90, 91, and 92 show the shield weights for the ablation plus TZM re-radiation heat shield. For a backface temperature of 422°K (300°F), the MPN is the lightest and for 589°K (600°F), the ESM is the lightest for the low backface temperature.

Comparing the two re-radiation systems, the ablation plus Rene' 41 is the lightest system at a backface temperature of 589°K (600°F), whereas the ablation plus TZM is lighter at 422°K (300°F).

c. Ablation plus Re-radiation plus Ablation over Re-radiation

This system consists of ablation and ablation over re-radiation in areas of high heat flux and re-radiation in areas of low heat flux. Two types were considered; ablation plus Rene' 41 re-radiation plus Rene' 41 composite, and ablation plus Rene' 41 re-radiation plus TZM re-radiation plus TZM composite. The Rene' 41 and TZM composite consist of an ablator directly over the re-radiation material.

For the ablation plus Rene' 41 re-radiation plus Rene' 41 composite, the following is a breakdown of the location of each system:

Ablation - nose, fin leading edge, flap, canopy

Rene' 41 re-radiation - same as previous case

Rene' 41 composite - all remaining areas

Figures 93, 94, and 95 depict the weights for the ablation plus Rene' 41 re-radiative plus Rene' 41 composite system. For this type of system, use of the ESM for both the 422 and 589°K (300 and 600°F) backface temperatures results in the minimum weight.

For the ablation plus Rene' 41 re-radiation plus TZM re-radiation plus TZM composite, the following is a breakdown of the location of each system (see Figure 84):

Ablation - same as previous case

Rene' 41 re-radiation - same as previous cases

TZM re-radiation

TZM composite - all remaining areas

Figures 96, 97, and 98 depict the weights for the ablation plus Rene' 41 re-radiation plus TZM re-radiation plus TZM composite. As shown, the use of ESM for the high backface temperatures results in the minimum weight system. The ablation material for the combined heat protection system which shows minimum weight for the low backface temperature depends on the re-entry condition application.

d. Comparison of the Three Heat Protection Systems

When comparing the various types of heat protection system based on weight, the most important consideration is the allowable backface temperature. This study clearly shows that the higher the backface temperature the lower is the weight of the resulting heat protection system. In order to evaluate the various systems based on minimum total weight, the weight of the substructure should also be considered.

Based on previous lifting vehicles studies conducted at General Electric, (Reference 51) it has been shown that minimum-gage structure is the governing criteria between 360 and $644^{o}K$ (200 and $700^{o}F$). As the structural backface temperature is increased, the shield weight decreases. Since the structure is minimum-gage in design, the same structure that would result at low backface temperature would suffice at higher temperature. The optimum backface temperature would be the maximum allowable temperature that the structural material could be subjected to without any substantial loss in material properties. The structural weight for both the $422^{o}K$ ($300^{o}F$) and the $589^{o}K$ ($600^{o}F$) backface temperatures would be essentially the same. Aluminum and titanium or steel are representative of typical structural materials for the application. The shield weight comparison shown previously with both backface temperatures is believed representative of the total heat protection system weight.

A comparison of the various heat protection system weights is shown on Figure 99 for a typical re-entry condition. It is clear that for the low backface temperature condition, the use of re-radiation and ablation over re-radiation on portions of the vehicle decreases the total shield weight. The extra complexity of this combined total system may be warranted for the application if the weight reduction is desired. The MPN ablation material shows somewhat lower weights for this low temperature condition.

When the backface temperature is high, the ablation system produces the lightest weight system and there is virtually no advantage for employing the re-radiation or the ablation over re-radiation system on portions of the vehicle. The ESM ablation material produces the lightest weight heat protection system at the high backface temperatures.

63

4.4 REFURBISHMENT

4.4.1 APPLICATION OF REFURBISHMENT ATTACHMENT SYSTEM

The refurbishment cycle consists of a combination of processes which, generally, provide for application of the thermal protection system to the structure, quality checking of the shield material and attachment after application, and, after flight, removing such remaining portions of the coating as are required to recycle the vehicle. To be practical, a refurbishment cycle should be capable of field application.

This section will discuss the applicability, fabricability, and ease of application and removal of each of the refurbishment attachment systems with MPN and ESM shield materials. MPN can also be bonded to the structure with a high temperature adhesive, such as HT 424 and Epon 934; however, this possibility will not be discussed, since it is not refurbishable under this definition.

4.4.1.1 Elastomeric Bond

The elastomeric bond is applicable only to ESM for both the 422 and 589°K (300 and 600°F) backface temperature requirements. Although it is the least adaptable to quick turnaround techniques, it does have the highest reliability at this stage of development. The fabricated ESM is directly bonded to the primed structure with the base elastomer. It is the simplest to fabricate, does not require modifications in the structure, and is highly attractive for weight considerations.

It has been well characterized and qualified by extensive ground and flight tests, and it is the standard bond system used with molded and sheet ESM, as described in Section 4.3.1.1.1.

4.4.1.1.1 Attachment

The procedure for bonding with RTV-560 is detailed in General Electric Material Specification R6328 and Manufacturing Standing Instruction (MSI) 242370. The materials acceptance criteria are listed for the adhesive and the metal primers in GE Acceptance Specifications 156A98174 and 128A5489, respectively.

After the ESM shield sections have been dry-fitted to the structure, the structure surface is wiped with clean unsized linen toweling, wet with acetone, until no residue remains on clean portions of the cloth. The SS4004 silicone primer is then applied to the structure surface by a clean white cloth to a thin uniform thickness. The RTV-560 is then mixed with 0.5 percent T-12 catalyst and applied to the structure surface. The adhesive is rolled out onto the structure surface with a clean paint roller to a thickness

of 0.127 to 0.254 mm (5 to 10 mils). (For molded sections only, an adhesive layer is applied to both bond surfaces.) The shield material is then applied to the structure surface, much like a "wallpaper" application, and the surface of the ESM is rolled with a clean paint roller to assure wetting and to eliminate any entrapped air in the bond. No pressure or external temperature is required to cure the bond. In areas such as the nose, where thicker shield sections are used, straps may be used to hold the shield in place during cure of the bond. Although the bond will cure sufficiently at room temperature to permit handling after twelve hours, a cure time of several days at room temperature is required to achieve full adhesive strength.

4.4.1.1.2   Refurbishment

For refurbishment after recovery, the shield material may be removed by either a hand tool or a mechanical technique and virgin shield material reapplied as discussed in the previous section.

a.   Removal Techniques

1)   Equipment and Solvents

(a)   Putty-knife type scraper with sharpened edges.

(b)   Paint scraping tool (Zipaway-Hunt Wilde Corp.) which has a three-inch razor edged blade.

(c)   Pneumatic drill equipped with a one-inch wide "disc-type" metallic brush.

(d)   Hand metallic brush with a metal softer than the structural metal.

(e)   Acetone and toluol.

2)   Hand Tool Removal

(a)   The scraper, either putty knife or scraping tool, is inserted in a joint at the interface of the bond and shield. The shield is removed in strips by scraping in one direction while maintaining fairly even pressure on the blade.

(b)   The remaining bond material is solvent-soaked with acetone and grossly removed by rescraping.

(c)   The surface is then wire brushed or scrubbed with copper or aluminum wool for removal of the final residue.

(d)   The metal surface is then solvent-wiped with toluol.

Although hand techniques are more time-consuming, certain areas of the structure may require this procedure. A final wiping with a toluol-dampened lint-free cloth will prepare the surface prior to bonding the next virgin shield.

3) Mechanical

After stripping the shield by the hand method, the residual bond material may be removed by high speed abrasion with a wire wheel. In this case, solvent-soaking is not required. A vacuum cleaning inlet would be located near the wire brush to protect the operator and the vehicle and hanger from the silicone dust.

4) Spray ESM

The application of spray ESM was included in the discussion on the "formulation and fabrication of ESM." Although no separate bond system is used, the spray material may be removed in the same manner as the sheet ESM. The scraping step may be eliminated, and all the material removed by high speed abrasion where the ablated shield thickness is less than 0.102 mm (0.040 inches).

4.4.1.2 Perforated Scrim

The perforated-scrim technique, also only applicable to ESM, is a compromise between the elastomeric bond and the other refurbishment techniques with respect to current flight and ground qualification and ease of removal. The scrim material is a 0.102 mm (0.004 in.) thin sheet of teflon-coated glass cloth. Elastomeric bond or spray ESM does not adhere to this scrim. Holes are punched in this scrim and the bond effected through these holes to the structure. The size and spacing of these perforations can be selected to achieve attachment strength to meet specific design requirements.

The adhesive is applied to the bond surface of the ESM. The shield is then applied to the structure in the same manner as the elastomeric bond with the perforated scrim between the shield and structure. After flight, the shield is removed by lifting a tab end and peeling. Little force is required to break each of the attachment points singly.

After shield removal, dots of the adhesive remain on the structure; these can be readily removed by the wire brush technique described in the section on refurbishment of the elastomeric bond.

This technique has been sucessfully demonstrated and flight-tested on sheet material and would be applicable to spraying ESM in the field. It may not be practical, however, for high shear areas, such as leading edges, where full adhesive strength capability is desired.

The perforated-scrim refurbishment technique is illustrated in Figure 100A.

4.4.1.3 "Nut-and-Bolt"

The nut-and-bolt attachment system shown in Figure 100B provides a positive technique for the attachment of the shield to the substructure and is applicable to both MPN and ESM. The bolt would be imbedded into the insulative portion of the shield and fixed through holes in the structure by a locknut at the inner side of the structure. A washer would be used at the head of the nut to increase the area of bearing load on the shield. A high temperature, load bearing, insulative material such as a glass-reinforced phenolic, polyimide, or polybenzimidazole would be used in the construction of the nut, bolt, and washer. The temperature capability of these materials exceeds the allowable limits of the thermal shield material. The size and spacing of these bolts can be varied, depending upon the structural design requirement.

This system can be fabricated by two different techniques. The simplest method involves normal fabrication of the shield section. After qualification and machining, cores the size of the washer could be made to a designed depth from the outer surface of the shield. The bolt hole would then be drilled in the center of this opening to the base of the shield. The bolts with washers would be dropped into this opening and shield material, equal in shape and size to the core, placed and bonded into the cored section. After final machining of the shield surface, the shield could be attached to the structure mechanically. If a self-locking bolt were used, the shield would be attached to the structure before the cores were refilled.

In a second approach, applicable only to molded MPN and molded ESM, the mold would be designed so that the bolts would be imbedded into the shield during the molding of the shield material.

4.4.1.4 Elastomeric Pillars

The elastomeric pillars approach is the other method that applies to both MPN and ESM. From a refurbishable viewpoint, it does not have particular advantages over other methods for ESM, but it can be used with MPN to make it attractive. In this instance, the shield is attached to the structure by a number of discrete pillars or columns of RTV silicone rubber as shown on Figure 101A. As in the case of the perforated scrim, the size and spacing of the pillars are designed to meet vehicle

station requirements. In addition to refurbishment, the pillar approach provides an insulating layer to the structure that could reduce shield weight and act as a compressible bond that would increase the low temperature thermal cycling capability of an MPN shield system.

Sheets of the pillar system are fabricated by placing a metal mold containing holes of the size, shape, and spacing of the pillars into a tray of catalyzed RTV silicone rubber. The RTV flows through these holes to the top surface of the flat mold. After curing in an oven at slightly elevated temperature, the excess material is cut from the top surface of the mold. The pillars, which are attached to a thin skin of RTV on the bottom surface of the mold, are removed from the mold. The skin surface of the pillar system is next bonded to the inner shield surface with RTV silicones. The shield sections are then ready for attachment to the structure. For attachment to ESM, the pillars can be fabricated and bonded to the surface of the ESM in one step, thus eliminating one of the bonding steps.

An adhesive layer is applied to the structure as in the case of the elastomeric bond system. The shield is held in place onto the structure while the bond cures and attaches the ends of the pillars to the structure.

For removal and refurbishment, a cutting tool would be inserted between the shield and structure, the pillars cut, and the shield lifted from the surface. The remaining bond material would be removed as in the case of the elastomeric bond system.

4.4.1.5 Loop and Pile

Loop and pile is a fabric fastening technique that has been adapted for rapid shield refurbishment. The hi-temp loop and pile is completely constructed of stainless-steel loops and stainless-steel piles integrally fabricated into a stainless-steel backing. The mid-temp loop and pile is a silicone resin-impregnated woven tape with stainless-steel loop and pile surfaces woven into the backing tape. It has the potential of having the shortest turn-around time of any refurbishment technique, but is only applicable to ESM as shown on Figure 101B.

Either the loop or the pile side is bonded directly onto the structure with the RTV elastomeric bond or other high temperature adhesive system and remains permanently attached to the structure for successive flights. For the hi-temp material only, the material may also be spot welded to the structure rather than adhesively bonded. The sheet and molded ESM is attached with the elastomeric bond to the other portion of the tape, cut to pattern, and attached to the structure by hand pressing in place.

After flight, the shield is removed by exposing a tab end and peeling. The installation process is then repeated for the following flight with prefabricated shield sections.

4.4.1.6   Mystic Tape No. 7000

The pressure-sensitive tape, Mystic No. 7000, is a 0.254 mm (0.010-in.) thick composite of fiberglass tape and pressure-sensitive silicone adhesive. The system can only be used with ESM and is only applicable for the 422°K (300°F) backface temperature condition. The system may be applied to the structure in two ways, as illustrated in Figure 102. The tape may be rolled onto the structure and the shield material attached to the tape with the elastomeric bond (Figure 102B). The pressure-sensitive tape may also be pre-bonded to the shield material, and after cutting to pattern, this system could be applied to the structure by rolling in place after removal of the tape's adhesive protection sheet (Figure 102A).

For removal after flight, a tab end is exposed and the tape and ablated shield material are stripped from the surface of the structure.

4.4.1.7   Discussion

Summaries of the weights and applications of the refurbishment systems to the design criteria for each shield material are shown in Table 2.

Each of the proposed refurbishment systems has attractive features with respect to application, reliability, cost, and weight. With the exception of the elastomeric bond, which is well-characterized, additional development effort is required on each system on scale-up and application data generation and thermo-mechanical analysis before a quantitative selection can be made of the most promising system for this application.

Stewart and Bloom have evaluated these refurbishment techniques against the system's criteria of cost, safety, and time (Reference 46). They concluded that the elastomeric bond, the mechanical attachment, the loop and pile, and the high temperature tape systems have the greatest potential for elastomeric thermal shields for payoff through further development. Their rating of each system against vehicle design requirements are shown in Table 7.

4.4.2   ESTIMATED COST OF REFURBISHMENT

A rough-order-of-magnitude (ROM) cost estimate has been prepared for refurbishment of an all ESM shield system for the M2-F2 vehicle with an elastomeric bond. This estimate is based on a vehicle of 4536 Kg (10,000 lb) weight, 7.92 mm (26 ft) length, 61.4 m² (678 ft²) surface area. Calculations were made for shield weights of about 409 and 1040 Kg (900 lb and 2,285 lb) for the 589 and 422°K (600 and 300°F) backface temperature conditions respectively. For cost purposes, we assume that

90 percent of the shield weight will be sheet ESM and 10-percent molded ESM. The cost includes fabrication of the shield material, application to the structure, and removal after flight which encompasses the refurbishment cycle. The estimate covers a range for each shield weight depending upon minimal and nominal quality control coverage, shield qualification criteria, etc. No allowance is made for the additional cost involved in fabrication and application of material to special application areas. The material costs includes molds, tooling, and normal production control activity. The estimate is based on a single refurbishment unit that should be reduced to some degree for multiple refurbishment applications. Other refurbishment techniques would generally require less labor for application and removal, but the fabrication costs would be somewhat higher, depending on the system.

The following assumptions on cost of fabrication, application, and removal should in no way be considered binding or official estimates from the General Electric Company due to the many variables inherent in a given program.

ROM cost based on single unit:

Material (includes labor and OH for fabrication)

422°K (300°F)

90% sheet stock at $110/Kg ($50/lb)	936Kg (2,057 lb)	$102,850
10% molded at $220/Kg ($100/lb)	104Kg (228 lb)	22,800
TOTAL	1040Kg (2,285 lb)	$125,650

589°K (600°F)

90% sheet stock	368Kg (810 lb)	$ 40,500
10% molded	41Kg (90 lb)	9,000
TOTAL	409Kg (900 lb)	$ 49,500

Application (same labor and materials for both backface conditions)

	Material $	Labor (hr)	Labor $ (@ $15/hr)
Surface preparation	20	60	900
Fitting and bonding	240	320	4,800

Removal

Shield removal	80	235	3,525

	Material $	Labor (hr)	Labor $ (@ $15/hr)

Special Equipment

Pneumatic brushes	1600		
Pneumatic scrapers	700		
Walk-in refrigerator, etc.	3500		
	$6,140		$9,225
SUB-TOTAL		$15,365	
Cost of fabrication	$125,650		$49,500
TOTAL	$141,015 at 422°K (300°F)		$64,865 at 589°K (600°F)

A second estimate has been made based on a ROM manufacturing cost prepared for fabrication, application, and removal of sheet and molded ESM to the X-15-2 aircraft. This estimate was based on a quantity of 35 units and does not include quality control costs. Gross assumptions were made to this estimate to account for the differences in required shield weight and surface area for the two vehicles.

Unit Average Shop Cost

	Material (incl. special equip.)	Labor	Total
422°K (300°F) backface	$16,000	$184,500	$200,500
589°K (600°F) backface	7,878	90,000	97,878

Based on two separate rough-order-of-magnitude estimates of cost for the complete fabrication, application, and refurbishment of the M2-F2 vehicle, not including quality control costs, a 409Kg (900 lb) ESM heat shield would cost between $65,000 and $100,000, and a 1040Kg (2,285 lb) heat shield would cost between $140,000 and $200,000.

As a basis of comparison, it is estimated that the MPN shield for a 422°K (300°F) backface condition may be three times the ESM cost and for the 589°K (600°F) case, five times the ESM cost. This added cost results from both the fabrication, which would require extensive molds and tooling, and the cost of application and refurbishment, since this material is not as applicable to refurbishment techniques. The estimate on MPN assumes that it can be made in large sections - a capability that has not yet been demonstrated.

4.5   ERROR ANALYSIS

The study made to obtain the heat protection system weights was based on certain
conditions as outlined previously. It is of interest to consider the effect on the shield
weights previously presented of various possible variations in the conditions and
analysis used throughout the study. The error analysis included the effects of transi-
tion criteria, aerodynamic coefficients, pressure distribution, trajectory perturbations,
heating evaluation, safety factors, material properties and performance, attachment
methods, weight, and length variations.

4.5.1   Transition Criteria

The transition criteria used for this study were based primarily on the results of
flight and ground test: (Section 4.2.2.2). The critical Reynolds number was considered
a function of the local Mach number. The available data indicates that an error in
Reynolds number of a factor of two will adequately cover the spread in data for these
flight vehicles (Figure 16). The maximum Reynolds number will thus reach twice the
nominal while the lowest Reynolds number may reach one-half the nominal. This
variation in transition Reynolds number will affect the local heating, total heating,
and therefore the heat protection system weights. The Reynolds number criteria for
this application has little effect on the location of the various heat protection systems
since transition occurs so late in flight that the turbulent heat flux is lower than the
maximum laminar heat flux occuring during earlier flight. The total heating change,
however, will affect the system weight. The effect of this transition Reynolds number
on the shield weight for a typical nominal vehicle is shown on Figure 103 for each of
the three basic re-entry trajectories. The influence of the ablation material and the
backface temperature is also shown. The shield weight will increase to a maximum of
about one to seven percent for the minimum transition Reynolds number. In general,
the ESM shield and the lower backface temperature requirement both show the least
weight change by the change in transition criteria. The higher Reynolds number criteria
will decrease the shield weight by about one-half to two percent, depending on the
conditions shown in Figure 103.

4.5.2   AERODYNAMIC COEFFICIENTS

The high, nominal, and low values of trimmed lift and drag coefficient versus pitch
angle of attack for Mach numbers above five in continuum flow are presented in
Reference 2. The predictions for lift have a lesser tolerance than those for drag,
being less influenced by viscosity effects that vary along the entry flight path.

The surface pressure distributions were obtained from Newtonian computations that
were compared to and then adjusted to the test levels of the M2-F1 data presented in

72

Reference 2.2*. The accuracy of the lower surface distributions was initially estimated at five percent for the most windward meridian, then varying to 10 percent for the side meridian.

The data of Reference 2.3 were closely examined to determine whether a single pressure distribution could adequately represent the relatively large Mach number range of $5 \leq M \leq 10$, and the consequent error introduced by that assumption. The analysis of Reference 2 showed that the initial accuracy assessment was valid and not overly conservative.

Since the F2 canopy is further forward and of different shape, and since no pressure data was available for the F2 configuration, the supplementary data of References 2.3 through 2.5 was employed to define the top centerline distribution as well as the variations between top centerline and side meridian. The F1 data and the supplementary data revealed that the presence of the canopy influenced the flow both ahead of and behind the canopy. A possible error of 20 percent was charged to the leeward data presented in Reference 2 as a result of these considerations. The possible overall averaged error for all of the meridians examined was well within the initial estimations.

The basic influence of variations in the aerodynamic coefficients will be in altering the vehicle flight path. The flight path variation will thereby affect the heating and therefore the heat shield weight. The aerodynamic lift and drag coefficients can vary from nominal values as discussed in Section 4.2.1.1. The individual values of C_D and C_L can be varied in four combinations: 1) high and low, 2) low and high, 3) low and low, and 4) high and high. The effect of these combinations on the heat shield weight is shown on Figure 104 for both ESM and MPN for the two pertinent backface temperatures. In general, the ESM material and the lower backface temperature show the lowest change in heat shield weights as a result of errors in aerodynamic coefficients. Combinations (1) and (4) produce lower shield weights while (2) and (3) result in higher shield weights. The influence of these aerodynamic variations will result in changes in shield weight of ± 9 percent, depending on the conditions. The re-entry condition selected for this comparison is that for a speed of 7,468 m/sec (24,500 ft/sec), which is more sensitive to performance errors caused by the wide variation in angle of attack during flight, and thus has more effect upon shield weight.

4.5.3 PRESSURE DISTRIBUTION

The maximum error in pressure distribution (Reference 2) varies from 5 to 20 percent, depending on the location on the vehicle. It is estimated that a variation of about

---

* References 2.2, 2.3, etc. - denotes References 2, 3, etc, cited in Reference 2 of this report.

± 5 percent on the windward side, ± 10 percent on the side meridian, and ± 20 percent on the lee side (aft portion) may occur. The change in local pressure will effect the local heating and the resulting heat shield weight. The shield weight will vary with pressure, as shown on Figure 105, for the various materials and backface temperatures for a typical re-entry flight of 9144 m/sec (30,000 ft/sec). Again the ESM material and the lower backface temperature condition show the smallest change in system weight by these errors. The maximum variation in system weights resulting from these pressure errors is about ± 3 percent.

4.5.4 TRAJECTORY PERTURBATIONS

The influence of the flight path on the local heating and, therefore, the heat shield weight, is obvious. The influence of the aerodynamic coefficients on the flight path was included in the previous discussion (Section 4.5.2). The trajectory may also be affected by atmospheric variations and the mode of entry. The atmospheric variation was established for standard cold day and a standard hot day and compared to the normal standard day atmosphere. It was clear, when comparing the performance under these two extreme conditions for entry at 7468 m/sec (24,500 ft/sec), that there was very little effect on total heating. The total heating for a standard cold day was about 0.2 percent less and for the standard hot day it was about 0.1 percent greater than the nominal total heating. The effect of these atmospheres on the total heat shield weight is, therefore, negligible.

Trajectories were investigated briefly for an undershoot boundary flight, instead of the overshoot boundary used for the nominal trajectories for both 9144 and 10,363 m/sec (30,000 and 34,000 ft/sec). Flights were made with a limit of about five normal g's maximum during flight (Section 4.1.1.2). The mode of flight was similar to the nominal three-phase flights. The undershoot boundary flight has the characteristics of shorter flight time, lower total heating, and higher maximum heat flux operation. The total heating for the undershoot boundary is about 47 percent and 38 percent of the nominal heating, for highest and lowest super-circular re-entry velocity, respectively. The corresponding local heat flux will increase by a factor of about 2.3 and 3.2 for these two flights. It is clear that the increase in local heat flux will influence the application of the re-radiation heat protection system, since it is temperature (or heat flux) limited. The ablation systems designed for the nominal trajectories will be adequate for this undershoot boundary condition. It should be noted that if the M2-F2 vehicle was designed for this new trajectory, an ablation system would require less total shield weight than the nominal shield. The high heating areas such as the nose, flaps, canopy, and fin leading edge would undoubtedly use a composite ablation-type system comprised of an outer dense material to minimize erosion and the present low density inner material for insulation. The ESM material is well-suited to this combined system. The MPN could also be made in the same manner, if desired.

The undershoot boundary flight will definitely influence the applicability of the re-radiation system as shown below:

Re-Entry Application

U_E m/sec (ft/sec)	Material	Undershoot Boundary (X/L)						
		Bottom	Top	Canopy	LE	Flaps	Fins	Rudder
9144 (30,000)	René 41	X	0.17	X	X	X	X	X
10363 (34,000)	René 41	X	0.20	X	X	X	X	X
9144 (30,000)	TZM	0.90	0.04	All	X	X	All	All
10363 (34,000)	TZM	0.95	0.05	All	X	X	All	All

The re-radiation heat protection system, if designed initially for the overshoot boundary and critical abort, will not meet the requirements for the undershoot condition. An ablation system, however, can meet both conditions. It may be possible to make the re-radiation system adaptable to both conditions if an ablation layer is added over the re-radiation surface to accept the extra heating load imposed. This, however, will increase the local weight of the system and therefore the total heat shield weight.

4.5.5 HEATING EVALUATION

The effect of heating on the total shield weight is quite clear. The shield weight requirement was evaluated for a variation of ± 10 percent in heating over the vehicle. This variation is considered well within the scatter of data obtained from a number of flight tests where the local conditions were well-established such as in the stagnation area using the methods of analysis described in Section 4.2.2.2. The Ablation shield weight comparison is shown on Figure 106 for the nominal re-entry trajectory speed of 9144 m/sec (30,000 ft/sec) and the nominal vehicle weight of 4536Kg (10,000 lb). The shield weight can vary by about +3 to -5 percent of the nominal values. The largest change is shown for the MPN material at the higher backface temperature requirement. The effect on shield weight using ESM and the lower backface temperature requirement is considerably smaller. The effect of heating on the re-radiation system will essentially alter the position of application, i.e., an increase in local heating will require the limiting surface to move downstream to areas of lower heating. A decrease in heating would likewise allow the application of each

system forward to a higher heating region. It is clear that if the heating is increased, the re-radiation system is less desirable, since it may require locally higher temperatures than allowable, and thereby possibly cause a failure. A similar increase in heat flux for the ablation system would not be of great concern as long as this increase is not a continuous increase of sufficient magnitude to use more total material than available, including the allowed safety factor.

There are a number of areas on the vehicle for which heating evaluations are more prone to error than others; namely, the fin leading edges, flaps, and canopy. The local heating for these items (shown on Figure 30) are based on evaluations made using the best available data and from the local pressure estimates in these areas. It is noted that heating evaluation errors for these local areas will not have a significant effect on the total shield weight because of the relatively low weights of these particular items. The fin leading edge for the nominal 4534-Kg (10,000-lb) vehicle, for the re-entry velocity of 9144 m/sec (30,000 ft/sec), weighs between one and two percent of the total shield weight, depending on material and backface temperature. The flaps are somewhat heavier, but only amount to about four to six percent of the total weight for the same reference conditions. The portion of the canopy of major interest is the high heating area on the front face. Still, the weight of this section amounts to less than one percent of the total shield weight. An increase in the local heating in these areas will have a relatively small effect on the total shield weight. For example, if the local heating was found to be increased by 30 percent, the total shield weight would be affected by about 0.6 and 1.8 percent as a maximum for the fin leading edge and flap, respectively. The effect of this heating variation on the canopy would be even smaller. A reduction in heat flux would produce a similar reduction in the shield weight.

The application of the re-radiation system was based on a maximum surface temperature of $1255^{\circ}K$ ($1800^{\circ}F$) for René 41 and $1755^{\circ}K$ ($2700^{\circ}F$) for TZM. The employment of this heat protection system (Table 4) will depend not only on the surface temperature but upon the surface emissivity which influences the maximum allowable heat flux. A change in the value of emissivity from 0.80 to 0.65 (Table 1) would reduce the maximum allowable heat flux by about 18.8 percent. A comparison of the effect of this change in emmisivity on the most critical location of the re-radiation system is given as follows:

Critical Position of Re-radiation System
X/L

	Bottom	Top	Canopy	LE	Flaps	Fins	Rudder
			$\epsilon = .8$				
René 41	X	0.13	X	X	X	X	X
TZM	0.75	0.03	X	X	X	All	All
			$\epsilon = 0.65$				
René 41	X	0.16	X	X	X	X	X
TZM	0.79	0.04	X	X	X	All	All

Note: (1) Values in the table represent the position on the vehicle in terms of X/L.
(2) X designates not applicable for given material.

The location of the re-radiation system will change to a position somewhat further aft on the vehicle when the surface emissivity is lowered. The effect of this change of location on the total weight would be negligible. It is noted that the re-radiation weights were based on the most severe condition for an emissivity of 0.80. The effect of using TZM or René 41 on parts of the forward portion of the leeward surface depends on the specific abort or re-entry condition.

The effect on weight between the least severe and most severe condition is less than 0.3 percent of the shield weight, hence quite negligible. The weights given, therefore, are applicable to all booster conditions.

4.5.6 SAFETY FACTORS

The heat protection system weights were based on using a safety factor of 1.2. This safety factor has been used throughout the study to make the heat shield weights more realistic. A safety factor of 1.2 has been used on current re-entry vehicle systems employing various types of heat protection materials for a variety of different applications. The safety factor provides excess margin to account for unexpected variations in both the thermal environment and in the performance of ablation materials due to variations in the material properties. The safety factor is used on the degraded material and not on the insulation requirement.

The effect of safety factor on total shield weight is shown on Figure 107 for the nominal vehicle for re-entry velocity of 9144 m/sec (30,000 ft/sec). The shield weight, of course, will increase with an increase in safety factor. The maximum increase will be equal to the increase in safety factor but, in general, is considerably less as shown

in Figure 107. For example, a change from 1.2 to 1.5 in safety factor will increase the shield weight from about 10 to 23 percent, depending on the material and backface temperature. Similiarily, a reduction in weight will occur when the safety factor is decreased.

4.5.7 MATERIAL PROPERTIES AND PERFORMANCE

Of fundamental importance to the adequacy of the REKAP models used as the basis of the analysis in this program are the physical properties which are determined by laboratory experiment. The most important of these, from the viewpoint of heat shield performance and weight, are thermal conductivity, injected species specific heat and molecular weight, and decomposition kinetics.

At temperatures much above $589^{\circ}K$ ($600^{\circ}F$), the determination of these properties becomes significantly complicated by the ablative material change of phase and decomposition, thus making accurate property measurements difficult to obtain. Thermal conductivity values obtained by steady-state techniques differ by factors of 2 to 4 from transiently obtained values. This large transient vs. steady-state discrepancy was studied in the early portion of the program and resulted in the selection of transient conductivity values for the shield performance analysis.

The property values used for the simulation of the ESM shield are reasonably well-defined, and the REKAP model has been verified with numerous ground tests. The MPN properties are not nearly as well-verified, nor have tolerances on properties been established. It will be assumed that tolerances for MPN would be reasonably in accord with other materials such as PN.

4.5.7.1 Effects of Uncertainties in Thermal Conductivity

The change in shield weight for a factor of two increase in char reference thermal conductivity varies from a 7 percent increase for the hyperbolic entry mission to a maximum of 12 percent for the equilibrium glide mission (Reference 47). The standard deviation tolerances usually assigned to char measurements (steady-state and transient) of approximately ± 25 percent result in a two to three percent increase in thermal shield weight. Interestingly, a similar variation in both undecomposed, virgin material and char conductivity produces a much more significant increase in shield weight. It would appear that reasonable observed uncertainties in virgin, undecomposed plastic thermal conductivity give weight changes comparable to those for the observed uncertainties in char thermal conductivity. It should be emphasized, however, that 10 to 15 percent increases in thermal shield weight, resulting from the differences between steady-state and transient thermal conductivity, can produce a significant increase for an optimized thermal shield design.

78

The tolerance on conductivity for ESM ranges from ± 10 percent at low temperatures to ± 20 percent at higher temperatures. This results in less than a 5 percent variation in shield weight, as shown on Figure 108A. A similar 5 percent variation in weight would occur for the assumed MPN tolerance of ± 30 percent, as shown on Figure 108B.

The marked attenuation of the effect of large variations in char properties on thermal shield weight is primarily a result of the self-regulatory mechanisms of energy absorption from the boundary layer gas-char interface to the zone in the decomposition region where significant gas generation occurs. Small temperature increases in the decomposition region will result in a much increased gas evolution rate because of the exponential form of the decomposition phenomena. The decomposition region, then, can be visualized as a nearly constant temperature region for a given external energy flux. The temperature of this region represents a "pseudo" boundary condition for interior, or virgin, material heat conduction. Consequently, the char layer processes are uncoupled, to a significant extent, from the heat conduction process in the uncharred plastic. Also, the high conductivity of the char permits a considerable portion of the sensible heat stored in the char to be conducted back towards the boundary layer-char interface during the cool-down, or "soak" portion of the entry phase. It is then lost convectively to the lower temperature airstream.

4.5.7.2 Decomposition Kinetics

Thermogravimetric analysis data is used to describe the kinetics of decomposition of charring plastics. The TGA data is normally obtained over a wide range of heating rates, but the typical heating rates obtainable in the laboratory are comparable to glide entry rate, therefore the errors in this area should be very small and contribute only a negligible error to the total system.

4.5.7.3 Heat Capacity and Molecular Weight of Injected Products of Pyrolysis

The energy absorption resulting from gas product enthalpy, ΔH_g, was considered to be a second-order energy absorption mechanism for the entry considered (based on REKAP analysis); however, mass transfer accounted for blocking approximately 20 to 50 percent of the incident energy flux. Mass transfer effectiveness is dependent upon injected species molecular weight (specific heat). The effect on shield weight of uncertainties in molecular weight is shown on Figure 108C, which depicts a variation in molecular weight ratio to a factor of 2.5. A reasonable range of ratios would be from 1.5 to less than one. The former would result in a shield weight error of two or three percent, the latter would mean the shield is conservative by some percentage. The heat capacity (gas specific heat) variations seem to have very little effect on shield performance for a wide range of tolerances.

The importance of transition on the blocking effectiveness of these pyrolysis gases was studied to determine if errors in this area would have appreciable effects on the system design. Turbulent heating has resulted in a maximum increase of 10 to 20 percent in total heating. At the time transition occurs, approximately 20 percent of the convective heat is blocked. There does not seem to be any large variation in this figure between laminar and turbulent blocking. Therefore, any discrepancy resulting from the use of a laminar rather than turbulent blocking term should be small, and in view of the fact that only a maximum of 20 percent of the total heating is being discussed, the overall effect on the system should be negligible. In addition, it should be noted that the greatest part of the erosion and degradation processes has been completed prior to the occurance of transition. Therefore, small changes in heating from this point on will not appreciably change shield performance.

The main emphasis of this work has been conduction and gas properties; other material properties (e.g., material specific heat) were not treated because of the general acceptance of the values used or the insignificance of their effect on overall shield performance. It should be noted that the tolerances discussed for each material characteristic would, in general, be root sum squared together rather than summed, to give a total variation. This would give a total tolerance of not substantially higher than the greatest variation.

4.5.8 HIGH EROSION EFFECTS ON SHIELD PERFORMANCE

The effect of a high erosion condition on heat shield performance was studied, with particular emphasis on the resultant backface temperatures. Results from the study indicate that substrate performance is not substantially effected by a high erosion condition.

An analysis was made of the effects of instantaneous char removal, on MPN substrate performance in areas where no erosion is expected (environmental conditions for a 9144 m/s (30,000 fps) trajectory, low heating point). The results are illustrated on Figure 109. They show that the char removal does not have a substantial effect on the shield performance. There is some rise in backface temperature, but safety margins would more than compensate for the latter if such erosion were to occur.

The most evident result in the high erosion case is surface removal during the flight; this has a two-fold effect. First, it exposes lower shield layers to higher heating earlier in the trajectory. Second, it removes from the system the heat that was stored in the char (which was removed), and therefore it (the heat in the char) cannot contribute to substrate heating during soak-out.

The study indicates, in the low heating areas (areas where no or minimal erosion is predicted — a major part of the vehicle) with long soak-out periods, the removal of

char caused by shear, oxidation, or any other mechanism, would not substantially effect shield performance.

An analysis was made to determine if a composite ESM on honeycomb filled with microquartz system would provide weight benefits over an all-ESM shield for the M2-F2 lifting vehicle. This is a result of material performance studies in which it became evident, for the environments studied, that approximately 1.81 cm (0.75 in.) of ESM was undegraded and essentially served only as insulation. This amount of ESM was replaced with a 0.254 mm (.010 in.) sheet of fiberglass on top of various thicknesses of honeycomb filled with micro-quartz. It was found that 2.54 to 3.81 cm (1-1.5 in.) of honeycomb will provide the same insulation as the ESM with a weight saving of approximately 2.44 Kg/m^2 (0.5 lb/ft^2).

The honeycomb without a micro-quartz filler (air-filled) has essentially the same thermal properties (specific heat, conductivity) as the system with micro-quartz. Therefore, if various schemes were used to reduce the radiation in the honeycomb, or if only a minimum amount of microquartz was used as a radiation inhibitor, additional weight savings might be possible.

4.5.9 WEIGHT AND LENGTH VARIATIONS

The shield weight required was presented for the nominal conditions of weight and length. Variations of both weight and length off the nominal conditions will also affect the shield weight. The shield weight and length were varied from the nominal conditions for each of the re-entry trajectories for both ablation materials and backface temperatures. The effect of total vehicle weight on the shield weight is shown on Figure 110 for each of the pertinent conditions. It is clear that there is only a minor influence on the shield weight by total weight changes of ± 10 percent. A 10 percent total weight reduction reduces the shield weight by from about 1 to 4 percent, while a 10 percent increase in total weight increases the shield weight by about 1 to 5 percent, depending on the trajectory material and backface temperature. The weight change essentially changes the vehicle W/C_LA, which effects the local heating and therefore the shield weight requirements. A variation in vehicle length has a much greater effect on the shield weight as shown on Figure 111. A reduction of 10 percent in length will reduce the shield weight by about 10 to 18 percent, while a 10 percent increase in length will increase the shield weight by about 12 to 18 percent, depending on the trajectory, material, and backface temperature. The length variation for a given vehicle total weight effects both the W/C_LA and the vehicle surface area, both of which influence the shield weight.

4.5.10 ATTACHMENT METHODS

Figure 76 shows the percent of the total ablation system weights that are contributed by both the ablation material and the refurbishment technique. As can be seen, the refurbishment system contributes a small amount of the total weight; therefore, large errors in refurbishment weights will result in negligible errors in the overall weight of the heat protection system.

Figure 76 also shows the percent refurbishment for the combined vehicle of ablation plus René 41 and TZM re-radiation plus ESM over TZM re-radiation. It has been stated previously that the refurbishment weight for the re-radiation panels with or without the overlay of ablation will be the same, so that the example will be sufficient to show the percentage of refurbishment for all cases of re-radiative panels. Therefore, the percentage error in total heat protection weight will be negligible due to large errors in the weight of refurbishment for the refurbishment schemes used in the study.

4.5.11 YAW EFFECTS

The influence of yaw was investigated on the heat protection system weights. It was assumed that the vehicle would be subject to yaw oscillations of $\pm 5^{\circ}$ during the nominal flight. Operation at an angle of yaw will influence the local heat flux primarily on the side of the vehicle. The heating on the windward and leeward rays will essentially remain unchanged, as will the total heating at any point on the vehicle. The ablation system, therefore, will not be affected. However, yaw will limit the re-radiation application if the system is utilized to its full capability along the heat flux isoclines (Figure 29) which are essentially in an axial direction. From a practical standpoint, the re-radiation-system was limited in application to a position on the side of the vehicle dictated by the material's maximum capability on the windward ray (Table 4). Thus, yaw will have little practical influence on either the shield weights or the heat protection application specified in this study.

4.6 FUTURE WORK RECOMMENDATIONS

During the performance of the study it became obvious that additional work was required in specific areas to improve performance predictions necessary in the design of future lifting vehicles, such as the M2-F2.

4.6.1 TRAJECTORY ANALYSIS

Three major areas of trajectory analysis merit further investigation:
  (1) Abort escape from the booster blast propagation.
  (2) Footprints for the various re-entry maneuvers.
  (3) Terminal landing maneuvers for safe touchdown.

The abort system requires the capability of escaping the shock wave and fireball that could result from a catastrophic booster malfunction at any point on the ascent trajectory. The blast propagation, residual fuel energy, and abort system performance should be investigated as a function of altitude.

The footprints for the various re-entry flight modes, ranges of weight, and WC_LA should be investigated to determine landing site selection capability.

The achievement of a tolerable sink rate at touchdown is a fairly difficult problem for a relatively low-lift vehicle such as the M2-F2. A study should be made of the optimum landing maneuver with consideration given to the influence of vehicle design parameters such as L/D, $C_{L\,max}$, and W/C_LA. Consideration should also be given to uncertainties (such as altitude measurement) and their effect on landing safety.

4.6.2 AERODYNAMICS

The major difficulty in providing adequate aerodynamic information for the use of other disciplinary effort during this study was the lack of data on the specific M2-F2 vehicle configuration. The desired data can only be provided by extensively testing pressure models of the F2 configuration at flight representative conditions. These tests should include mass addition simulation, Schlieren photographic coverage, and a finer mesh of pressure taps to the canopy, upper surface, fin-body intersection, inboard and outboard fin surface, boattail, and control surface areas of the tunnel models. Additional testing of F2 force models is desirable, but is not as critically needed for heat shield design as the pressure information.

The possibility of generating heat shield data from flying test bed experiments for the M2-F2 vehicle should be investigated. Such data could markedly improve predictive accuracy on heat shield design and permit a lighter, more reliable configuration. Test-bed experiments to determine heat shield material capability have already been flown on the X-15 aircraft.

Test-bed vehicles designed primarily for material testing have been used successfully by GE-RSD for several years. The latest such GE-RSD proposal has the acronym SLAMAST, for $\underline{S}$cout $\underline{L}$aunched $\underline{A}$dvanced $\underline{M}$aterials $\underline{A}$nd $\underline{S}$tructures $\underline{T}$est-bed. It should be possible to either test full-scale M2-F2 panels on such a lifting re-entry vehicle or, alternatively, fly a sub-scale M2-F2 model with the SLAMAST internal subsystems.

Another area that will require future attention is that of possible windshield distortion, pitting, or fogging caused by deposits from products of ablation. The pilot must have a windshield as free as possible from such deposits so that he may clearly and reliably see terrain and runway in the process of a routine safe landing. Investigation of ablation products and their deposition may point to simple aerodynamic fixes that will ensure clear canopies for safe piloted landings.

In addition to the mandatory pressure tests and the desirable force tests, updating and upgrading the current pressure predictions should be continued by application of three -dimensional flow field theory, as well as comparison with configurations whose flow fields exhibit local similarities. As the results of new experimental work become available, the pressure predictions should be modified to include the effects of mass addition from the ablative process, the local effects of gaps, steps, and joints, and the changes dictated by more adequate definition of control surface and stabilizing surface pressures. The subsystem (environmental control system, structural loads, etc) requirements on vent locations and sizes may require detailed local assessments of pressure levels.

The recommended future aerodynamic work for the M2-F2 heat shield design is as follows:

(1) Test the M2-F2 model at a Mach number of ten or greater, the model having closely spaced pressure taps in the following areas:

    (a) Upper surface in the nose cap/canopy, canopy/body flat, fin/body, and control surface/boattail intersection areas.

    (b) Fin inboard and outboard surfaces from the leading edge back one-third the local chord and at several spanwise locations.

    (c) Control surface edges and near-edge locations.

The model should have moderately spaced pressure taps in those flat upper surface areas and lower surface boattail areas not covered by the closely spaced taps, and widely spaced taps over the lower nose cap and conically wrapped surface areas.

(2) Mass-addition effects should be simulated on a M2-F2 model either separately or in combination with the tests envisioned in (1). Schlieren or shadowgraph photographic records should be considered a necessary part of the test data.

84

(3) Continue force tests of the M2-F2 shape to better define the aerodynamic force and moment characteristics throughout the expected flight ranges of Mach number and altitude.

(4) Employ available analytical tools, such as three-dimensional flow field theory, for analyses of the M2-F2 configuration to better define vehicle characteristics, particularly where test data is either unobtainable or inconclusive.

(5) Consider body-fin and other interaction zone testing through use of the Malta, or other comparable, facility.

(6) Initiate a feasibility study of test-bed design and experimentation directed toward higher confidence levels in heat shield design for selected materials.

(7) Consider an aerodynamic investigation into the problems of ablation product contamination of windshield, vent, control gap, and other critical surface areas.

4.6.3 HEATING EVALUATION

The thermal protection requirements are largely a function of the heating. Therefore, it is highly recommended that additional work be done to obtain a better definition of the thermal environment over the vehicle for the conditions of prime interest. Detailed thermal distributions, such as obtained by thermal sensitive paint techniques, should be obtained for a variety of angle-of-attack and yaw conditions. Test conditions should include angles of attack of 0 to 40 degrees and yaw angles of 5 and 10 degrees.

Both laminar and turbulent flow conditions are required to obtain the desired heat flux distributions. Special emphasis should be placed on the heat flux contours and the high heating interaction areas over the vehicle.

In order to obtain a better definition of the heating on the leeward surface, fins, flaps, canopy, and interaction areas, quantitative tunnel tests with sufficient instrumentation should be run at various Mach number and Reynolds number conditions. Photographs should be made to establish the flow field definition, with such tests covering a range of angle-of-attack and yaw conditions that would include both laminar and turbulent flow conditions for the M2-F2 configuration, with and without a canopy.

Considerable effort is being expended on transition from laminar to turbulent flow, including the Re-entry F flight experiment sponsored by NASA Langley Research Center. The problem is complex, due to the large number of variables (wall cooling, roughness, mass addition, angle of attack, etc.) that appear to be important. This work should continue and is directly applicable to lifting vehicle application.

4.6.4 HEAT PROTECTION SYSTEM

The heat shield weights evaluated for the various heat protection systems, re-entry conditions, and vehicles were based on the best estimated performance properties of the systems involved. The ablation systems are dependent on the ablation material performance. The performance of ESM is fairly well established, but there is a lack of information avaiable for MPN. A number of performance tests should be made on MPN at various facilities to obtain actual performance data by instrumented models for a variety of heating rates, enthalpy levels, and shear levels for various conditions of total time. The MPN requires gaps for expansion over the vehicle surface. The performance of the MPN in the gap region must also be evaluated.

Areas, pertaining to re-radiation systems, requiring further analysis are maximum surface temperature sensitivity, coatings, and the effect of discontinuities. Additionally, the use of microquartz (Dyna Quartz) at high temperature conditions, active cooling system relaibility, and proper use of air gaps and construction techniques, are all items that must be further studied for design optimization. In this regard, the latter could concern such items as air gaps near the re-radiation material (rather than next to the backface), several air gaps in series, filling air gaps with extremely lightweight materials to inhibit substructure radiation, and double wall construction.

The ablation over re-radiation sytem is quite attractive for the low backface temperature shield. This system relies on the ablation material to provide the necessary protection until the re-radiation material can be used. The actual performance of the various ablation materials and the bonds to this application are of prime importance. A number of performance tests must be made to determine the adequacy and the design requirements for the system. Special emphasis should be placed on the thin coatings of ablation material over the re-radiating surface. The performance of the ablating material and the effect on the re-radiating surface, especially the TZM coating, must be evaluated.

The methods used in joining adjacent heat protection systems, is an area needing intensive investigation. Passive-type joints between two dissimilar systems should be tested to determine the adequacy and requirements for a realistic design. Joint configurations that adapt to the surface contour (active joints) may be required. The gaps required at hinges and between adjacent hot structures must also be tested to evaluate their adequacy.

The use of a composite type of ablation system consisting of a variety of ablation materials in depth was discussed in section 4.3.2.1.1.3. ESM is ideally suited to composite application (graded properties in depth). A number of such ESM Composites have been tested. A composite of PN and MPN could also be produced but with much greater difficulty. Composites with different base materials may offer special advantages, but a suitable bond must be developed for these composite systems. Analytical and experimental studies should be made to further explore composite heat protection systems characteristics.

4.6.5 MATERIALS

4.6.5.1 Metallic Materials

One heat protection system concept that should be investigated is the combined ablator over re-radiative panels in which the ablator would provide protection during early re-entry (high heat flux) while the re-radiative elements functioned during the longer, low-heat-flux portion of the flight. Optimization of such a system is dependent on a number of design-limiting factors such as the requirements of complete removal of the spent ablator and spread of temperatures of ablator bond and re-radiative panel operating temperatures. The system in its simplest form would consist of a layer of ESM 1004 bonded to the structure on re-radiative panels with RTV 560. Local ablator thickness would be a function of heat load, and re-entry heating would result in removal of spent ablator at a certain point in the trajectory. Since ablation may be non-uniform over portions of the vehicle, this system would be limited to those applications where surface irregularities resulting from incomplete removal of the ablator would not adversely affect boundary flow conditions.

Positive control of ablator removal could be achieved by several methods. One simple mechanical means would require the introduction of a thin layer of a high-modulus metal such as beryllium between the ablator bond and the structure skin. An explosive device could be actuated to open the heat protection composite into a petal configuration at the forward portion of the vehicle. The whole components would then be cleanly stripped from the vehicle exposing the re-radiative surface.

Another concept has been tried in the laboratory. Magnesium foil was bonded to a thin 0.788 mm (0.031 in.) strip of 6061 aluminum using RTV 560. ESM 1004 was bonded to the 0.153 mm (0.006 in.) magnesium foil with RTV 560. One edge of the ablator and attached magnesium foil was peeled from the aluminum and loaded with a small weight to permit access of air heated by an oxy-acetylene torch. The magnesium foil ignited and burned, completely destroying the bond holding the ablator to the aluminum strip. Heat of combustion of the foil was so small that the aluminum was undamaged. The reaction could be initiated by an explosive ring device located immediately behind the nose cap. This would push the leading edge of the ablator composite into the slip stream. The high temperature capability of either Rene 41 or TZM would make this concept completely feasible, in view of the experience with aluminum. Further investigation of these and other concepts are required before this system can be used.

Another field for development is in the realm of extended capability adhesives or the use of metallic deposits deposited on the re-radiative panels or vehicle structure. The metals could be selected on the basis of melting temperatures, and the flame-sprayed metallic substrate for the ablator bond would be removed without leaving any residue when the melting point of the metal was reached.

4.6.5.2 Plastic Materials

The following additional work is recommended on the candidate ablative and attachment material systems, assuming that sufficient potential has been shown for each one from the analytical study. The rationale for this effort was included in the discussion of each of the material systems.

(1) MPN

    (a) Definition of the fabrication technique for producing full-scale vehicle sections.

    (b) Generation of design data for analysis on representative samples.

    (c) Cost estimate based on the defined fabrication process.

    (d) Develop bonds for high temperature application.

(2) ESM

    (a) Selection of optimized ESM formulation to specific body station requirements.

    (b) Define production application of spray ESM.

    (c) Evaluate performance at nose and leading edge areas. Select other candidate materials for these areas and compare performance.

    (d) Develop bonds for high temperature application.

(3) Refurbishment Attachment Systems

    (a) Define production fabrication technique for:

        - Elastomeric-pillars and Nut-and-Bolt with MPN.
        - Loop-and-pile with ESM.

    (b) Generate thermo-mechanical design data for each of the selected attachment systems for the applicable shield material.

    (c) Conduct trade-off analysis and select best attachment system(s) for each shield material.

(4) Special Application Areas

    (a) Select, define, and generate thermo-mechanical data on sealant material for joints and gaps with MPN.

    (b) Define most promising technique for access panel attachment for each shield material.

(c) Develop and define technique for thermal protection of control surface gaps for each shield material.

(5) Jointure of Ablative and Re-radiative Thermal Protection Systems

(a) Define fabrication technique for each of the proposed methods.

(b) Qualify the techniques in a simulated re-entry thermal environment.

(6) Test Vehicle

After previous studies are completed, select most promising systems, fabricate and apply to a recoverable instrumented re-entry test vehicle, conduct flight test, qualify systems, and analyze performance against analytical and ground test data.

4.6.6 STRUCTURES

As was discussed in Section 4.3.4, the main structural interest in obtaining the optimum heat protection system is the determination of the optimum backface temperature that will result in the minimum weight of the sum total of the shield plus the substructure. As the backface temperature is increased to 644°K (700°F), the weight of the shield decreases and the weight of the structure increases because of the reduction in mechanical properties. To determine the optimum heat protection system, it is recommended that an integrated study be made including both the shield and the substructure over a wider range of backface temperatures than used in this study. A range in temperature from about 366°k (200°F) to 810°k (1000°F) should cover the region desired so that an optimum may be established. The temperature variation should be investigated, both uniform value and as a variable over the portions of the vehicle.

4.6.7 SHIELD OPTIMIZATION

The extension of the shield performance analysis beyond the material and environmental constraints for this study would be useful from a shield optimization standpoint. The applicability of the M2-F2 configuration to other missions would also be determined. The most promising area for optimization is the shield-structure trade-off with backface temperature, as mentioned in Section 4.6.6. This trade-off would not only establish the optimum operating backface temperature for minimum weight for a passive system but also for active cooling schemes. In addition to internal active cooling, the use of transpiration cooling during specific portions of flight and on local areas of the vehicle may also show a weight advantage for the system. The transpiration cooling system could be either active or passive, depending on the local application.

The data obtained from the model testing suggested in Section 4.6.3 would aid in the determination of weight penalties for performing a wide range of missions which differ from those in this study. The study should include both terrestrial and extra-terrestrial missions. The latter appear to be a relatively minor problem for a planetary atmosphere such as Mars (Reference 49) but would be of interest for Venus, Mercury, and Saturn. There is interest in using the same shield for use in planetary entry and then using it again during earth entry. The REKAP program is compatible with this multiple use requirement.

5. CONCLUSIONS

This study was made to evaluate the heat protection system weights for lifting vehicles having a moderate L/D for a variety of weights and sizes. These vehicles would be capable of re-entry at a variety of flight entry velocities, after launch from a number of boosters, and would also be capable of abort. A variety of heat protection systems were considered consisting of a number of different materials and several backface temperatures.

The boosters considered included Titan II, Titan III-C, and Saturn I-B. The re-entry trajectories included one subcircular and two supercircular velocities; namely, 7468, 9144, and 10,363 m/sec (24,500, 30,000, 34,000 ft/sec). The nominal vehicle sizes varied from 6.71 to 9.14 m (22 to 30 ft) and 3172 to 6804 kg (7000 to 15,000 lb). The basic lifting body used in the study was the M2-F2 NASA configuration. Heat protection systems included ablation; ablation plus re-radiation; and ablation, re-radiation, and ablation over re-radiation. The materials included an elastomeric shield material (ESM) and microballoon phenolic nylon (MPN) for the ablation material, a super alloy (René 41), and a refractory alloy (TZM) for the re-radiation system, and micro-quartz and foamed-pyrolytic graphite for insulation of the re-radiation systems. The heat protection system weights were evaluated for backface temperatures of 422 and 589°K (300 and 600°F).

Trajectories were obtained for the wide variety of vehicle sizes and weights for both re-entry and abort conditions of interest. The flow fields and pressure distributions were determined over the entire vehicle at various angles of attack. The heat flux distribution was determined by reference enthalpy methods for both laminar and turbulent flow, as required. The methods employed in the study have been used extensively in re-entry vehicle design. Transition criteria for the critical Reynolds number was determined as a function of local Mach number. Transition occured at the very end of the flight and was included in the analysis.

Model tests were run at Rhodes and Bloxom to obtain the heat transfer distribution at 30 degrees angle of attack. The heating evaluation clearly showed that the convective heating during re-entry and abort was most critical. The heat protection system requirement was established by a Reaction Kinetics Ablation Program (REKAP) analysis for both ESM and MPN. The REKAP model has been well-established for ESM and was adapted to MPN. Demonstration of its prediction capability of degradation and erosion is described in the Appendix.

The heat protection system weights were dependent on both the re-entry and abort trajectories. The application of the ablation system was essentially based on the re-entry trajectories that imposed the highest total heating (greatest shield requirement), while the re-radiation system application was primarily limited by the critical abort flights that imposed the highest heat flux. The ablation over re-radiation system

weight was based on both re-entry and abort. The minimum ablation thickness for this system was imposed by the abort, while the higher total heating capability was determined by re-entry. The heat protection requirements were determined primarily for the three trajectories used as nominal typical flight paths with three basic phases (pull-out, constant altitude, and equilibrium glide). The nominal supercircular flights were based on the overshoot boundary. The subcircular flight was investigated for several variations; those requiring the heaviest heat shield were used in the study (constant altitude phase to L/D max). Flights with a constant altitude phase to C_L max showed appreciably lower total heating and therefore lower shield weight requirement. Operation at bank angle with C_L max will produce a still lighter shield requirement.

The shield weights, based on a safety factor of 1.2, vary from about 8 to 25 percent of the total vehicle weight for the conditions examined. The major influence on the shield weight requirement was the backface temperature. For the low backface temperature condition of $422^\circ K$ ($300^\circ F$), the all-ablation type heat protection system requires about 17 to 25 percent of the total vehicle weight. Of the two ablation materials investigated, MPN requires somewhat less weight than for the ESM all-ablation system. The TZM material, using a maximum allowable temperature of $1755^\circ K$ ($2700^\circ F$), requires a shield of less weight than that for Rene 41 (maximum temperature $1255^\circ K$ ($1800^\circ F$)). The combined ablation, re-radiation, ablation over re-radiation system requires the lowest weight shield.

The comparison of weights for the higher backface temperature $589^\circ K$ ($600^\circ F$) shows the opposite trend. The high backface temperature reduces the ablation system requirements considerably. The ablation shield is by far the lightest and consists of about 8 to 17 percent of the total vehicle weight. The heat shield using ESM material is considerably lighter than that using MPN. The systems using re-radiation and ablation over re-radiation show higher weights than the ablation system.

The heat shield systems were all refurbishable. The weight penalty associated with refurbishment varies from about 3 to 12 percent, depending on the material, system, backface temperature, and application. The refurbishment system for the all-ablation ESM system can use the perforated scrim approach for all applications and tape for the lower backface condition. The MPN ablation material requires the elastomeric-pillar system. The maximum refurbishment system weight requirement for ESM is about 58 percent of that for MPN and about 66 percent of that for the re-radiation system using rods and clips. The ease of refurbishment is clearly reflected in the cost estimate for these typical systems. A typical cost (rough estimate) of the ESM ablation system for the nominal 4536-kg (10,000-lb) vehicle will be about $85,000 for the 808-kg (900-lb) shield and $175,000 for the 1070-kg (2285-lb) shield. A comparable cost of the MPN system is estimated at about $420,000 to $530,000 for the similar shields.

The heat protection system study shows that for the application intended, the local heat flux is sufficiently high that ablation must be used for specific portions of the vehicle (nose, flaps, fin leading edge, canopy, etc). Although re-radiation may be used for some portions of the vehicle, this system exhibits a high sensitivity to changes in the flight path. The ablation system has more versatility and shows definite weight saving for the higher backface temperature condition. The ESM material, besides being less expensive, has a definite advantage not only in manufacture and refurbishment but is more adaptable to cold-soak and has thermal expansion compatability with the structure. MPN is generally limited to about 150°K (-190°F) cold-soak and requires local expansion gaps over the vehicle. ESM has no such limitation.

The ablation-type heat protection system selected is considered to be the most reliable at the present time. The use of the materials, the manufacture, and repair are such as to present us with the utmost confidence in this system for the intended application. The re-radiative system, which can be used for only part of the vehicle, has the basic limitation of being sensitive to local heat flux which is closely dependent on the flight path requirements. The coatings required for TZM make the handling and re-use capability of special concern. The re-radiation heat protection system can use passive or active cooling. The passive system is more reliable but it requires greater shield thickness and greater shield weight than the active system. The active (closed loop) system utilizes pumping equipment, heat exchanger and coolant (ethylene-glycol water solution) which is cooled in a boiler and the steam generated is discharged over board. The active cooling system used in conjunction with an air gap is desireable from a weight standpoint but requires somewhat greater shield thickness. The use of microquartz for insulation, compared to foamed-pyrolytic graphite, shows a weight advantage of about 5 percent. The ablation over re-radiation system for low backface temperature applications appears very attractive. The relatively clean removal of the outer ablation layer and its effect on the coating for TZM is of some concern for the proper application of this system. The necessity of an active cooling system with the re-radiation system adds somewhat to its complexity and reduces its reliability.

The error analysis considered for this study indicates that the weight evaluations may be considered reasonable for the intended application. Individual variations in the various aspects of the study can be readily evaluated in terms of heat shield weights. Future work recommendations have been established for this application in each of the major technical areas.

The study shows the advantage of higher backface temperature design. About 24 percent of the vehicle weight represents the shield at the low backface temperature of 422°K (300°F), which can be lowered to about 8 percent when the temperature is raised to 589°K (600°F) for ESM. It is further suggested that in special areas such as the fins, flaps, and aft section of the vehicle (away from the pilot area), the local backface temperature be increased to even higher values through the use of structures such as beryllium or boron fibers which will further reduce the shield weight.

6. REFERENCES

1. Hiatt, E., "Aerodynamics of Space Flight," Astronautics Vol. 4, No. 2, Feb. 1959, Pg. 24-25.

2. Brunner, M., and Barté, G.R., Jr., "Study of Thermal Protection Requirements for a Lifting Body Entry Vehicle Suitable for Near Earth Missions," Auxiliary Final Report, GE TIS 66SD254, May 12, 1966.

3. Dewees, L., "Re-entry Vehicle Design Program," GE TIS R59SD391, July, 1959.

4. Logan, J., and Treanor, C., "Tables of Thermodynamic Properties of Air From 3000°K to 10,000°K," Cornell Aeronautical Laboratory Report No. BE-1077-4-3, Jan. 1957.

5. Dewees, L., "Afterbody Design Program," GE TIS R59SD393, July 1959.

6. Shaw, T., et al, "Final Summary of Aerothermydynamic Analysis Mark 2 Data," GE TIS R60SD481, Jan. 1961.

7. Kivel, B., and Bailey, K., "Tables of Radiation from High Temperature Air," Res. Rept. 21 (Contracts AF04(645)-18 and AF49(638)-61), AVCO Res. Lab., Dec. 1957.

8. Breene, et al, "Radience of Species in High Temperature Air," GE TIS R53SD3, June 1963.

9. Brunner, M., Dohner, C., Langelo, V., and Rie, H., "Flow Field Prediction and Analysis — Project FIRE," NASA CR-60451, GE 64SD727, May 1964.

10. Moyer, R., "Heat Transfer at Angle of Attack for Conical Bodies," GE Thermodynamics Fundamentals Memo. No. 015, July 1963.

11. Heins, A., and Estes, T., "Effect of Angle of Attack on Laminar Convective Heat Transfer for Sharp and Blunt Bodies," GE TIS 61SD70, April 1961.

12. Haviland, R., "Handbook of Satellites and Space Vehicles," D. VanNostrand Co., Inc., New York, 1965, Pg. 354 - 374.

13. Saydah, A., "Presentation and Analysis of Heat Transfer Data Obtained in Support of the Maneuvering Re-entry Vehicle Study (DA85)," TDM-8151-012, July 18, 1963.

14. Rennika, A., "Analysis of Wind Tunnel Data on the MBRV Configuration," August 1964.

15. Shaw, T., and Nestler, D., "Heat Transfer and Ablation Phenomena in the Interaction Zones of Fin-Body Configurations in Hypersonic Flow," GE Aerophysics Technical Memo 198, April 1961.

16. Probstein, R., and Kemp, N., "Viscous Aerodynamic Characteristics in Hypersonic Rarefied Gas Flow," J A/S Sciences, Vol. 27, No. 3, March 1960, Pg. 174 - 192.

17. Hayes, W., and Probstein, R., "Hypersonic Flow Theory," Academic Press, New York, 1959.

18. Ferri, et al, "Heat Transfer at Hypersonic Speeds and Low Reynolds Numbers," JAS Vol. 21, Pg. 130, 1954.

19. Van Dyke, M., "Higher Approximations in Boundary Layer Theory," J. Fluid Mech., V. 14, 1963, Pg. 161ff and 481ff.

20. Roth, N., and Lenard, M., "Vorticity Effect on Stagnation Point Flow of a Viscous Incompressible Fluid," JAS 1959, Vol. 26, No. 8, Pg. 542.

21. Maslen, S., AIAA J. Vol. 1, 1963, Pg. 33.

22. Davis, R., and Flugge-Lotz, Int. J. of Heat and Mass Transfer, Vol. 7, 1964, Pg. 341.

23. Hickman, R., and Giedt, W., AIAA J. Vol. 1, 1963, Pg. 665.

24. Van Dyke, M., "Rarefied Gas Dynamics - Supplement 2," Vol. 2, Academic Press, New York, 1963, Pg. 212.

25. Ferri, A., Zakkay, V., and Tung, L., "Blunt Body Heat Transfer at Hypersonic Speed and Low Reynolds Number," JAS Vol. 28, Pg. 962, No. 12, Dec. 1961.

26. Hecht, A., Personal Communication.

27. Larson, H., "Heat Transfer in Separated Flows," JAS Vol. 26 No. 11, Pg. 731 - 8, Nov. 1959.

28. Dolan, C.M., Axelson, J.S., and Curtis, F.P., "Development of Elastomeric Thermal Shield Materials (ESM 1000) for Satellite and Space Vehicle Re-entry Vehicles," Plastics Technology TIS Report No. 64SD225, March 5, 1964.

29. Dolan, C.M., "Study for Development of Elastomeric Thermal Shield Materials," NASA CR-186, March 1965.

30. Fehl, C.J., "Recommended Machining Procedure for ESM." Plastics Technology PIR 8158-1212, October 19, 1964.

31. Dow, M.B., and Brewer, W.D., "Performance of Several Ablation Materials Exposed to Low Convective Heating Rates in an Arc-Jet Stream," NASA TN D-2577, January 1965.

32. Chapman, A.J., "An Experimental Evaluation of Three Types of Thermal Protection Materials at Moderate Heating Rates and High Total Heat Loads," NASA TN D-1814, July 1963.

33. Peters, R.W., and Wadlin, K.L., "The Effect of Resin Composition and Fillers in the Performance of a Molded Charring Ablator, NASA TN D-2024, Dec. 1963.

34. Dow, M.B., and Swann, R.T., "Determination of Effects of Oxidation on Performance of Charring Ablators," NASA TR R-196, June 1964.

35. Chapman, A.J., "Effect of Weight, Density, and Heat Load on Thermal Shielding Performance of Phenolic Nylon," NASA TN D-2196, June 1964.

36. Clark, R.K., "Effect of Environmental Parameters on the Performance of Low Density Silicone-Resin and Phenolic-Nylon Ablation Materials," NASA TN D-2543, January 1965.

37. Wilson, R.G., "Thermophysical Properties of Six Charring Ablators from 140° to 700°K and Two Chars from 800° to 3000°K," NASA TN D-2991.

38. Florence D., "Development of an ESM 1001 PS REKAP Model," Thermodynamics Technology Component Technical Data Memo. No. 8151-040, Dec. 1964.

39. Brunner, M.J., "Phenolic Carbon Heat Protection System Requirements for Ballistic and Maneuvering Applications," GE - RSD TIS 65SD252, May 17, 1965.

40. Wichorek, G.R., and Stein, B.A., "Experimental Investigation of Insulating Refractory Metal Heat Shield Panel," NASA TN D-1861, Dec. 1964.

41. Cline, P.B., "Internal Structure Cooling System for Lifting Re-entry Vehicles," Thermodynamics Technology Component PIR-8151-560, April 18, 1966.

42. Rizzo, J., and Merlo, G., "Potential Interface Concepts — Lifting Body Entry Vehicles," Structural Mechanics PIR-8156-AA5-1992, April 7, 1966.

43. Wichorek, G.R., and Stein, B.A., "Experimental Investigation of Insulating Refractory-Metal Heat Shield Panels," NASA TN D-1861, Dec. 1964.

44. Wilson, R.G., "Thermophysical Properties of Six Charring Ablators from 140° to $700^\circ K$ and Two Chars from 800° to $3000^\circ K$," NASA TN-2991, Oct. 1965.

45. Myskowski, E., Unpublished Test Results, Composite System Operation.

46. Stewart, J.D., and Bloom, H.L., "Refurbishable Thermal Shields for Lifting-Entry Vehicles," ASSET/Advanced Lifting Re-Entry Technical Symposium, Dec. 1965.

47. Shaw, T.E., Garner, D., and Florence D., "The Effect of Uncertainties in Thermophysical Properties on the Ablative and Insulative Efficiency of Char-Forming Materials in Intense Convective and Radiative Heat Transfer Environments," AIAA Paper No. 65-639, September, 1965.

48. Kratsch, K., Hearne, L., and McChesney, H., "Thermal Performance of Heat Shield Composites During Planetary Entry," AIAA Meeting, Oct. 1963.

49. Brunner, M.J., "Mars Excursion Module Study," Doc. No. 65SD918, Oct. 12, 1965.

50. NASA/Ames Specification for "A Study of Thermal Protection Requirements for a Lifting Body Entry Vehicle Suitable for Near-Earth Missions," Spec. No. A-9758, Feb. 1965.

51. Dolan, C.M., Edighoffer, H.H., Cline, P.B., and Reinecka, E.A., "Elastomeric Thermal Shield Systems for Lifting Re-entry Vehicles," AIAA Sixth Structures and Materials Conference, April 5, 1965.

52. Brazel, J., Tanzilli, R., and Begany, A., "Determination of the Thermal Performance of Char Under Heating Conditions Simulating Atmospheric Entry," AIAA Paper 65-640, Sept. 1965.

53. Brazel, J., "Transient Determination of Thermal Conductivity of a Low-Density Phenolic Nylon Char," Final Report NASA Contract L-2979, July 1965.

7. APPENDIX

7.1 SAMPLE ABLATION ANALYSIS (GROUND AND FLIGHT TEST)

Thermodynamic analysis was made of the ground and flight test for the microballoon phenolic nylon (MPN) for the two following test conditions:

(1) Ground test

heat flux = 141.5 w/cm^2 (125 Btu/ft^{2}sec)

enthalpy = 23.2 KJ/g (10,000 Btu/lb)

time = 60 sec.

(2) Flight test

flight path (Reference 50)

max heat flux = 795 w/cm^2 (700 Btu/ft^2-sec)

The analysis utilized the Reaction Kinetics (REKAP) and Ablation Design Computer programs.

The conduction properties for the virgin material are well established (References 37, 50). The char conductivity based on transient conditions is shown on Figure 112A as a function of temperature. As shown, the transient conductivity is considerably lower than the steady-state values but more realistic for utilization in the reaction kinetic analysis of charring ablation materials (Reference 52). The transient values were based on recent GE tests for NASA-Langley (Reference 53). The specific heat is shown on Figure 112B for the material and on Figure 112C from the TGA data as a function of temperature (Reference 50). The pyrolysis gas properties shown on Figure 112B as a function of temperature are based on information from phenolic nylon and are believed applicable to the MPN material. The emittance data is shown on Figure 112D (Reference 50). The NASA data has been utilized throughout the study for the MPN material except as specifically noted.

The thermodynamic performance of the ground test sample is illustrated by the degradation and erosion shown on Figure 113 and the temperature distribution shown on Figure 114 as a function of time. The degradation is shown for the amount of material charred to a density less than 95 percent virgin density. The degradation calculated was about five percent higher than tested and the erosion calculated was about 13 percent higher than tested. It is noted that, since only one test (NASA) was run for this case, the comparison cannot necessarily be called representative because of the lack of statistical

data. In any case, however, the calculated degradation and erosion appears somewhat conservative. The maximum surface temperature calculated is about 30 percent lower than tested. This considerable difference may be due either to a local test facility characteristic or to measurment difficulties. It has been the general characteristic of the usual REKAP analysis to slightly overpredict the subsurface and backface temperature as determined by measurements usually more reliable than surface temperature. It is believed that the subsurface and backface temperature calculations are representative of actual test conditions.

The flight test heat flux is shown on Figure 115 as a function of time. The performance of the material is also shown on Figure 116 as a function of time. The temperature is shown on Figure 116 for various locations beneath the surface. The degradation and erosion during flight are shown on Figure 117 as a function of time. The calculations indicate that about 1.66 cm (0.66 inches) of material will degrade and about 1.31 cm (0.515 inches) of material will erode for the flight condition of interest. At the present time no flight tests have been made for these conditions.

7.2 GROUND TEST MATERIAL PERFORMANCE

REKAP analyses were conducted in order to calculate phenolic nylon (PN) performance for three ground test conditions.

The material and local laminar conditions studied were:

Phenolic Nylon 1.2 g/cm^3 (75 lb/ft^3)

(a) Condition I

1.	Enthalpy	9.280 KJ/g	(4000 Btu/lb)
2.	Nose radius	44.5 mm	(1.75 in.)
3.	Heating rate (cold wall)	908 w/cm^2	(800 Btu/ft^2-sec)
4.	Pressure	2.62 atm	
5.	Material thickness	2.54 cm	(1.00 in.)
6.	Duration of heating	30 sec	
7.	Heating rate (combust)	284 w/cm^2	(250 Btu/ft^2-sec)

(b) Condition II

1.	Enthalpy	23.200 KJ/g	(10,000 Btu/lb)
2.	Nose radius	6.35 cm	(2.50 in.)
3.	Heating rate (cold wall)	152 w/cm^2	(134 Btu/ft^2-sec)
4.	Pressure	0.021 atm	
5.	Material thickness	1.9 cm	(0.75 in.)
6.	Duration of heating	60 sec	
7.	Heating rate (combust)	102 w/cm^2	(90 Btu/ft^2-sec)

(c) Condition III

1.	Enthalpy	7.150 KJ/g	(3080 Btu/lb)
2.	Nose radius	9.5 mm	(0.375 in.)
3.	Heating rate (cold wall)	184 w/cm^2	(162 Btu/ft^2-sec)
4.	Pressure	0.045 atm	
5.	Material thickness	1.52 cm	(0.60 in.)
6.	Duration of heating	25 sec	
7.	Heating rate (combust)	68 w/cm^2	(60 Btu/ft^2-sec)

The results of the analysis are depicted in graphical form on Figure 118 through 128. The data is presented for the conditions listed above, with and without combustive heating. The values used for the combustive heating are only representative of possible heating levels and are shown to indicate the effect of this mechanism on material performance.

The ablation and degradation histories for each of the above conditions are shown on Figures 118 and 119, respectively. They depict an essentially linear increase in degradation and erosion with time which ends at the termination of heating (i.e., no appreciable degradation appears during soakout). The addition of combustion heating causes from 0.508 to 1.524 mm (20 to 60 mils) of additional degradation. This is about twice the effect produced for the erosion 0.254 to 0.762 mm (10 to 30 mils). A comparison between conditions I, II, and III shows the increase in degradation and erosion due to high heating in condition I and the effect of the high enthalpy (condition II) in depressing the erosion and degradation rates by increasing the blocking effectiveness of the pyrolysis gases.

The temperature and density profiles (Figures 120 to 128) are typical of phenolic nylon test results, showing relatively narrow reaction zones.

The effects of combustive heating are most dramatically demonstrated by surface temperatures shown on Figures 126 through 128. They illustrate the 278 to 556°K (500 to 1000°R) increase in surface temperature due to combustion heating.

It should be noted that the erosion characteristics are based on the recommended erosion criteria used for the program, which was determined from ground and flight test data. The use of different erosion characteristics (which, though different from the criteria might fall well within the substantial scatter of the test data) will profoundly effect other material performance parameters (e.g., degradation depths).

TABLE 1. TYPICAL PROPERTIES OF RENE 41 AND TZM

	TZM	René 41
Emittance (A)	0.80	0.80
(B)	0.65	0.65
Tensile Yield Strength x 10^{-3} KN/m^2 (lb/in^2)	13.7 (20)	20.7 (30)
Young's Modulus x 10^{-6} KN/m^2 (lb/in^2)	10.3 (15)	13.7 (20)
Density g/cm^3 (lb/ft^3)	10 (624)	8.11 (506)
Coefficient of Expansion x 10^6 $^{\circ}K$ ($^{\circ}R$)	5.4 (3)	16.2 (9)
Elongation (%)	40	25

(A) Pre-oxidized Matte finish

(B) Typical Operational Value

TABLE 2. REFURBISHMENT SYSTEM WEIGHTS

	Refurbishment Technique	Design Backface Temp. $^\circ K$ ($^\circ F$)	MPN	Shield Material Kg/m^2 (lb/ft^2) ESM Sheet	ESM Spray
1.	Elastomeric Bond	589 (600)	N.A.*	0.366 (0.075)	0.000
2.	Perforated Scrim	589 (600)	N.A.	0.488 (0.100)	0.122 (0.025)
3.	Nut and Bolt	589 (600)	0.537 (0.011)	0.537 (0.011)	N.A.
4.	Elastomeric Pillars	589 (600)	1.13 (0.232)	0.766 (0.157)	N.A.
5.	Hi-Temp. Loop & Pile	589 (600)	N.A.	4.94 (1.012)	4.57 (0.937)
6.	Mid-Temp. Loop & Pile	422 (300)	N.A.	2.83 (0.581)	2.47 (0.506)
7.	Mystic Tape No. 7000	422 (300)	N.A.	0.674 (0.138)	0.307 (0.063)

*N.A. - Not Applicable

TABLE 3. MINIMUM ABLATION THICKNESS FOR COMBINED (ABLATION OVER RE-RADIATION) SYSTEM FOR MAXIMUM CRITICAL ABORT APPLICATION
(Saturn I-B, L/D max)

V_E Condition m/sec (ft/sec)	Ablation Material	Required Thickness* mm (in.)
10,363 (34,000)	ESM	0.356 (0.014)
	MPN	0.254 (0.010)
9144 (30,000)	ESM	2.16 (0.085)
	MPN	1.53 (0.060)
7468 (24,500)	ESM	1.91 (0.075)
	MPN	1.35 (0.053

*TZM Re-Radiation Material

TABLE 4. HEAT PROTECTION SYSTEM APPLICATION - RE- RADIATION

		Bottom (X/L +)	Top	Canopy	L.E.	Flaps	Fins	Rudder

Abort Conditions

1. L/D Max

A. René 41

		Bottom (X/L +)	Top	Canopy	L.E.	Flaps	Fins	Rudder
Titan II	max. $W/C_L A$	0.74	0.07	X	X	X	All	All
	min. $W/C_L A$	0.66	0.045	X	X	X	All	All
Titan III-C	max. $W/C_L A$	0.82	0.11	X	X	X	All	All
	min. $W/C_L A$	0.74	0.07	X	X	X	All	All
Saturn I-B	max. $W/C_L A$	0.85	0.13	X	X	X	All	All
	min. $W/C_L A$	0.70	0.06	X	X	X	All	All

B. TZM

		Bottom (X/L +)	Top	Canopy	L.E.	Flaps	Fins	Rudder
Titan II	max. $W/C_L A$	0.26	0.02	X	X	X	All	All
	min. $W/C_L A$	0.095	0.02	All	X	X	All	All
Titan III-C	max. $W/C_L A$	0.446	0.03	X	X	X	All	All
	min. $W/C_L A$	0.255	0.02	X	X	X	All	All
Saturn I-B	max. $W/C_L A$	0.48	0.03	X	X	X	All	All
	min. $W/C_L A$	0.17	0.02	All	X	X	All	All

2. L/D = 1.0

A. René 41

		Bottom (X/L +)	Top	Canopy	L.E.	Flaps	Fins	Rudder
Titan II	max. $W/C_L A$	0.92	0.04	All	X	X	All	All
	min. $W/C_L A$	0.86	0.03	All	X	X	All	All
Titan III-C	max. $W/C_L A$	1.05	0.075	X	X	X	X	X
	min. $W/C_L A$	0.90	0.036	All	X	X	All	All
Saturn I-B	max. $W/C_L A$	1.02	0.06	X	X	X	All	X
	min. $W/C_L A$	0.91	0.04	All	X	X	All	All

TABLE 4.   HEAT PROTECTION SYSTEM APPLICATION - RE-RADIATION (Cont'd)

			Bottom $(X/L\,+)$	Top	Canopy	L.E.	Flaps	Fins	Rudder

Abort Conditions

2. L/D = 1.0 (cont)

B.   TZM

			Bottom $(X/L\,+)$	Top	Canopy	L.E.	Flaps	Fins	Rudder
Titan II	max.	$W/C_L A$	0.56	0.02	All	All	X	All	All
	min.	$W/C_L A$	0.42	0.02	All	All	X	All	All
Titan III-C	max.	$W/C_L A$	0.69	0.02	All	X	X	All	All
	min.	$W/C_L A$	0.51	0.02	All	All	X	All	All
Saturn I-B	max.	$W/C_L A$	0.68	0.02	All	All	X	All	All
	min.	$W/C_L A$	0.54	0.02	All	All	X	All	All

Re-Entry

1. René 41

$$V_E$$
m/sec (ft/sec)

			Bottom $(X/L\,+)$	Top	Canopy	L.E.	Flaps	Fins	Rudder
10,363 (34,000)	max.	$W/C_L A$	X	0.08	X	X	X	X	X
	min.	$W/C_L A$	0.93	0.06	All	X	X	All	All
9144 (30,000)	max.	$W/C_L A$	0.90	0.04	All	X	X	All	All
	min.	$W/C_L A$	0.78	0.03	All	X	X	All	All
7468 (24,500)	max.	$W/C_L A$	0.91	0.05	X	X	X	All	All
	min.	$W/C_L A$	0.8	0.03	X	X	X	All	All

2. TZM

			Bottom $(X/L\,+)$	Top	Canopy	L.E.	Flaps	Fins	Rudder
10,363 (34,000)	max.	$W/C_L A$	0.75	0.03	All	X	X	All	All
	min.	$W/C_L A$	0.57	0.02	All	All	X	All	All
9144 (30,000)	max.	$W/C_L A$	0.53	0.02	All	All	X	All	All
	min.	$W/C_L A$	0.16	0.02	All	All	X	All	All
7468 (24,500)	max.	$W/C_L A$	0.55	0.02	All	X	X	All	All
	min.	$W/C_L A$	0.22	0.02	All	X	X	All	All

TABLE 5.   RE-RADIATION SYSTEM WEIGHTS

	René 41		TZM	
	Kg/m^2	(lb/ft^2)	g/cm^2	(lb/ft^2)
Outer surface material	2.90	(0.594)	4.65	(0.954)*
Insulation weight	Based on conduction-solution			
Supports and attachments	.293	(0.060)	.361	(0.074)
Refurbishment (Channels and Rods)	1.02	(0.209)	1.02	(0.209)

*includes coating

TABLE 6. TYPICAL ABLATION HEAT PROTECTION SYSTEM

Velocity   = 9144 m/sec (30,000 fps)
Vehicle Length = 7.92m (26.00 ft)
Vehicle Weight = 4536 Kg (10,000.00 lb)
Safety Factor = 1.200

$$\frac{\text{Weight of Shield}}{\text{Weight of Vehicle}} \times 10^4$$

Location	ESM (A)	ESM (B)	MPN (A)	MPN (B)	
1	15.05	7.56	14.51	11.23	
2	19.11	10.39	20.47	16.66	
3	7.92	3.11	5.76	3.66	
4	30.67	10.42	19.54	10.67	
5	39.98	13.23	24.87	13.15	
6	43.71	12.04	25.83	11.96	
7	47.73	9.05	25.94	8.99	
8	51.18	9.70	27.81	9.64	
9	111.81	19.00	59.53	18.87	
10	60.66	10.31	32.30	10.24	
11	5.00	0.94	2.71	0.94	
12	29.08	8.86	17.66	8.80	
13	64.68	30.18	57.14	42.02	
14	65.01	32.66	62.69	48.52	T_{BF}
15	74.18	41.78	80.95	67.05	(A) 422°K
16	125.88	56.07	105.45	74.86	(300°F)
17	116.15	54.20	102.61	75.47	
18	124.51	62.56	120.07	92.93	(B) 589°K
19	83.38	35.87	67.11	46.29	(600°F)
20	179.44	82.50	155.86	113.39	
21	57.96	23.50	43.58	28.48	
22	167.06	67.75	125.60	82.08	
23	55.06	23.24	43.37	29.43	
24	51.44	21.29	39.61	26.40	
25	35.58	14.42	26.75	17.48	
26	18.81	7.39	13.69	8.69	
27	87.53	36.24	67.40	44.93	
28	37.73	17.34	32.77	23.84	
29	11.53	2.61	6.50	2.59	
30	97.79	39.82	73.88	48.48	
31	96.95	20.20	53.69	20.07	
32	40.93	16.94	31.52	21.01	
33	5.17	0.54	2.57	0.53	
34	106.27	62.12	117.98	99.59	
35	67.05	12.71	36.43	12.63	
36	1.88	0.71	1.33	0.82	
37	9.13	3.47	6.45	3.97	
38	24.02	8.57	16.00	9.23	
39	17.77	6.04	11.32	6.18	

Subtotal Weights	ESM (A)	ESM (B)	MPN (A)	MPN (B)
Nose Cap	34.16	17.95	34.99	27.89
Upper Surface	427.79	96.72	242.01	96.96
Lower Surface	1113.35	510.37	964.46	700.58
Sides	193.37	79.36	147.46	97.51
Fins	244.02	79.99	166.86	94.99
Control Surface	219.45	92.33	188.51	133.78
Canopy	52.82	18.81	35.11	20.21
Total Refurbishment Weight	93.56	93.56	157.30	157.30
Total Vehicle	2377.55	989.13	1936.74	1329.25

TABLE 7. TYPICAL REFURBISHMENT EVALUATION MATRIX

Refurbishment Concept / Criteria	Re-radiation	Ablation				
		Bond	Mechanical Attachment	Loop & Pile	Perforation Scrim	High-Temp. Tape
Cost						
C-1 Material	4	1	2	3	2	1
C-2 Inspection	6	5	2	1	4	3
C-3 Application	5	3	2	1	4	1
C-4 Quality Assurance	6	2	1	4	5	3
C-5 Design	2	1	2	4	5	3
Safety						
S-1 Complexity	5	1	2	3	4	3
S-2 Weight	1	1	4	3	2	1
S-3 Environment	3	1	2	1	1	1
S-4 Compatibility	3	1	2	1	1	1
Time						
T-1 Inspection	5	4	3	1	4	2
T-2 Removal	3	2	2	1	2	1
T-3 Refurbishment	4	3	2	1	3	1
T-4 Quality Assurance	4	3	1	1	3	2
Total	51	28	28	25	40	23
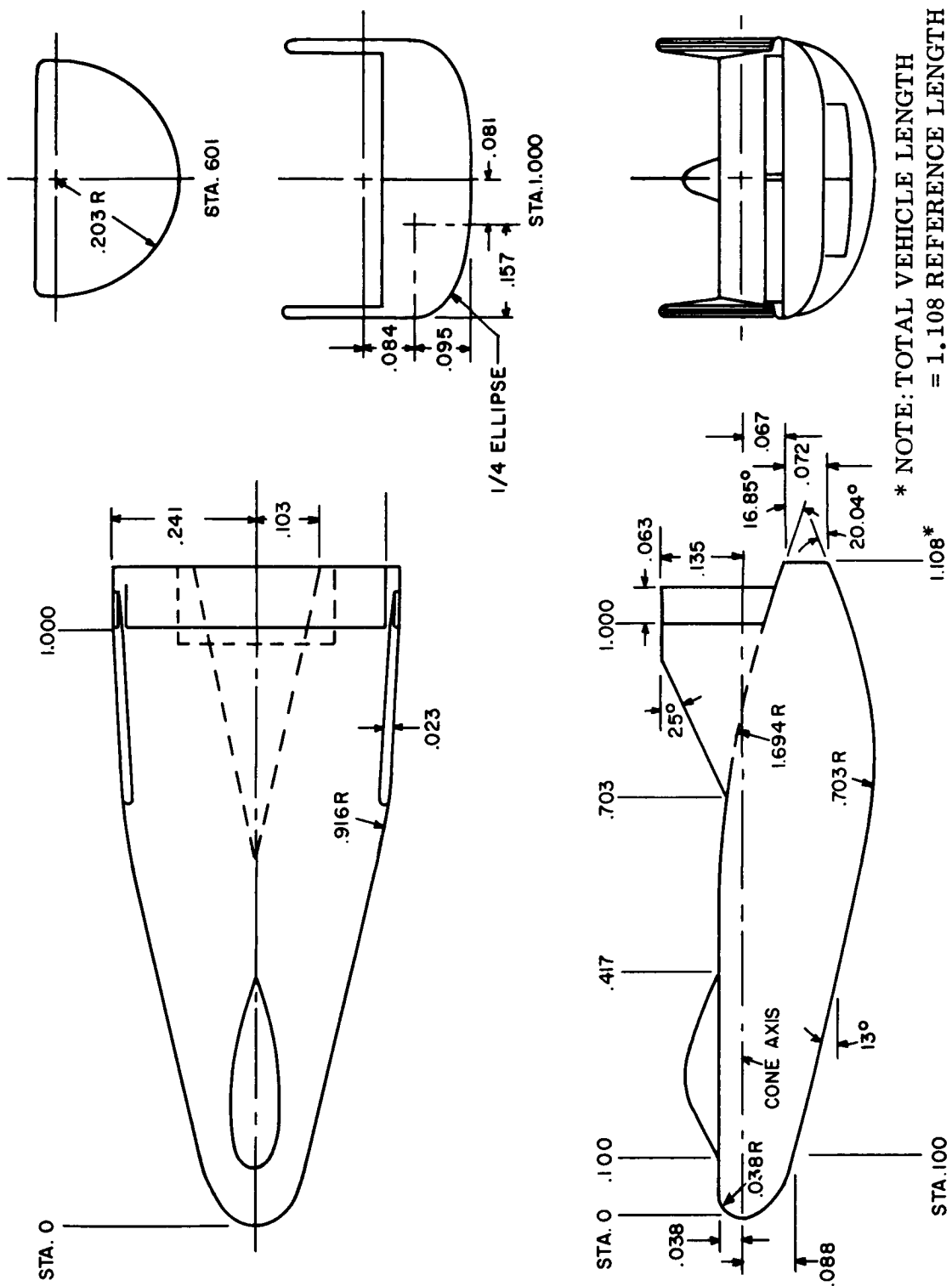
Figure 1. Configuration of M2 – F2 (NASA Vehicle)

* NOTE: TOTAL VEHICLE LENGTH
= 1.108 REFERENCE LENGTH
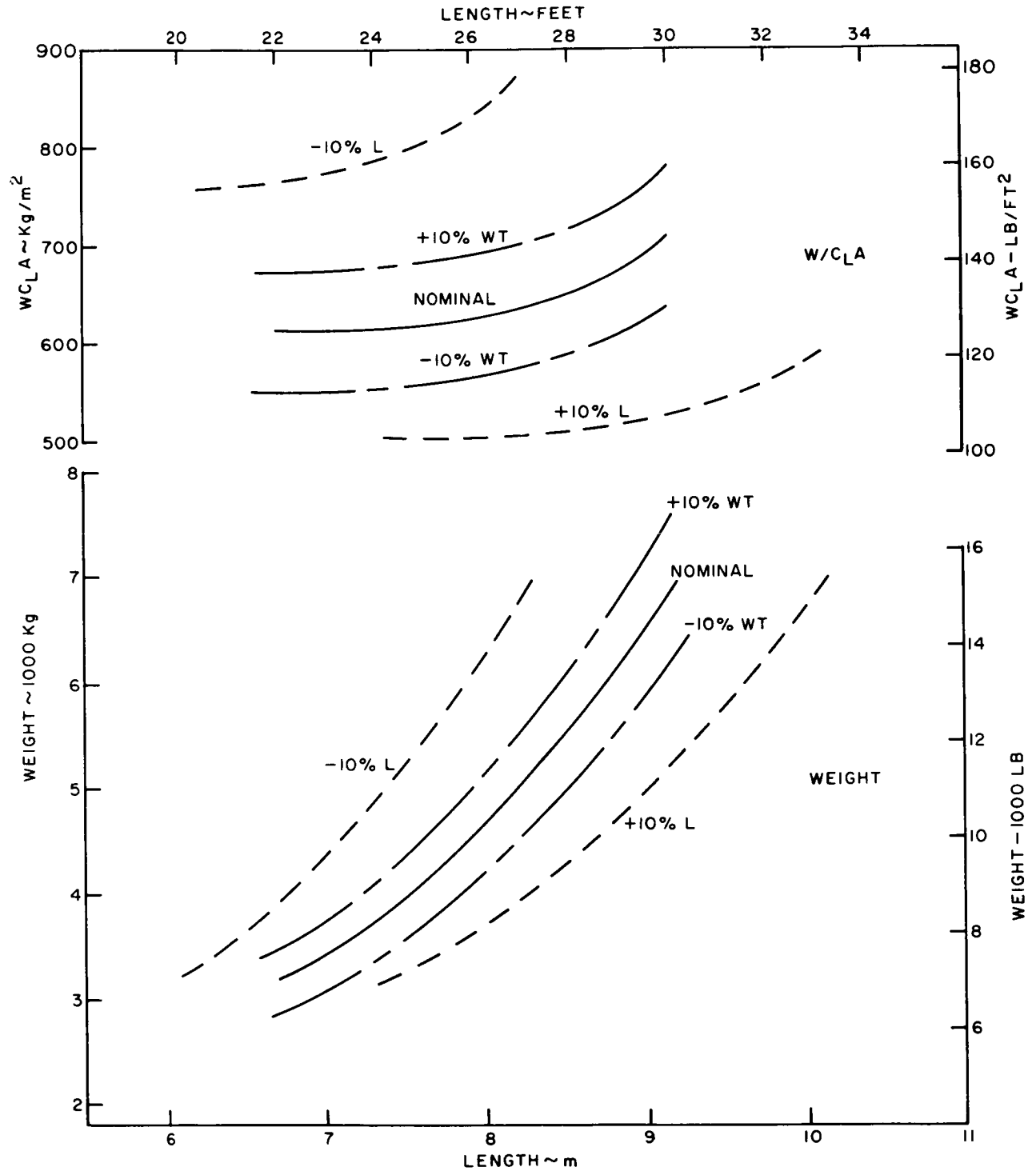
Figure 2. Scope of M2 - F2 Study - Weight and $W/C_L A$ vs. Length
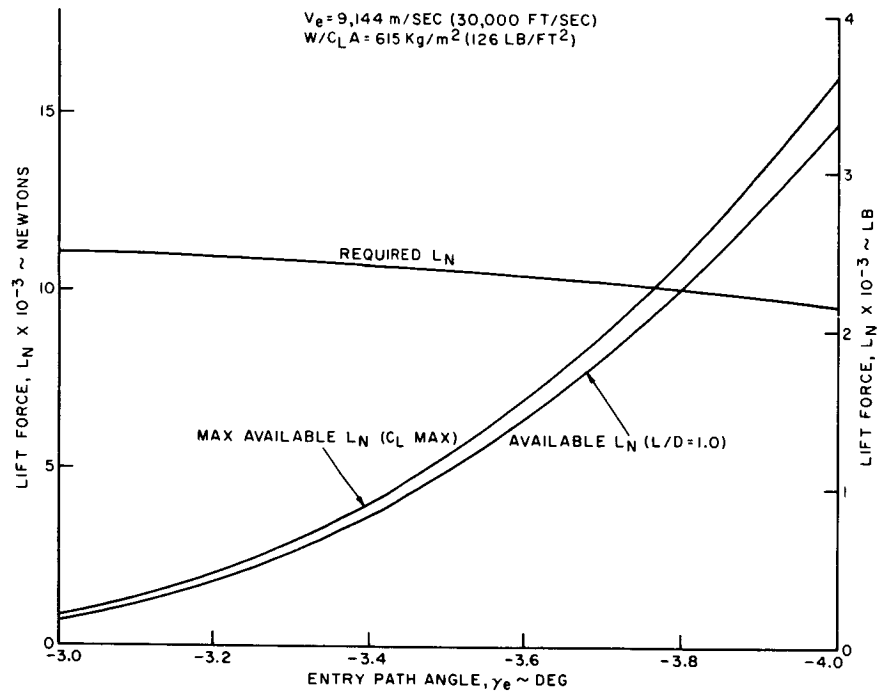
Figure 3. Overshoot Boundary Definition - Lift Force vs. Path Angle
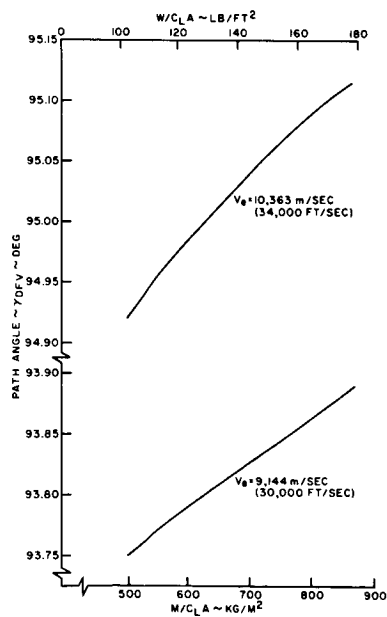
Figure 4. Overshoot Boundary Definition - Path Angle vs. W/C_LA
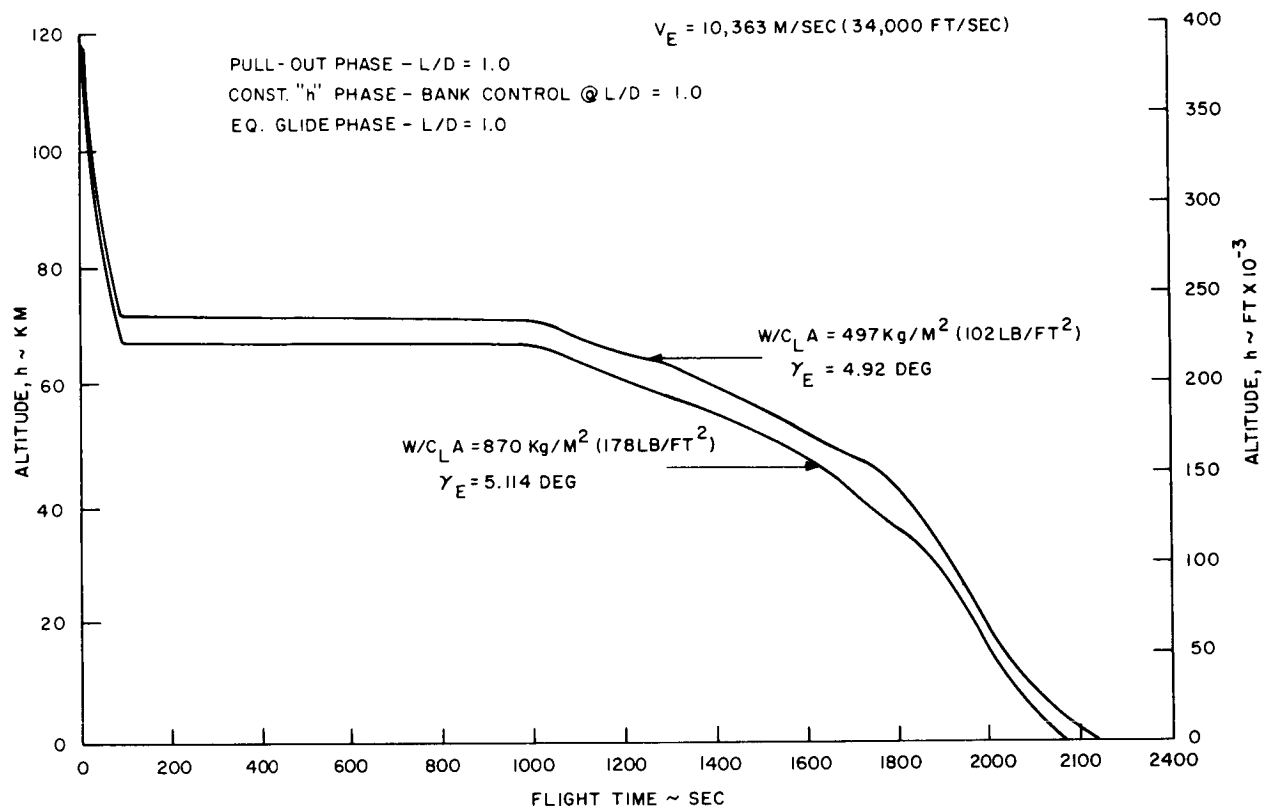
Figure 5. Overshoot Boundary Definition – Altitude vs. Flight Time
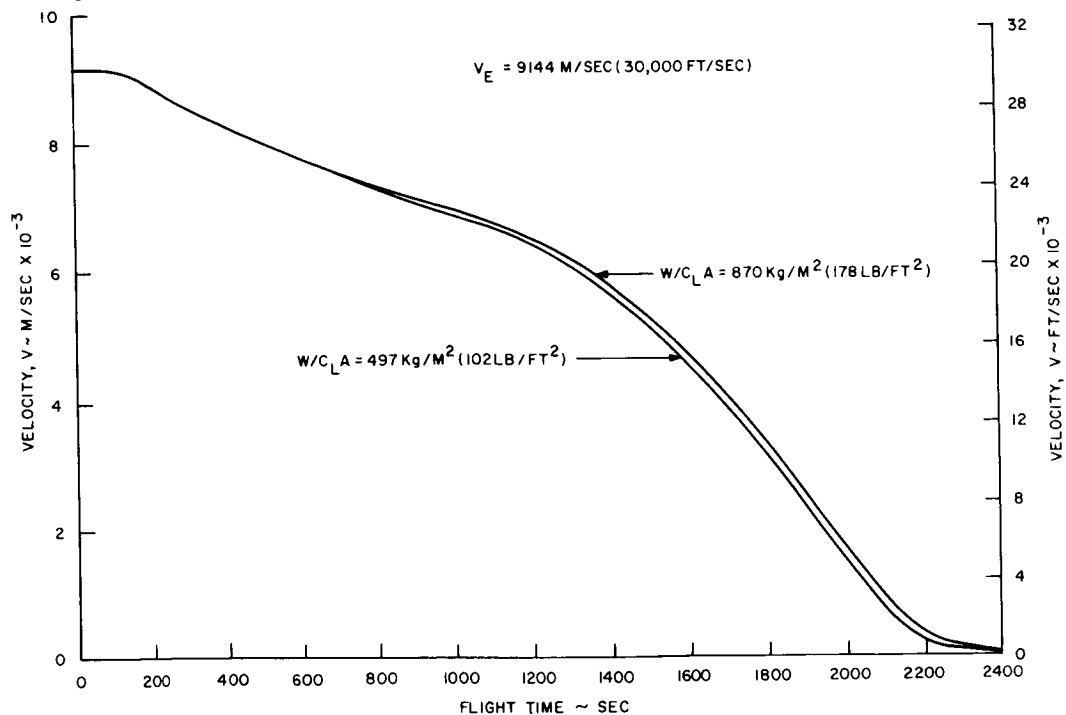
Figure 6. Overshoot Boundary Definition – Velocity vs. Flight Time

F4
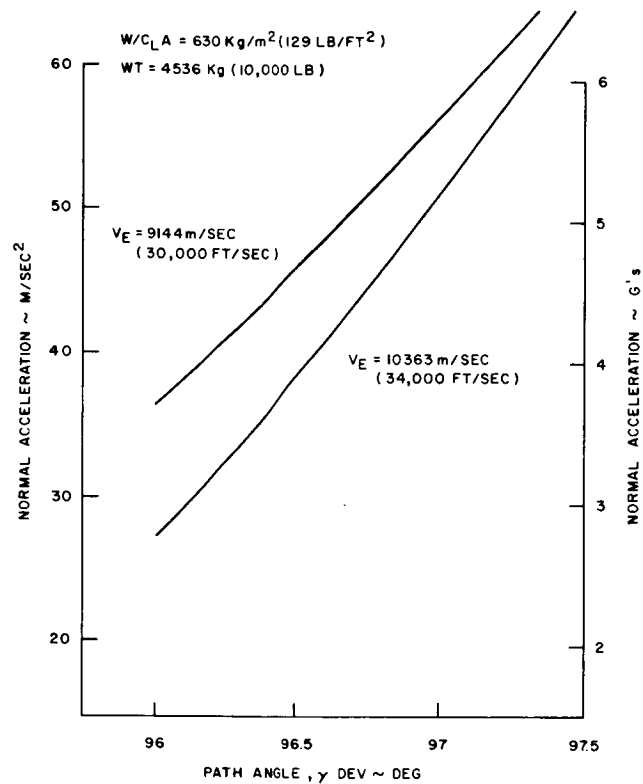
Figure 7. Undershoot Boundary Definition - Normal Acceleration vs. Path Angle
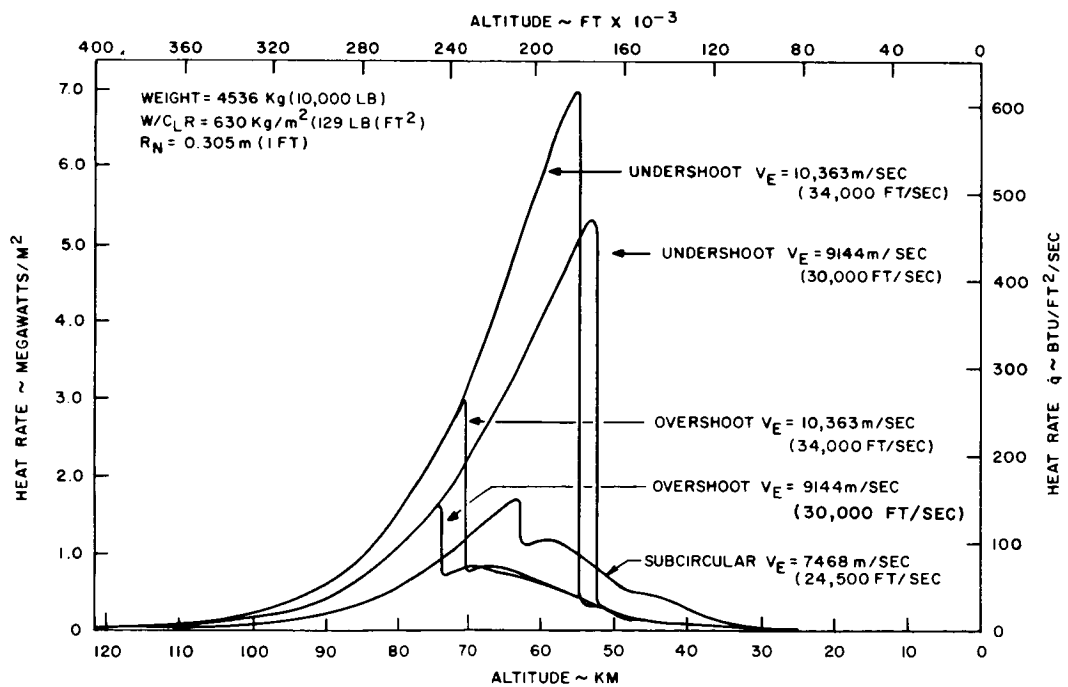
Figure 8. Heat Flux Profiles for Typical Re-entry Trajectories
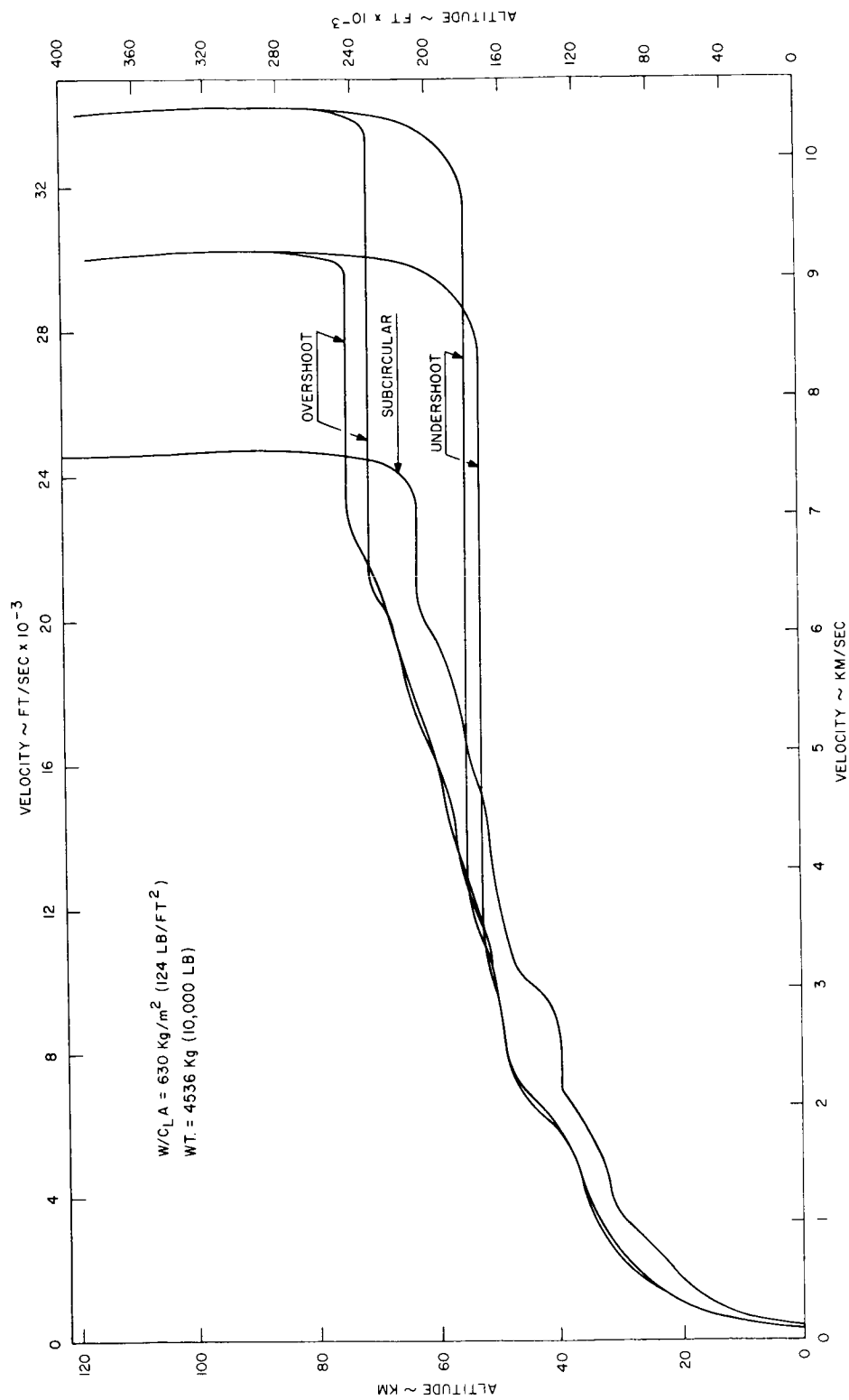
Figure 9. Altitude-Velocity Profiles for Typical Re-entry Trajectories

F6
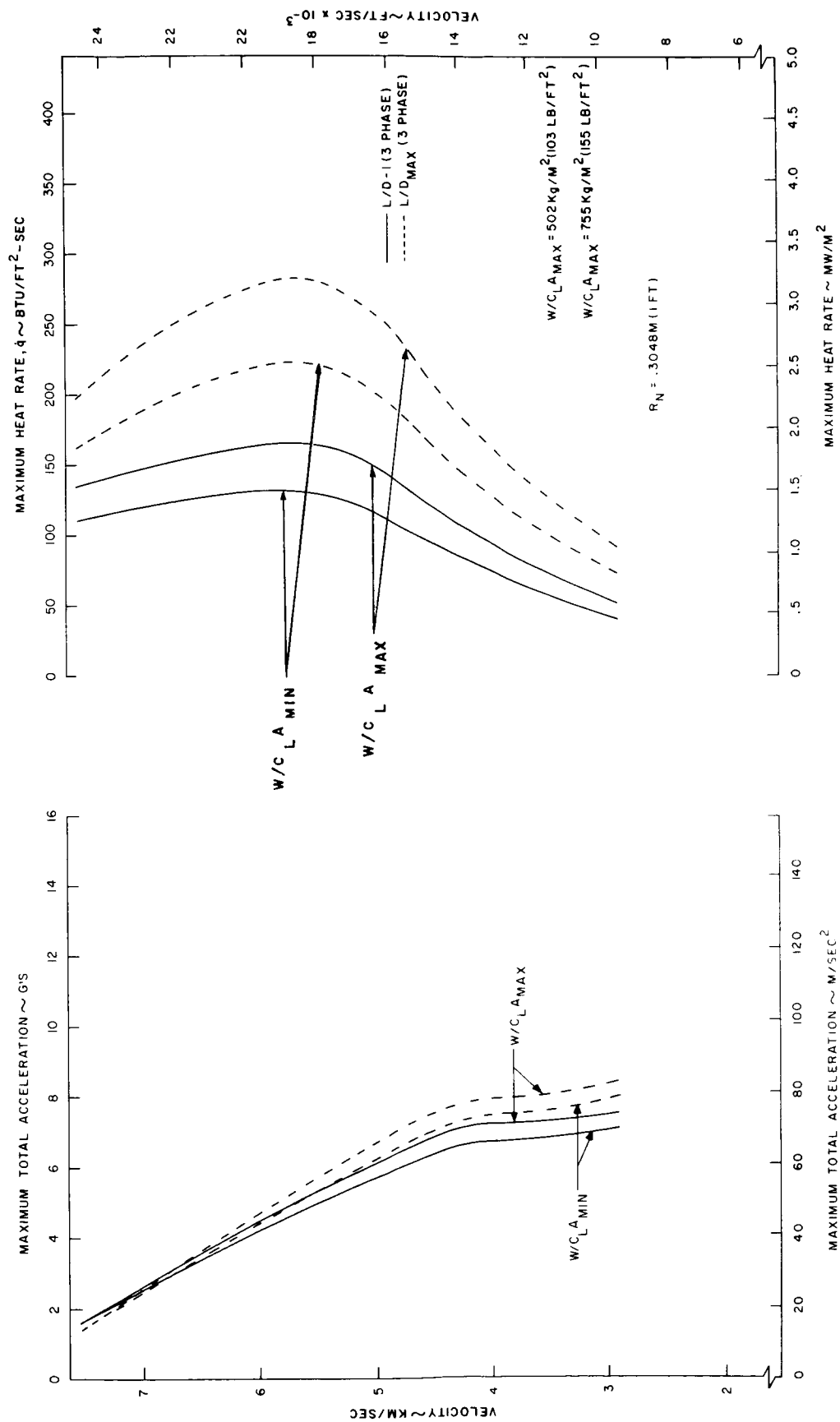
Figure 10. Critical Ascent Abort From Titan II – Velocity vs. Total
Acceleration and Maximum Heating Rate
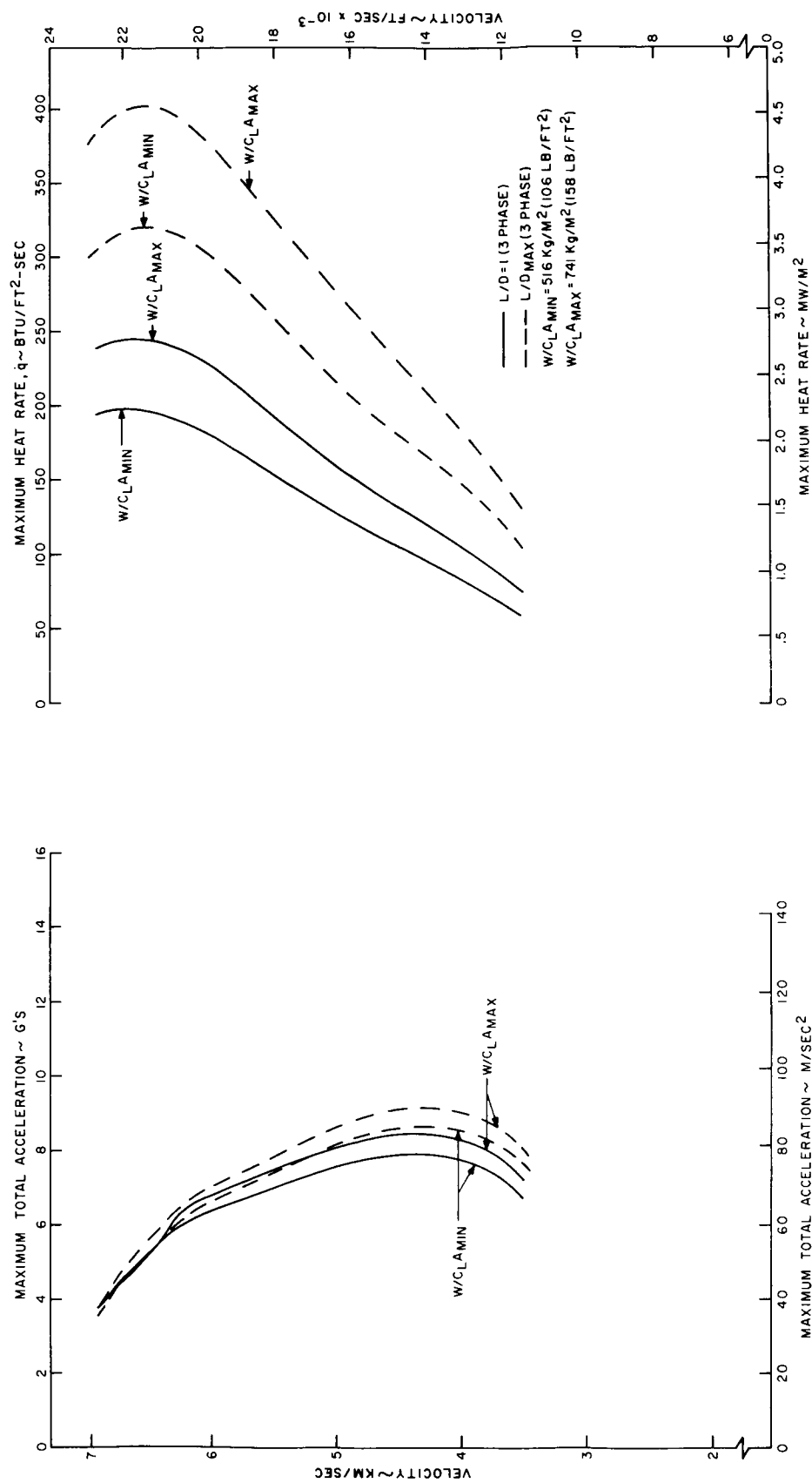
Figure 11. Critical Ascent Abort From Titan IIIC – Velocity vs. Total Acceleration and Maximum Heating Rate

F8
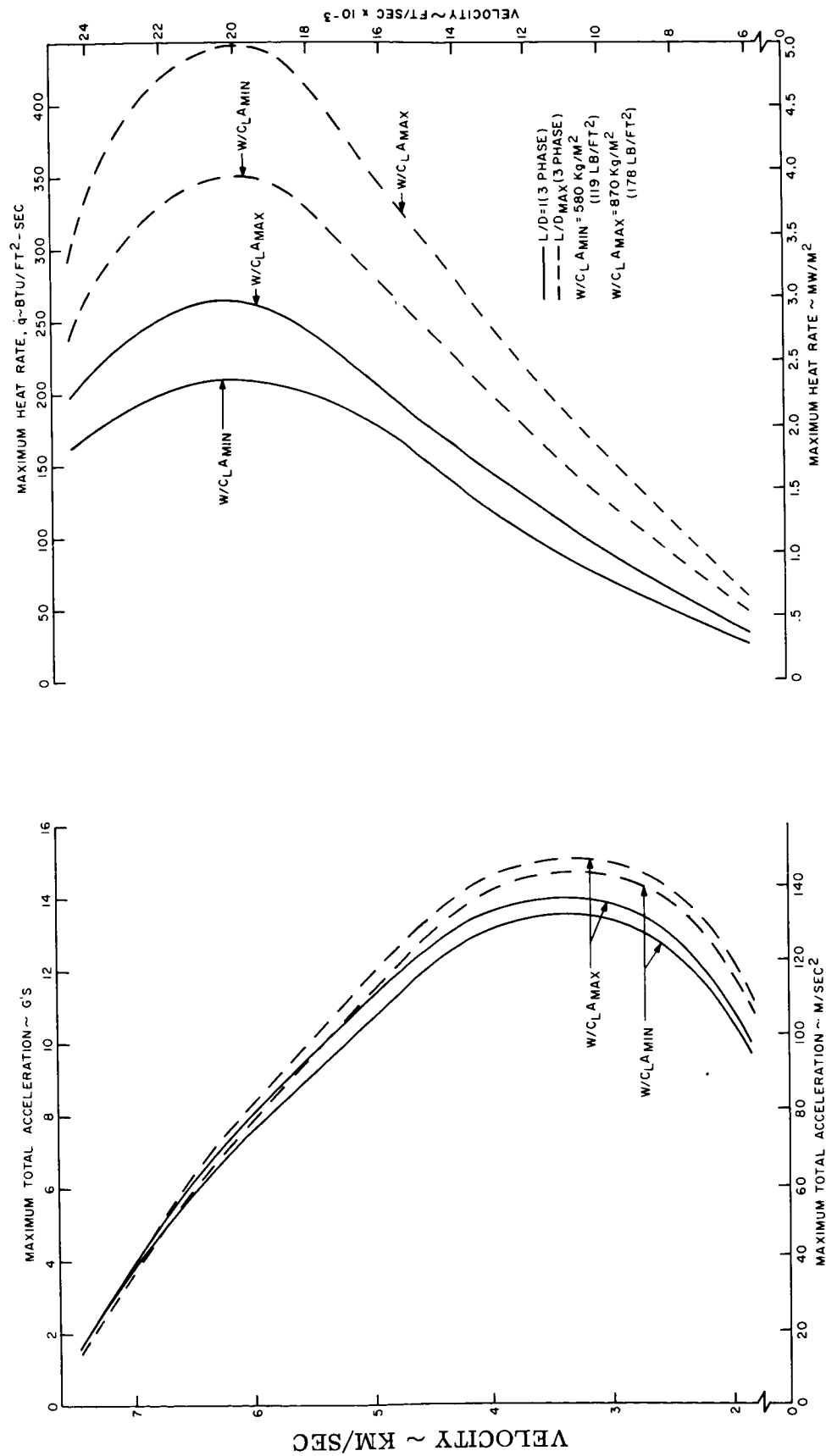
Figure 12. Critical Ascent Abort From Saturn IB - Velocity vs. Total
Acceleration and Maximum Heating Rate
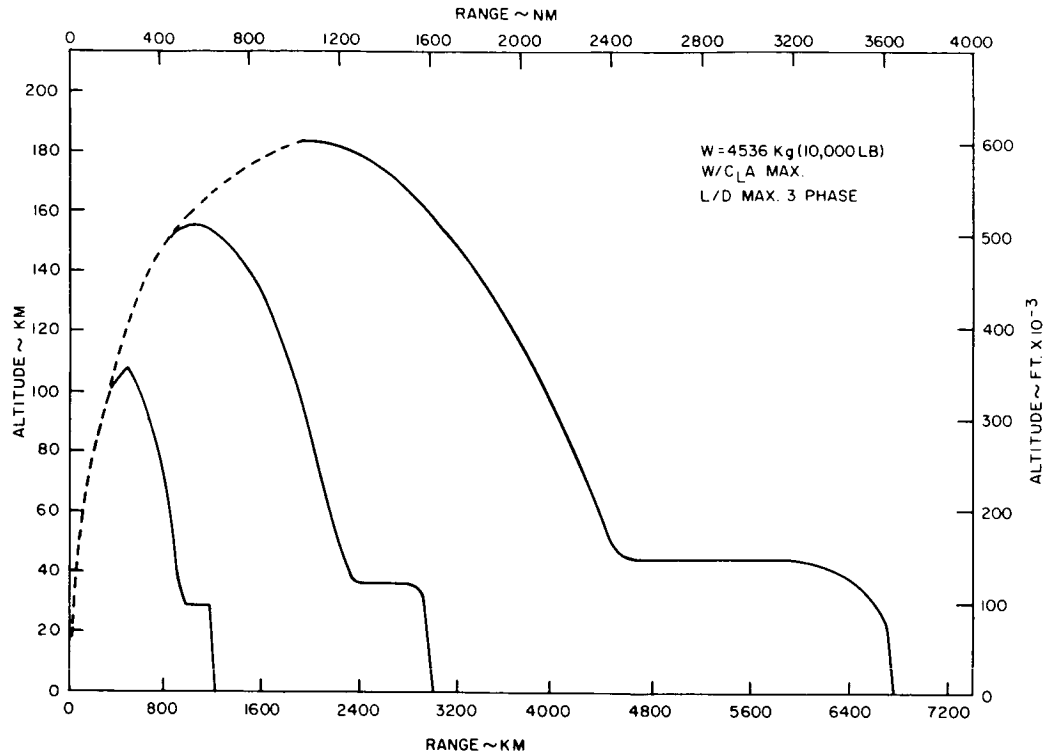
Figure 13. Typical Critical Ascent Abort Profiles for Titan IIIC - Altitude vs. Range
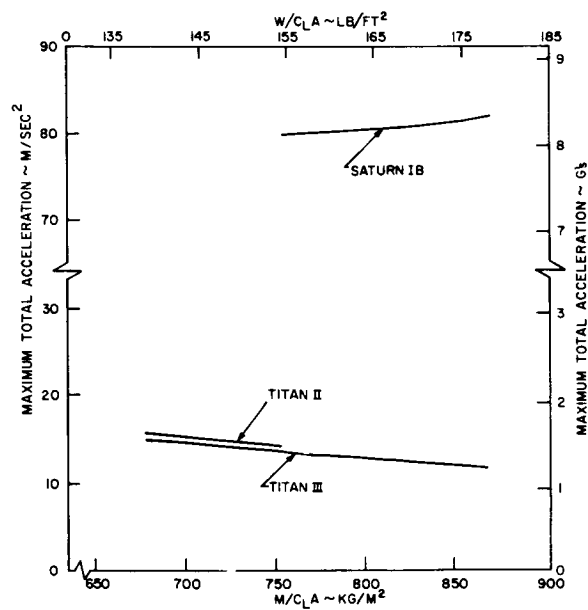
Figure 14. Maximum Total Acceleration for Maximum Dynamic Pressure Abort

F10

Figure 16. Transition Reynolds Number Criteria

Figure 15. Total Acceleration Profile for
Maximum Dynamic Pressure Abort

F11
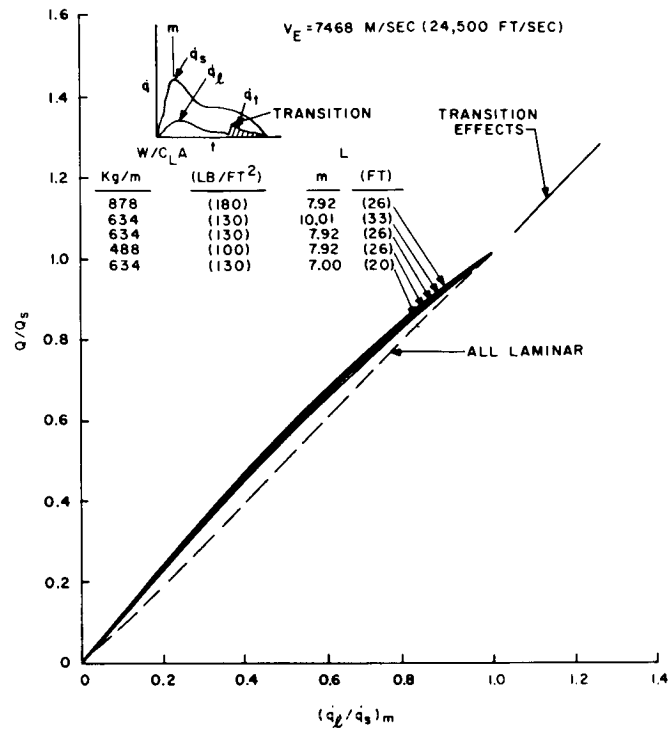
Figure 17. Transition Effects on Total Heating as a Function of $W/C_L A$
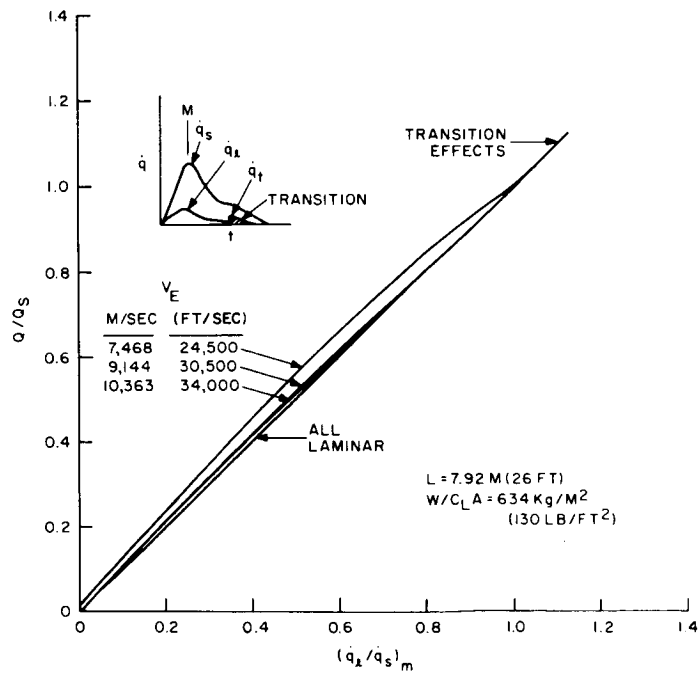
Figure 18. Transition Effects on Total Heating as a Function of Re-entry Velocity

F12
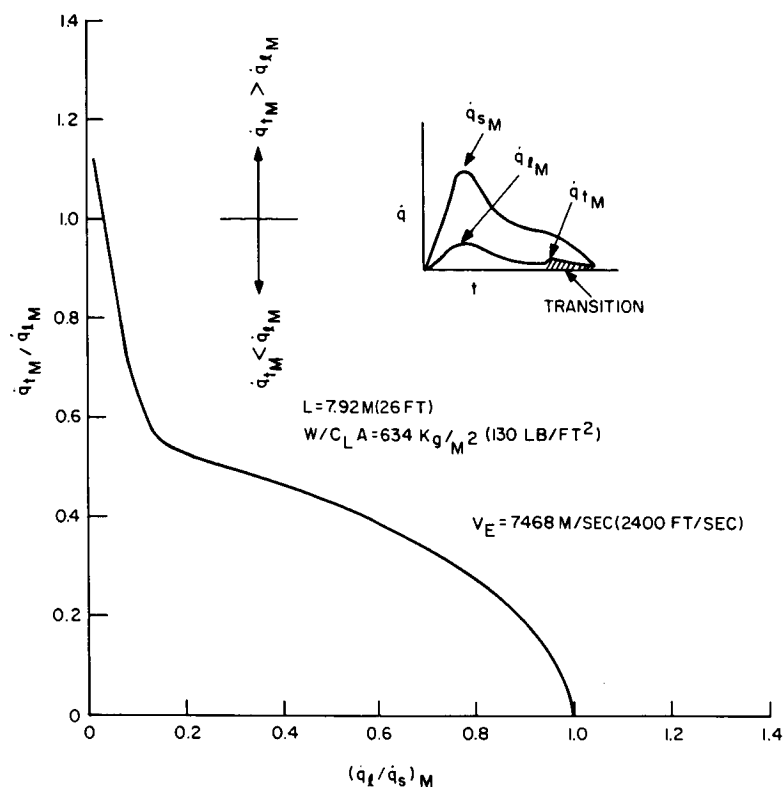
Figure 19. Transition Effects on Maximum Turbulent Heat Flux
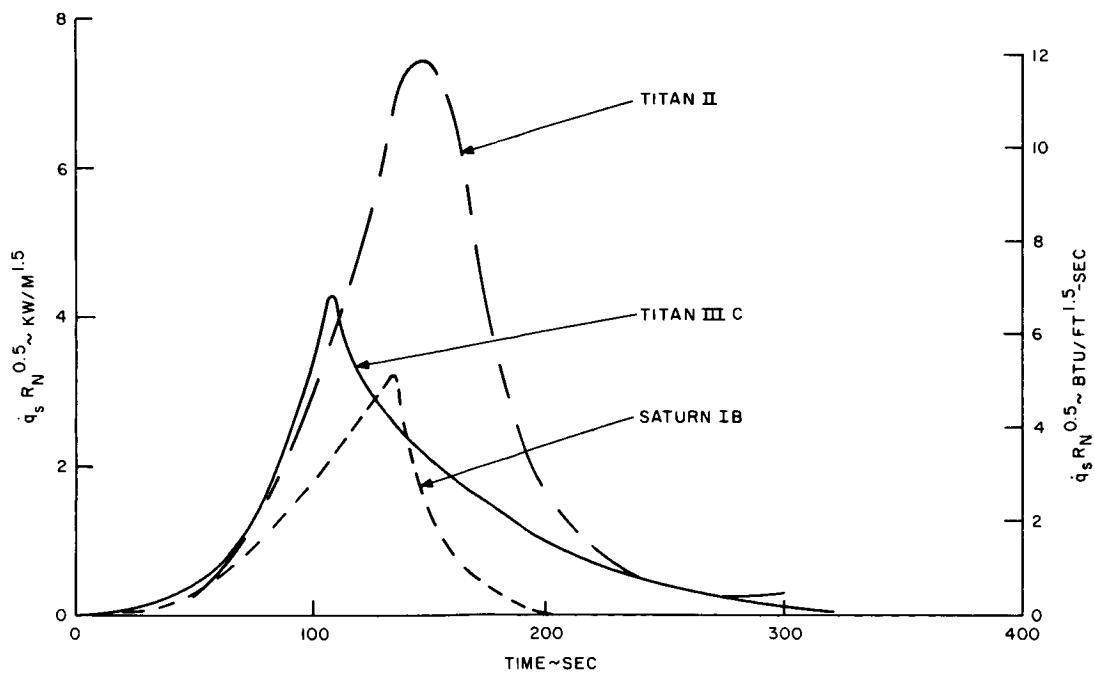
Figure 20. Ascent Heating

F13
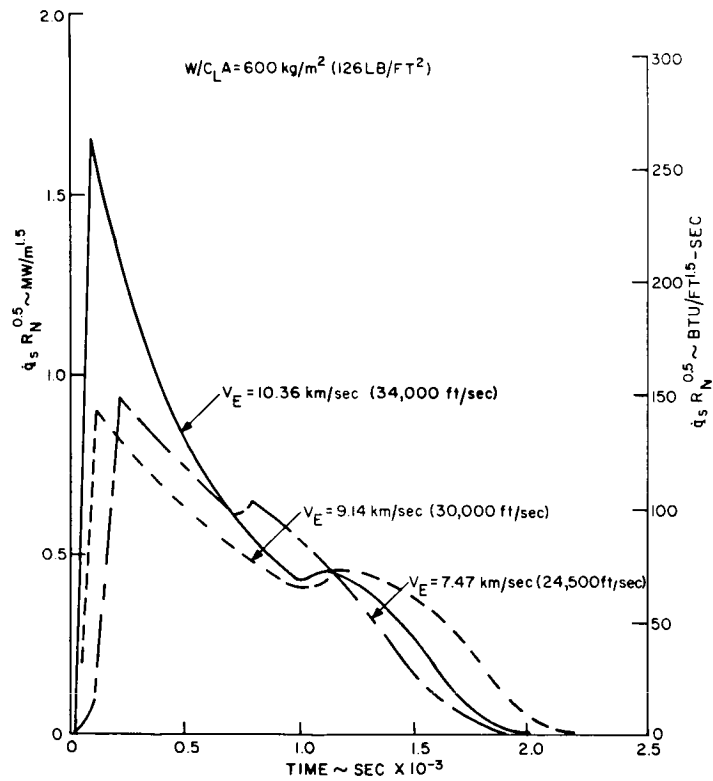
Figure 21. Typical Re-entry Stagnation Heat Flux Environments
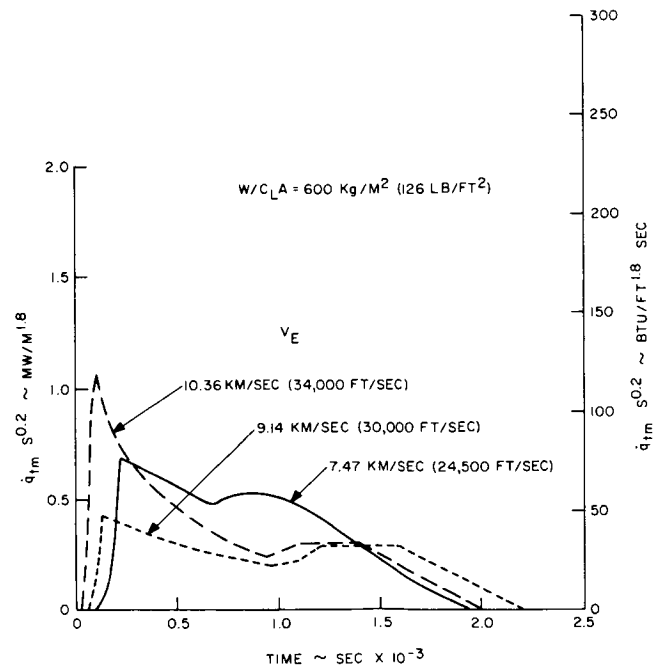
Figure 22. Maximum Turbulent Heat Flux for Re-entry
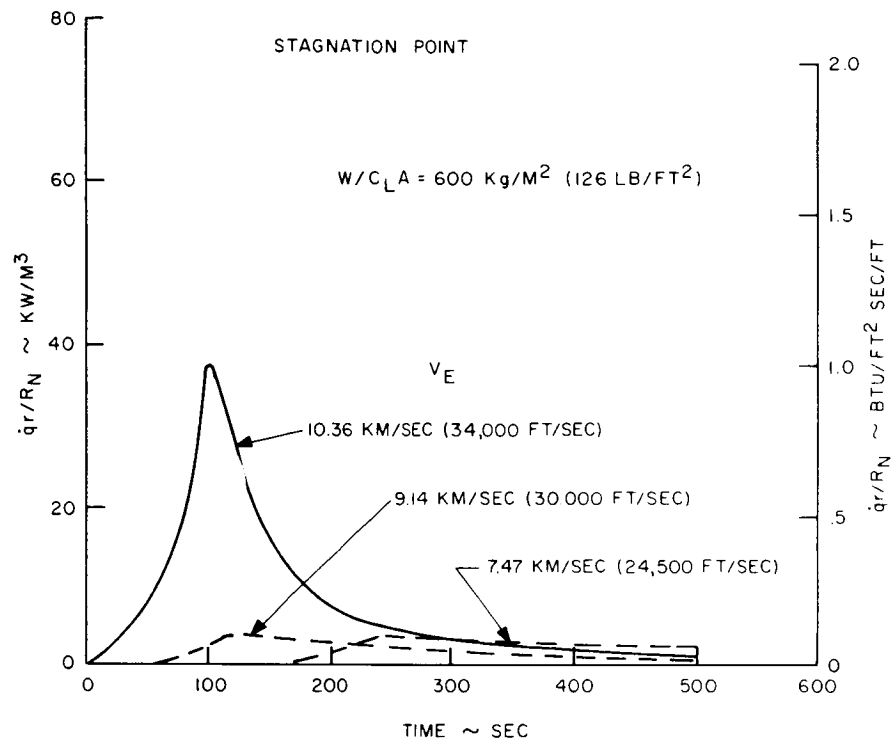
Figure 23. Typical Hot Gas Radiation at the Stagnation Point for Re-entry
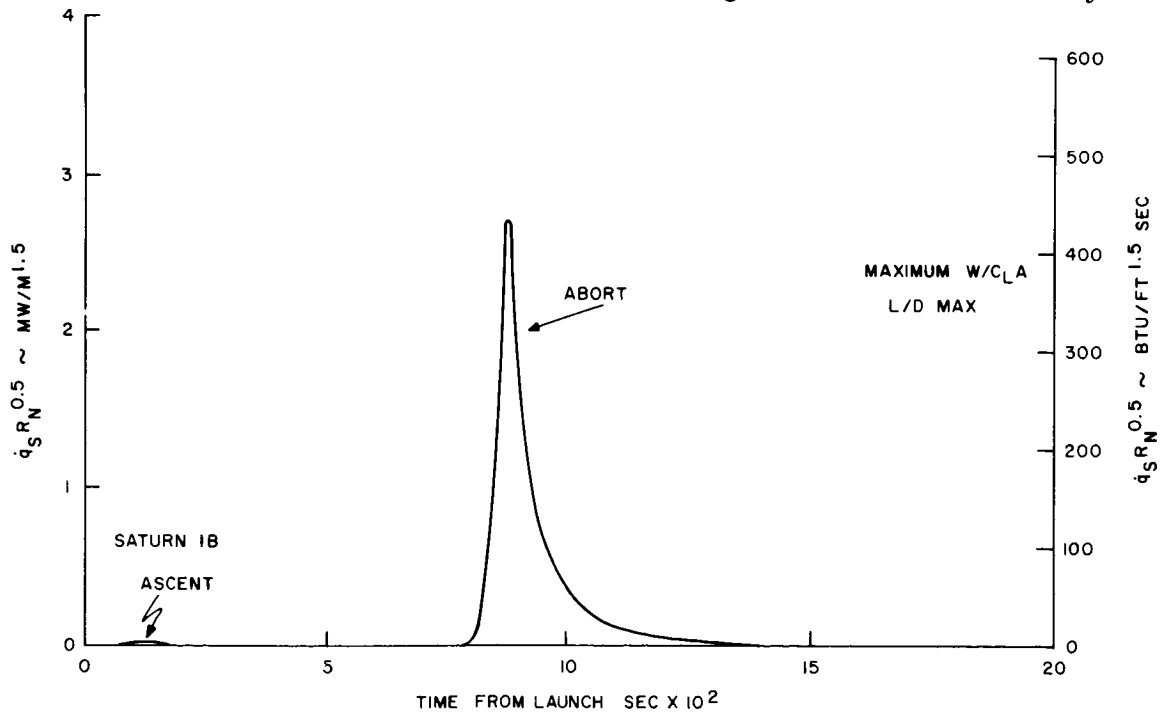
Figure 24. Typical Stagnation Heat Flux for the Critical
Ascent Abort Flight (L/D max.)
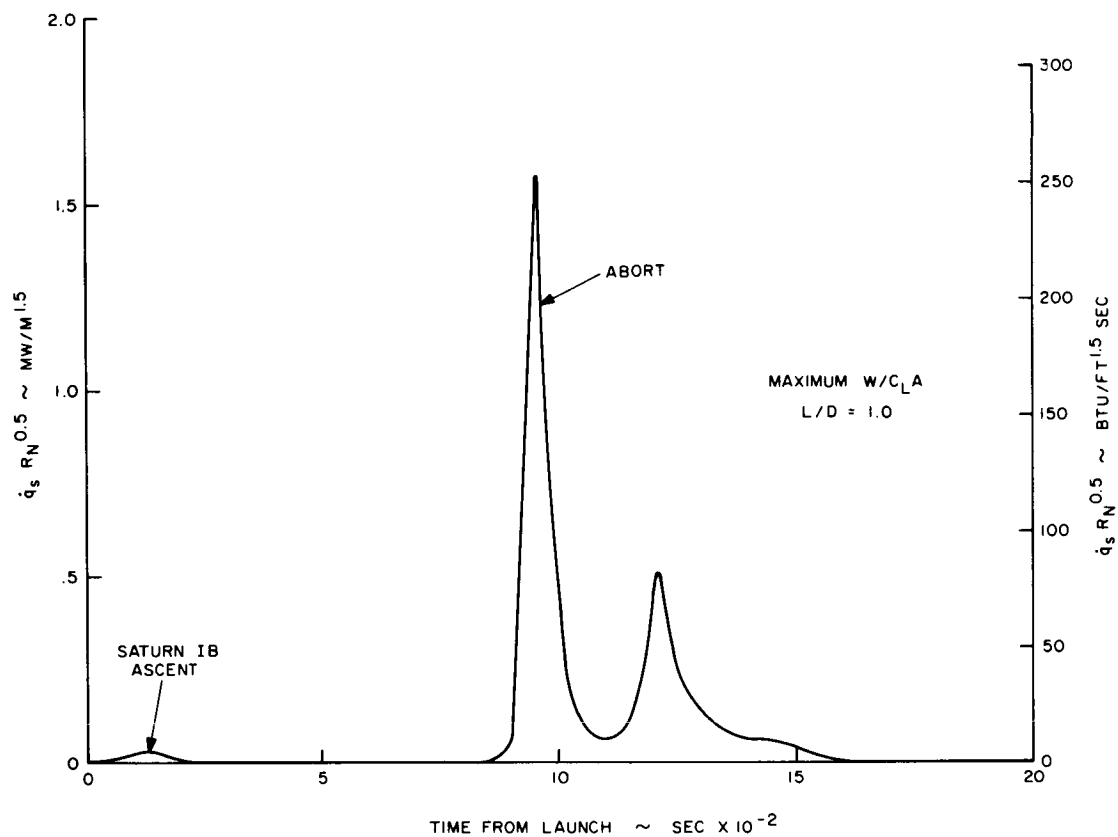
Figure 25. Typical Stagnation Heat Flux for the Critical
Ascent Abort Flight (L/D = 1)
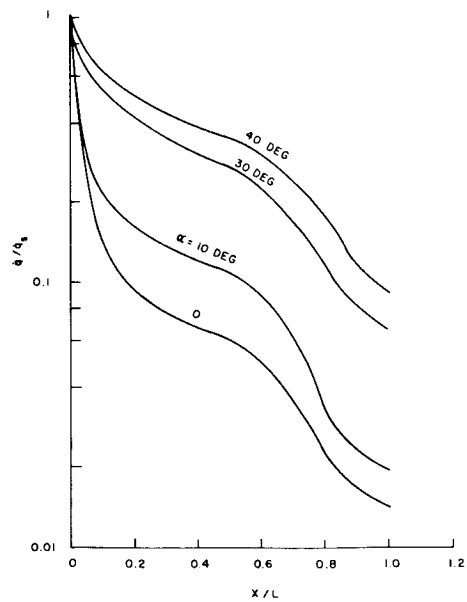
Figure 26. Laminar Heat Flux Distribution on Windward Ray
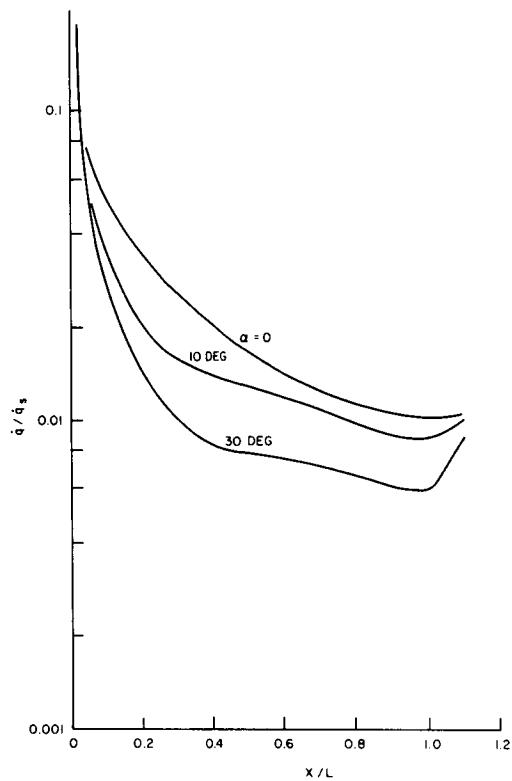
Figure 27. Laminar Heat Flux Distribution on Leeward Ray
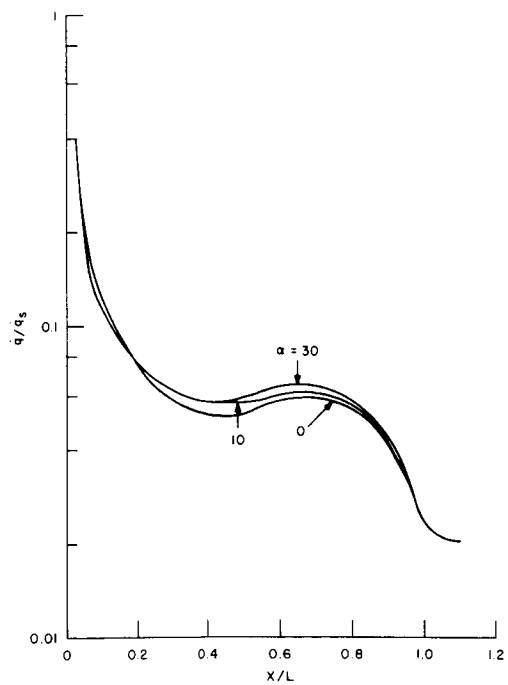
Figure 28. Laminar Heat Flux Distribution on Side Meridian

F17
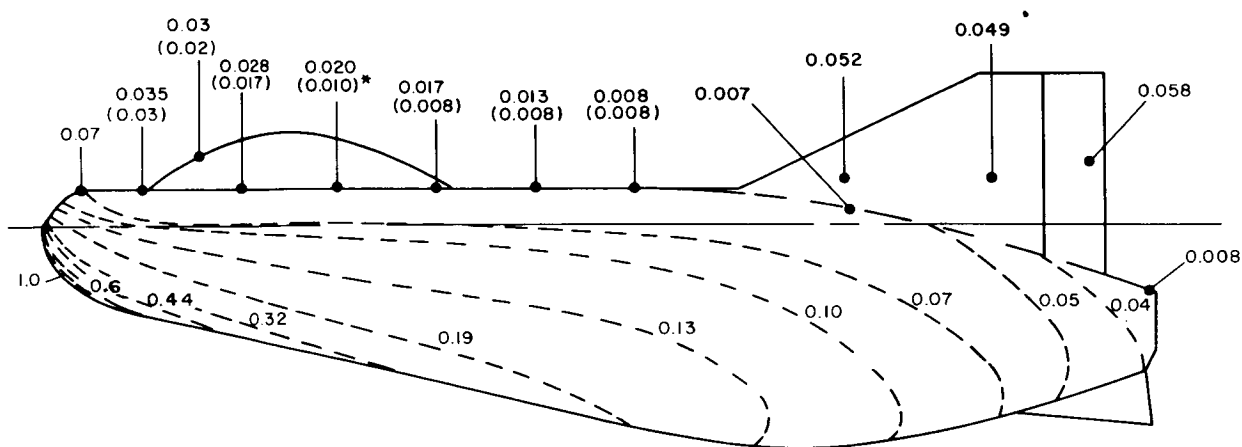
Figure 29. Typical Laminar Heat Flux Distribution at 30-Degrees
Angle of Attack
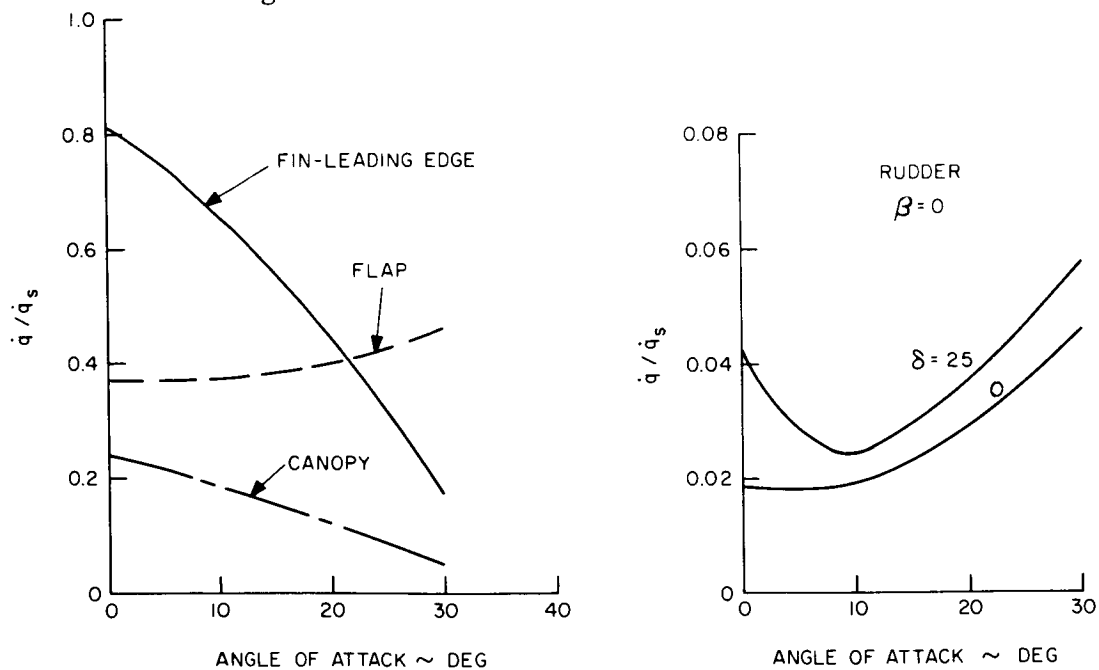
Figure 30. Laminar Heat Flux Distribution vs. Angle of Attack for Flaps,
Fin Leading Edge, Canopy and Rudder
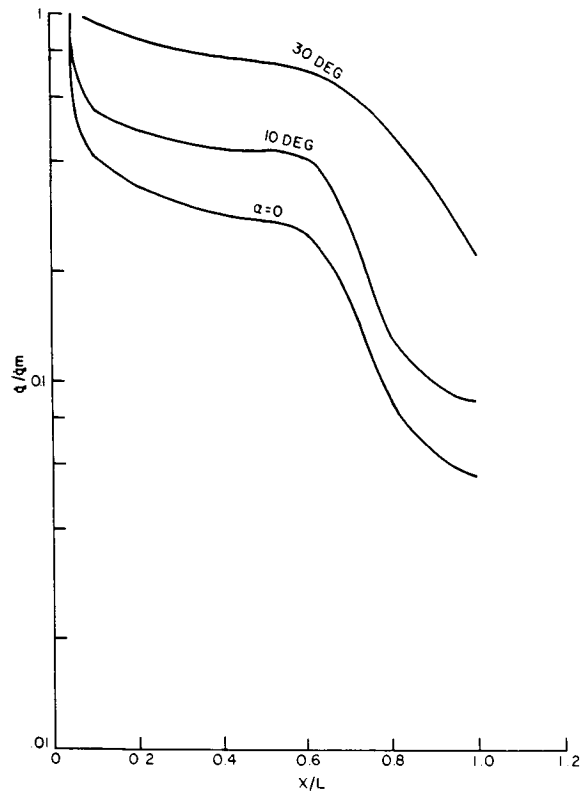
Figure 31. Turbulent Heat Flux Distribution on Windward Ray
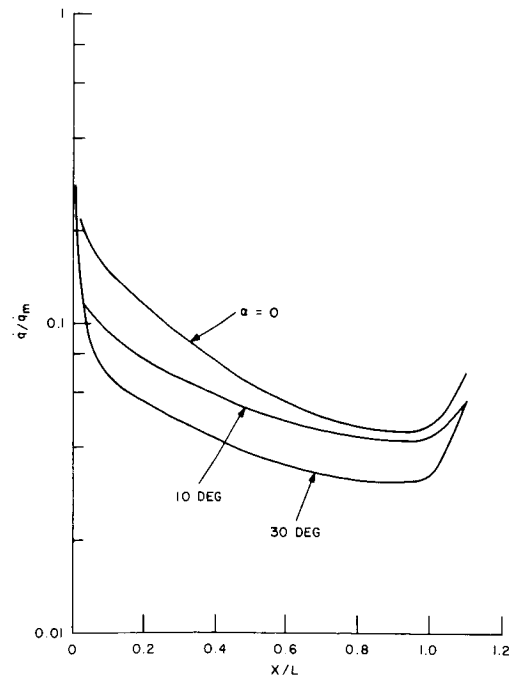
Figure 32. Turbulent Heat Flux Distribution on Leeward Ray
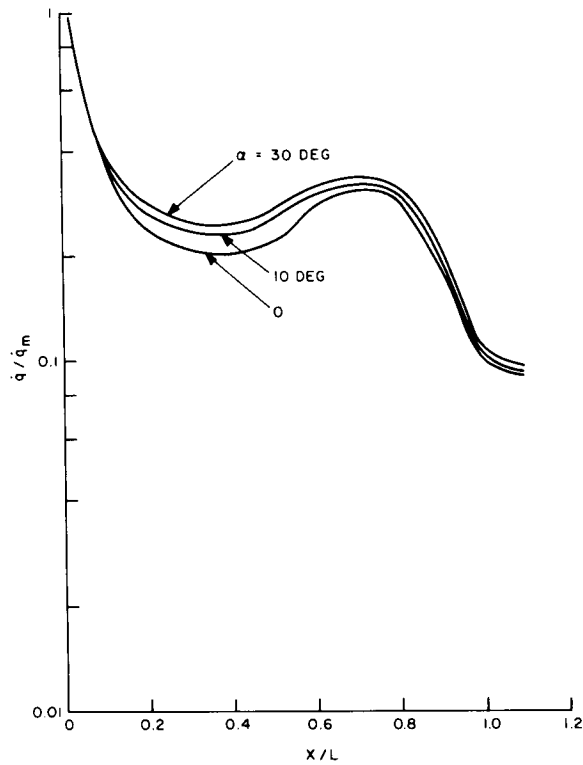
Figure 33. Turbulent Heat Flux Distribution on Side Meridian
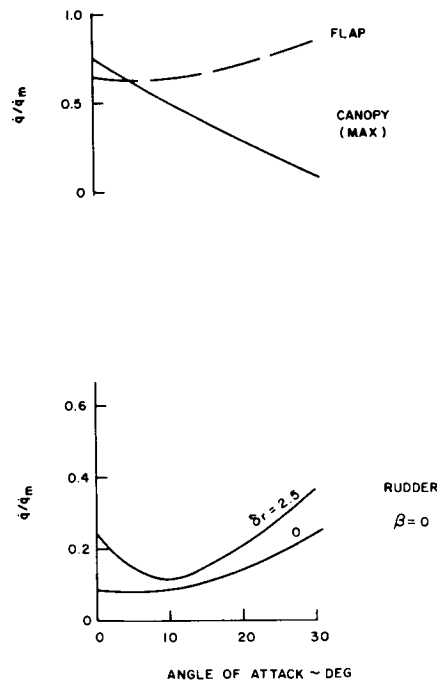
Figure 34. Turbulent Heat Flux vs. Angle of Attack for the
Flaps, Canopy, and Rudder
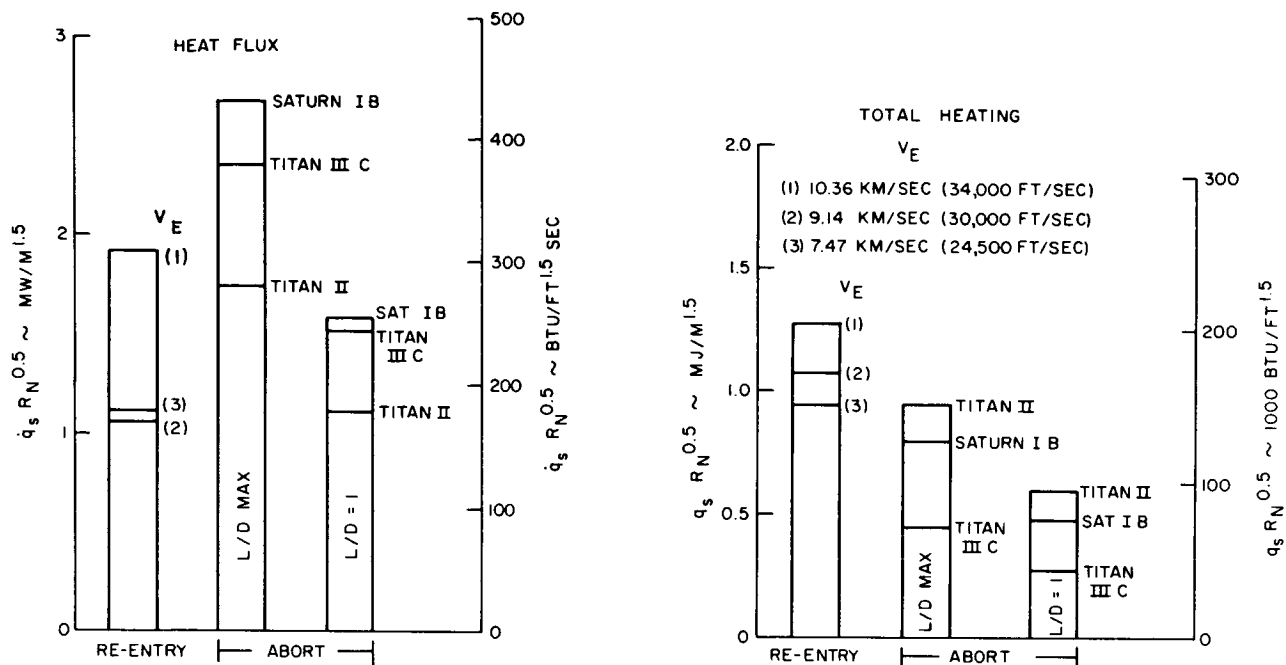
Figure 35. Re-entry and Abort Heating Comparison at Maximum
Stagnation Point (Heat Flux and Total Heating)
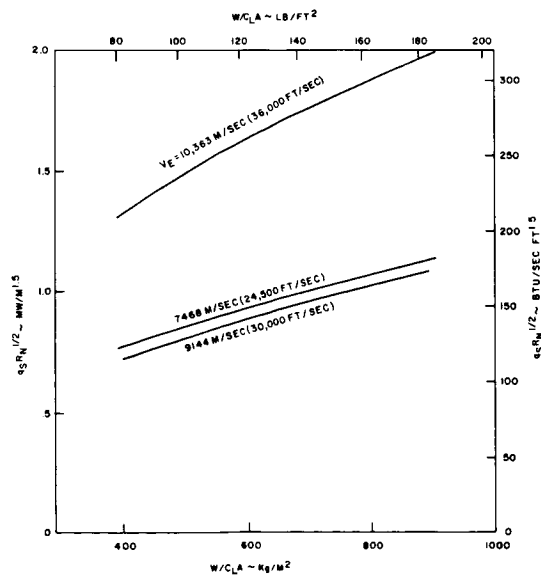
Figure 36. Maximum Stagnation Heat Flux for
Re-entry as a Function of $W/C_L A$
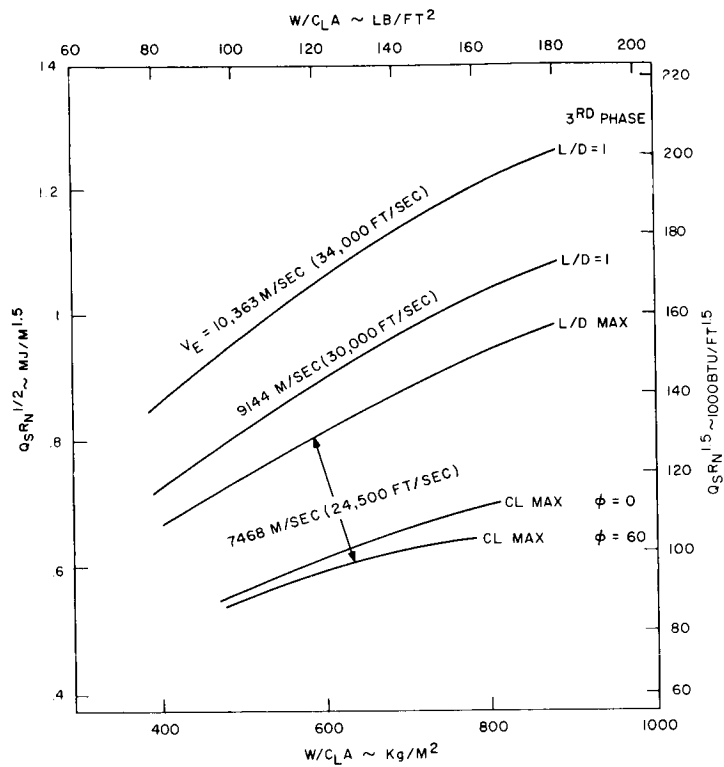
Figure 37. Maximum Total Stagnation Heating for Re-entry as a Function of $W/C_L A$
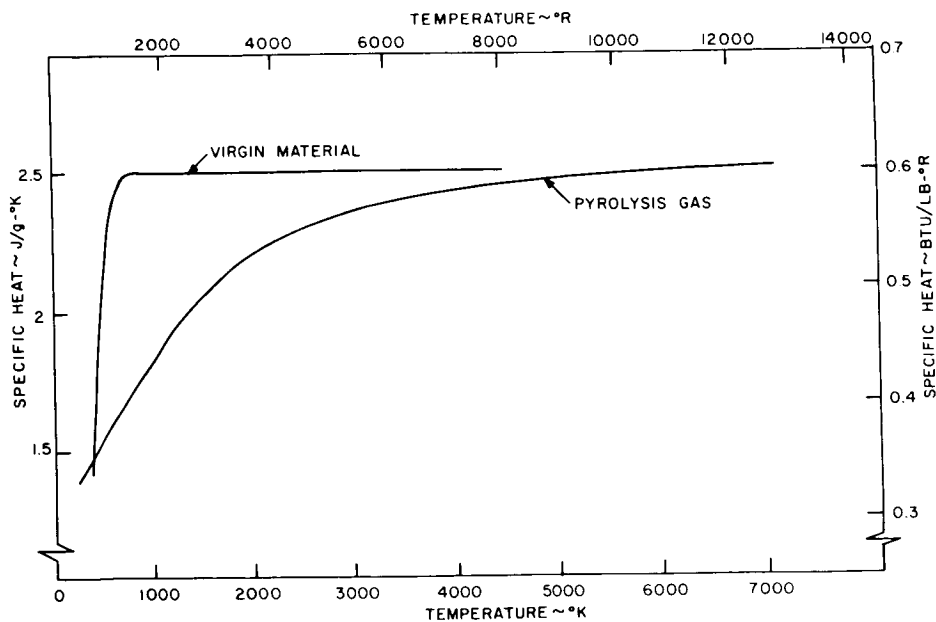
Figure 38. Specific Heat of ESM (Virgin Material and Pyrolysis Gas)
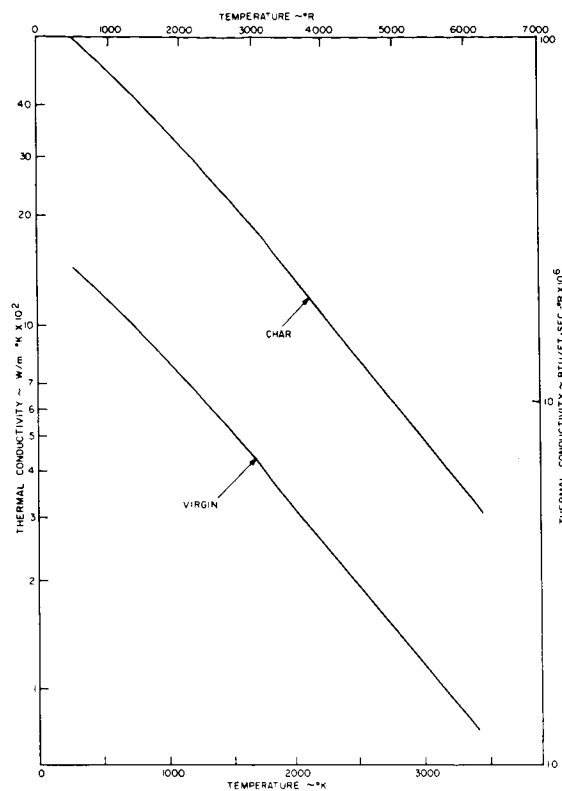
Figure 39. Thermal Conductivity of ESM (Virgin Material and Char)
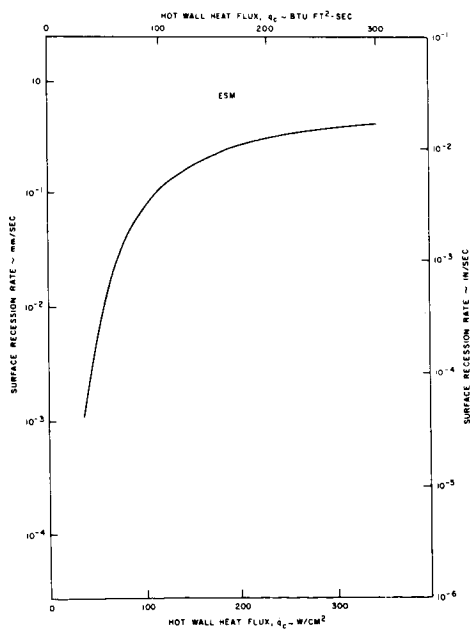
Figure 40. Surface Recession Rate for ESM vs. Heat Flux
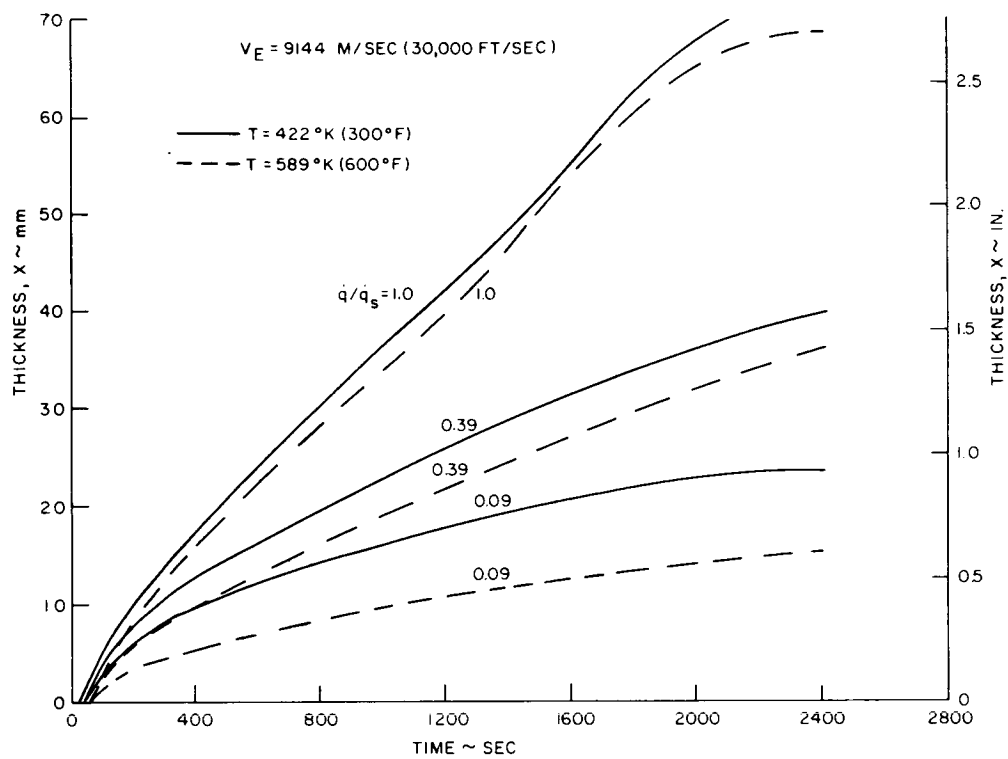
Figure 41. Temperature Histories for Typical MPN REKAP Analysis
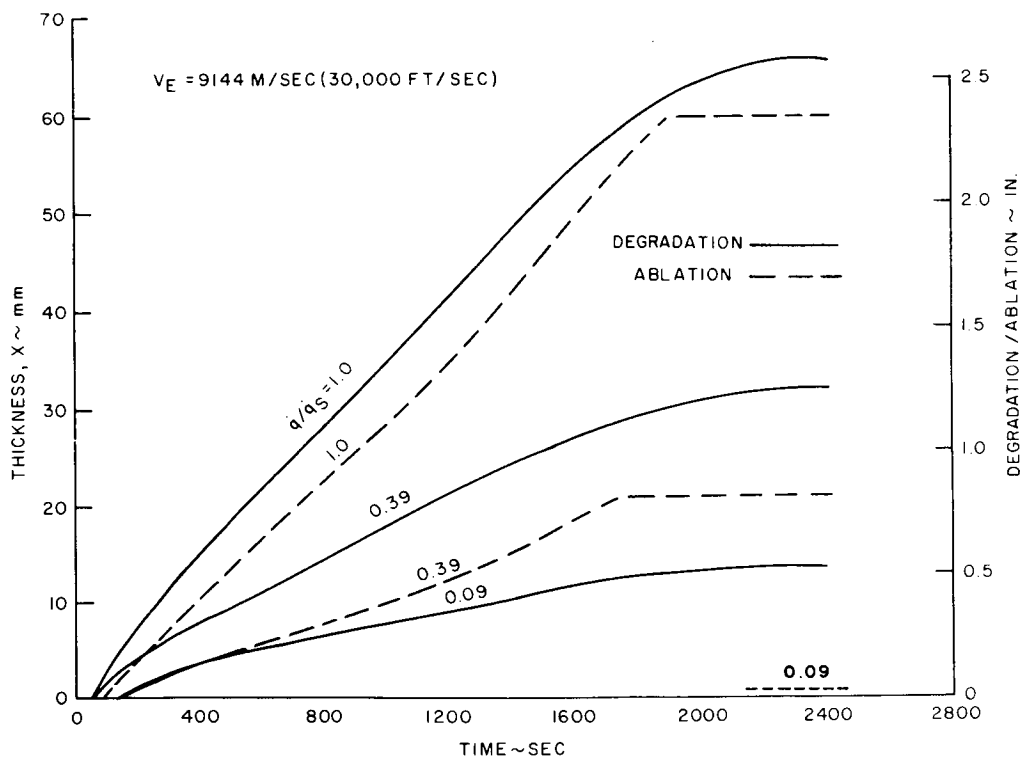
Figure 42. Degradation and Ablation Histories for MPN Typical REKAP Analysis

F24
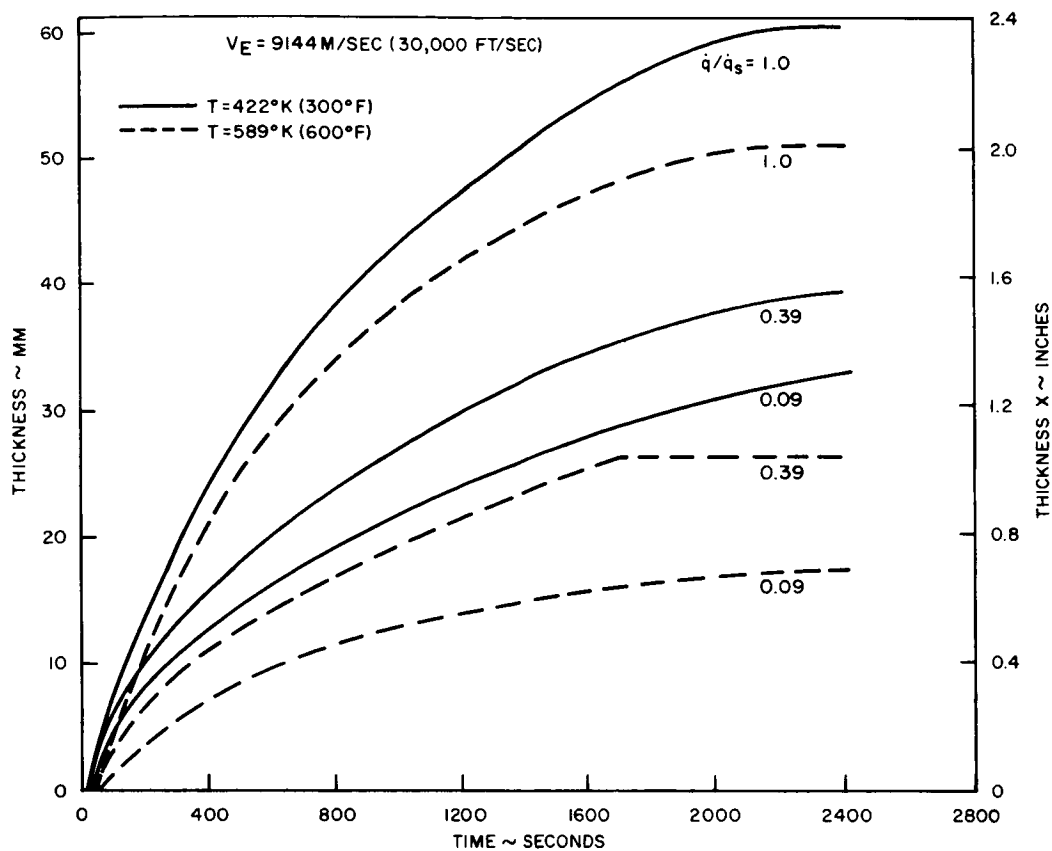
Figure 43. Temperature Histories for Typical
ESM REKAP Analysis
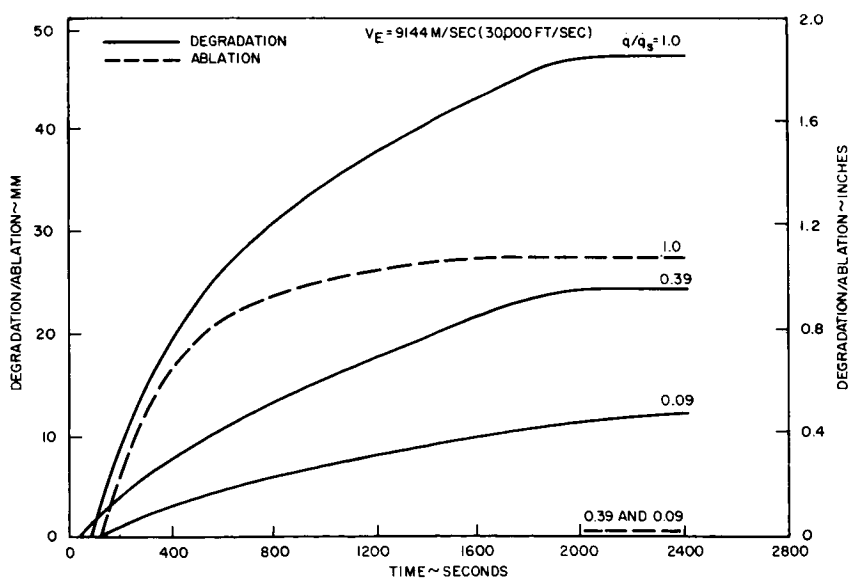
Figure 44. Degradation and Ablation Histories for
Typical ESM REKAP Analysis

LOW HEATING ($Q_T \approx 5.56$) KJ/CM^2 (4900 BTU/FT^2)

V_E = 9144 m/SEC (30,000 FT/SEC)

TIME ~ SEC
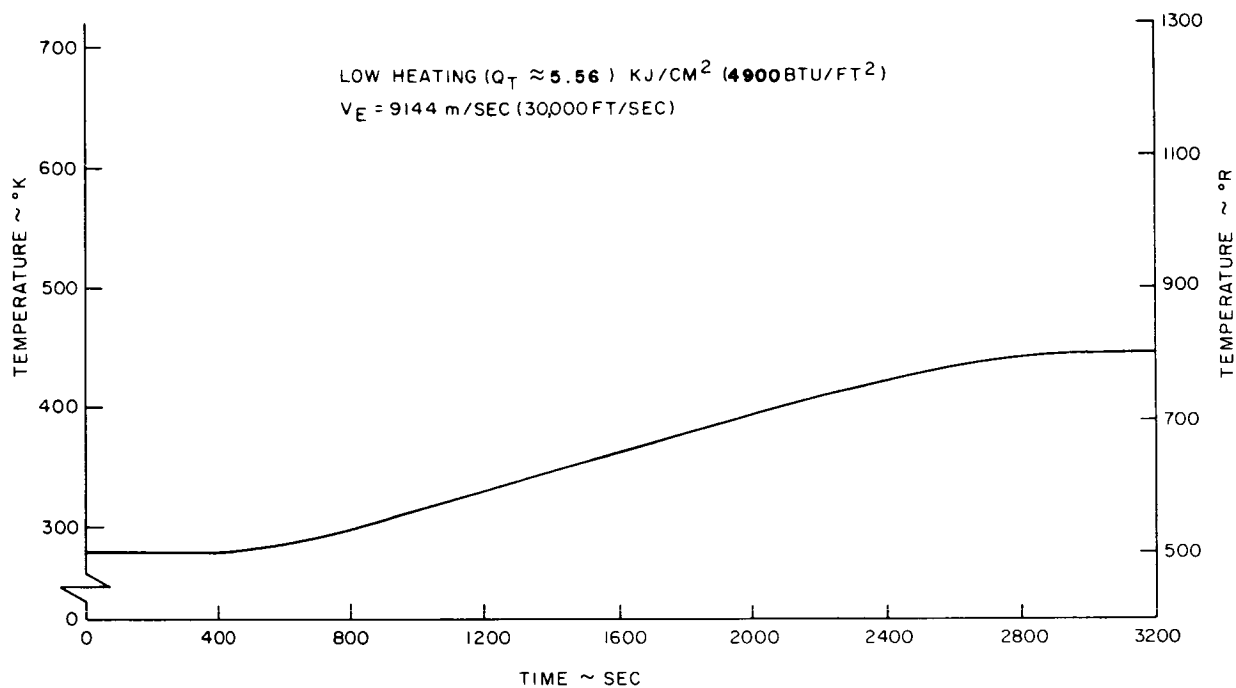
Figure 45. Temperature-Time Histories for ESM at a Typical Low
Heating Rate Condition (Aluminum Structure)

LOW HEATING ($Q_T \approx 5.56$ KJ/CM^2) (4900 BTU/FT^2)

V_E = 9144 M SEC (30,000 FT/SEC)

TIME ~ SEC
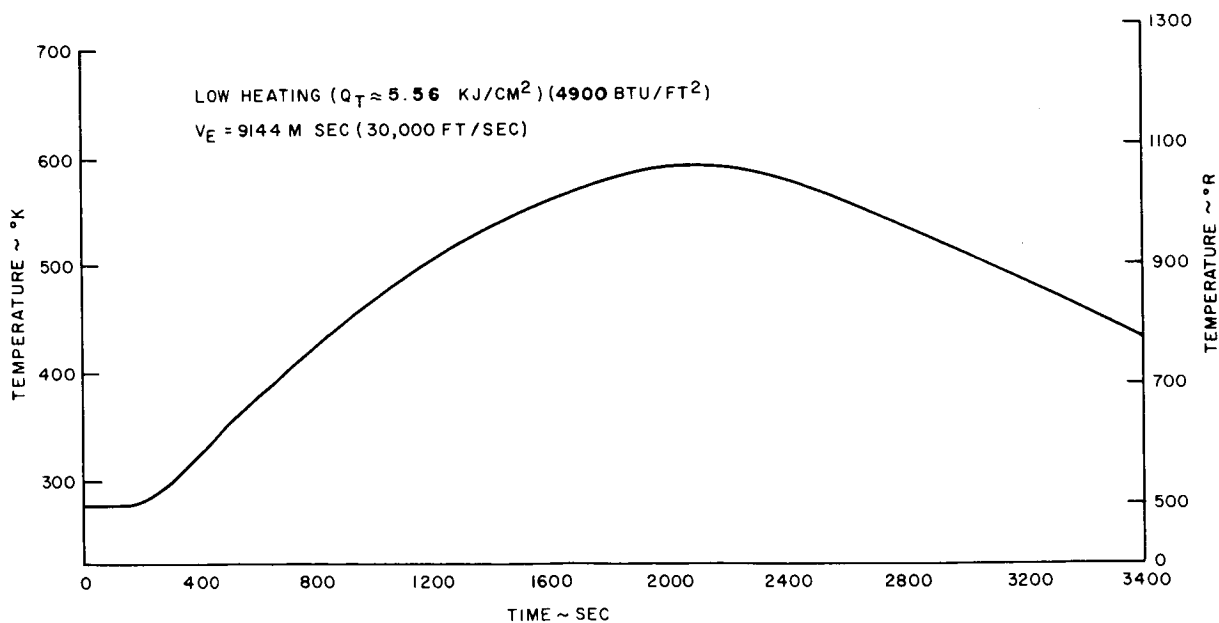
Figure 46. Temperature-Time Histories for ESM at a Typical Low
Heating Rate Condition (Steel Structure)
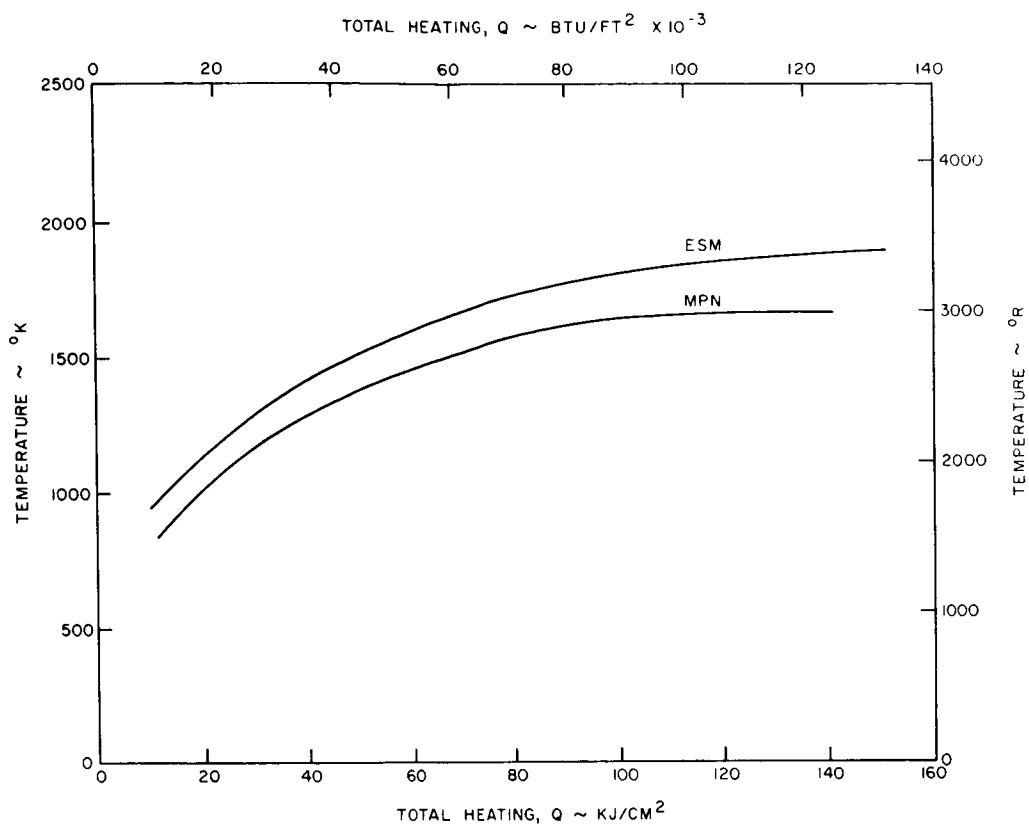
Figure 47. Maximum Surface Temperature vs. Total Heating for ESM and MPN
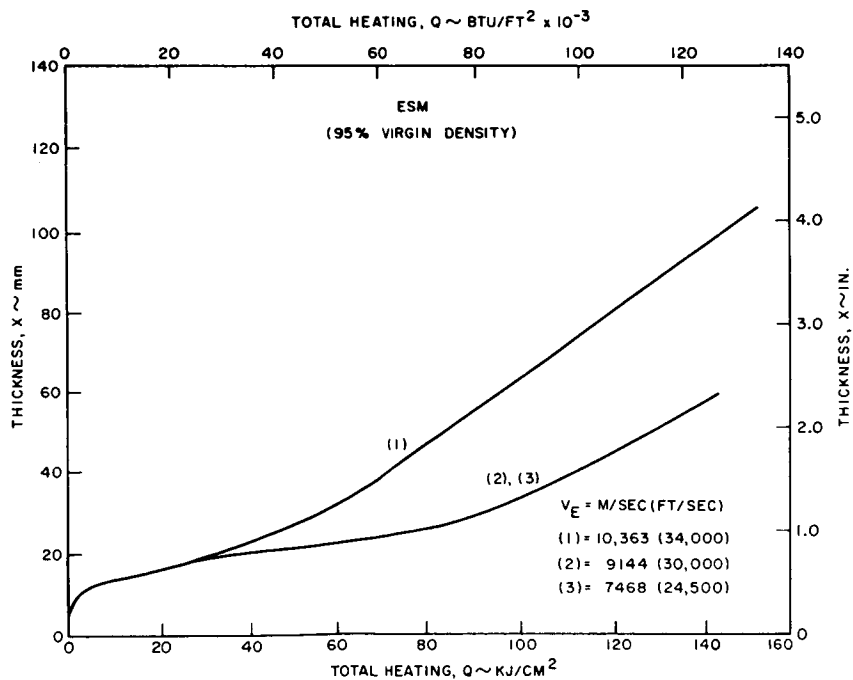
Figure 48. ESM Degradation vs. Total Heating for Re-entry

F27
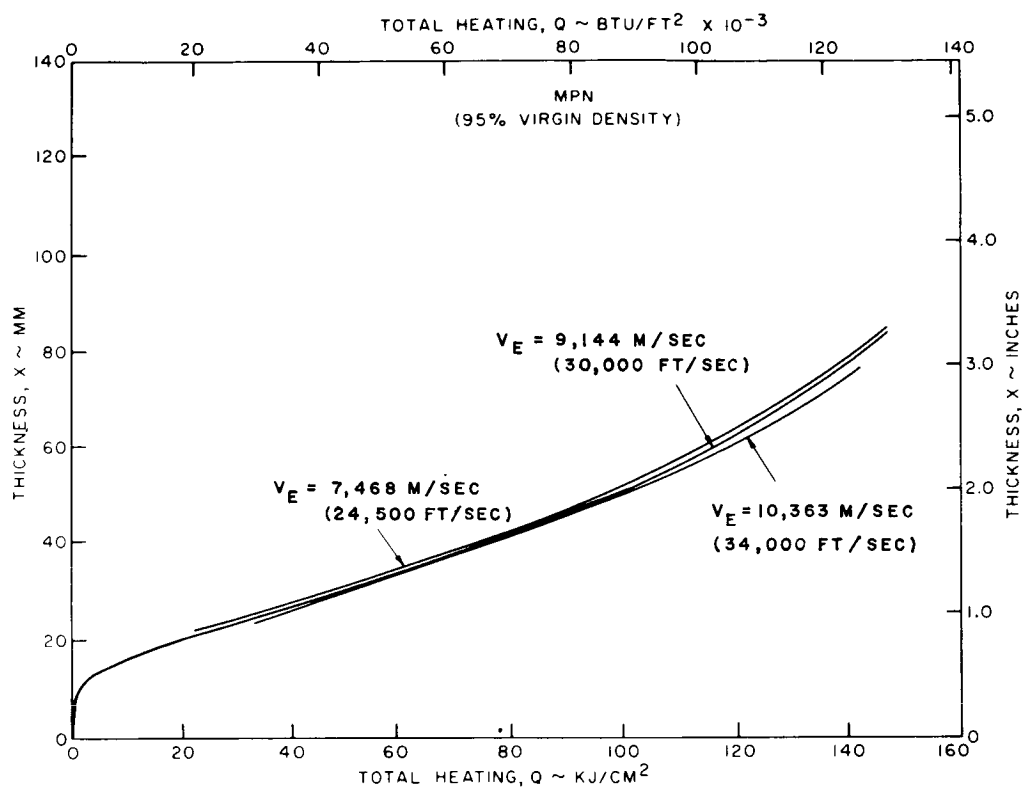
Figure 49. MPN Degradation vs. Total Heating for Re-entry
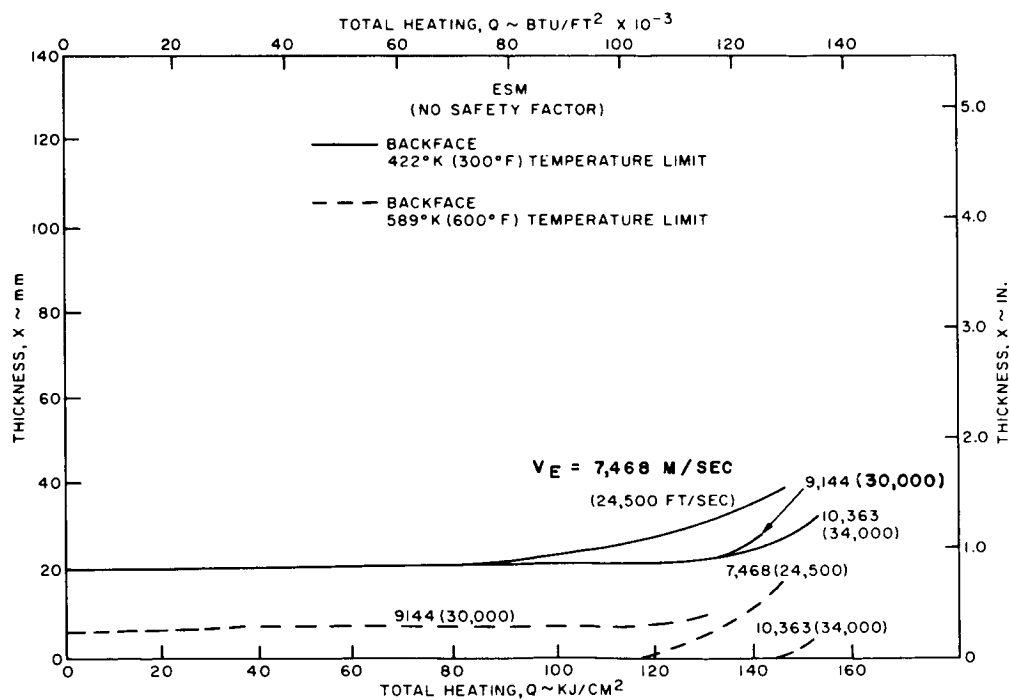
Figure 50. ESM Insulation Requirements vs. Total Heating

F28
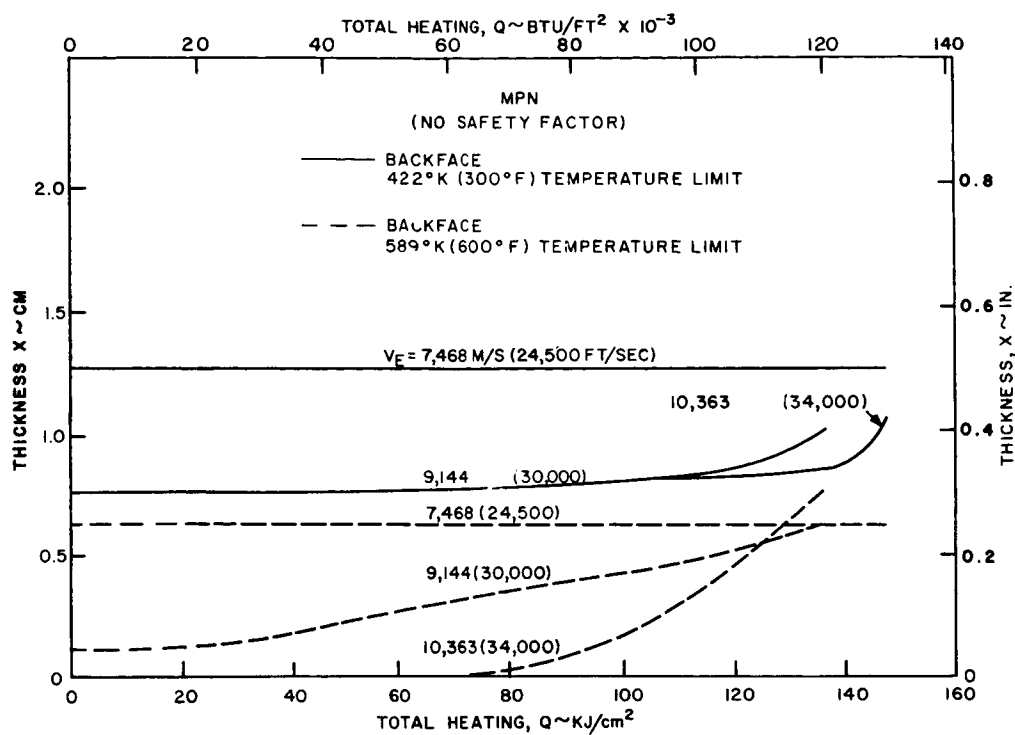
Figure 51. MPN Insulation Requirements vs. Total Heating
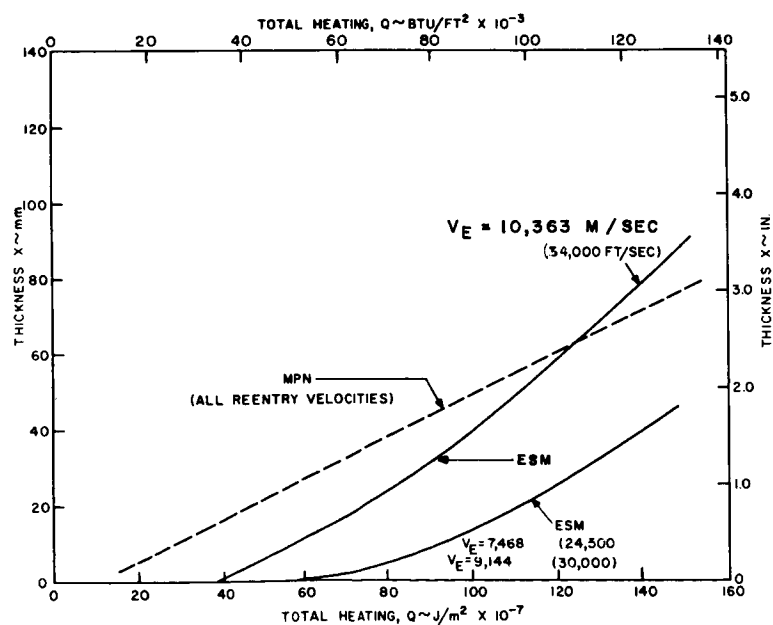
Figure 52. Surface Recession vs. Total Heating for ESM and MPN

ATTACHMENT CLIPS

FLIGHT
DIRECTION

A   A

TRAILING EDGE OF EACH PANEL   FASTENING BOLT AT AFT
RERADIATIVE SURFACE   OVERLAPS THE SUCCEEDING PANEL   APEX OF EACH PANEL

INSULATION   SELF-LOCKING ANCHOR   STIFFENING RINGS   VEHICLE SHELL
                 NUT

SECTION A-A

(A) DIAMOND-SHAPED PANEL

FLIGHT
DIRECTION

B   B

C

EXPANSION GAP

VIEW AT C

CORRUGATED PANEL
SHIELD SUPPORTS   ATTACHMENT ROD   INSULATION PADS   SPACER RIVETS

VEHICLE SHELL   STIFFENING RINGS

SECTION B-B

(B) CORRUGATED PANEL

Figure 53. Typical Re-Radiation Thermal Shield Concepts

F30

HEAT SHIELD

INSULATION

15.2 Cm
(6 IN.)

1.90 Cm (0.75 IN.)

CHANNEL

SHIELD
SUPPORT

ROD
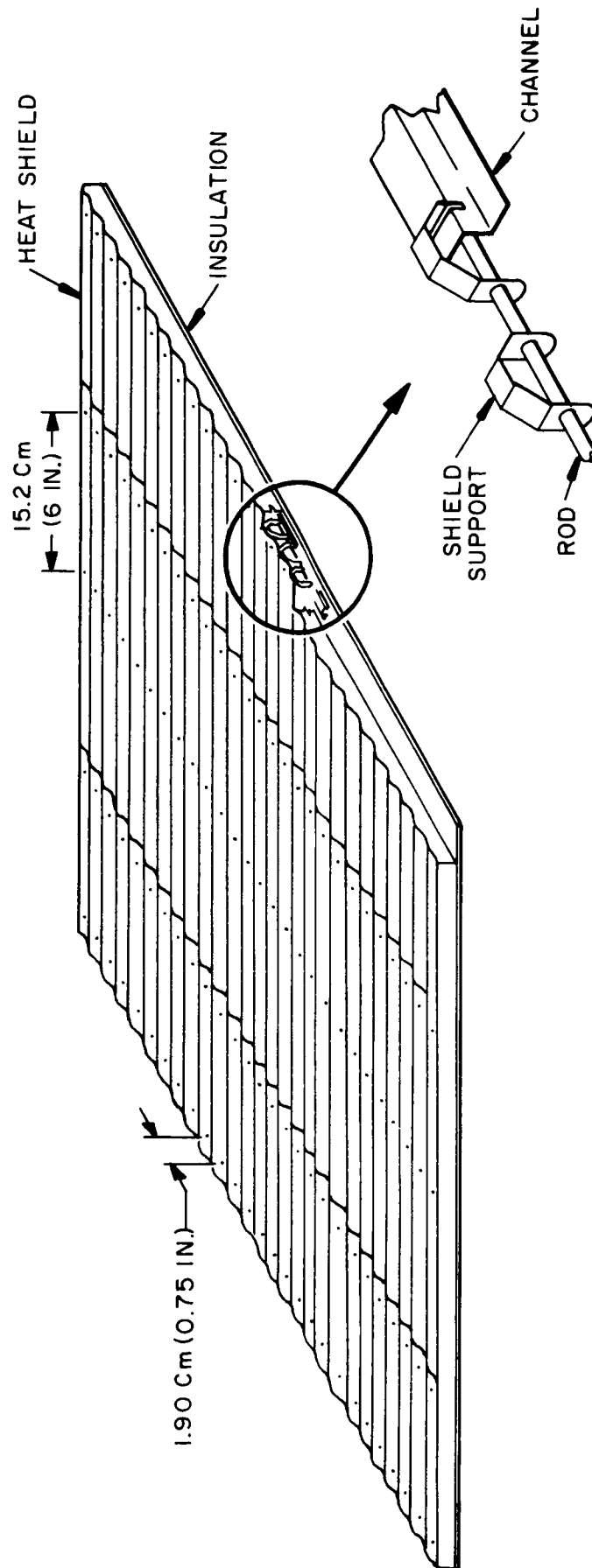
Figure 54. Typical Corrugated Panel Design Showing Clips and Fasteners

Figure 56. Effective Thermal Conductivity
for Re-Radiation Structure
(Rene 41 and TZM)

Figure 55. Specific Heat vs. Temperature for
Micro-quartz, Foam Pyrolytic
Graphite, Rene 41, and TZM

F32
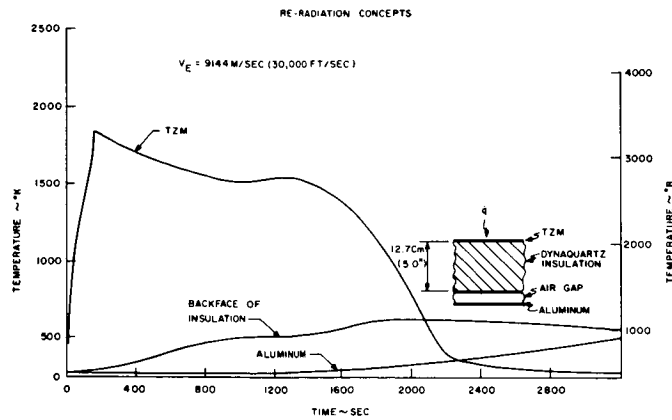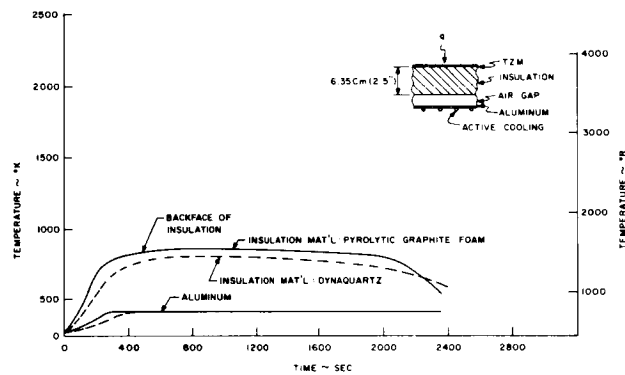
A. Panel with Air Gap

B. Panel with Air Gap plus Cooling
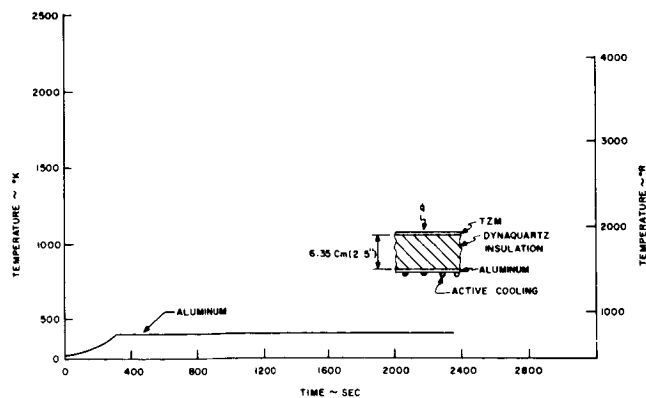
C. Panel with Cooling

Figure 57. Typical Temperature Histories for Re-Radiating Concept
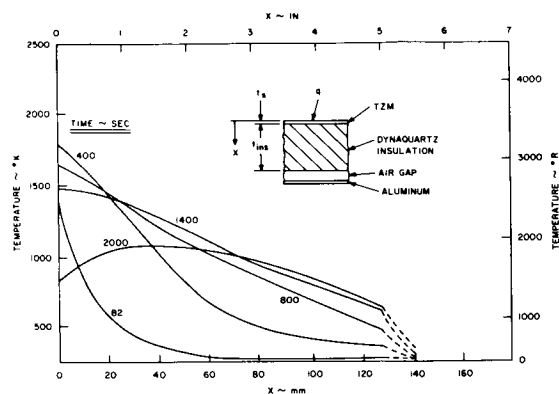
A. Panel with Air Gap
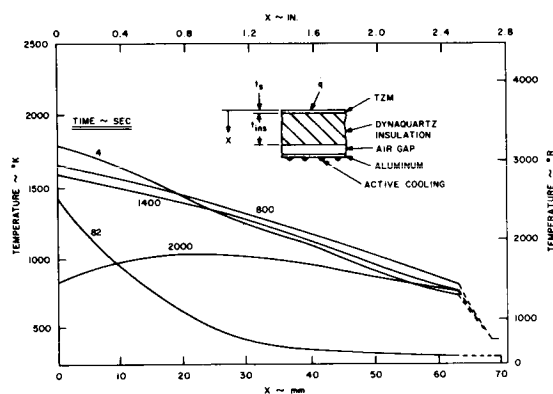
B. Panel with Air Gap plus Cooling
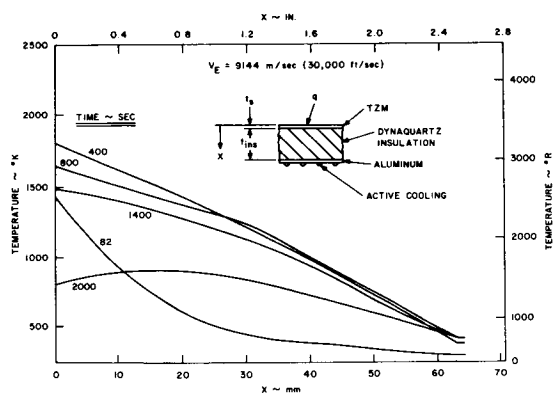
C. Panel with Cooling

Figure 58. Typical Temperature Profiles for Re-Radiating Concept

F34
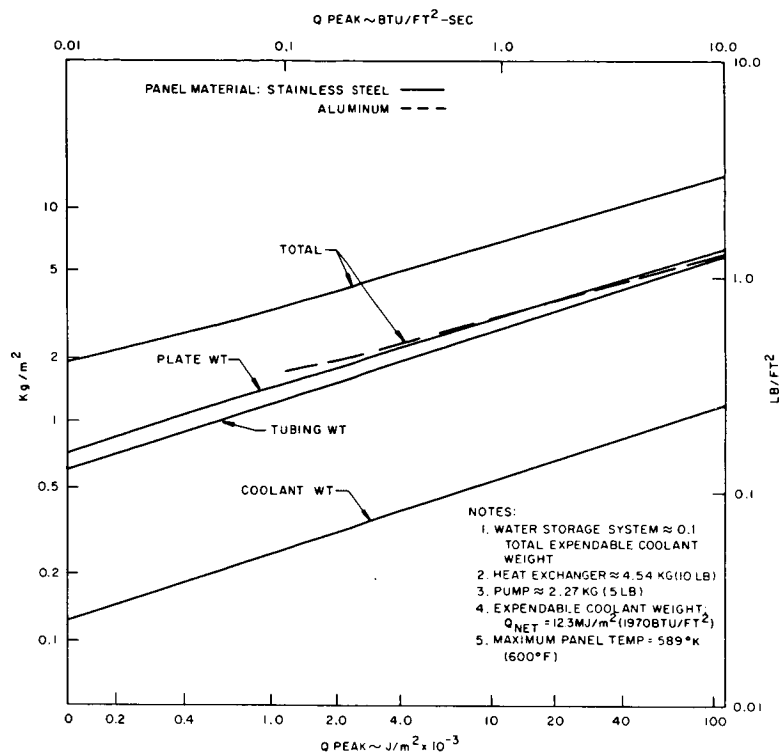
Figure 59. Weight Requirement for Closed-Loop Cooling
System vs. Maximum Heat Flux
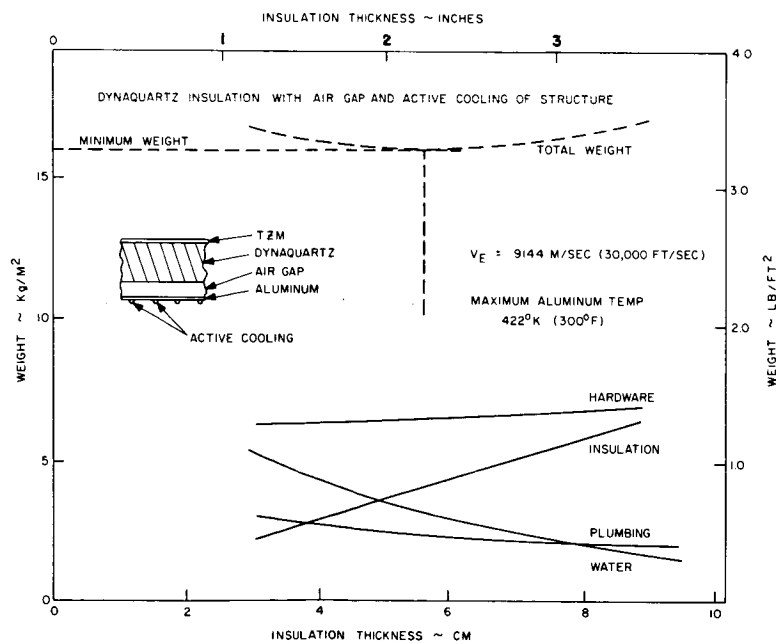
Figure 60. Typical Minimum Weight Optimization of Re-Radiation
Structure with Air Gap and Active Cooling
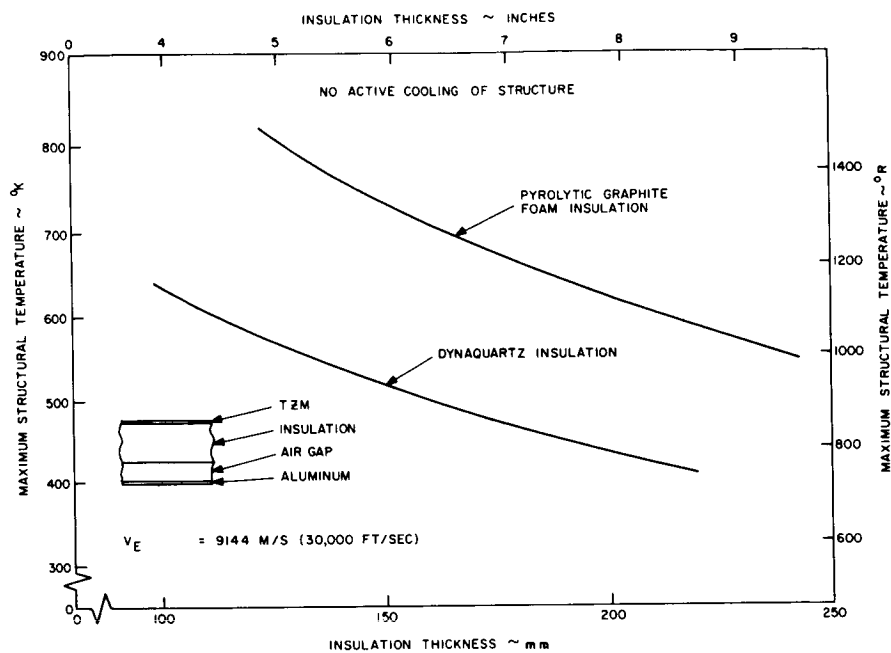
Figure 61. Typical Insulation Requirements for Re-Radiation
Structure without Cooling
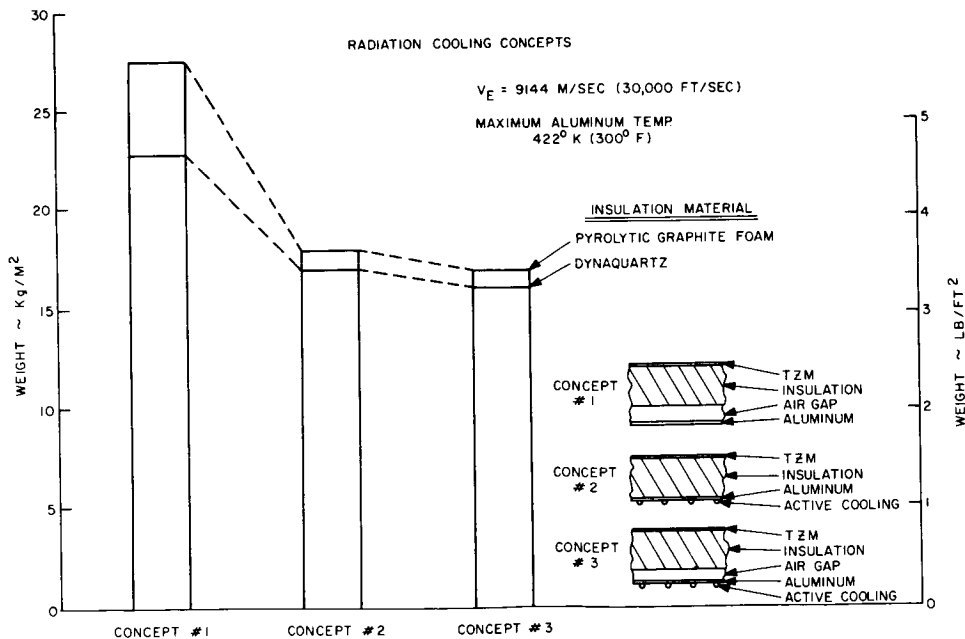
Figure 62. Weight Comparison of Re-entry Cooling Concepts
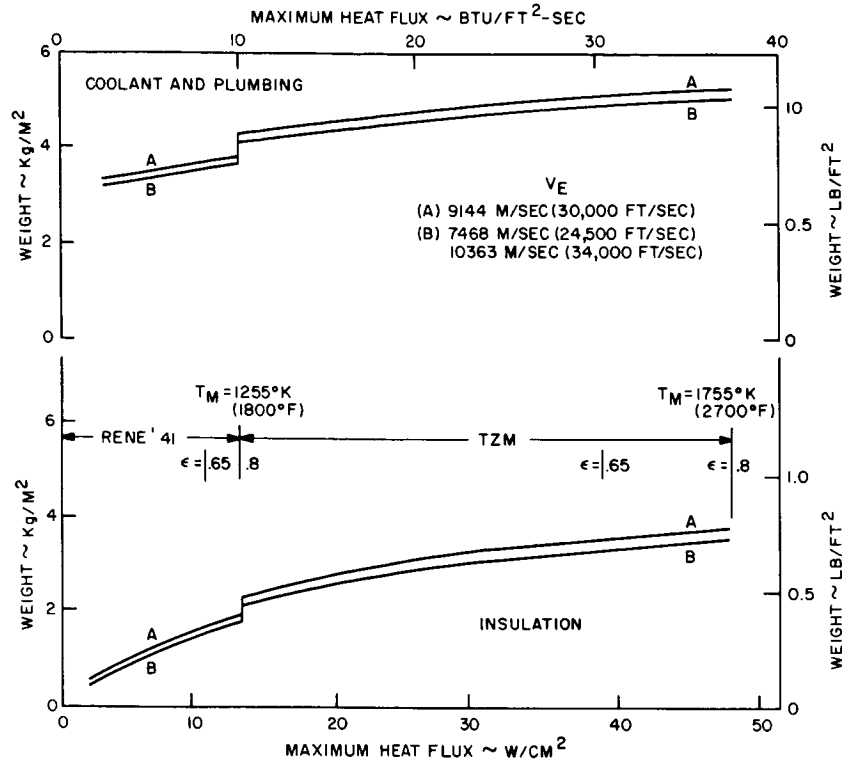
Figure 63. Re-Radiation Requirements vs. Maximum Heat Flux
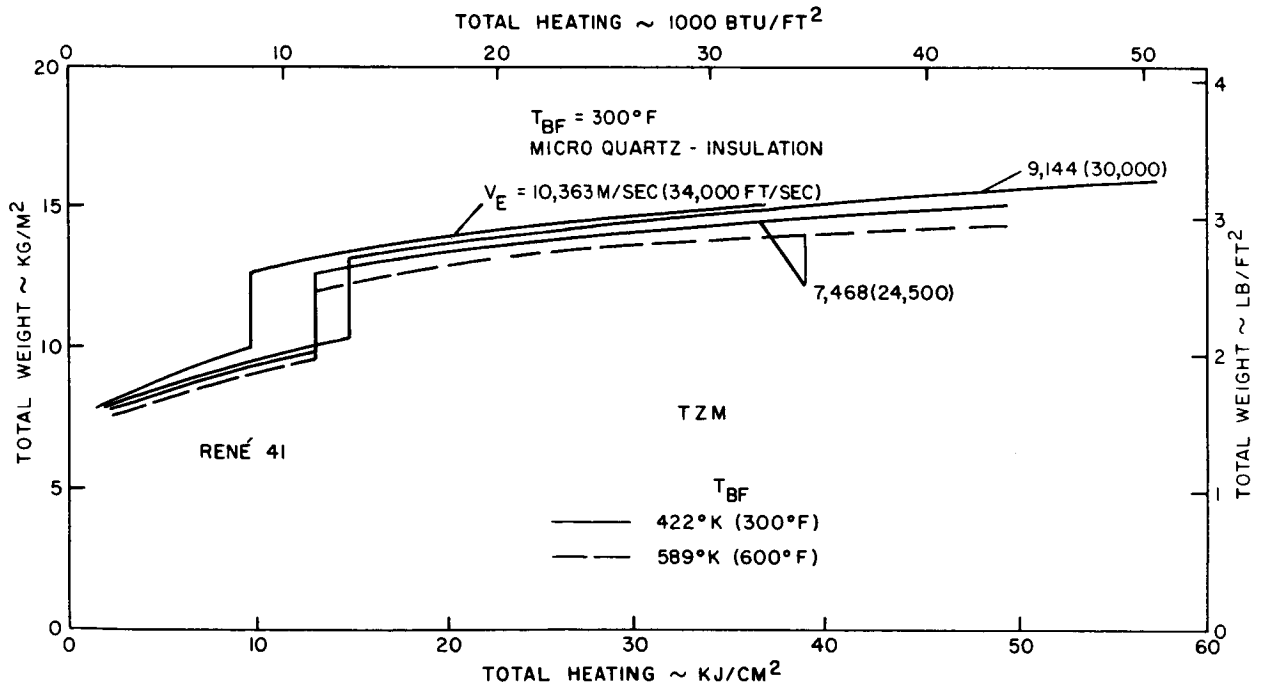
Figure 64. Re-Radiation Shield Requirements vs. Total Heating

F37
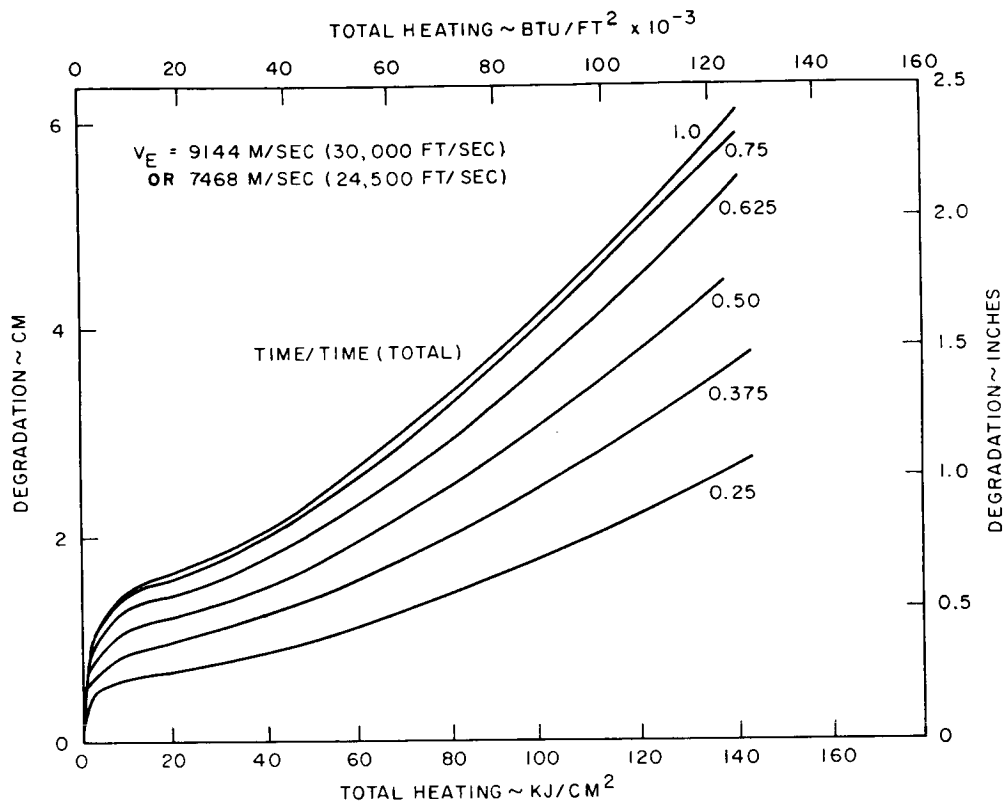
Figure 65. ESM Ablation Requirements for the Ablation over
Re-Radiation Heat Protection System
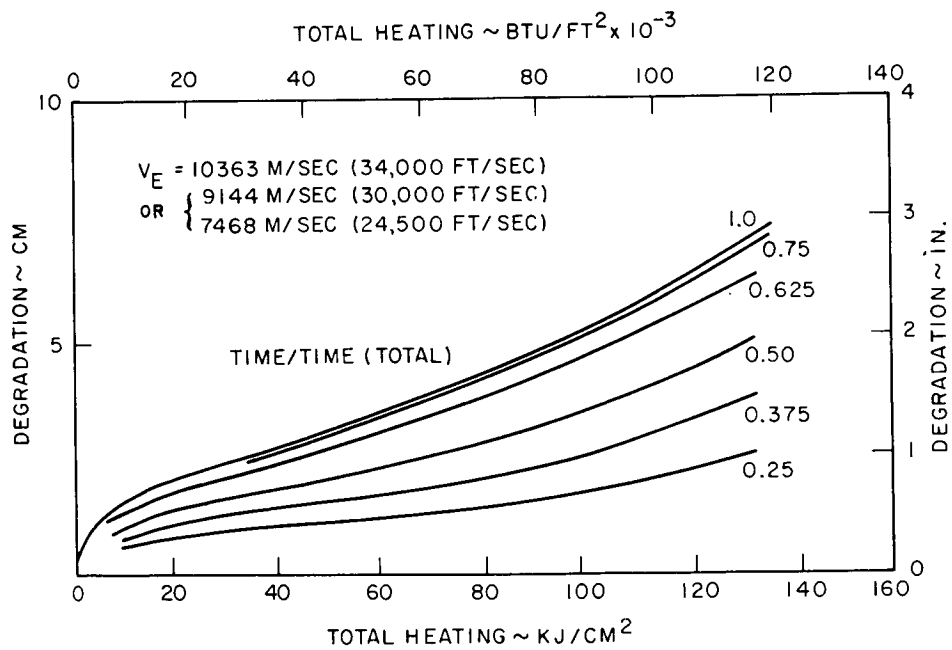
Figure 66. MPN Ablation Requirements for the Ablation over
Re-Radiation Heat Protection System

F38
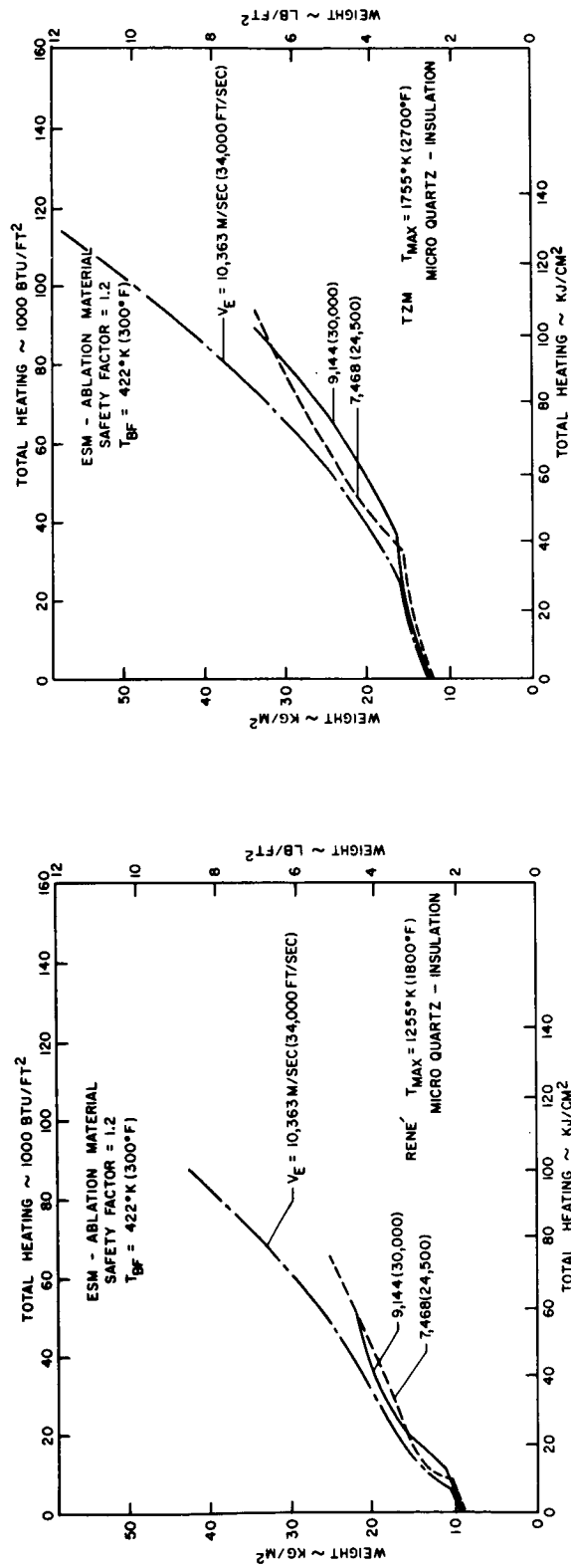
A. Rene 41 Re-Radiation Material   B. TZM Re-Radiation Material

Figure 67. Ablation Over Re-Radiation Heat Protection Weight Requirement for ESM
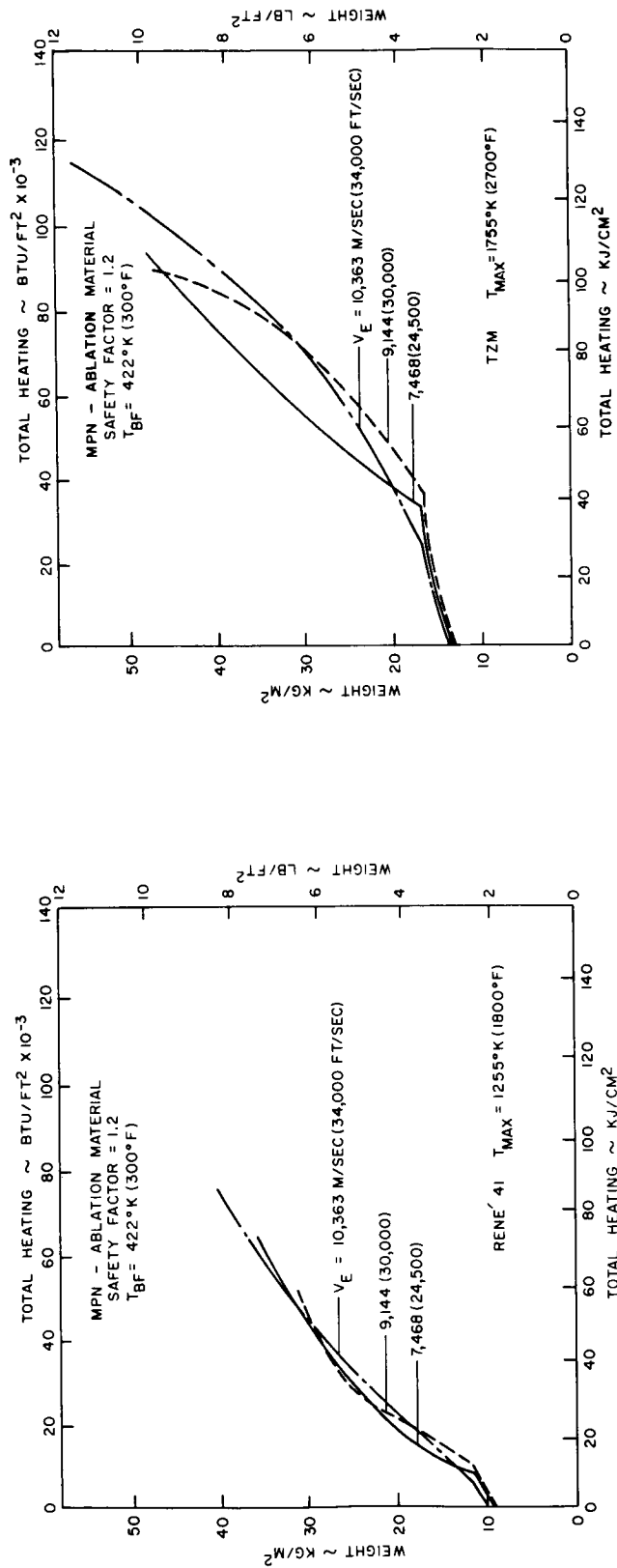
A. René 41 Re-Radiation Material

B. TZM Re-Radiation Material

Figure 68. Ablation Over Re-Radiation Heat Protection Weight Requirement for MPN
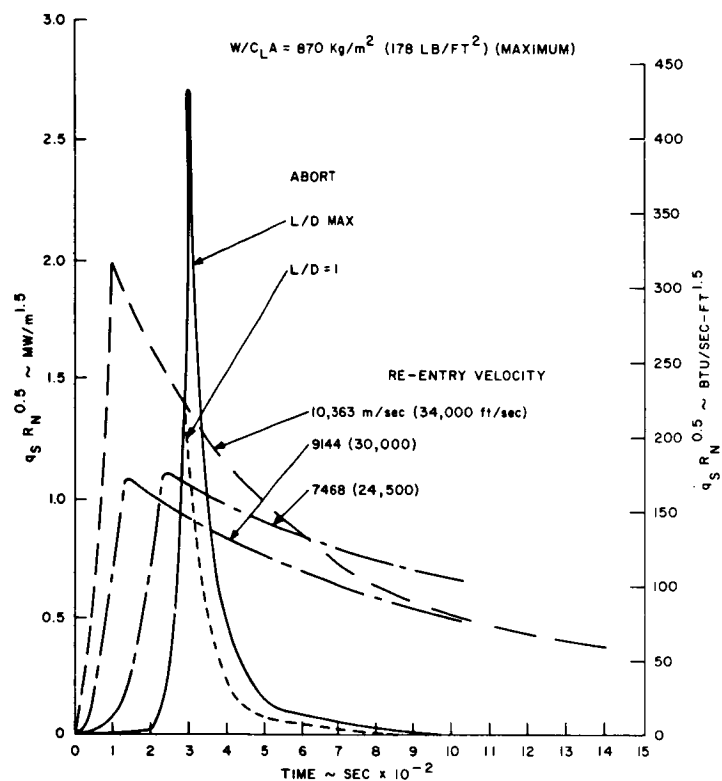
Figure 69. Re-entry and Abort Heat Flux Comparison (Initial Phase of Flight)
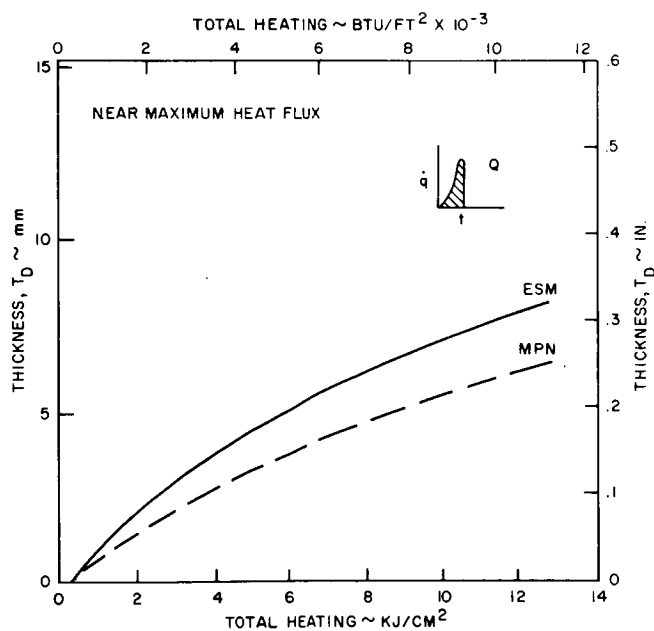
Figure 70. Ablation Requirement for the Initial Phase of Flight
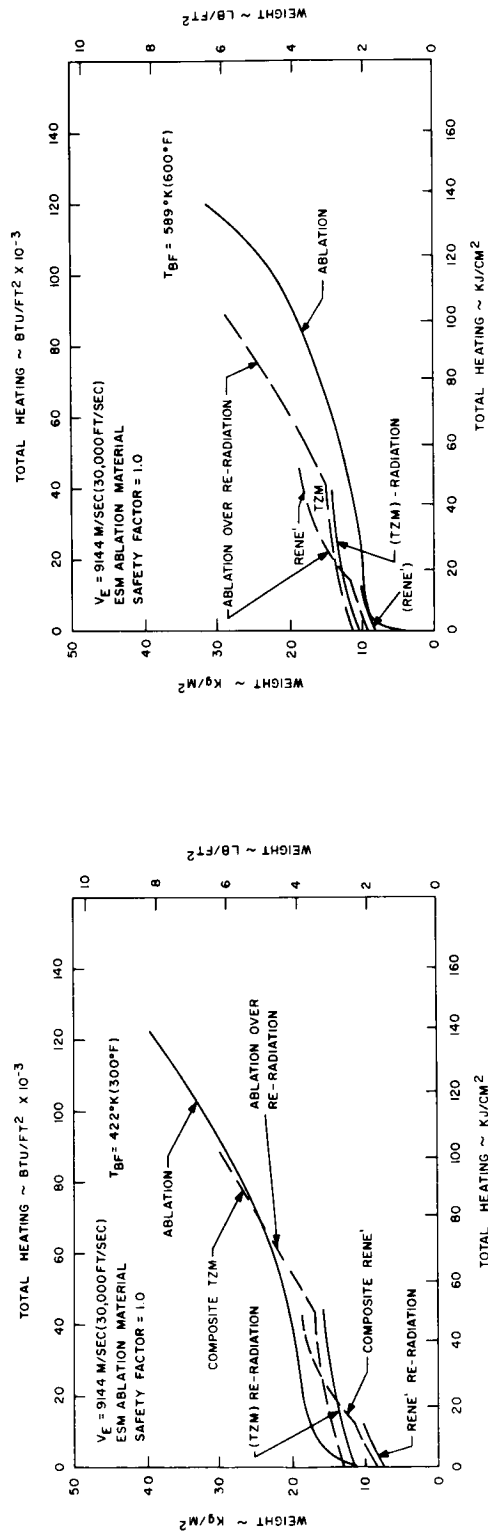
(A)

(B)

Figure 71. Typical Ideal Heat Protection System Weight Comparison for ESM
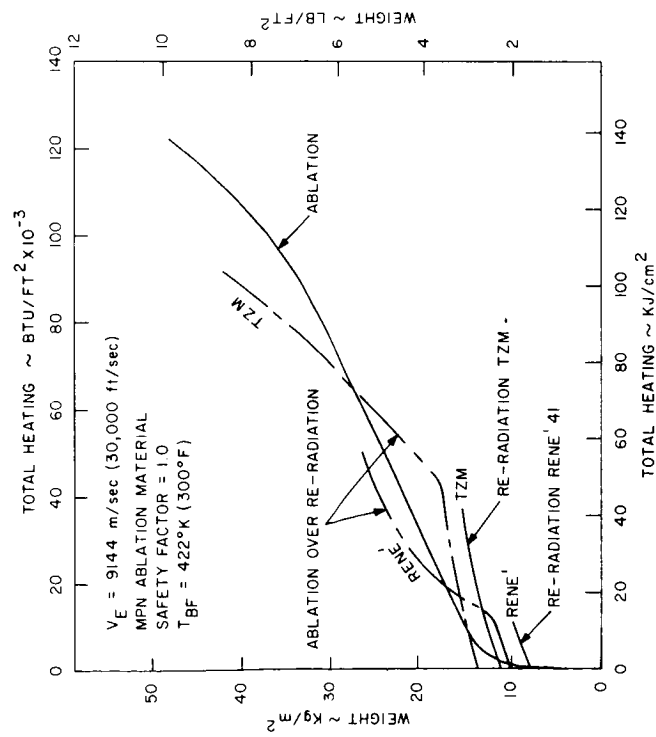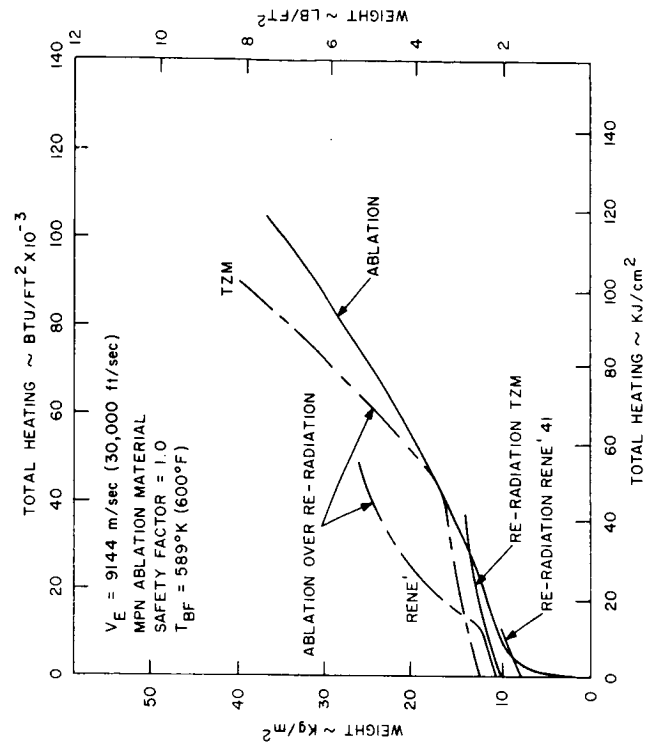
Figure 72. Typical Ideal Heat Protection System Weight Comparison for MPN
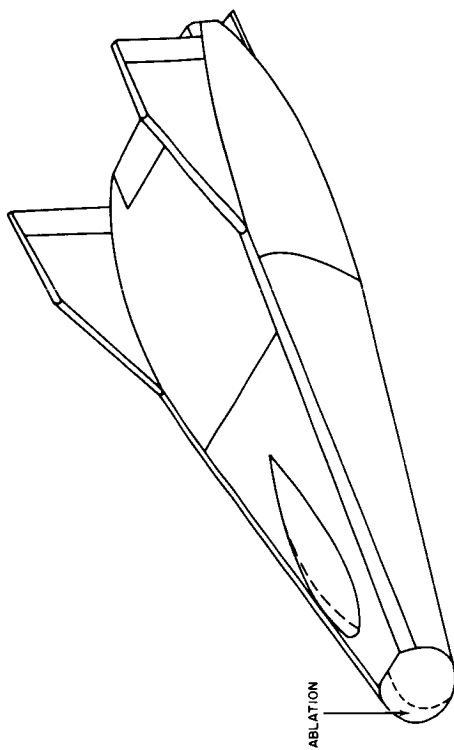
A. Ablation
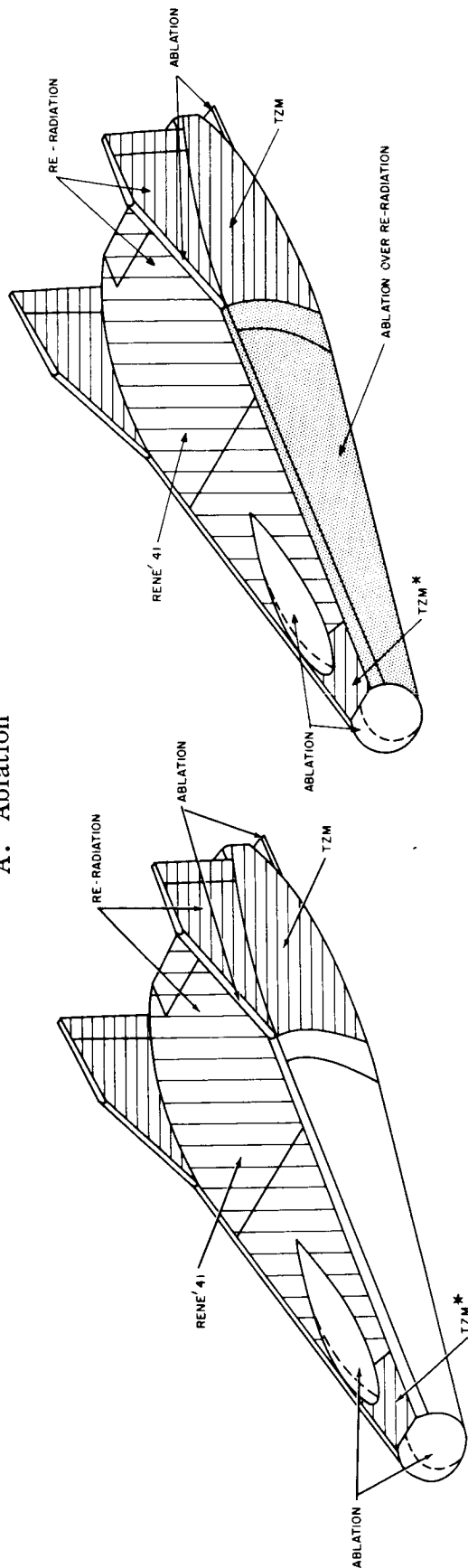
B. Ablation and Re-Radiation

C. Ablation, Re-Radiation, and Ablation over Re-Radiation

Figure 73. Typical Heat Protection System Application

F44
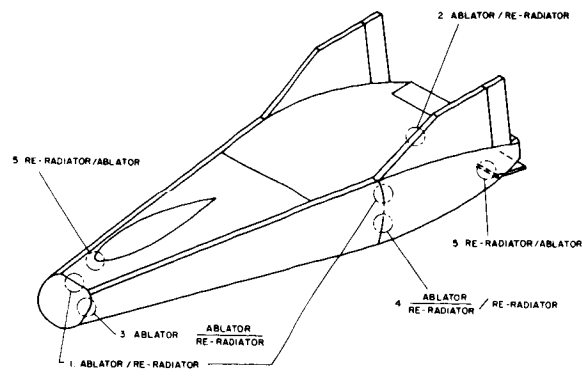
A. Location of Joints
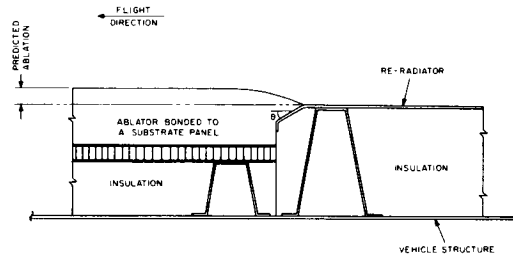
B. Joint #1

(B)
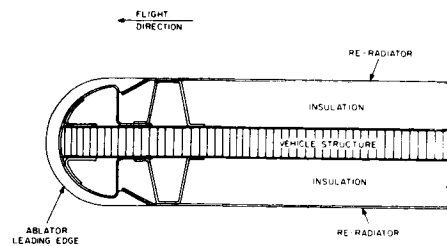
C. Joint #2

Figure 74. Typical Joint Concepts (Sheet 1 of 2)
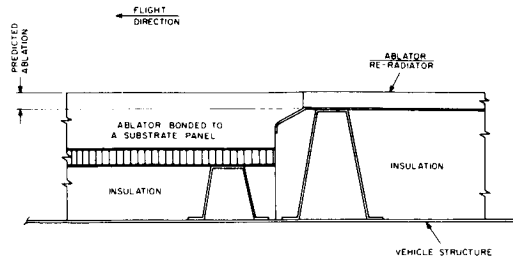
D. Joint #3

(D)
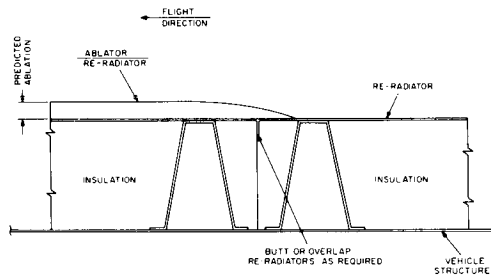
E. Joint #4
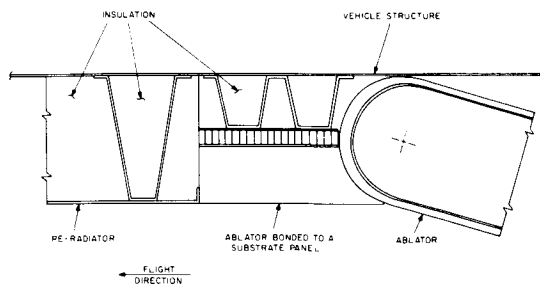
F. Joint #5

Figure 74. Typical Joint Concepts (Sheet 2 of 2)

F46

SUBSTRUCTURE SKIN

ACCESS DOOR GAP

BOLT

THERMAL SHIELD

BEVELED
PANEL EDGES

PLUG

THERMAL
SHIELD

FLOW
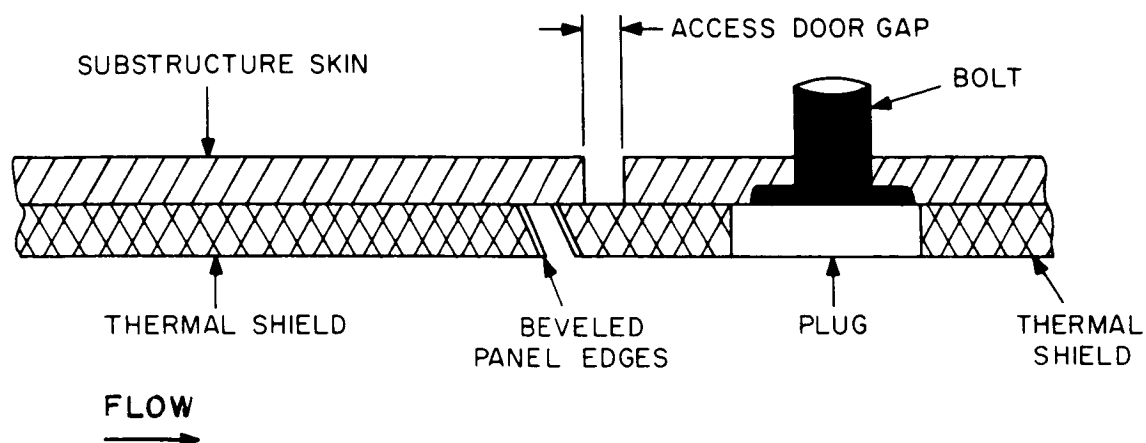
A. Reduction of Gaps Via Beveled Edges

SUBSTRUCTURE
SKIN

STRUCTURAL
HINGE

SUBSTRUCTURE
SKIN

THERMAL
SHIELD

ESM "HINGE"
TO CLOSE LEADING
EDGE GAP (FIBER RE-
INFORCED, POSSIBLY FAB-
RICATED WITH OR WITHOUT GROOVE)

THERMAL
SHIELD
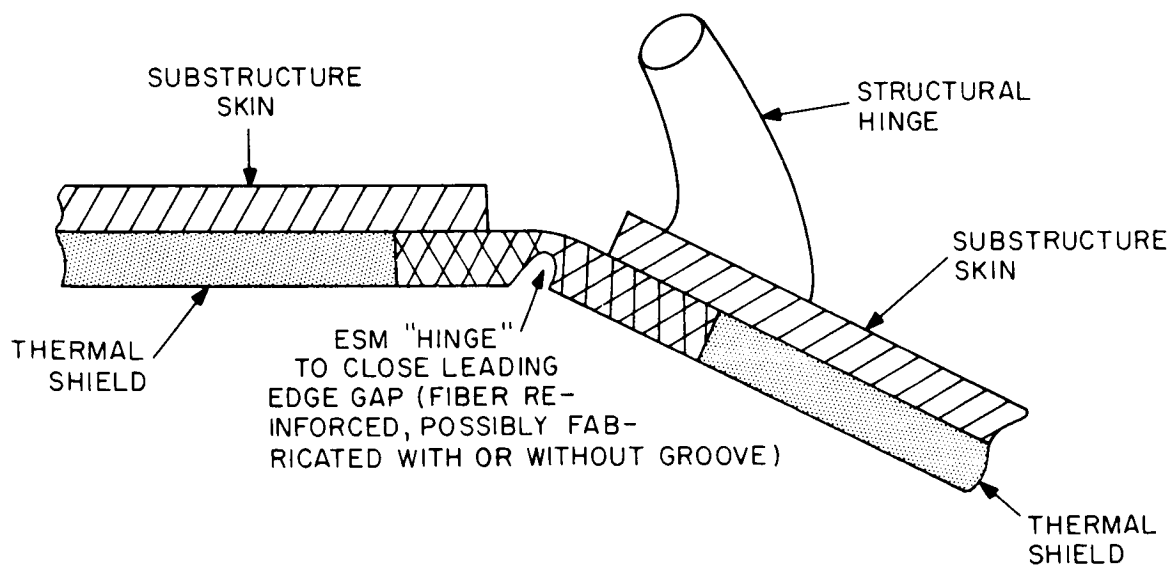
B. Proposed Hinged Closures Arrangement

Figure 75. Typical Hinge and Gap Concepts
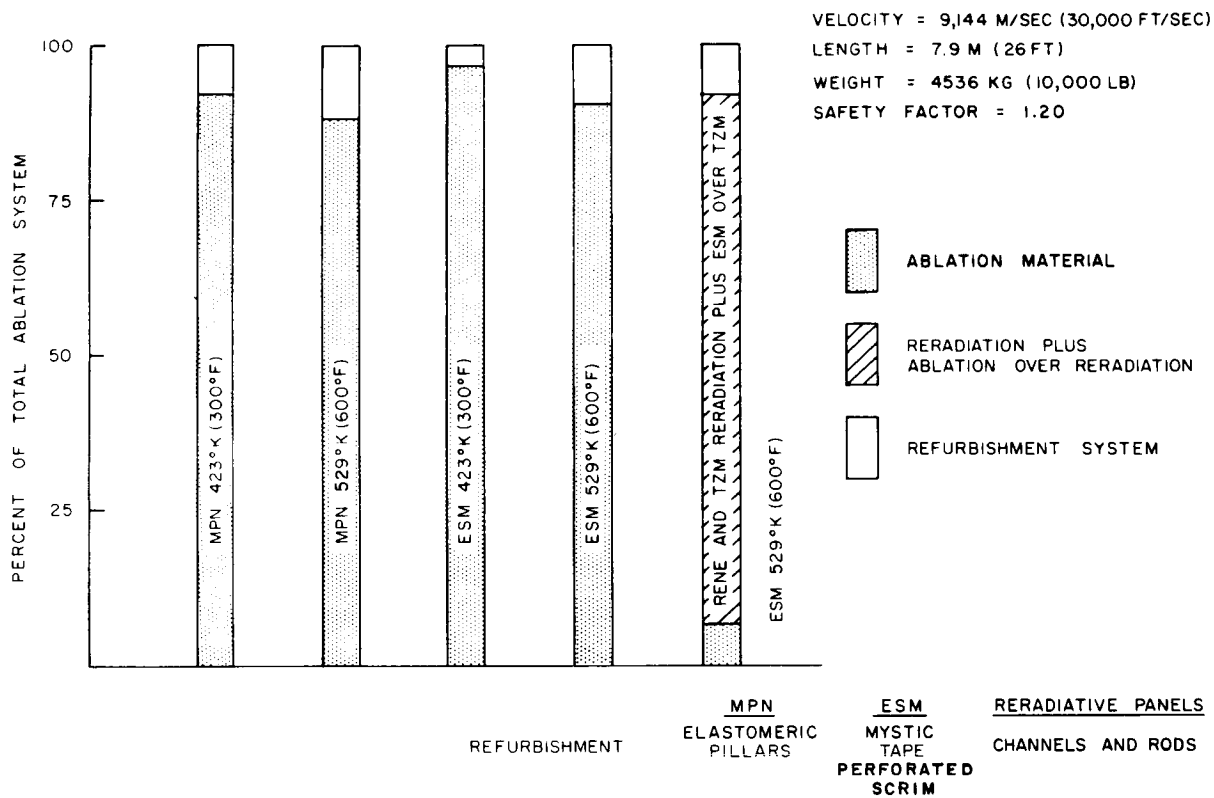
Figure 76. Refurbishment Weights for Various Heat Protection Systems
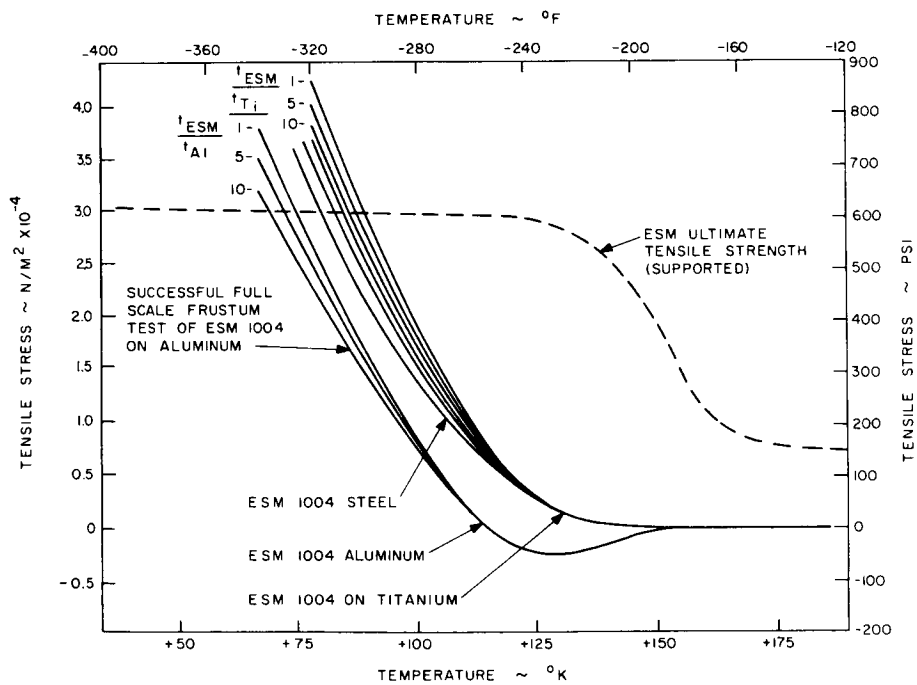
Figure 77. Typical ESM Orbit Stress Levels
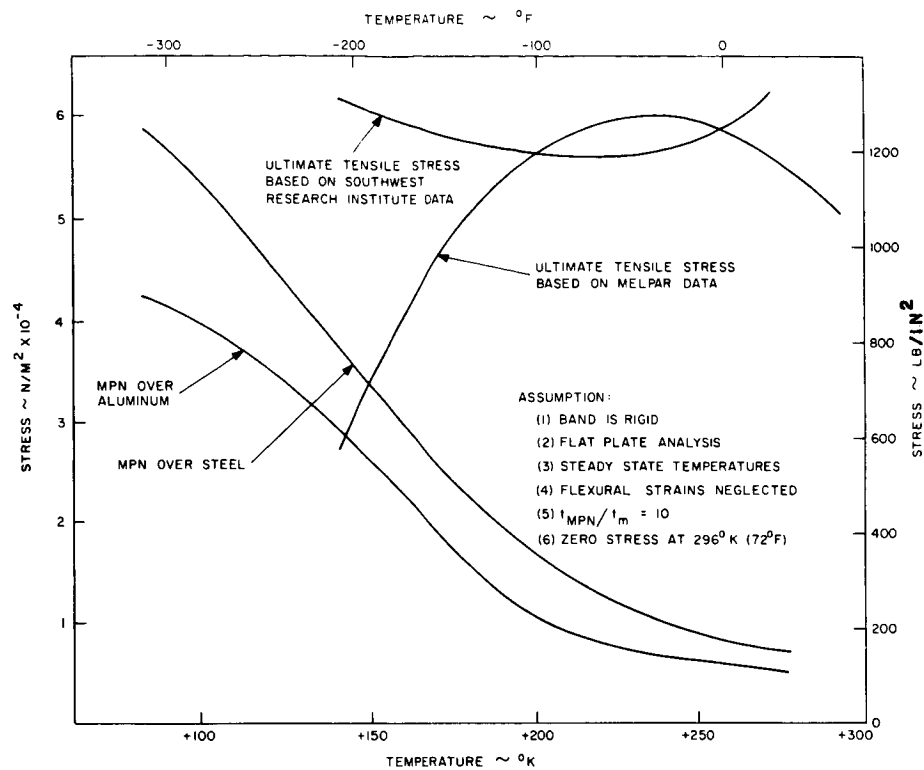
Figure 78. Typical MPN Orbit Stress Levels
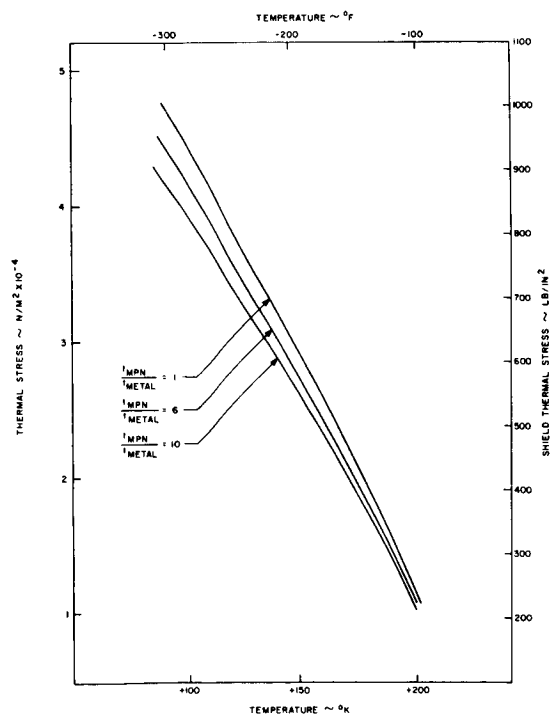
Figure 79. Effect of Shield Thickness on Orbit Stress Levels
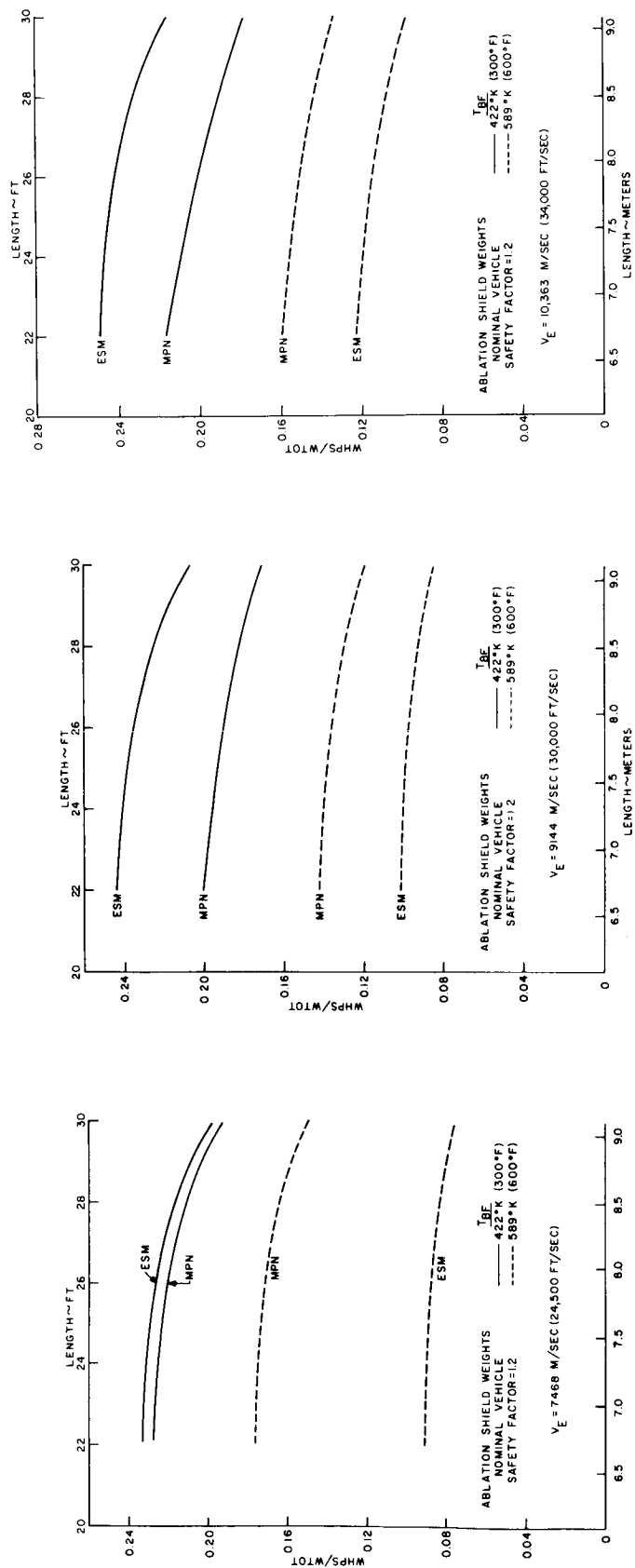
Figure 80.   Ablation Shield Weights for Nominal Vehicle (V_E = 7468 m/sec (2450 ft/sec))

Figure 81.   Ablation Shield Weights for Nominal Vehicle (V_E = 9144 m/sec (30,000 ft/sec))

Figure 82.   Ablation Shield Weights for Nominal Vehicle (V_E = 10,363 m/sec (34,000 ft/sec))

VELOCITY = 9144/SEC (30,000 FPS)
LENGTH = 7.92 M (26 FT)
WEIGHT = 4536 Kg (10,000 LBS)
SAFETY FACTOR = 1.20
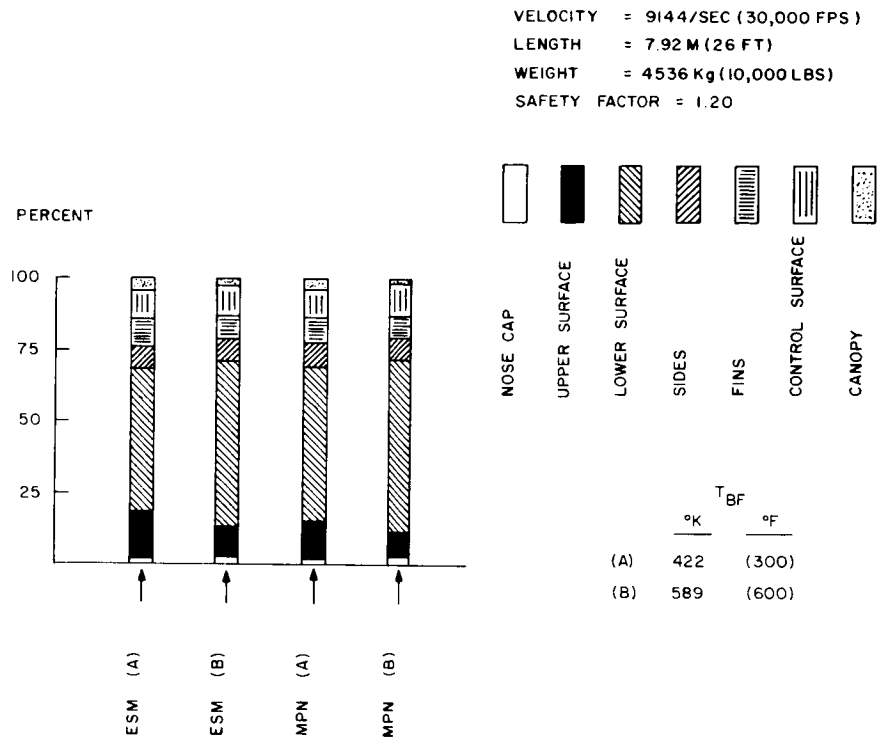
Figure 83. Typical Distribution of Ablation Shield Weights
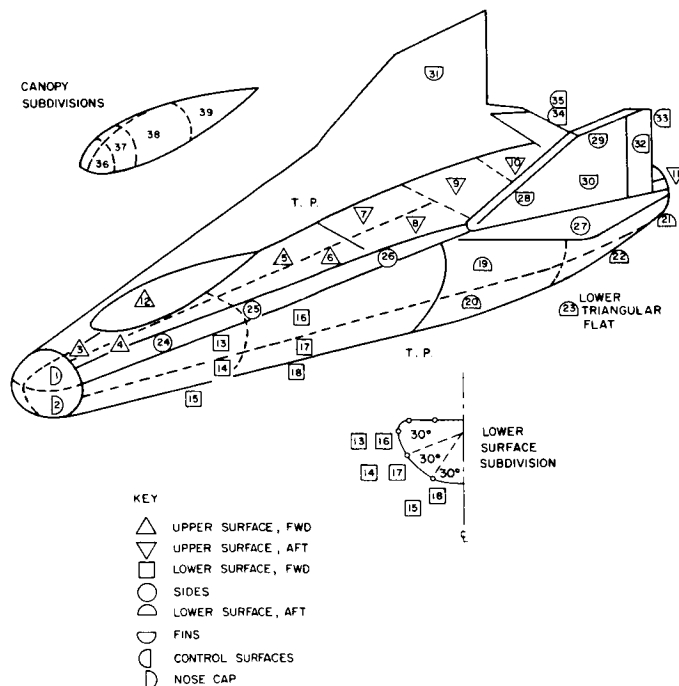
Figure 84. Area Designations for the M2-F2 Vehicle
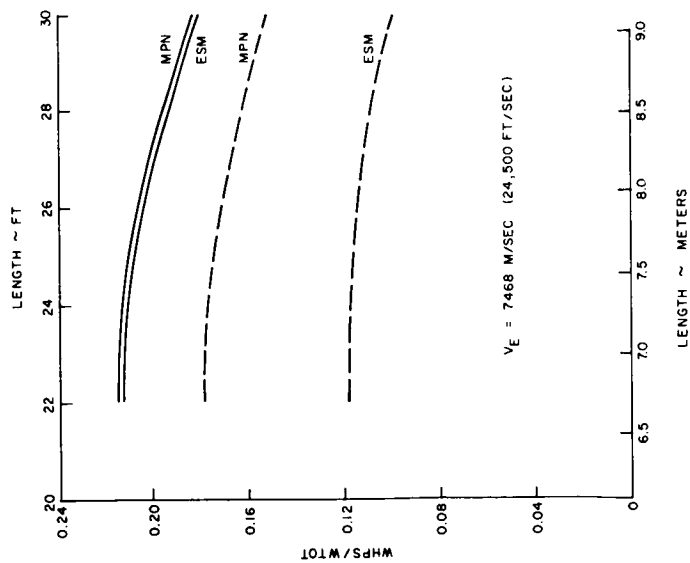
Figure 85. Combined Shield Weights for the Ablation Plus Rene 41 Re-Radiation Systems (V_E = 7468 m/sec (24,500 ft/sec))
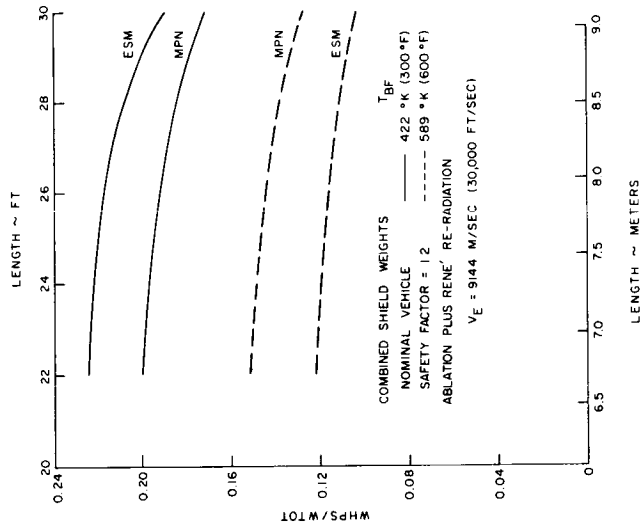
Figure 86. Combined Shield Weights for the Ablation Plus Rene 41 Re-Radiation Systems (V_E = 9144 m/sec (30,000 ft/sec))
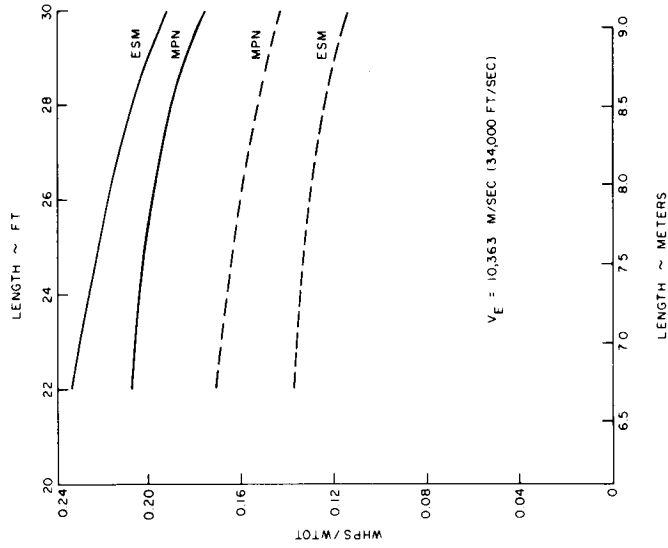
Figure 87. Combined Shield Weights for the Ablation Plus Rene 41 Re-Radiation Systems (V_E = 10,363 m/sec (34,000 ft/sec))

F52

VELOCITY = 9144 M/SEC (30,000 FT/SEC)
LENGTH = 7.92 M (26 FT)
WEIGHT = 4536 Kg (10,000 LB)
SAFETY FACTOR = 1.20
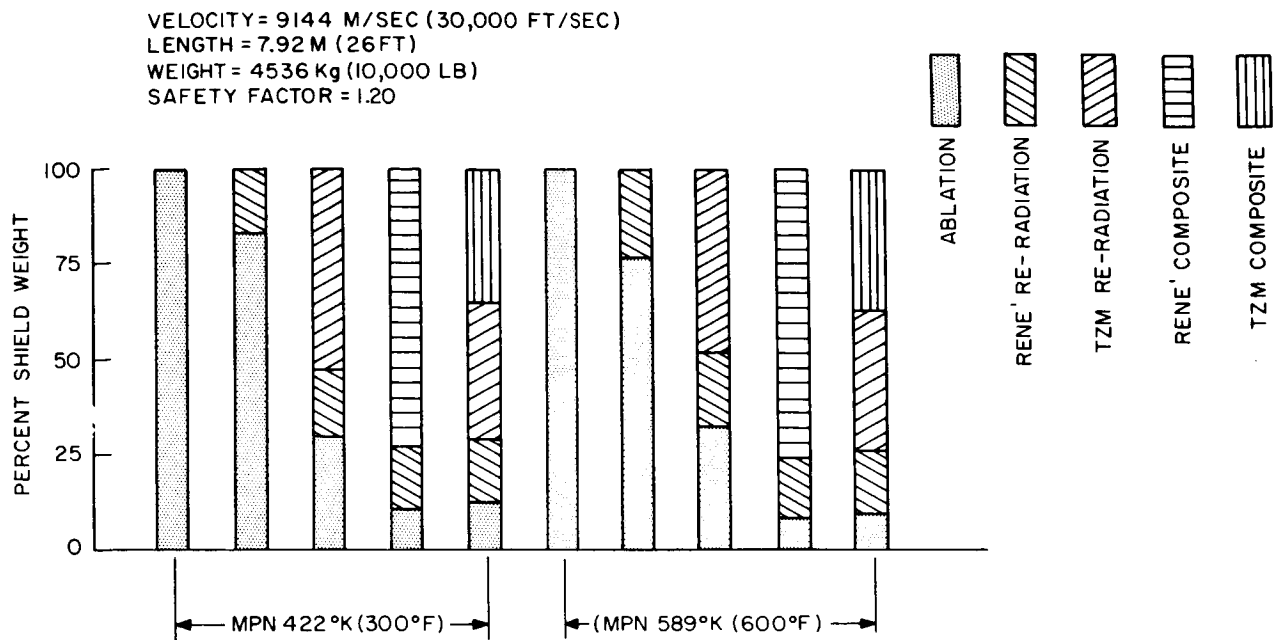
Figure 88.   Typical Weight Comparison for the Various Heat Protection
Systems for MPN

VELOCITY = 9144 M/SEC (30,000 FT/SEC)
LENGTH = 7.92 M (26 FT)
WEIGHT = 4536 Kg (10,000 LB)
SAFETY FACTOR = 1.20
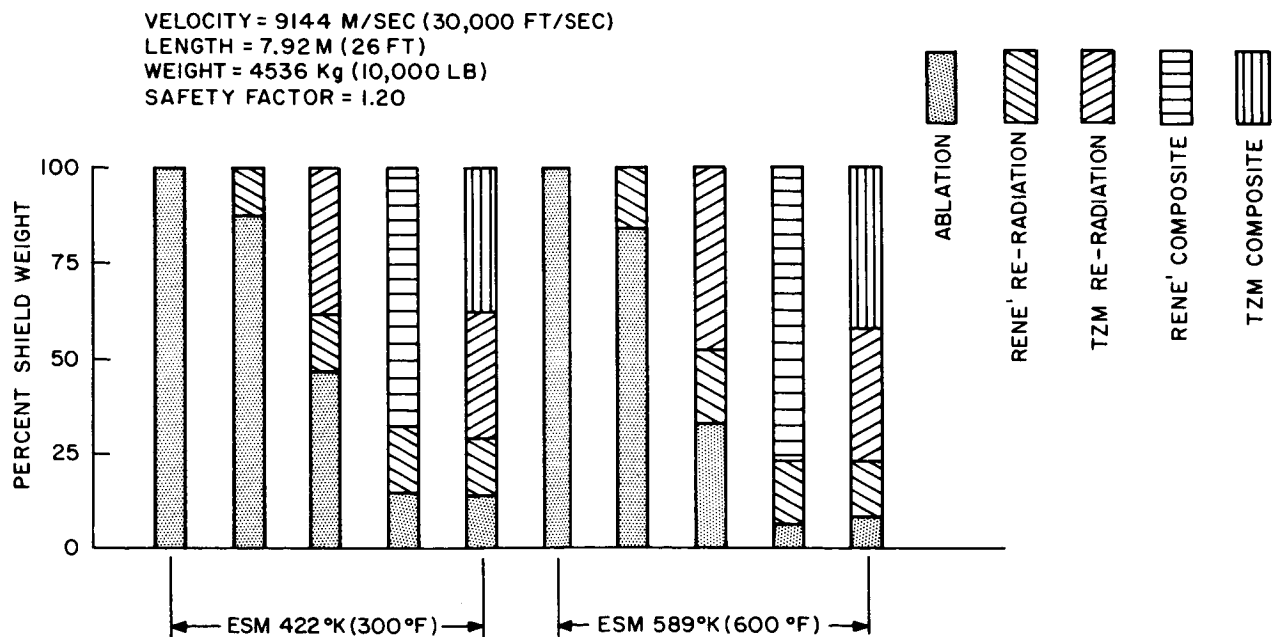
Figure 89.   Typical Weight Comparison for the Various Heat Protection
Systems for ESM
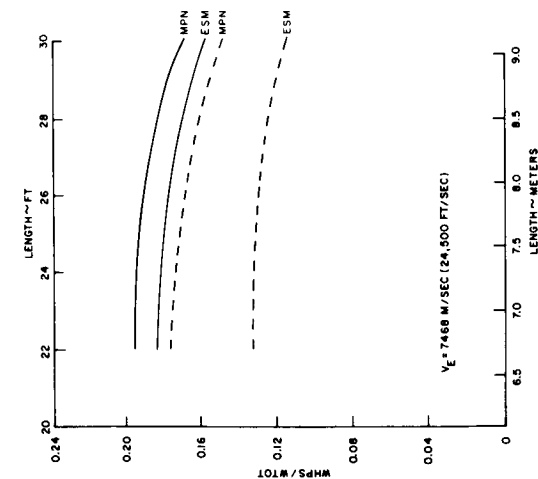
Figure 90. Combined Heat Shield
Weights for the
Ablation Plus TZM
Re-Radiation Heat
Protection System
(V_E = 7468 m/sec
(24,500 ft/sec))
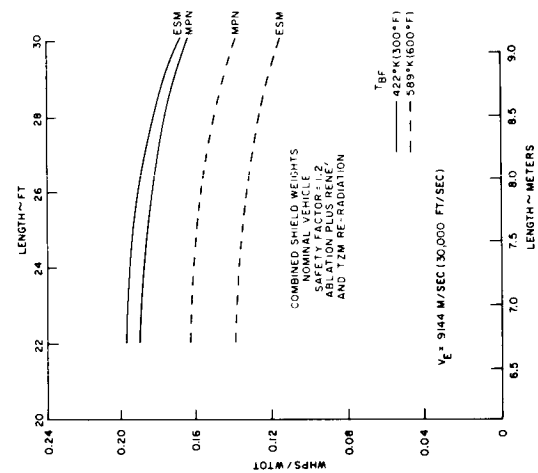
Figure 91. Combined Heat Shield
Weights for the
Ablation Plus TZM
Re-Radiation Heat
Protection System
(V_E = 9144 m/sec
(30,000 ft/sec))
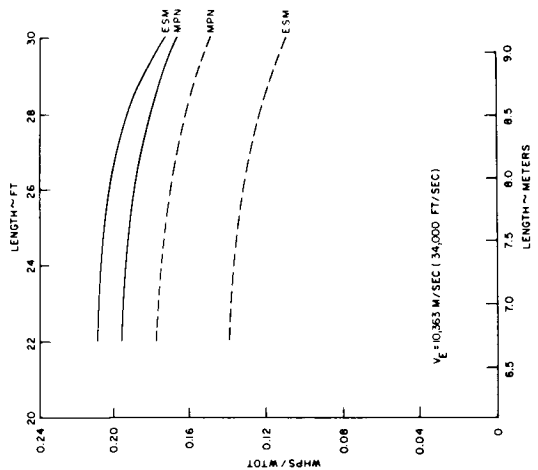
Figure 92. Combined Heat Shield
Weights for tne
Ablation Plus TZM
Re-Radiation Heat
Protection System
(V_E = 10,363 m/sec
(34,000 ft/sec))
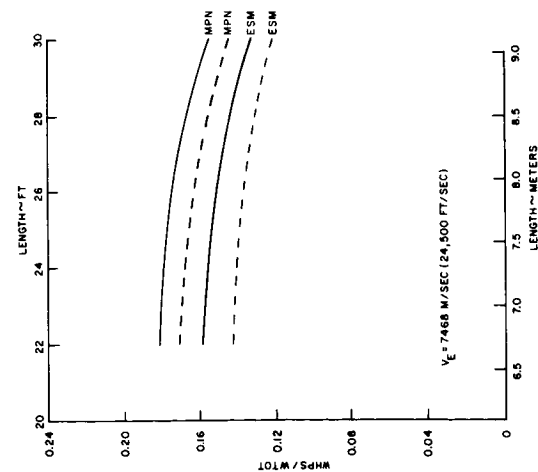
Figure 93. Combined Heat Shield
           Weights for Ablation
           Plus Rene Re-Radiation
           and Ablation over Rene
           Re-Radiation Heat
           Protection Systems
           (V_E = 7468 m/sec
           (24,500 ft/sec))
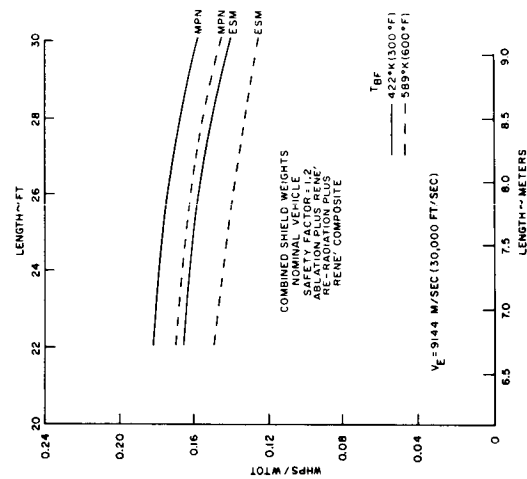
Figure 94. Combined Heat Shield
           Weights for Ablation
           Plus Rene Re-Radiation
           and Ablation over Rene
           Re-Radiation Heat
           Protection Systems
           (V_E = 9144 m/sec
           (30,000 ft/sec))
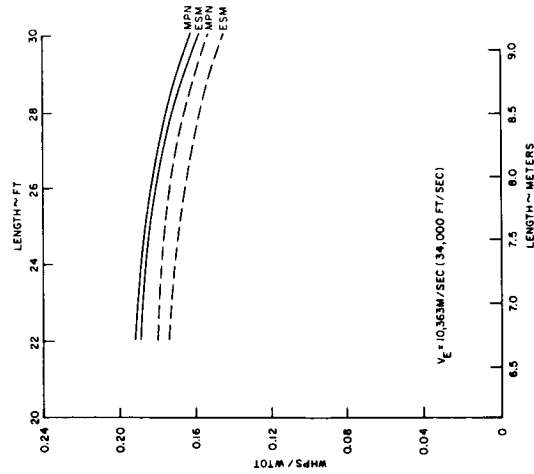
Figure 95. Combined Heat Shield
           Weights for Ablation
           Plus Rene Re-Radiation
           and Ablation over Rene
           Re-Radiation Heat
           Protection Systems
           (V_E = 10,363 m/sec
           (34,000 ft/sec))
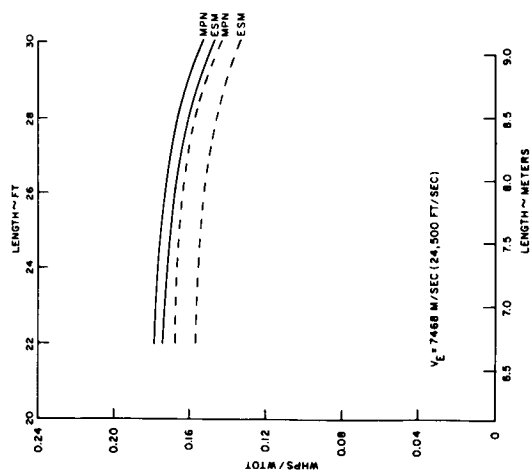
Figure 96. Combined Heat Shield
Weights for Ablation
Plus TZM Re-Radiation
and Ablation over Rene
Heat Protection Systems
(V_E = 7468 m/sec
(24,500 ft/sec))
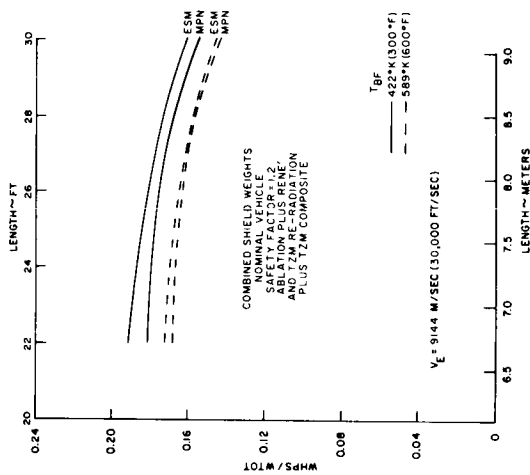
Figure 97. Combined Heat Shield
Weights for Ablation
Plus TZM Re-Radiation
and Ablation over Rene
Heat Protection Systems
(V_E = 9144 m/sec
(30,000 ft/sec))
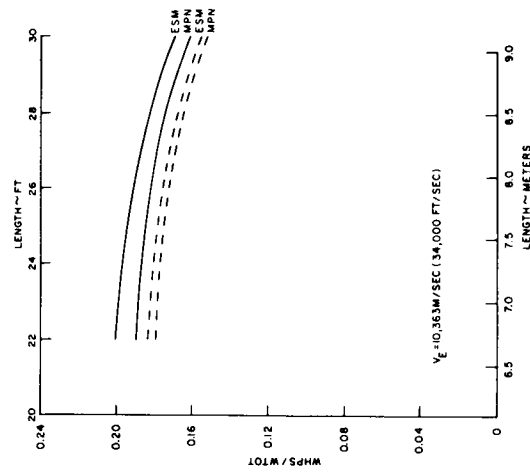
Figure 98. Combined Heat Shield
Weights for Ablation
Plux TZM Re-Radiation
and Ablation over Rene
Heat Protection Systems
(V_E = 10,363 m/sec
(34,000 ft/sec))
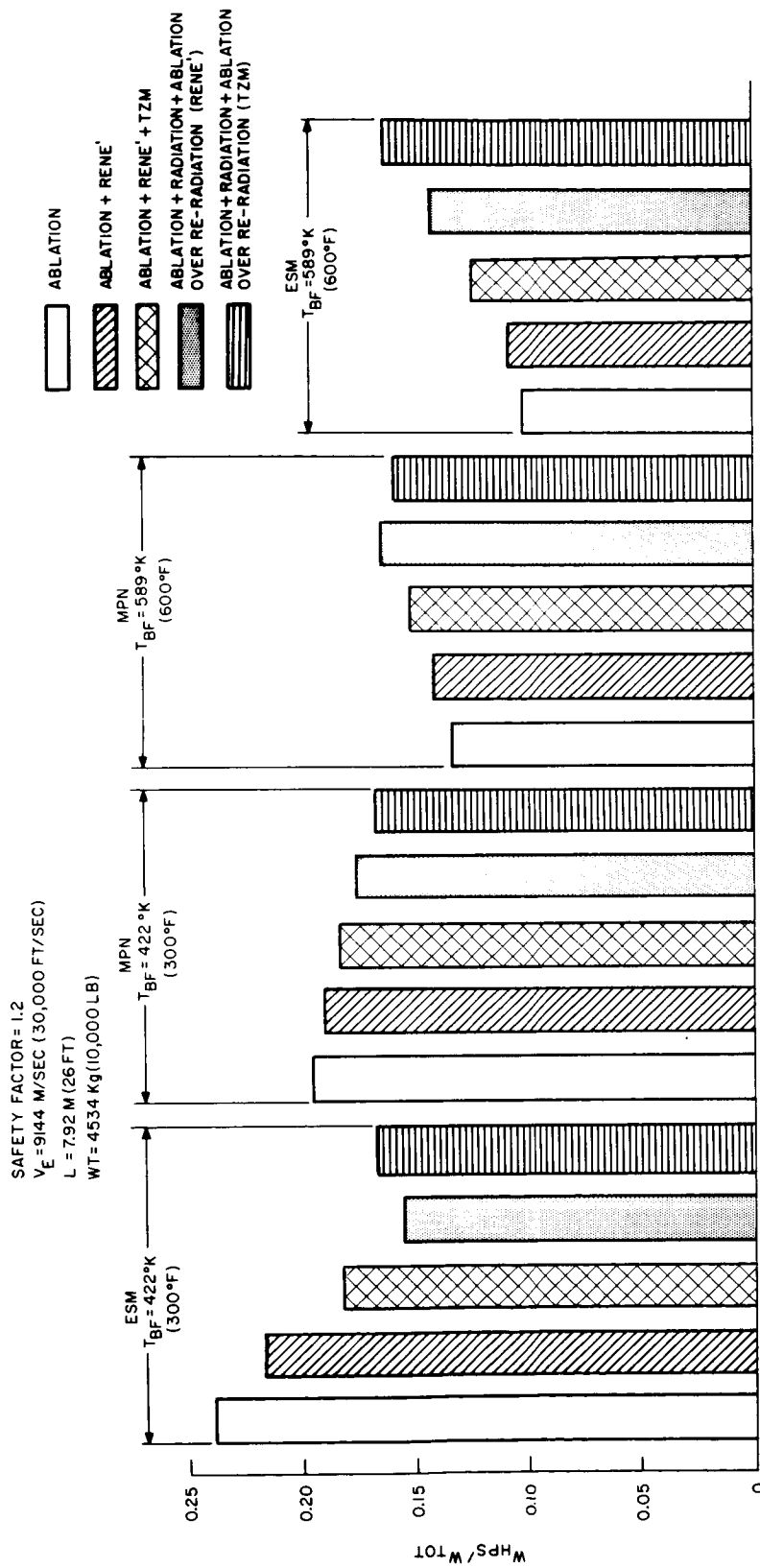
Figure 99. Typical Heat Protection System Weight Comparison for V_E = 9144 m/sec (30,000 ft/sec)

F57

ESM SHIELD

STRUCTURE

PERFORATED TEFLON
COATED GLASS FABRIC

A. Perforated Scrim

BONDED OR MOLDED-IN
ATTACHMENT

THERMAL SHIELD
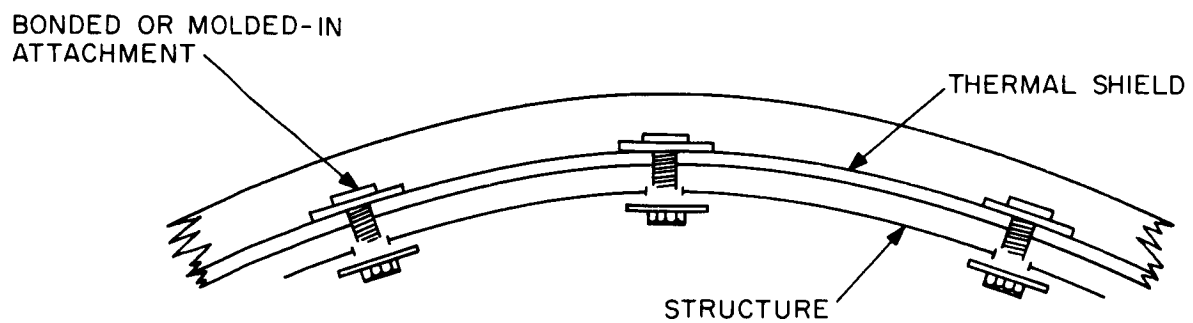
STRUCTURE

B. Nut and Bolt

Figure 100. Refurbishment Techniques

BOND — SHIELD
ELASTOMERIC PILLARS
STRUCTURE

A. Elastomeric Pillars

ESM SHIELD
STAINLESS STEEL PILE
STAINLESS STEEL LOOP
STRUCTURE
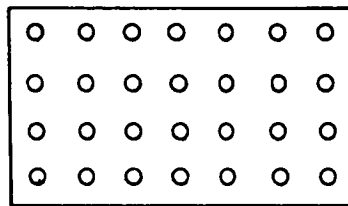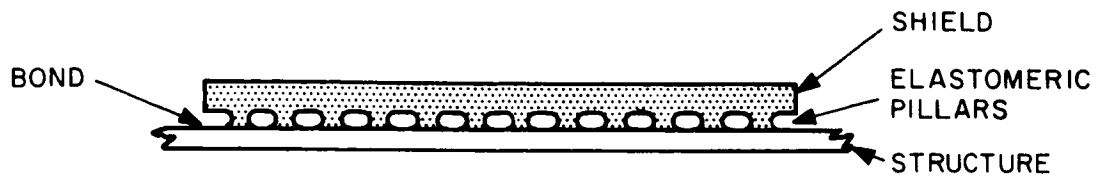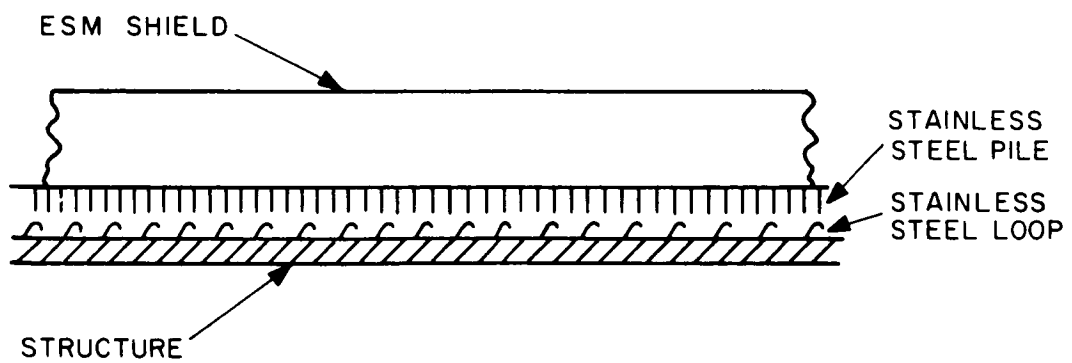
B. Loop and Pile

Figure 101. Refurbishment Techniques

F59

ROLLER

ESM SHIELD

TAPE-SHIELD BOND (RTV 560)

PRESSURE SENSITIVE TAPE
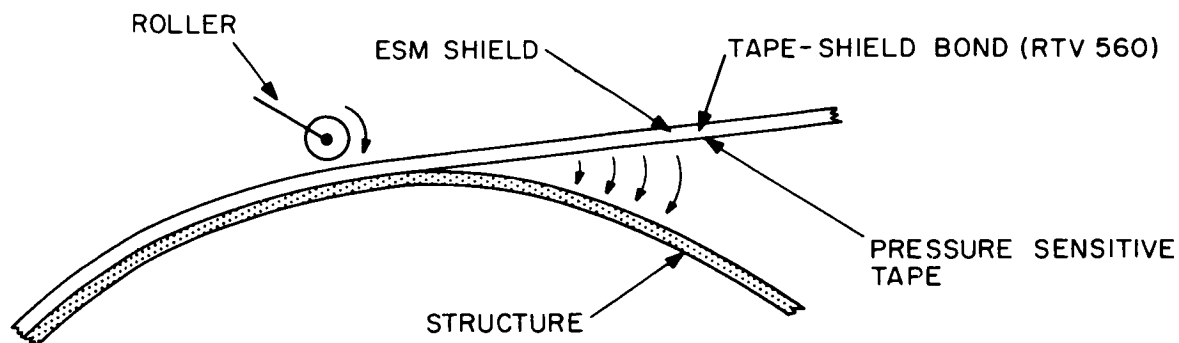
STRUCTURE

(A) PRE-BONDED SHEET OR SPRAY MATERIAL ABLATION

STRUCTURE

STRUCTURE

PRESSURE SENSITIVE TAPE

TAPE-BUTT SEAM

1. SURFACE PREPARATION
2. PRESSURE SENSITIVE TAPE APPLICATION
3. PRIMER APPLICATION
4. SPRAY OR SHEET APPLICATION
5. REMOVAL FOR REFURBISHMENT

STEPS   1   2   3   4   5
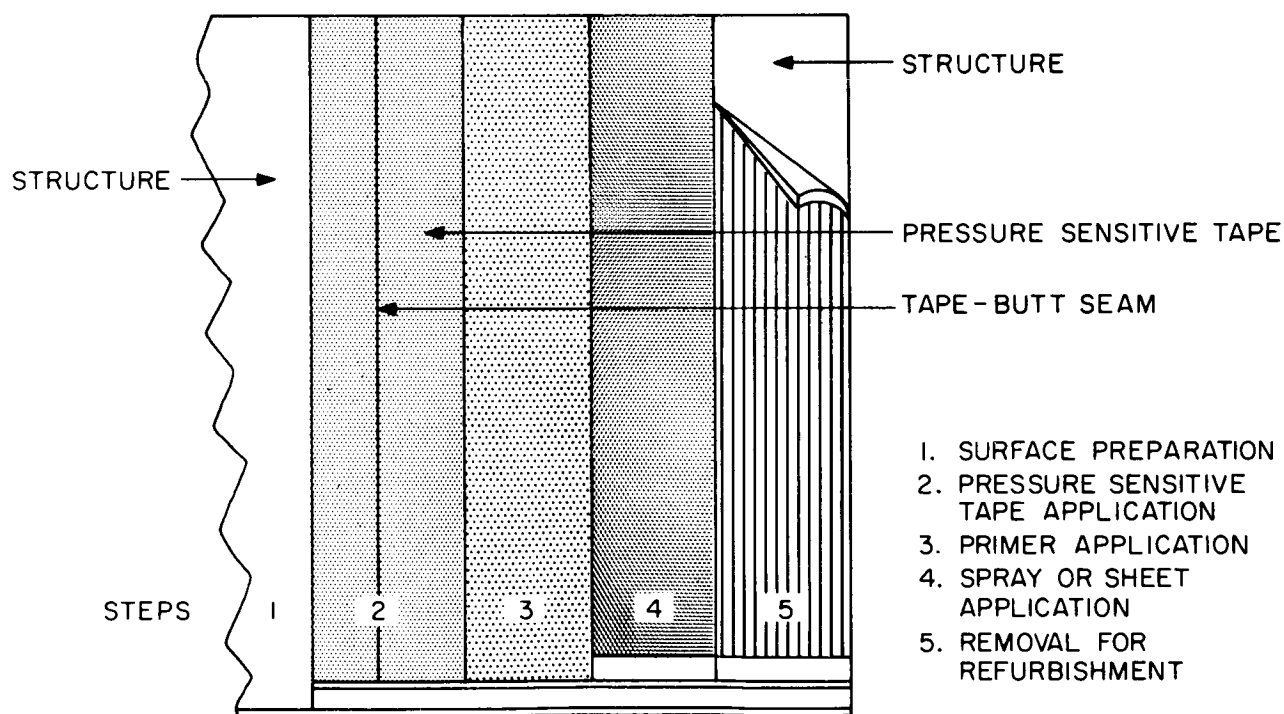
FIELD BONDED SHEET OR SPRAY MATERIAL APPLICATION TO THE STRUCTURE

(B) PRESSURE SENSITIVE TAPE

Figure 102. Refurbisnment Techniques
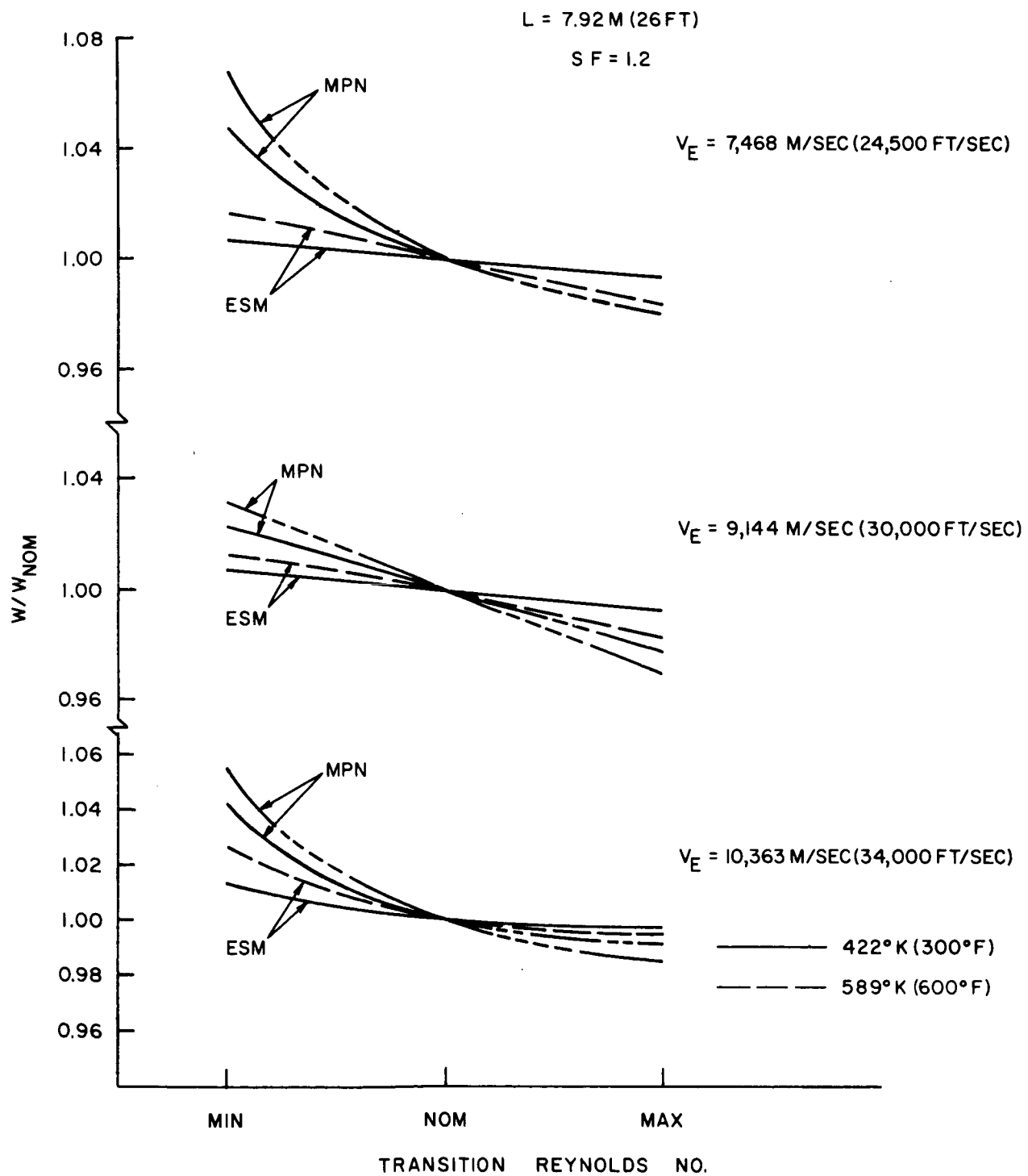
Figure 103. Effect of Transition on Heat Protection System Weight
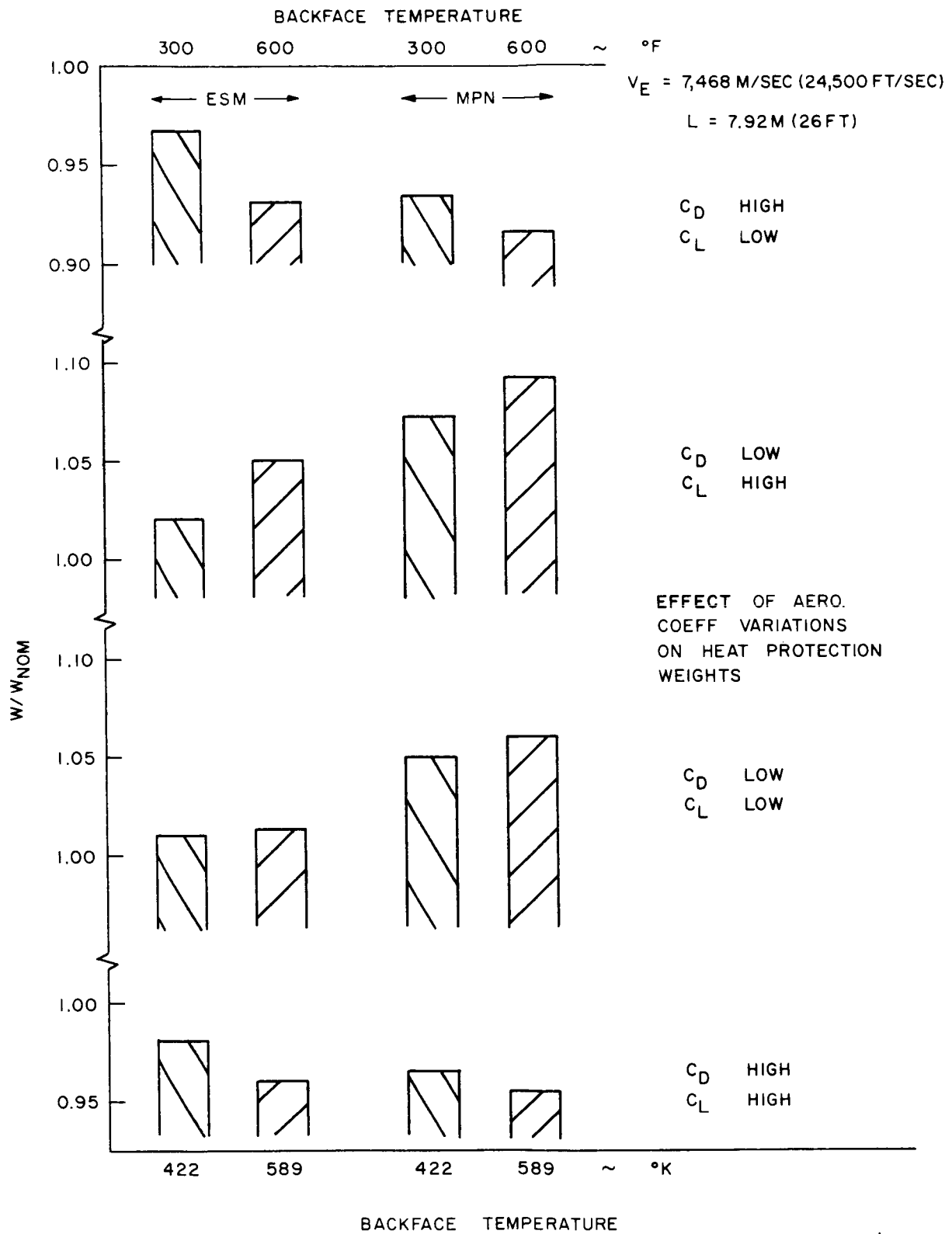
Figure 104.   Effect of Aerodynamic Coefficients on Heat Protection System Weights
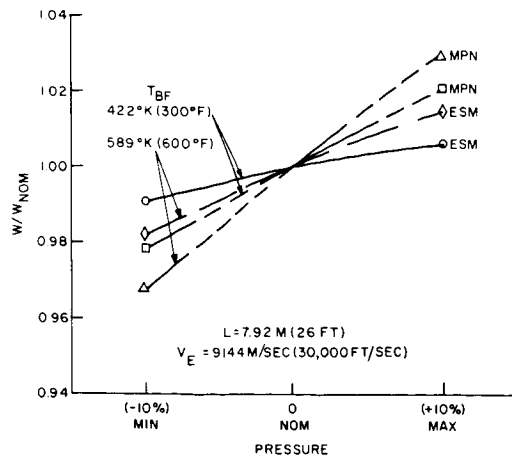
Figure 105.   Effect of Pressure Distribution on Heat Protection System Weights
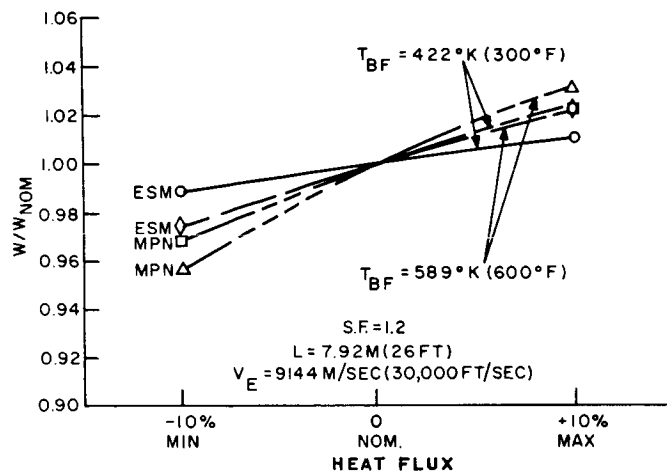
Figure 106.   Effect of Heat on Heat Protection System Weights
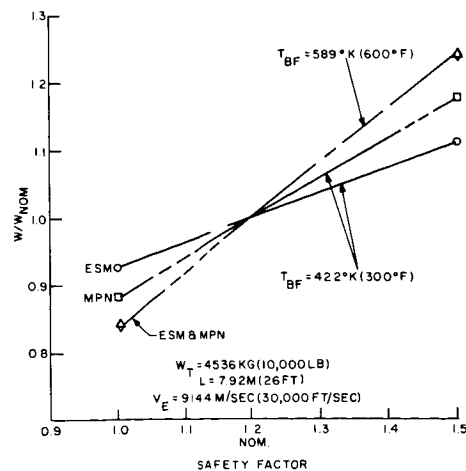
Figure 107.   Effect of Safety Factor on Heat Protection System Weights

A. Char Conductivity of ESM

B. Char Conductivity of MPN

C. Injected Gas Molecular Weight
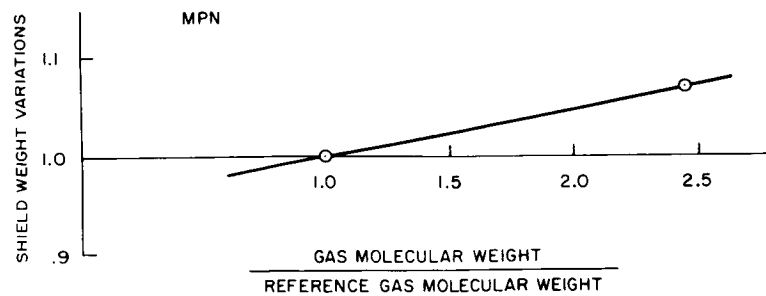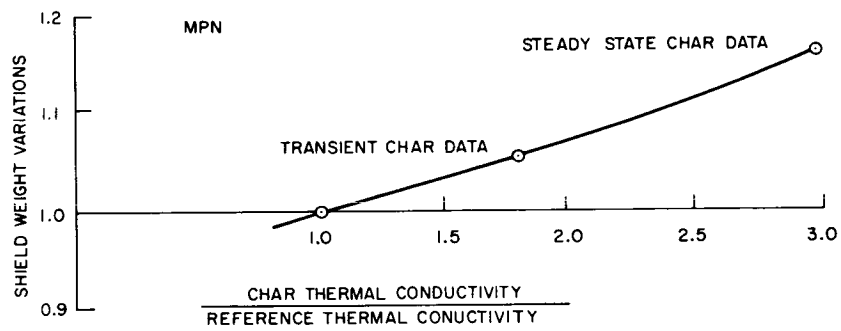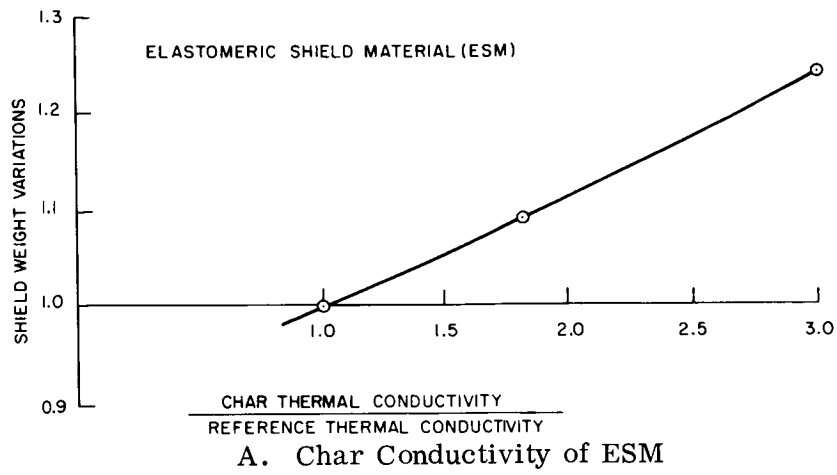
Figure 108. Effect of various Material Properties on Weights

A. Normal Erosion Case
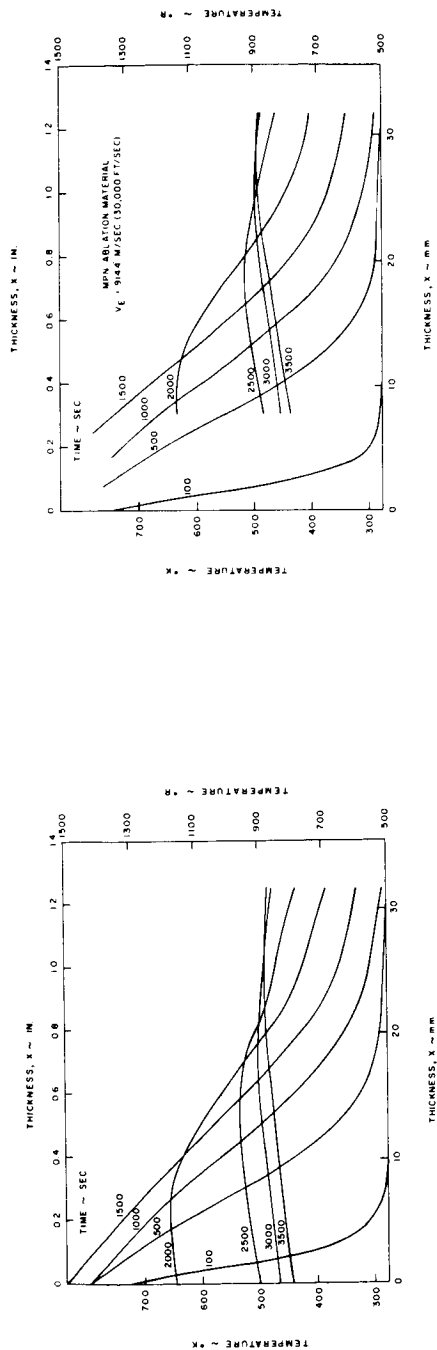
B. High Erosion Case
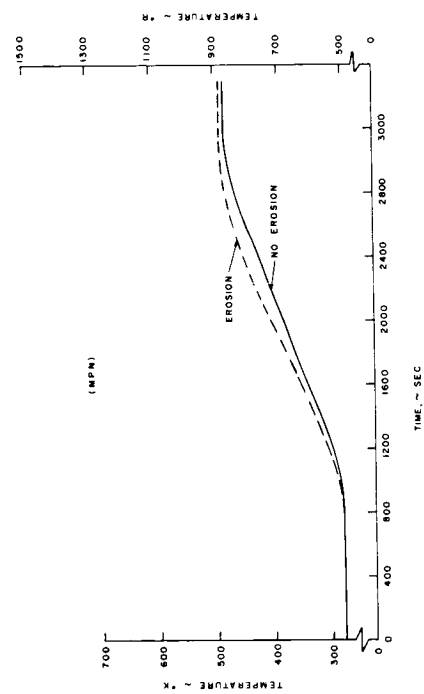
C. Backface Temperature History

Figure 109. Temperature Profiles for MPN ₁or Typical Ablation (V_E = 9144 m/sec (30,000 ft/sec))
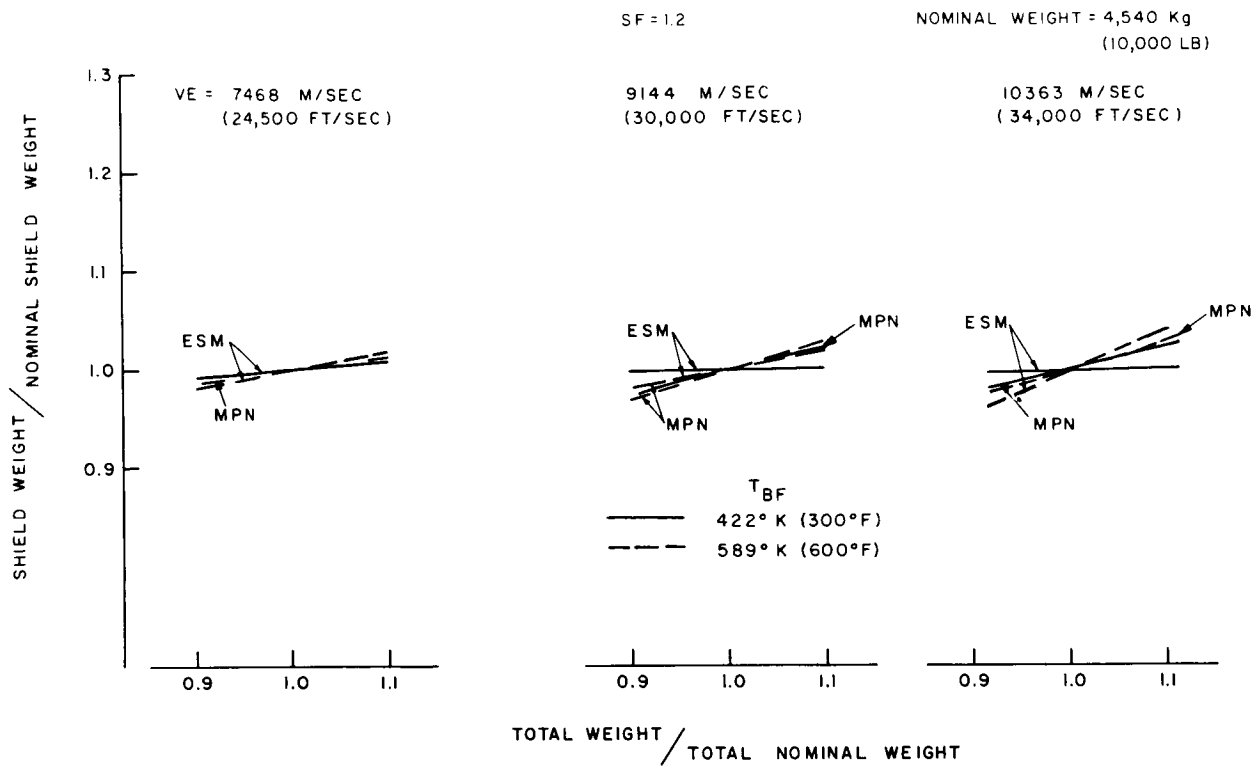
Figure 110. Effect of Total Vehicle Weight Variation on Shield Weight
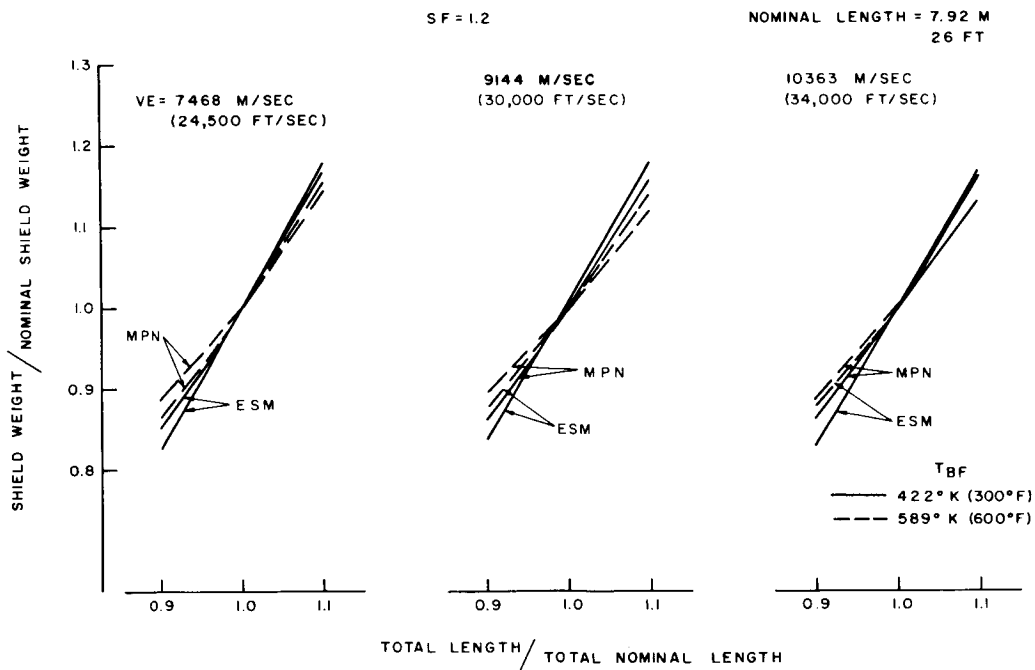
Figure 111. Effect of Total Vehicle Length on Shield Weight
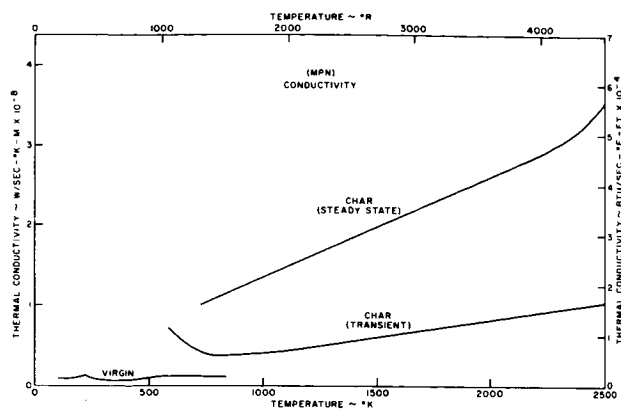
A. Thermal Conductivity
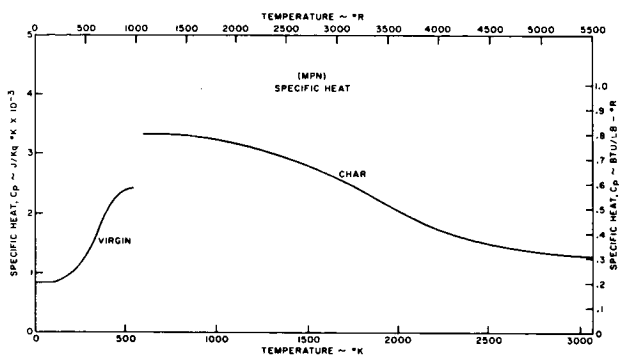
B. Specific Heat
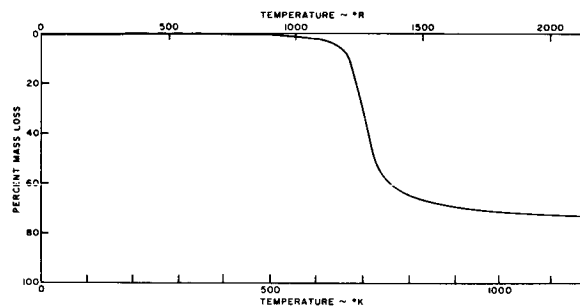
C. Thermogravimetric Data
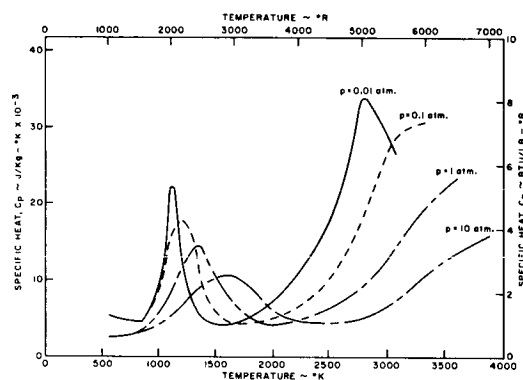
D. Pyrolysis Gas - Specific Heat
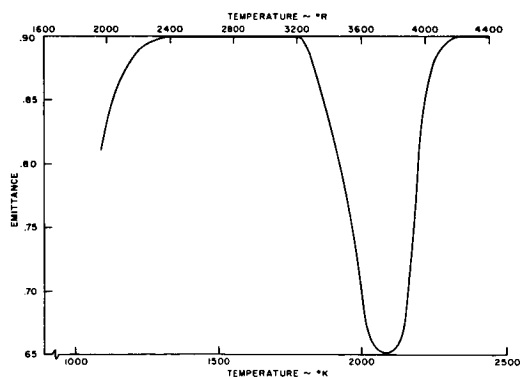
E. Emittance

Figure 112. Properties of MPN
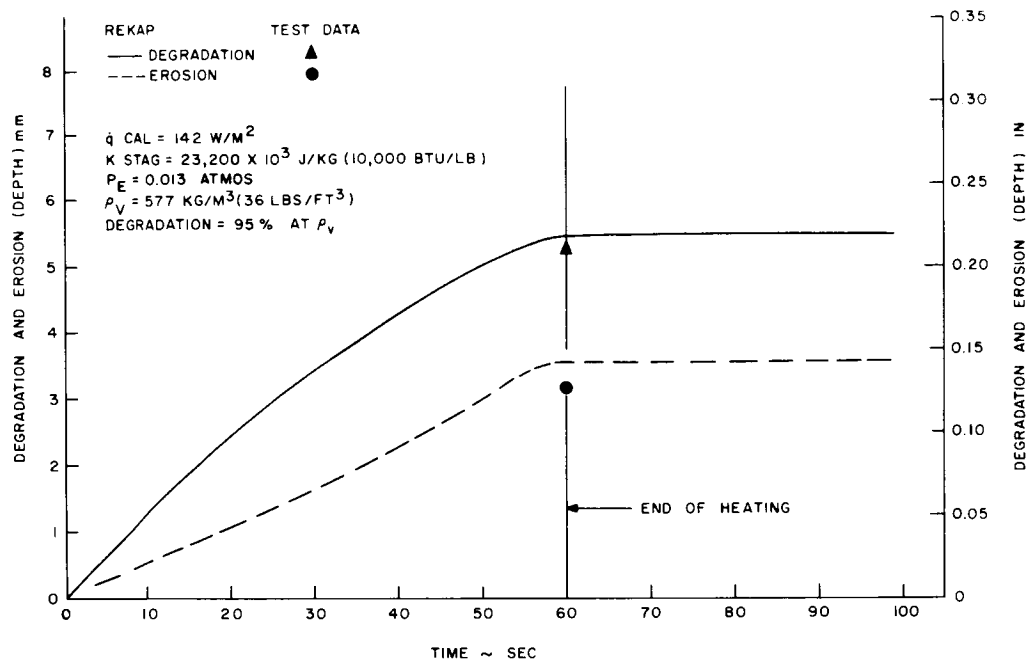
Figure 113. Degradation and Ablation of MPN for Ground Test Conditions
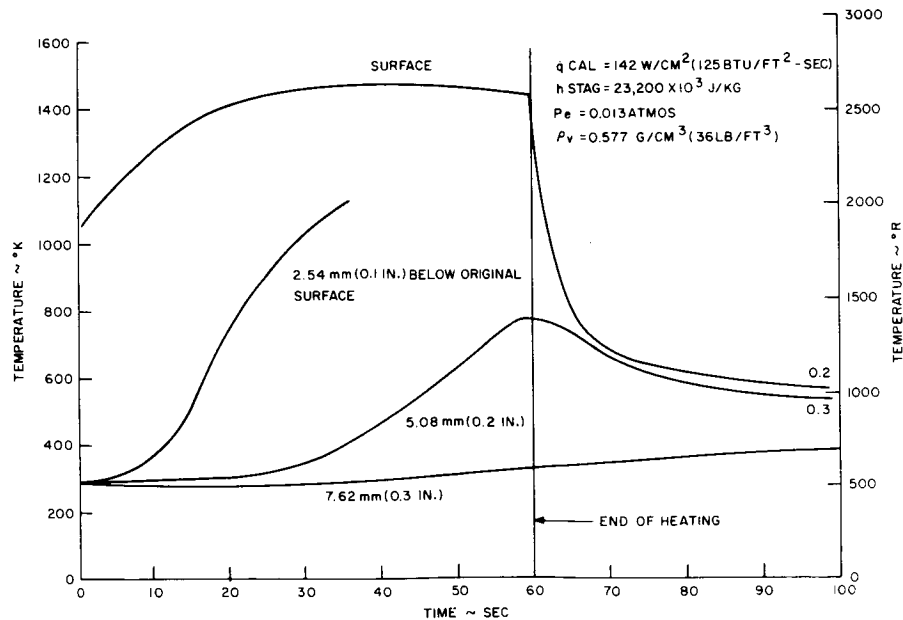
Figure 114. Temperature Response of MPN for Ground Test Conditions
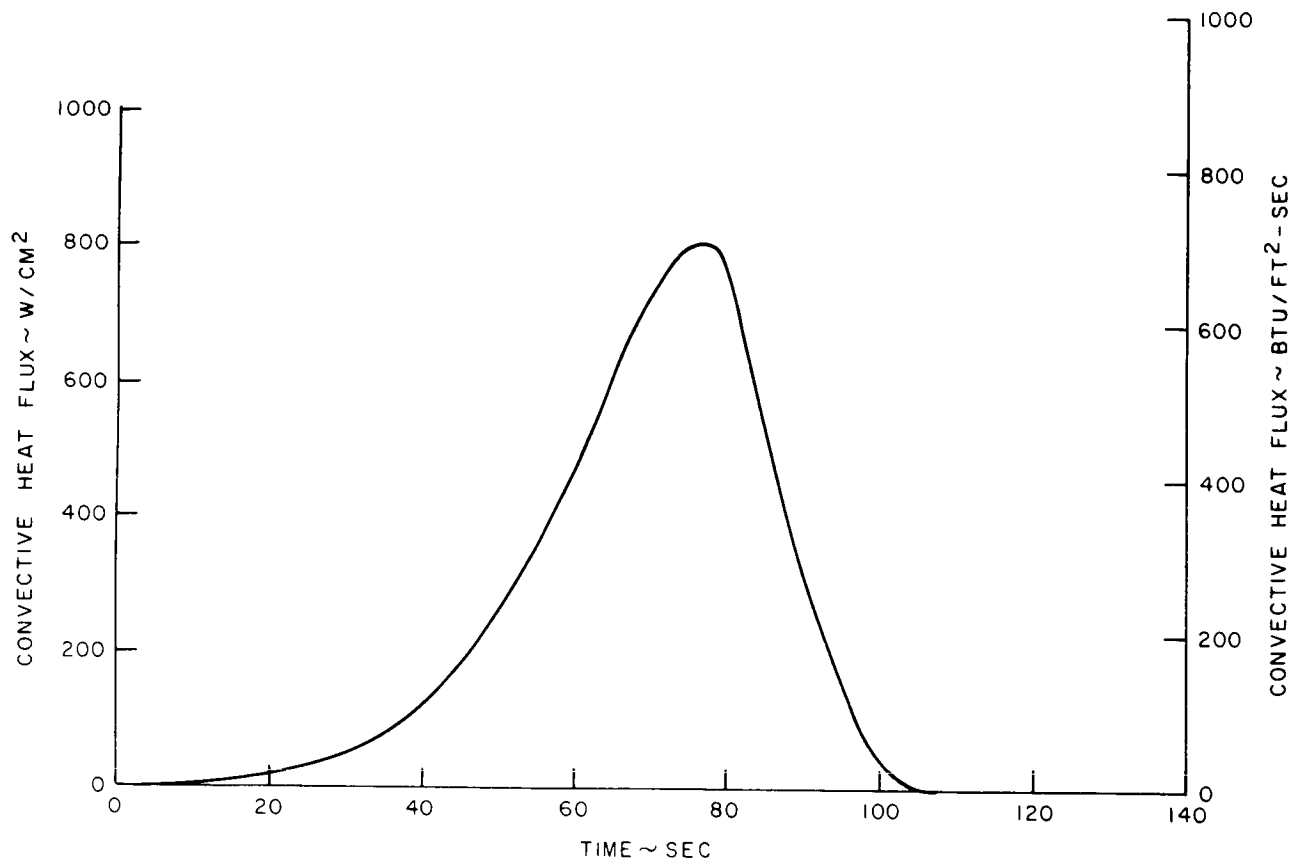
Figure 115.   Convective Heat Flux for Flight Test Conditions
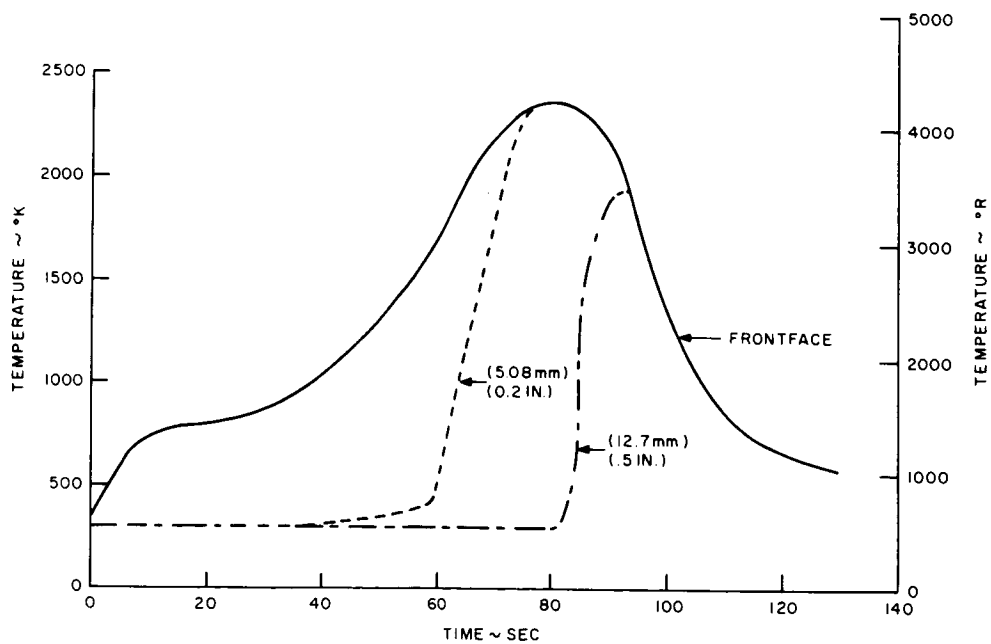
Figure 116.   Temperature Response of MPN for Flight Test Condition
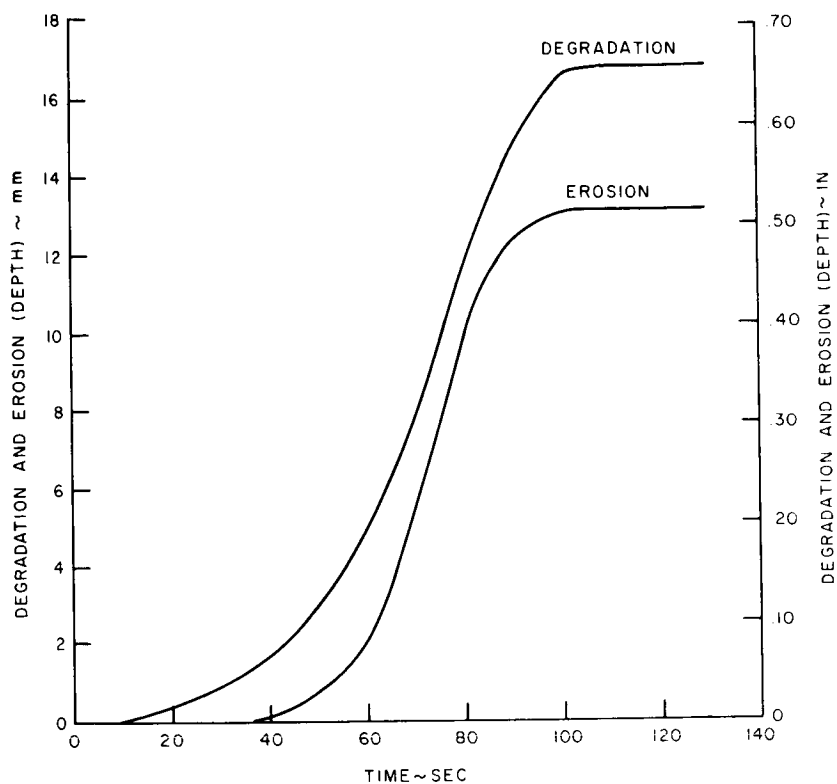
Figure 117. Degradation and Ablation of MPN for Flight Test Condition
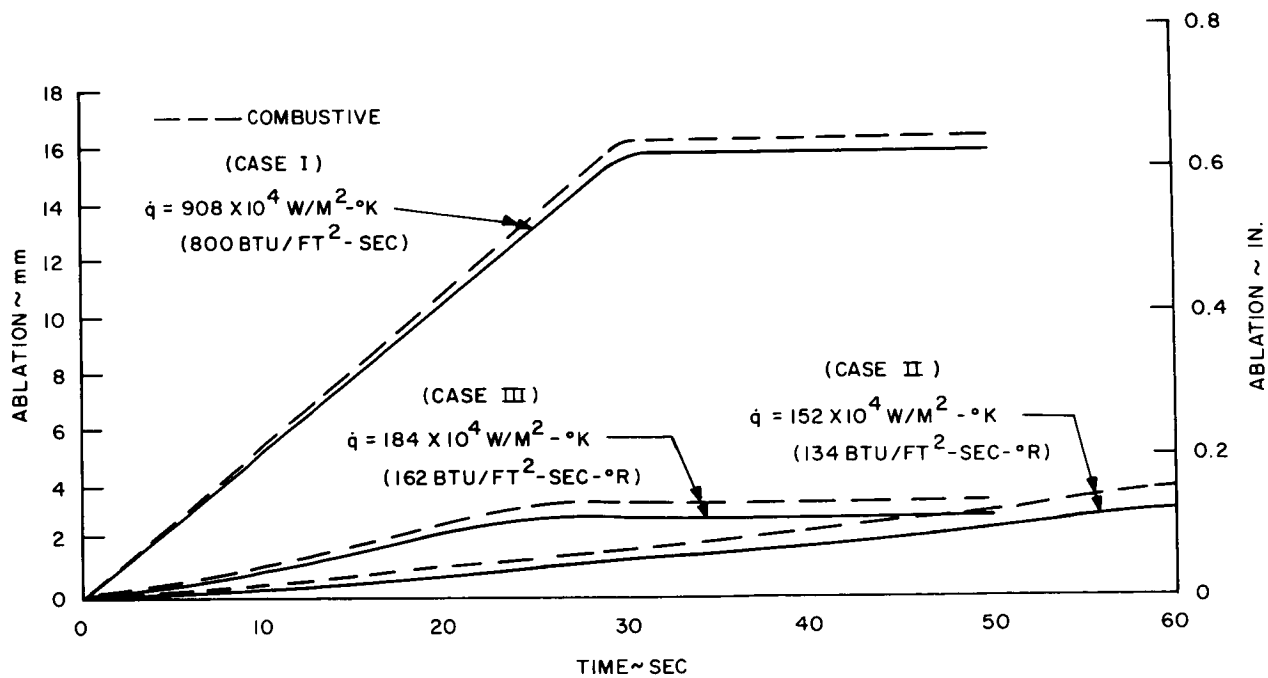
Figure 118. Ablation Histories of PN Ground Test Conditions for Case I, II and III

F70
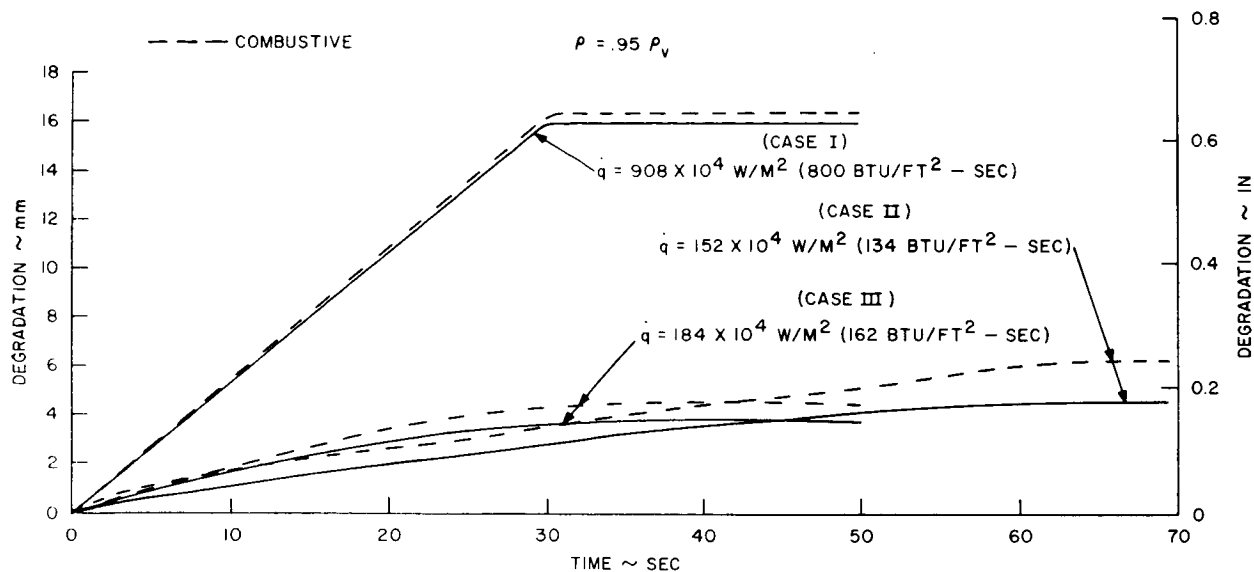
Figure 119.   Degradation Histories of PN Ground Test Conditions for Case I, II, and III
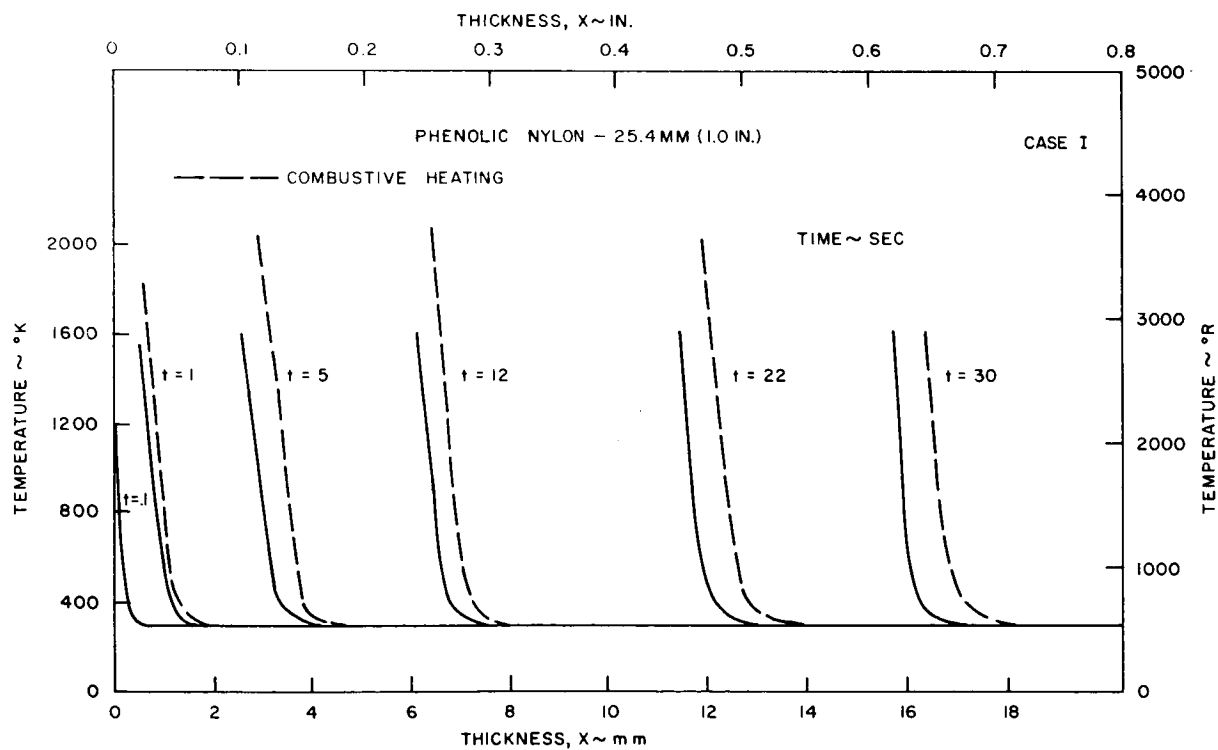
Figure 120.   Temperature Profiles for PN Ground Test Condition Case I
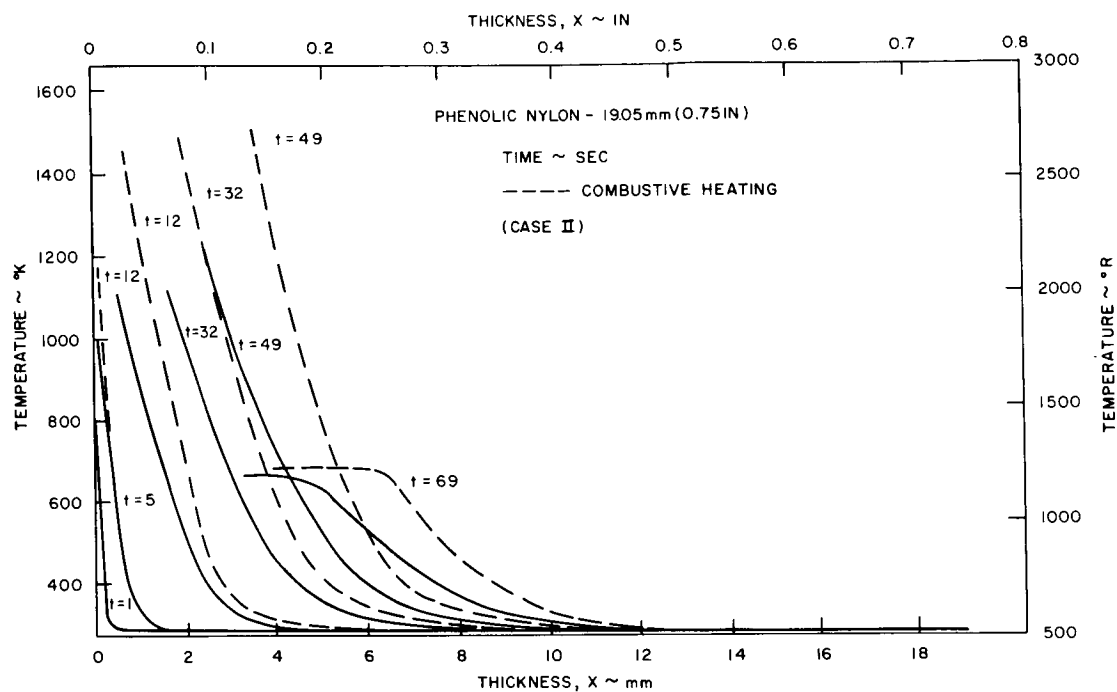
Figure 121. Temperature Profiles for PN Ground Test Condition Case II
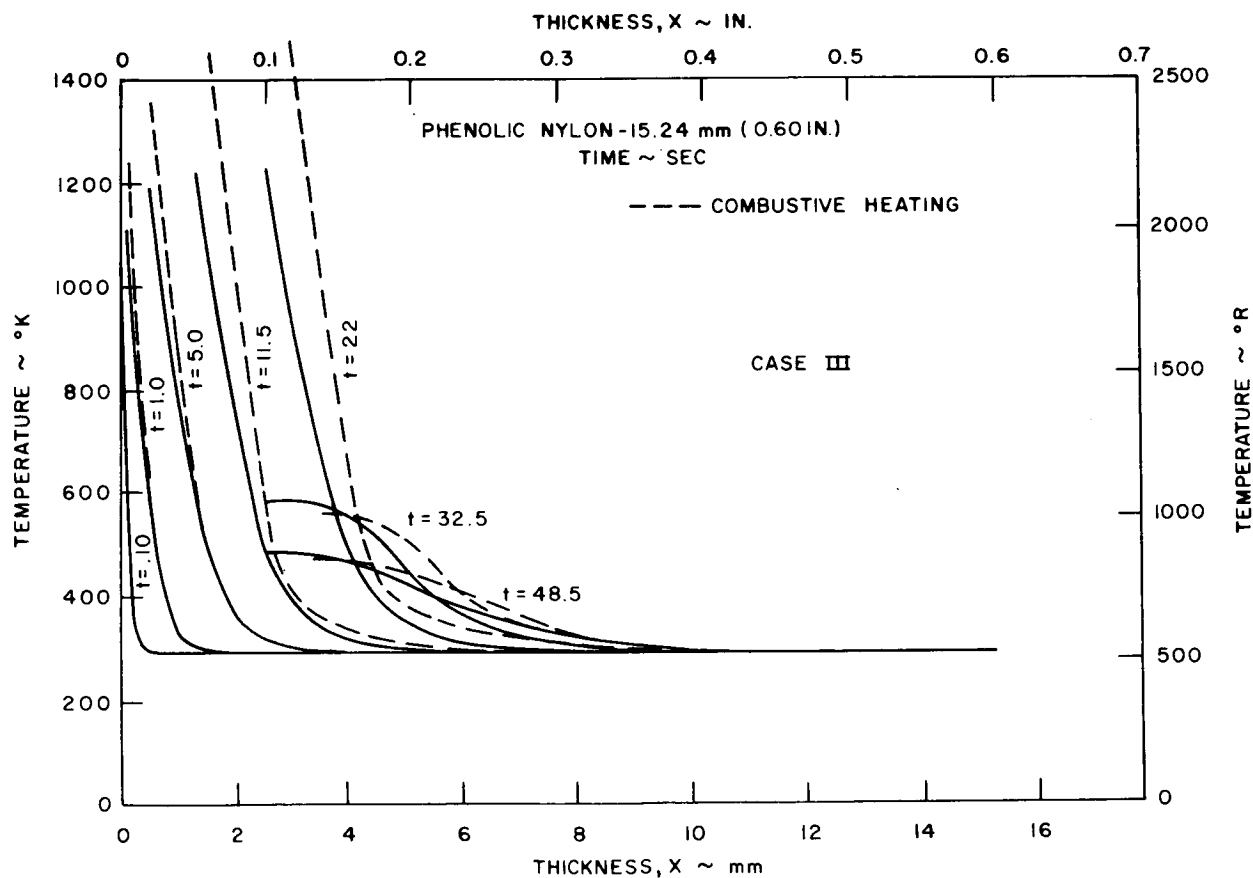
Figure 122. Temperature Profiles for PN Ground Test Condition Case III

F72
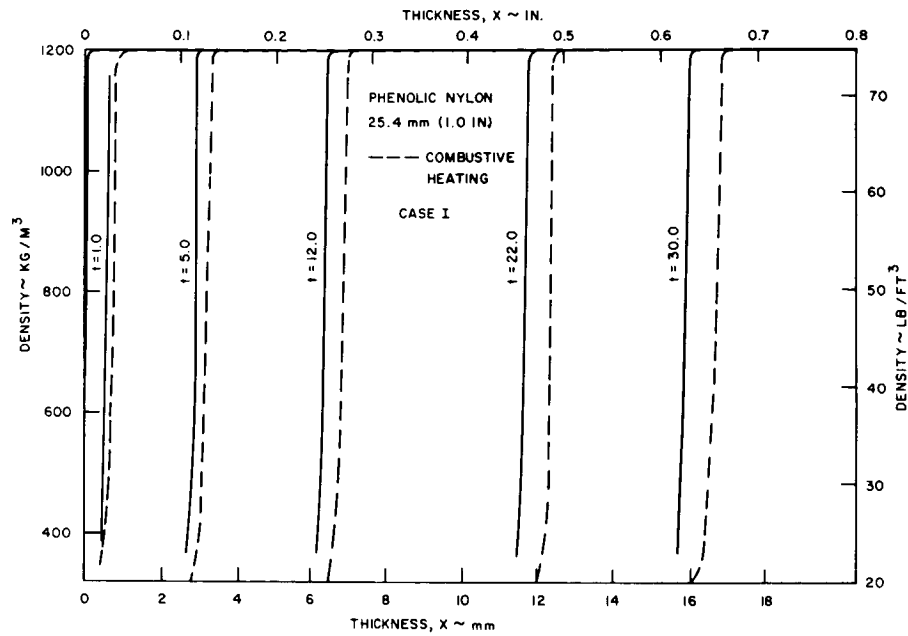
Figure 123. Density Profiles for PN Ground Test Condition Case I
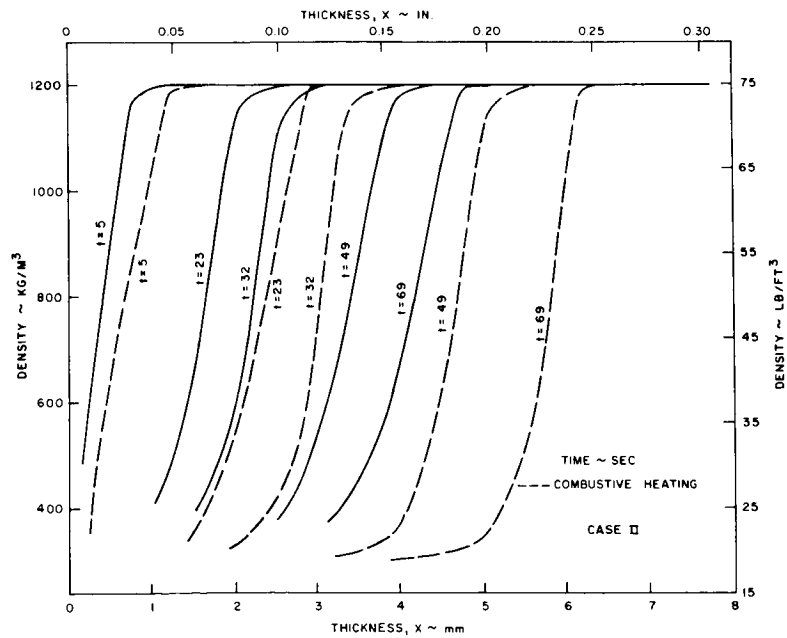
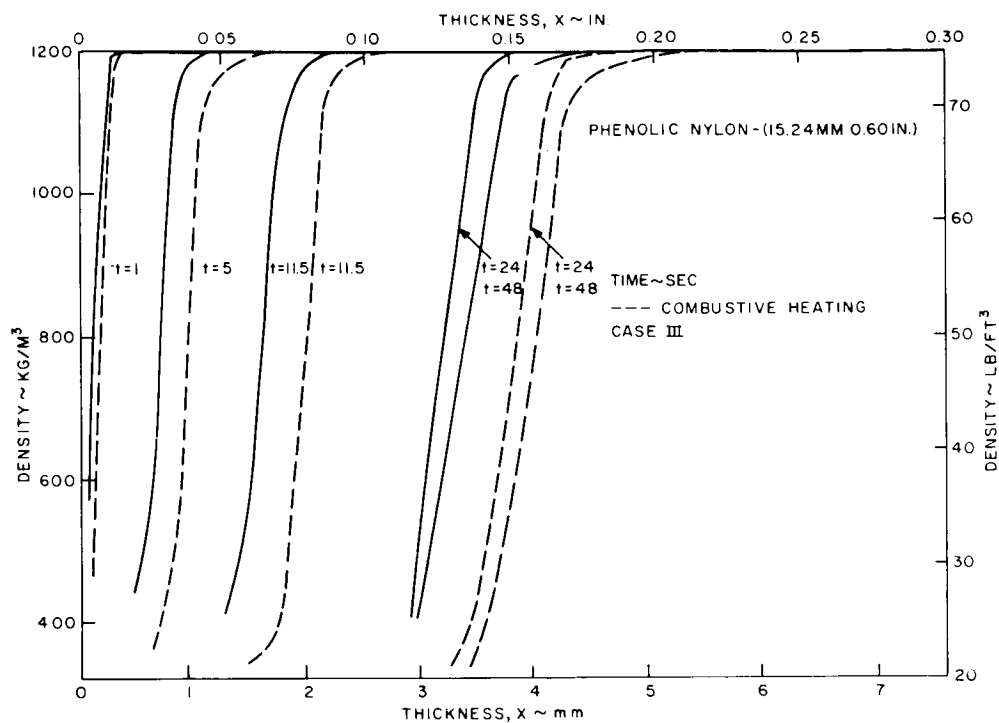Figure 124. Density Profiles for PN Ground Test Condition Case II

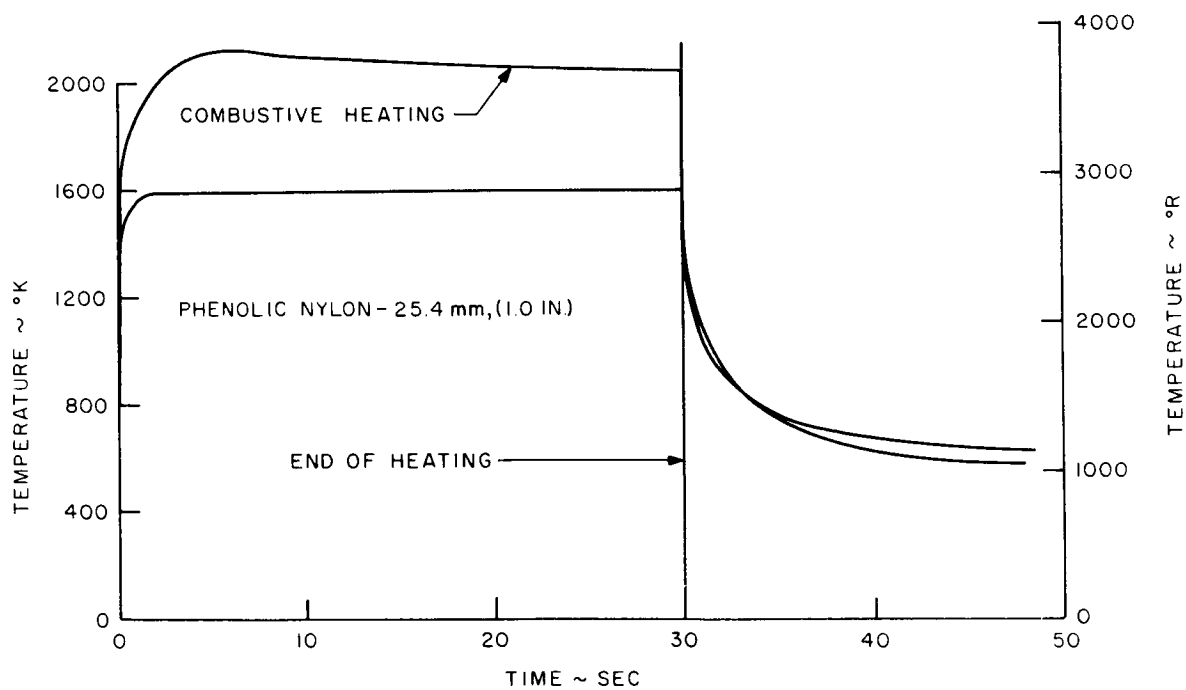Figure 125.   Density Profiles for PN Ground Test Condition Case III

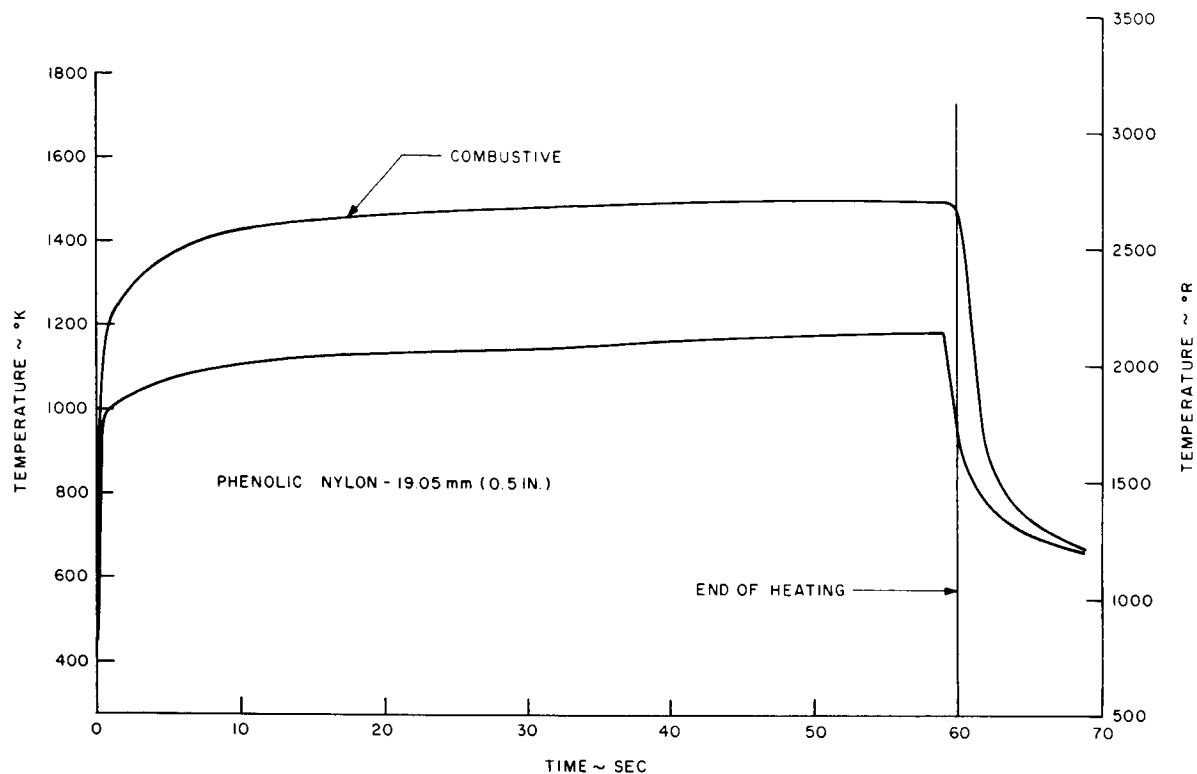Figure 126.   Surfact Temperature Histories for PN Case I
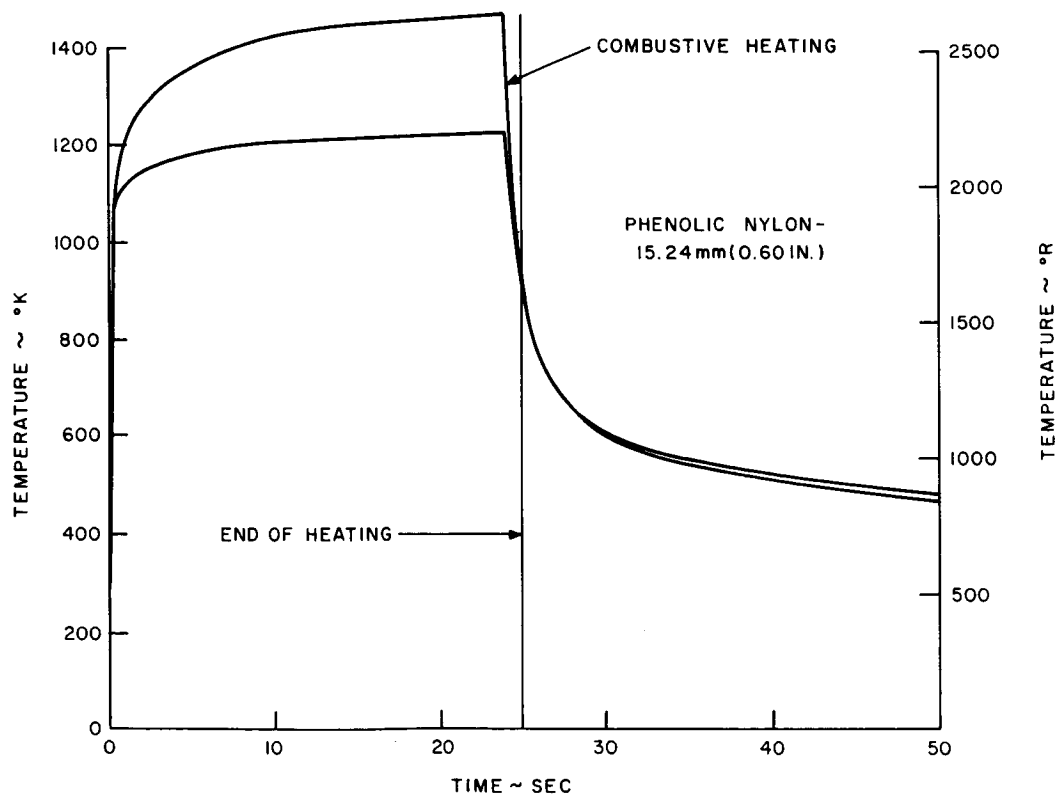
Figure 127. Surface Temperature Histories for PN Case II

Figure 128. Surface Temperature Histories for PN Case III